Titre: Title:	Shear and Tension Capacity of Arc-Spot Weld connections for Multi-Overlap Roof Deck Panels
Auteur: Author:	Nadir Guenfoud
Date:	2009
Type:	Mémoire ou thèse / Dissertation or Thesis
Référence: Citation:	Guenfoud, N. (2009). Shear and Tension Capacity of Arc-Spot Weld connections for Multi-Overlap Roof Deck Panels [Mémoire de maîtrise, École Polytechnique de Montréal]. PolyPublie. https://publications.polymtl.ca/188/

UNIVERSITÉ DE MONTRÉAL

SHEAR AND TENSION CAPACITY OF ARC-SPOT WELD CONNECTIONS FOR MULTI-OVERLAP ROOF DECK PANELS

NADIR GUENFOUD
DÉPARTEMENT DES GÉNIES CIVIL, GÉOLOGIQUE ET DES MINES
ÉCOLE POLYTECHNIQUE DE MONTRÉAL

MÉMOIRE PRÉSENTÉ EN VUE DE L'OBTENTION
DU DIPLÔME DE MAÎTRISE ÈS SCIENCES APPLIQUÉES
(GÉNIE CIVIL)
NOVEMBRE 2009

UNIVERSITÉ DE MONTRÉAL

ÉCOLE POLYTECHNIQUE DE MONTRÉAL

Ce mémoire intitulé:

SHEAR AND TENSION CAPACITY OF ARC-SPOT WELD CONNECTIONS FOR MULTI-OVERLAP ROOF DECK PANELS

Présenté par : GUENFOUD Nadir
en vue de l'obtention du diplôme de : Maîtrise ès sciences appliquées
a été dûment accepté par le jury d'examen constitué de :

M. BOUAANANI Najib, Ph.D, président
M. TREMBLAY Robert, Ph.D, membre et directeur de recherche
M. ROGERS Colin, Ph.D, membre et codirecteur de recherche
M. TRIGO Gil, M.B.A., membre

ACKNOWLEDGEMENTS

I would like to thank the Natural Sciences and Engineering Research Council of Canada (NSERC), the Canadian Sheet Steel Building Institute (CSSBI), the Steel Structures Education Foundation (SSEF) of the Canadian Institute of Steel Construction (CISC) for their support in sponsoring this project. The collaboration of the Canam Group for supplying the material for the test specimens is most appreciated... I wish to thank Professor Colin Rogers from McGill University and Professor Robert Tremblay from École Polytechnique de Montréal for their guidance and dedication throughout the entire length of my studies. I wish to thank M. Gil Trigo for sharing his knowledge and experience. I must also recognize the contribution of Patrice Bélanger, Denis Fortier and Viacheslav Koval from the laboratory at École Polytechnique who were always available to help during the experimental program. Finally I would like to thank all my friends and family for making this time so enjoyable.

RÉSUMÉ

Ce projet de recherche a pour but d'évaluer la résistance en cisaillement et en traction des soudures à l'arc utilisées pour l'assemblage de plusieurs épaisseurs de tôle métallique à une structure en acier. Ce type d'assemblage survient dans les diaphragmes de toit des bâtiments, quand les feuilles se chevauchent le long du périmètre des feuilles. A ces endroits, les limites imposées par la norme pour l'épaisseur maximale des tôles soudées et pour le ratio d'épaisseur de la plaque de support sur l'épaisseur totale des feuilles de tôle, peut être dépassée si des tôles épaisses sont utilisées. Le premier objectif de ce projet fut de déterminer une méthode de soudage qui permet de maximiser la qualité des soudures fabriquées dans plusieurs tôles épaisses. Les résultats ont démontré que les facteurs les plus importants à contrôler sont l'intensité du courant, le type d'électrode et la technique du soudeur. Au cours de cette étude, toutes les soudures furent fabriquées par un soudeur professionnel et certifié. Des soudures furent fabriquées avec 1, 2 et 4 feuilles de tôle avec des épaisseurs variant de 0.76 mm à 1.52 mm et une procédure de soudage a été développée pour chaque configuration. Plusieurs configurations de feuilles de tôle furent mises à l'essai pour reproduire le plus fidèlement possible les cas de chargement que l'on retrouve dans un diaphragme de toit. Au moins 3 essais furent complétés avec chaque épaisseur de tôles pour chaque configuration. Des essais furent réalisés pour 72 échantillons soumis à un chargement monotonique en traction. De plus, des essais en cisaillement furent réalisés sur 107 échantillons, dont 76 furent soumis à un chargement monotonique et 31 à un chargement cyclique. Ce type de chargement a été utilisé pour observer le comportement des soudures soumises à des sollicitations dynamiques telles qu'imposées lors d'un séisme. De plus la résistance, la déformation ainsi que le mode de rupture furent relevés pour chaque spécimen. Par ailleurs, le diamètre effectif de la soudure fut mesuré pour les spécimens où il y a eu rupture de la soudure. Les résultats obtenus durant les essais furent comparés aux valeurs prédites par la norme CSA S136 (2007) pour en évaluer la précision.

Nous avons observé que les diamètres effectifs des soudures mesurés pendant la période d'essais étaient, en moyenne, plus grands que les diamètres effectifs prédits par la norme CSA S136 (2007). Cette différence s'accroît quand l'épaisseur des tôles augmente. L'analyse des résultats démontre

qu'une limite inférieure du diamètre effectif devrait être imposée à l'équation E2.2.1-5 de la norme CSA S136 (2007) pour améliorer sa précision. La résistance en cisaillement moyenne mesurée lors des essais était aussi plus élevée que celle prédite par la section E2.2.1 de la norme CSA S136 (2007). Les résultats indiquent que la modification de l'équation E2.2.1-2 permettrait d'améliorer la précision de la prédiction de la norme. Les résultats des essais en cisaillement avec chargement cyclique ont permis d'observer que la résistance ultime des spécimens n'était pas affectée après avoir été soumis à plusieurs cycles de chargement à un niveau inférieur puis égal à la résistance pondérée. Ces essais ont aussi permis d'observer un mode de rupture ductile lorsque la rupture est associée à une pression diamétrale excessive dans la direction parallèle à la charge appliquée, une situation qui se produit quand le diamètre effectif de la soudure est relativement grand par rapport à l'épaisseur de la tôle,.

Pour les essais en traction, la résistance moyenne mesurée pour les spécimens où la rupture est survenue par le déchirement de la tôle fut plus élevée que les valeurs prédites par la section E2.2.2 de la norme CSA S136 (2007). Ces résultats montrent que la réduction de résistance en traction de 30% qui est spécifiée par la norme ne devrait pas s'appliquer aux spécimens qui ont ce mode de rupture. Cependant, pour les spécimens qui ont subi une rupture de la soudure en traction, la résistance en traction moyenne mesurée fut inférieure à celle prédite par la norme CSA S136 (2007). Ce résultat indique que la réduction en résistance de traction de 30% devrait être maintenue pour la rupture de la soudure. L'application de cette réduction pourrait même être élargie pour inclure les soudures fabriquées avec une seule feuille de tôle, car il n'y a pas d'indice qui porte à croire que la résistance en traction reliée à la rupture de la soudure soit influencée par la configuration de plusieurs feuilles de tôle.

ABSTRACT

This research project was undertaken to investigate the shear and tensile capacity of arc-spot welds connecting overlapped deck sheets to underlying steel framework. Such connection configurations typically occur in roof deck constructions when steel sheets are stacked at a sidelap or endlap or at both. At these specific locations, the limits on the thickness of the thinnest connected part and on the ratio of supporting steel to sheet steel thickness imposed by the CSA S136 Specification (2007) can be exceeded if thick steel sheets are used. The first step of the project was to determine a welding procedure that would maximize the quality of arc-spot welds when fabricated through thick sheets. It was found that the most important factors to control during the welding of thick steel sheets were the current setting (high intensity), the electrode type (E6011) and the welding technique. During this study welds were fabricated by a certified welder through 1, 2 and 4 layers of steel sheets with thicknesses ranging from 22 gauge (0.76 mm) to 16 gauge (1.52 mm) and a welding procedure was developed for each case. Different sheet steel configurations were used to reproduce the typical loading conditions found in roof deck construction. A minimum of 3 tests were completed for each configuration with each steel sheet thickness. Monotonic tensile resistance tests were carried out on 72 specimens. A total of 107 shear resistance tests were also completed. Of this total, 76 specimens were loaded with a monotonically increasing load while 31 specimens were loaded with a reversed cyclic protocol used to gain insight on the behaviour of arc-spot welds subject to dynamic loading, such as that imposed under seismic ground motions. The resistance, deformation and failure mode was recorded for each specimen. Moreover, the effective weld diameter was recorded for specimens that failed due to weld failure. The results obtained during this study were compared with the current provisions of the CSA S136 Specification to verify if these provisions are applicable to multi-overlap configurations.

The effective weld diameter was recorded for all specimens where weld failure was observed. The average effective weld diameter recorded was larger than the effective weld diameter predicted by CSA S136 Specification . This difference between the measured and predicted values increased as the sheet steel thickness increased. These results demonstrated that a lower limit should be imposed on

Equation E2.2.1-5 of CSA S136 to improve its precision when dealing with large thicknesses of sheet steel. In the monotonic shear tests, the average shear resistance recorded was greater than the average resistance predicted by section E2.2.1 of CSA S136. A modification to this section is proposed to improve its overall precision. During the cyclic tests, the results demonstrated that the resistance of the specimens did not decrease after sustaining several loading cycles at load levels smaller than and then equal to the factored resistance. The results from the cyclic tests also showed that ductile failure can occur when the sheet bearing failure mode is engaged. This failure mode was observed for some specimens where the average weld diameter was relatively large when compared to the steel sheet thickness.

During the tensile resistance tests, specimens where the sheet tearing failure mode governed presented an average measured tensile resistance higher than the average resistance predicted by the section E2.2.2 of the CSA S136 Specification . These results showed that the 30% reduction in capacity specified in CSA S136 for specimens fabricated through more than one layer of sheet steel should not apply to specimens governed by the sheet tearing failure mode (Equation E2.2.2-2). However, for specimens that failed due to tensile weld fracture, the average measured resistance was lower than the values predicted by CSA S136, which indicates that the 30% reduction in strength should apply to this case. The 30% strength reduction related to weld failure should also be applied to welds fabricated in standard 1-layer configurations as there is no evidence to suggest that the resistance of arc-spot welds in tension is influenced by the lapped configuration.

CONDENSÉ EN FRANÇAIS

Introduction

En Amérique du Nord, les diaphragmes au toit font souvent partie du système de reprise des charges latérales des bâtiments d'un étage. Le système de reprise des charges latérales est utilisé pour résister aux charges provenant du vent ou des séismes. Un diaphragme au toit est généralement composé de plusieurs tôles métalliques qui sont attachées les unes aux autres ainsi qu'à la structure du bâtiment. Les différentes techniques pour fixer les tôles métalliques sont notamment à l'aide de vis, de clous ou de soudures. Grâce à sa polyvalence, sa vitesse d'exécution et son faible coût, le soudage à l'arc est un choix populaire très répandu dans l'industrie de la construction. Quand les soudures sont utilisées pour solidariser les feuilles de tôle métallique, les soudures doivent être capable de transférer des efforts de cisaillement. Ces efforts doivent passer d'une feuille à l'autre, ou d'une feuille à la structure, avant de pouvoir être retransmis aux contreventements verticaux qui sont généralement placés au périmètre de la structure. Ces soudures doivent aussi résister aux efforts de traction provenant du soulèvement occasionné par le vent. Les soudures fabriquées là où les tôles se chevauchent doivent être réalisées et assurer le transfert des efforts au travers de plusieurs épaisseurs de tôle métallique.

La norme canadienne CSA S136 (2007) présentement en vigueur spécifie les méthodes de calcul pour déterminer la résistance des soudures à l'arc. Une limite de 3.81 mm est imposée dans la norme comme l'épaisseur maximale de l'élément le moins épais à fixer à l'aide d'une soudure. De plus l'épaisseur maximale de deux feuilles de tôles ne doit pas dépasser 2.5 mm et le ratio de l'épaisseur de la plaque de support sur l'épaisseur totale des feuilles de tôles doit être plus grand ou égale à 2.5. Lors des modifications apportées aux dispositions parasismiques du Code National du Bâtiment du Canada (CNBC 2005) et de la norme CSA-S16 (2001), la méthode de conception par capacité est devenue obligatoire pour la plupart des systèmes de résistance aux forces sismiques. Selon cette méthode, la résistance pondérée en cisaillement du diaphragme au toit doit être supérieure à la résistance probable des contreventements verticaux. Cette nouvelle approche donne lieu à des efforts plus importants dans les diaphragmes de toit, ce qui force l'utilisation de tôles métalliques plus

épaisses. Il est maintenant courant de voir des tôles métalliques d'une épaisseur allant jusqu'à 1.52 mm. Quand ces tôles sont superposées l'une sur l'autre au périmètre des feuilles, les limites imposées par la norme CSA S136 (2007) sont dépassées. Il existe peu d'informations pour aider les concepteurs à déterminer la résistance des soudures pour ces cas particuliers.

Objectif

Le premier objectif de cette recherche est de développer une technique de soudage qui maximisera la qualité des soudures fabriquées au travers de plusieurs épaisseurs de tôles métalliques. Par la suite, cette recherche a pour but de déterminer la résistance en cisaillement et en traction de soudures fabriquées au travers de plusieurs épaisseurs de tôle métallique. À l'aide des résultats obtenus en laboratoire, il sera possible de déterminer si les clauses présentement en vigueur dans le CSA S136 (2007) sont valables pour les cas où il y a plusieurs épaisseurs de tôle.

Revue de littérature

Une revue de la littérature disponible sur le sujet indique que plusieurs travaux de recherche ont déjà été effectués sur la résistance des soudures à l'arc. Cependant, aucune étude n'a évalué le comportement des soudures à l'arc lorsque fabriquées avec plusieurs épaisseurs de tôle. La norme CSA S136 (2007) est la référence la plus reconnue pour la conception des membrues et assemblages impliquant des tôles minces en acier. La section E.2-2-1 de cette norme donne des équations pour la résistance en cisaillement des soudures tandis que la section E.2-2-2 donne des équations pour déterminer la résistance en traction des assemblages soudés. La section E.2-2-1 s'appuie en grande partie sur la recherche effectuée par Peköz et McGuire (1979) à l'Université Cornell. Leur programme expérimental comprenait entre autres 126 spécimens fabriqués avec des tôles d'une épaisseur variant de 0.38 mm à 3.42 mm. Les équations développées suite à cette étude sont encore celles qui se retrouvent aujourd'hui dans la norme CSA S136 (2007). Selon la norme, la résistance en cisaillement d'une soudure à l'arc doit être le moindre des résultats des équations E2.2.1-1 à E2.2.1-4 reprises ici:

$$P_n = \frac{\pi d_{eff}^2}{4} 0.75 F_{xx} \qquad (1-2)$$

$Pour\ (d_a/t) \leq\ 0.815\sqrt{E/F_u}$:

$$P_n = 2.20 t d_a F_u \qquad (1-3)$$

$Pour\ 0.815\sqrt{E/F_u} < (d_a/t) < 1.397\sqrt{E/F_u}$:

$$P_n = 0.280 \left[1 + 5.59 \frac{\sqrt{E/F_u}}{d_a/t}\right] t d_a F_u \qquad (1-4)$$

$Pour\ (d_a/t) \geq\ 1.397\sqrt{E/F_u}$:

$$P_n = 1.40 t d_a F_u \qquad (1-5)$$

où :

$P_n = Résistance\ nominale\ en\ cisaillement$

$d = \ Diamètre\ visible\ à\ la\ surface\ extérieure\ de\ la\ soudure$

$d_a = (d - t)\ = Diamètre\ moyen\ de\ la\ soudure$

$d_e = \ 0.7d - 1.5t \leq 0.55d = Diamètre\ effectif\ de\ la\ soudure$

$t = \ Épaisseur\ totale\ de\ tôles\ métalliques$

$F_{xx} = Limite\ ultime\ de\ l'électrode$

$F_u = Limite\ ultime\ de\ la\ tôle\ métallique$

$E = Module\ d'élasticité\ de\ la\ tôle\ métallique$

L'équation 1-2 a été développée pour représenter le comportement quand la rupture se produit par rupture en cisaillement dans la soudure. Les équations 1-3, 1-4 et 1-5 ont plutôt été développées pour représenter la déchirure de la ou des feuilles de tôle au périmètre de la soudure causée par l'effort de cisaillement.

Peuler (2002) a entrepris un program d'essais pour évaluer la réponse inélastique en cisaillement des soudures. Des essais en cisaillement ont été effectués avec des chargements monotonique et

cyclique. Des chargements de type sismique ont aussi été effectués pour reproduire les sollicitations d'un séisme. Pendant l'étude, différent types d'électrodes ont été évalué pour permettre de conclure que l'électrode E4311 est plus pénétrante que l'électrode E4310. L'étude a aussi permis de conclure que l'utilisation de rondelles lors de la soudure permet un comportement plus ductile lors de la rupture.

Récemment, Easterling and Snow (2009) ont effectué une série d'essais sur la résistance en cisaillement des soudures fabriquées au travers de plusieurs épaisseurs de tôle métallique. Des essais ont été réalisés avec des tôles d'épaisseur de 0.76, 0.91, 1.21 et 1.52 mm. Les résultats des essais au laboratoire ont démontré que les équations pour déterminer la résistance en cisaillement des soudures de la norme CSA S136 (2007) sont conservatrices. Cependant, ils n'ont pas été en mesure de produire des soudures convenables quand l'épaisseur totale des tôles était supérieure à 3.81 mm. Ils ont donc recommandé qu'aucune soudure ne soit fabriquée au-delà de cette limite.

La section E2.2.2 qui permet de déterminer la résistance en traction des soudures a été élaborée en grande partie selon la recherche de LaBoube et Yu (1991). Plusieurs essais ont été effectués pour déterminer la résistance en traction des soudures à l'arc. Une série d'essais a notamment été effectuée avec des échantillons de tôles superposées. Un maximum de deux tôles avec une épaisseur de 0.76 mm chacune ont été mises à l'essai. Les résultats ont démontré que la résistance en traction des soudures dans des configurations avec chevauchement des feuilles était moindre que la résistance des soudures dans des configurations standard. Ceci a amené la norme CSA S136 (2007) à imposer une réduction en résistance de 30% pour les soudures fabriquées dans une configuration superposée. Selon la norme CSA S136 (2007), la résistance en traction des soudures pour une épaisseur de tôle est égale au moindre des résultats des équations E2.2.2-1 et E2.2.2-2:

$$P_n = \frac{\pi d_e^2}{4} F_{xx} \qquad (1-6)$$

$$P_n = 0.8\left(F_u/F_y\right)^2 t d_a F_u \qquad (1-7)$$

où

$F_y = Limite\ d'écoulement\ de\ la\ tôle\ métallique$

L'équation 1-6 traite de la rupture en traction au travers la soudure tandis que l'équation 1-7 considère la rupture quand il y a déchirure de la tôle au périmètre de la soudure.

Montages en laboratoire

Dans ce projet, deux montages ont été conçus pour effectuer les essais au laboratoire. Le premier montage illustré à la Figure 3.1 a servi lors des essais en cisaillement. Les spécimens sont faits de deux feuilles de tôle, ou de deux paires de feuilles de tôle, qui sont assemblées par une soudure réalisée sur une plaque d'acier qui représente la structure du toit dans un bâtiment. Pour certains spécimens, une des paires de feuilles de tôle est remplacée par une plaque d'acier pour représenter l'assemblage du tablier métallique à la structure périphérie du diaphragme de toit dans un bâtiment. Les échantillons sont fixés au montage à l'aide de 8 boulons. La moitié des boulons servent à ancrer les feuilles de tôle sur un côté de l'assemblage soudé à une pièce fixe tandis que l'autre moitié des boulons servent à assembler les feuilles de tôle de l'autre côté de l'assemblage soudé à une pièce mobile qui est fixée à un vérin qui impose les déplacements ou charges de cisaillement à l'échantillon.

Le second montage, illustré à la Figure 3.3, a servi lors des essais en traction. Les spécimens représentent des segments de tablier métallique de toit. Ils sont préalablement soudés à une cornière d'acier qui représente la structure du toit d'un bâtiment (corde supérieure d'une poutrelle de toit). La cornière d'acier est liée à un point fixe par 2 boulons tandis que les feuilles de tôle sont insérées dans la tête du montage qui est assemblée au vérin imposant le déplacement ou la charge verticale. Quand le vérin se déplace, l'effort de traction est ainsi transmis au tablier, puis à la soudure.

Programme d'essais en laboratoire

Dans le cadre de l'étude expérimentale, 107 essais en cisaillement et 72 essais en traction ont été complétés. Toutes les soudures ont été fabriquées à l'aide d'une l'électrode de 3.2 mm (1/8 po.)

de type E6011 (E4311). L'acier des tôles métalliques était de type ASTM A653. L'épaisseur des tôles métalliques était de 0.76, 0.91, 1.21, 1.52 mm. Les propriétés mécaniques réelles de la tôle ont été déterminées pour chaque épaisseur selon la norme ASTM A370 (2009).

Pour les essais de cisaillement, des feuilles de tôle métallique de 100 x 275 mm ont été assemblées selon 3 différentes configurations pour bien représenter les cas de chargement qui peuvent survenir dans un tablier métallique. La première est une configuration à 2 feuilles (Figure 3.5) qui représente une soudure fabriquée au chevauchement des feuilles du côté long. La configuration à 2 feuilles comprend deux feuilles de tôle métallique qui se recouvrent au centre de l'échantillon par-dessus une plaque d'acier. La soudure est localisée au milieu de l'échantillon et sert à transférer l'effort d'une tôle à l'autre.

La deuxième est une configuration à 4 feuilles (Figure 3.7) où quatre feuilles de tôles métalliques se recouvrent au centre de l'échantillon. Elle sert à modéliser les endroits où quatre feuilles se chevauchent au coin des feuilles de tôle. Dans ce cas, la soudure sert à transférer l'effort des deux feuilles supérieures aux deux feuilles inférieures de tôle métallique. Les configurations à 2 feuilles et à 4 feuilles ont été mises à l'essai avec des plaques de support en acier de 3.2 et 6.4 mm d'épaisseur.

Une troisième configuration fut utilisée pour modéliser les soudures qui sont fabriquées au périmètre des bâtiments. À ces endroits chaque feuille de tôle est chevauchée par une autre à son extrémité. Cette configuration en périmètre (Figure 3.9) contient deux feuilles de tôle métallique soudées à une plaque de support de 6.4 x 100 x 275 mm.

Pour tous les essais en traction, des feuilles de tôle utilisées ont été pliées pour représenter les nervures qu'on retrouve habituellement dans les tabliers métalliques. Les essais en traction ont été effectués avec 3 différentes configurations. La première configuration à 2 feuilles (Figure 3.11) contient 2 feuilles de tôle soudées à un angle de support (63 x 63 mm) et sert à modéliser les soudures fabriquées là où les feuilles se chevauchent du côté long.

La deuxième est une configuration à 4 feuilles (Figure 3.13) semblable à celle utilisée pour les essais en cisaillement. Les configurations à 2 feuilles et 4 feuilles ont été fabriquées avec des angles de support de 3.2 et 6.4 mm.

La troisième est une configuration à 1-feuille où une seule feuille de tôle est soudée à un angle de 6.4 mm.

Protocoles de chargement

Tous les échantillons en traction ainsi que 76 des échantillons en cisaillement ont été soumis à un chargement monotonique avec une vitesse de chargement de 0.5 mm/minute. Ce type de chargement permettait de bien évaluer la résistance ultime de chaque échantillon, de même que le comportement post-pic. Au total, 31 essais en cisaillement ont été effectués avec un chargement cyclique. Ce type de chargement représente les sollicitations auxquelles peuvent être soumis les assemblages de tabliers métalliques pendant un tremblement de terre. Les résultats de ces essais cycliques permettent de déterminer si le chargement cyclique peut affecter la résistance ultime des assemblages et de caractériser le comportement des soudures sous des sollicitations extrêmes.

Modes de ruptures observés

Lors des essais en cisaillement, trois différents modes de rupture ont été observés. Ces modes de rupture sont les mêmes que ceux qui ont été observés par Peköz et al. (1979) lors de leur recherche. Le premier mode de rupture est défini par la rupture en cisaillement de la soudure. La rupture est soudaine et le niveau de déformation est peu élevé, ce mode de rupture peut donc être qualifié comme étant fragile. Le deuxième mode de rupture est défini par la déchirure de la feuille de tôle sur le périmètre de la soudure, perpendiculairement à la direction de la charge appliquée. Lors de ce type de rupture, l'échantillon continue de se déformer après la rupture tandis que la résistance diminue de façon graduelle et constante. Lors du troisième mode de rupture observé, la feuille de tôle métallique se déchire parallèlement à la charge appliquée. Ce mode de rupture est très ductile puisque de grandes déformations ont été observées, sans baisse prononcée de la résistance, après avoir atteint la charge ultime de l'échantillon.

Les essais en traction ont permis d'observer deux différents modes de rupture. Le premier mode de rupture est associé à la rupture de la soudure en traction. La soudure se rompt de façon soudaine et fragile. Les déformations observées avant la rupture sont faibles. Le deuxième mode de rupture est caractérisé par la déchirure de la tôle autour de la soudure. Après avoir atteint la charge ultime, l'échantillon continue de se déformer tandis que la résistance de l'échantillon diminue de façon graduelle et constante.

Résultats

Le diamètre effectif des soudures a pu être mesuré avec un pied à coulisse pour les échantillons qui ont subi une rupture de la soudure. Les résultats illustrés dans la Figure 4.12 montrent que les diamètres effectifs mesurés pendant les essais sont systématiquement plus élevés que les valeurs prédites par la norme CSA S136 (2007). Ces résultats sont semblables à ceux avancés par Easterling and Snow (2009). Cette étude a permis aussi d'observer que l'équation E2.2.1-5 de la norme CSA S136 (2007) est beaucoup trop conservatrice pour les cas avec plusieurs feuilles de tôle épaisse. Les résultats démontrent qu'une limite inférieure du diamètre effectif devrait être ajoutée à l'équation E2.2.1-5 pour améliorer la précision de cette dernière quand elle est utilisée avec des tôles épaisses.

Le temps nécessaire pour fabriquer les soudures a été mesuré pour chaque échantillon. Les résultats montrent que plus l'épaisseur totale de tôle à traverser pour fabriquer la soudure est grande plus le temps nécessaire pour fabriquer la soudure est long. De plus il a été observé que le temps nécessaire pour fabriquer les soudures avec des plaques de support de 3.2 mm d'épaisseur est plus court qu'avec des plaques de support de 6.4 mm d'épaisseur. Ceci indique que les plaques de support plus épaisses sont de meilleurs dissipateurs de chaleur, ce qui oblige le soudeur à prendre plus de temps pour fabriquer la soudure.

Les résultats des essais monotoniques en cisaillement ont permis de démontrer que les équations fournies dans la section E2.2.1 de la norme CSA S136 (2007) sont conservatrices. En effet, que ce soit pour la configuration à 2 feuilles, à 4 feuilles ou pour la configuration avec feuilles soudées à une plaque d'acier au périmètre du bâtiment, la résistance en cisaillement mesurée au

laboratoire était généralement plus élevée que celle prédite par la norme. L'évaluation des résultats reliés à l'équation E2.2.1-1 montre que l'équation pourrait être modifiée pour améliorer sa précision. Les essais cycliques en cisaillement ont permis de vérifier que les échantillons étaient capables de résister à des charges dynamiques à un niveau de chargement tel que prévu par la norme CSA S136 (2007). Ces essais ont aussi permis de vérifier que les échantillons avaient la même résistance ultime après avoir été soumis à plusieurs cycles de chargement d'amplitude inférieure et égale à la résistance pondérée. De plus, les essais cycliques ont aussi démontré que le mode rupture où la feuille de tôle métallique se déchire parallèlement à la charge appliquée est un mode de rupture ductile puisque les échantillons démontraient encore une résistance appréciable après avoir été soumis à des déplacements de 6 mm.

Les essais en traction ont permis d'évaluer les équations fournies dans la section E2.2.2 de la norme CSA S136 (2007). La norme spécifie une réduction de 30% de la résistance en traction des soudures fabriquées avec plusieurs épaisseurs de tôle. Les résultats obtenus lors de cette étude montrent que cette réduction n'est pas nécessaire quand le mode de rupture est la déchirure de la tôle. La résistance moyenne en traction des échantillons dont la tôle s'est déchirée est supérieure aux valeurs prédites par la norme CSA S136 (2007). Cependant, selon les données de cette étude, la réduction semble nécessaire quand le mode de rupture est la rupture en traction de la soudure.

Conclusion

Cette étude a permis de déterminer les facteurs importants à contrôler qui permettent de fabriquer des soudures de bonne qualité. En plus d'utiliser une électrode de type E4311 (E6011) et une intensité de courant très élevée il est important que le soudeur utilise la technique appropriée pour garantir une bonne qualité de soudure. Les essais ont aussi démontré que le temps requis pour fabriquer une soudure à l'arc peut varier selon l'épaisseur de la plaque de support. En effet, pendant cette étude, les soudures fabriquées avec des plaques de support plus épaisses ont nécessité plus de temps pour la fabrication car les plaques de support plus épaisses agissent comme des meilleurs dissipateurs de chaleur. Les essais avec chargement monotonique en cisaillement et en traction ont permis de démontrer que la résistance des soudures fabriquées avec

plusieurs épaisseurs de tôle est influencée par les même facteurs qui avaient été déterminés auparavant par les recherches de Peköz et McGuire (1979). Les tests ont montré que la résistance des échantillons dont la rupture est caractérisée par la déchirure des feuilles de tôle est influencée par l'épaisseur des feuilles de tôle et par le diamètre moyen de la soudure. Pour les échantillons dont la rupture se produit par rupture de la soudure, les essais ont démontré que la résistance est influencée par le diamètre effectif de la soudure. Les diamètres effectifs mesurés lors de l'étude ont été comparé aux valeurs prédites par l'équation E2.2.1-5 de la norme CSA S136 (2007). La comparaison a permis de démontrer que l'équation E2.2.1-5 est trop conservatrice dans les cas où la soudure est fabriquée au travers de plusieurs feuilles de tôle épaisse. Ces résultats ont démontré qu'une limite inférieure du diamètre effectif devrait être ajoutée à l'équation E2.2.1-5. Les essais cycliques en cisaillement ont démontré que la résistance des échantillons ne diminue pas après avoir été soumis à plusieurs cycles de chargement d'amplitude inférieure et égale à la résistance pondérée. Les résultats ont démontrés que l'équation E2.2.1-2, qui prédit la résistance en cisaillement des échantillons est conservatrice. Une modification de cette équation pourrait améliorer sa précision. De plus les essais en traction ont démontré que la réduction de 30% de la résistance spécifiée par la section E2.2.2 ne devrait pas s'appliquer aux échantillons dont la rupture se produit par la déchirure des feuilles de tôle.

TABLE OF CONTENTS

LIST OF TABLES

LIST OF FIGURES

LIST OF SYMBOLS

$A_{ne} = \ net\ effective\ weld\ area$

$d_a = Average\ weld\ diameter\ at\ mid\ thickness\ of\ t\ for\ max.of\ 4\ lapped\ sheets$

$d_e = \ effective\ weld\ diameter\ (MSSDD)$

$d_{eff} = Effective\ weld\ diameter\ \ at\ plane\ of\ maximum\ shear\ transfer$

$d_o = Hole\ diameter$

$d_s = Effective\ weld\ diameter\ (Eurocode)$

$d_{vis} = \ Visible\ diameter\ of\ outer\ surface\ of\ arc\ spot\ weld$

$d_w = \ visible\ weld\ diameter\ (MSSDD\ \&\ Eurocode)$

$E = Young's\ modulus\ of\ sheet\ steel$

$F_p' = Nominal\ strength\ of\ arc\ spot\ weld\ (MSSDD)$

$F_u = Ultimate\ tensile\ strength\ of\ sheet\ steel$

$F_{uw} = minimum\ ultimate\ tensile\ strength\ of\ welding\ electrodes\ (Eurocode)$

$F_{W,Rd} = Nominal\ strength\ of\ arc\ spot\ weld\ (Eurocode)$

$F_{xx} = Tensile\ strength\ of\ electrode\ classification$

$F_y = Yield\ strength\ of\ sheet\ metal$

$h = \ panel\ depth$

$l_v = \ purlin\ spacing$

$n_e = \ number\ of\ edge\ connectors\ between\ cross\ supports$

$n_p = \ number\ of\ purlins\ excluding\ \ those\ located\ at\ ends\ or\ end\ laps$

$n_s = \ number\ of\ stich\ connectors$

$P_n = Nominal\ strength\ of\ arc\ spot\ weld$

$Q_f = Nominal\ strength\ of\ arc\ spot\ weld\ (SDI)$

$Q_s = Nominal\ strength\ of\ arc\ spot\ weld\ at\ sidelap\ (SDI)$

$t = Total\ combined\ base\ steel\ thickness\ (exclusive\ of\ coatings)$

$t_d = total\ sheet\ steel\ thickness\ above\ shear\ plane$

$\alpha_1 = end\ distribution\ factor$

$\alpha_2 = purlin\ distribution\ factor$

$\sigma_u = ultimate\ tensile\ strength\ of\ sheet\ metal\ (MSSDD)$

$\sigma_{uw} = nominal\ tensile\ strength\ of\ filler\ metal\ (MSSDD)$

LIST OF APPENDICES

CHAPTER 1. INTRODUCTION

1.1 Background

In North America, roof deck diaphragms are commonly used as part of the wind and earthquake lateral load resisting system. These diaphragms are composed of rectangular corrugated steel panels that are connected to the underlying structure by arc spot welds, powder actuated fasteners or screws in order to develop shear strength and stiffness. Due to wind loads that cause uplift forces to act on roofs, these connectors must also resist tension forces. At the perimeter of each deck panel, sidelap and endlap fasteners are used to connect the panels together. Figure 1.1 illustrates the different fastener configurations typically found in roof deck diaphragm construction.

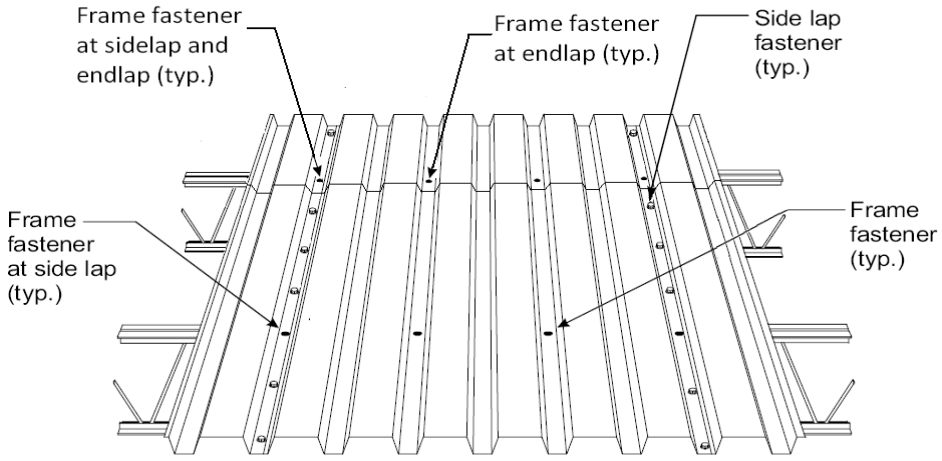

Figure 1.1 Typical fastener arrangement for roof deck diaphragms

Sidelap and endlap fasteners are used to transmit forces from one panel to another while the deck to underlying structure connections are used to transfer forces to the supporting joists, trusses or beams, and eventually to the vertical bracing elements of the lateral load resisting system. The overall shear resistance of a roof deck diaphragm is largely dependent on the strength of its connections. Arc spot welds are the most commonly used type of connection because they can be fabricated rapidly at a relatively low cost.

Provisions to determine the shear and tensile resistance of arc spot welds can be found in the CSA S136 North American Specification for the Design of Cold-Formed Steel Structural Members (CSA 2007). The current provisions for shear strength of arc spot welds are based on the research of Peköz and McGuire (1979), while the equations given to determine the tensile resistance were recommended by LaBoube and Yu (2001). These provisions are mainly based on tests that were carried out using thin deck panels because at the time, the vast majority of roofs were composed of deck with thicknesses of 20 and 22 gauge (0.91 mm and 0.76 mm). When changes were made to the seismic design provisions in the 2005 National Building Code (NRCC, 2005) and the CSA S16 Standard (2001), a capacity based design approach was adopted. The use of this approach for the design of a seismic force resisting system requires the roof deck diaphragm to have a shear capacity higher than the probable resistance of the vertical bracing elements. Consequently, the use of 16 and 18 gauge (1.21 mm and 1.52 mm) decks has become more common as stronger and stiffer diaphragms are required.

To fasten the deck panels together they are overlapped at their perimeter. Therefore, the welds at these locations must be fabricated through multiple steel layers. Multi-layer deck situations occur when the ends or sides of two deck panels overlap, or when the ends and sides of four deck panels overlap. These overlap situations are commonly found in all roof deck configurations. The CSA S136 Specification currently limits the combined thickness (deck thickness x number of deck layers) of an arc spot weld connection to 3.81 mm. Appendix B of the CSA S136 specification also states that the maximum single sheet thickness shall be 2.0 mm and that the maximum aggregate sheet thickness of double sheets shall be 2.5 mm. Furthermore the specification also requires that the thickness of the underlying supporting member be at least 2.5 times the steel sheet thickness. These limits are exceeded when 16 and 18 gauge deck panels in the four panel overlap/endlap configuration are required. Furthermore, the current design provisions are based mainly on tests where a single layer of sheet steel is welded to a steel plate. A complete testing program that incorporates all possible multi-layer configurations has not been carried out to verify if the current design provisions in CSA S136 for arc spot welds are valid.

1.2 Objective

The first objective of this research program is to develop a welding technique that consistently produces quality welds in the case where multiple layers of sheet steel are connected to the underlying framing members. A second objective of this study is to evaluate the applicability of the current design provisions for arc spot welds. To achieve these objectives, mechanical testing has been carried out to determine the shear and tension strengths of connections for multi-layer deck configurations typically found in roof deck diaphragms. This report also seeks to provide guidance in order to adapt the current design provisions to a new reality where thicker deck panels are commonly specified by designers. As the current design provision are based on tests with monotonically increasing load, shear tests will also be conducted under cyclic loading to reproduce loading conditions in diaphragms subjected to seismic force demand. Information will thereby be obtained to verify the validity of the current design provisions under this particular type of loading.

1.3 Scope

A series of practice runs was scheduled to determine the conditions required to fabricate quality welds through multi-layer configurations. Afterwards, to evaluate the shear and tension strength of multi-layer steel deck connections, mechanical testing was carried out on 189 specimens (107 shear tests and 72 tension tests) encompassing all multi-layer configurations typically found in roof deck construction. Test specimens were fabricated using the typical deck thicknesses (0.76, 0.91, 1.21, and 1.52 mm) and joist chord thicknesses (3.2 to 6.4 mm) used in the construction industry. Tension strength tests were performed under monotonically increasing load with sheet samples representative of the popular 38 mm deep x 914 m wide deck profile with flutes spaced 152 mm o/c. The shear strength tests were conducted under both monotonic and reversed cyclic loading.

1.4 Thesis organization

A review of the relevant research and design standards currently available is enclosed in Chapter 1 of this text. An analytical study of a typical roof deck diaphragm illustrating the flow of forces follows in Chapter 2. The description of the test set-up, test specimens, welding procedure and loading protocols is contained in Chapter 3. The results obtained during the testing program are presented and analysed in Chapter 4. This includes results for welding time, effective weld diameter, shear and tensile resistance. Finally, conclusions and recommendations are made in Chapter 5.

1.5 Literature review

1.5.1 Yarnell and Peköz (1973)

Yarnell and Peköz (1973) conducted a study on field welded puddle (arc-spot) and fillet welded connections. The research program included 122 specimens, tested under slowly increasing monotonic load on a hydraulic testing machine. The steel sheets, which were welded to a hot rolled steel plate, were loaded in tension which induced shear in the puddle weld.

Specimens were fabricated using 12 gauge (2.66 mm), 18 gauge (1.21 mm) and 28 gauge (0.38 mm) sheet steel. The 12 and 18 gauge steel sheets were made from A446 Grade A steel while the 28 gauge steel sheets were made from A446 Grade E steel. Weld washers were used only for the specimens with 28 gauge sheet steel. Single and double sheet specimens were welded using Lincoln Fleetweld 5P E6010 electrodes. A total of 31 arc-spot weld connection tests were completed, including 12 tests with double sheet specimens. The ultimate load of the specimen was recorded and a description of whether failure occurred in a sudden or gradual manner was provided for each test. The authors observed that most specimens with single sheets failed in a

gradual manner, while the specimens with double sheets failed in a sudden manner. The study concluded that this may be due to a lack of connectivity for the double sheet specimens.

The authors noted that when the specimens were properly welded the behaviour of puddle welds resembled that of a bolted connection. The steel sheet would break away on the tension loaded side of the weld and material would pile up on the opposite side of the puddle. The authors experienced difficulty to produce such welds due to a lack of fusion in the cover plate. In some cases, for specimens with 12 gauge or 18 gauge sheets, only 10% of the weld perimeter was connected to the sheet steel resulting in ineffective connections.

1.5.2 Struble et al. (1978)

In 1978, Struble et al. conducted a series of tests on 90 specimens to determine the shear capacity of arc-spot welds. The objective was to verify the effect of four parameters on the capacity of these welds. The four varying parameters were: edge distance, weld diameter, cover plate thickness, and the use of oblong welds. The test set up consisted of two 11.1mm thick hot rolled plates that were butted together with steel sheets welded on each side of heavy plates. Of the 90 specimens, 38 consisted of double sheet specimens where two steel sheets were welded on each side of the hot rolled plates. The testing program included seven gauges of sheet steel; the 10 gauge (3.42 mm), 12 gauge (2.66 mm), 14 gauge (1.90 mm), 18 gauge (1.21 mm) and 22 gauge (0.76 mm)sheets were of ASTM A446 Grade E steel while the 24 gauge (0.61 mm) and 28 gauge (0.38 mm) sheets were of ASTM A446 Grade A steel. All welds were fabricated with E6010 Fleetweld 5P electrodes. Due to the relative high strength of the hot rolled plates, the thickness of the connecting plates was not considered as a variable in the study. The specimens were tested under monotonically increasing shear load on a Baldwin Southwark hydraulic testing machine; associated displacement and visible diameter were recorded for every test.

Struble et al. recorded three different failure modes. For the thicker plates, specimens with 10 and 12 gauge sheets and specimens with double 14 gauge sheets, the failure occurred by shearing of the weld. For specimens with single and double 18 gauge sheets, the failure mode was described

as transverse tearing of the plate perpendicular to the applied load. For the thinner sheets, single 24 gauge sheet specimens and double 28 gage sheet specimens, the failure occurred from shearing of the sheet steel along lines parallel to the applied loads.

Based on the test results, Struble et al. proposed the following equation to predict the ultimate load of specimens that fail due to shearing of the weld:

$$P_u = 2\left(\frac{\pi d_{eff}^2}{4}\right)\left(\frac{3F_{xx}}{4}\right) \qquad (1-1)$$

Where d_{eff} is the effective weld diameter that will be defined in section 1.6.1 and F_{xx} is the nominal tensile strength of the deposited weld metal.

A factor of 2 is included at the beginning of equation 1-1 because each specimen tested during the study contained two welds. For the capacity of the weld in shear, the average value of the observed strength was 1.31 times the capacity predicted with the proposed equation (eq. 1-1). As each specimen contained two arc-spot welds the resistance of each weld is equal to half of the value predicted by Equation 1-1. The observed specimen strengths had a high variability in all circular-weld specimens. No distinction was made between the single and double sheet specimens.

1.5.3 Peköz and McGuire (1979)

Peköz and McGuire (1979) investigated the performance of arc-spot welds. Tests on the most common types of puddle welds conducted at Cornell University were summarized and interpreted in order to revise the welding provisions available at the time. The testing program included 126 tests on arc-spot welds carried out using specimens with single-ply and double-ply sheets. The welds were loaded in shear and no weld washers were used. Welds were made with E6010 electrodes for all specimens and the sheet steel used was A446 Grade A. Six different sheet thickness were tested; 10 gauge (3.42 mm), 12 gauge (2.66 mm), 14 gauge (1.90 mm), 18 gauge

(1.21 mm), 24 gauge (0.61 mm), and 28 gauge (0.38 mm). The sheets were welded to 11.1mm hot-rolled steel plates made of A36 steel.

Three failure modes were encountered by Peköz and McGuire during their investigation: i) failure by transverse tearing of the sheet along the contour of the weld spreading across the sheet, ii) failure by longitudinal tearing of the sheet followed by buckling of the end zone which results in the ploughing of the weld into the end material, and iii) failure by pure shear through the weld.

The results noted by Peköz and McGuire suggest that failure generally implicates a combination of basic failure modes, accompanied by significant out of plane deformations. The results were therefore separated in two categories. One containing the specimens that failed due to pure shear in the weld, the other including all other failure modes. Equations proposed for each category were then compared with the test results. Large scatters were observed due to the variability in quality of the arc-spot welds. No clear distinction could be made between the results for single-ply and double-ply sheets.

The welding procedures for the tests specified that arc-spot welds should have a fused nugget of at least ½ inch diameter into the supporting piece. To preserve uniformity in the welds, effective control of the current and regulation of the electrode burn-off rate was maintained. The authors also expressed concern that the coating on some electrodes may break down and produce insufficient penetration due to the high currents used for the arc spot welding. To avoid such problems, a suggestion was put forward to limit the number of welds made in rapid succession.

1.5.4 LaBoube and Yu (1991)

LaBoube and Yu (1991) conducted a research program that studied the tensile strength of arc spot welds in order to formulate comprehensive design guidelines. The tests were made with varying parameters. Specimens were fabricated from ASTM A446 Grade C and ASTM A446 Grade E decks. Manual welding using a SMAW process done by a local welding supplier was compared with an automated welding process done in the laboratory. Both welding processes used E70

electrodes to fabricate specimens. Typical field conditions were simulated by testing single sheet, double sheet and lapped sheet connections. The testing program included single connection tests and full panel tests.

For single connection tests, specimens were subjected to direct tension. The parameters recorded for all tests were; failure load, sheet thickness, visible diameter and weld time. When the weld was loaded symmetrically, LaBoube and Yu observed that the connection capacity is independent of the supporting plate thickness. Furthermore, the manual and automated welding processes proved to be equivalent for this series of tests. The authors also observed that for steel sheets thinner than 26 gauge (0.46 mm), the capacity of arc spot welds could be predicted suitably only when welding washers were used. The authors concluded that the parameters that influence the tensile strength of arc-spot weld connections are the thickness of the sheet, the diameter of the weld, and the tensile strength of the sheet.

When the weld is loaded eccentrically to simulate the condition along the perimeter of a building, a reduction in capacity of 40% was noted. This reduction can be attributed to the peeling effect caused by the eccentric configuration. Test results showed that the 40% reduction could be counterbalanced by using welding washers. However, welds of proper quality with welding washers could not be achieved using the automated welding process.

The study also investigated two types of nested configurations. For specimens tested with the configuration shown in Figure 1-2, the results indicated the capacity of the weld could be predicted by taking the sum of the thickness of each sheet as the sheet thickness in the corresponding design equations. The configuration shown in Figure 1-3 simulates a typical sidelap connection. With this configuration the weld capacity could not be predicted adequately. The length of the un-stiffened flange and the amount of weld provided for the top sheet lap, the dimension d', proved to have a significant influence on the capacity of the weld.

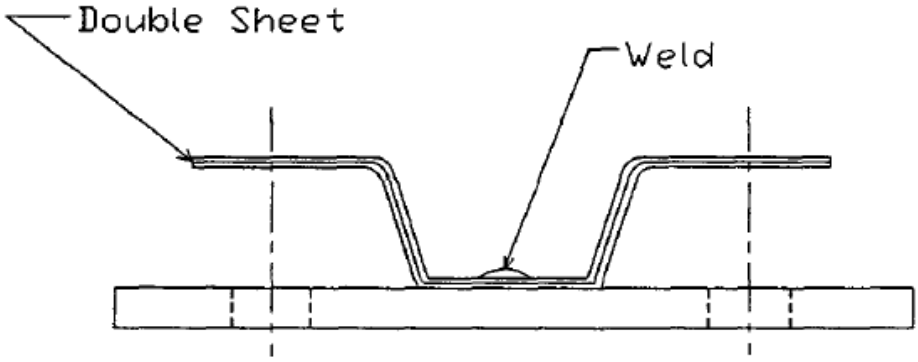

Figure 1.2 Cross-section of double sheet specimens (LaBoube and Yu 1991)

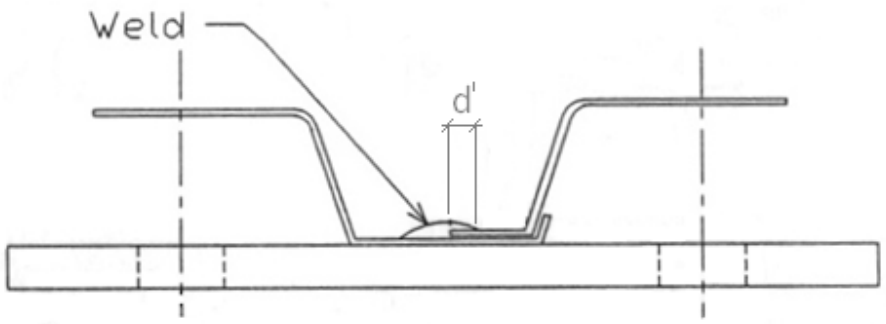

Figure 1.3 Cross-section of lap connection specimens (LaBoube and Yu 1991)

Six full panel tests were completed in the testing program to verify the validity of the results obtained from single connection tests. The tests included four standard configurations and two perimeter configurations that contained a sidelap connection. When Grade C steel sheets (nominal F_y = 275 MPa, F_u = 379 MPa) were used, the tests results confirmed those obtained through single connection tests. However, when Grade E steel sheets, with nominal F_y = 550 MPa and F_u = 570 MPa, were used, the test results did not support the results from the tests on single connections. According to the authors this variability is perhaps due to the lack of ductility in Grade E steel sheets. In the perimeter configuration, the specimens made with Grade C and Grade E steel sheets exhibited similar results to those obtained with single connection tests.

1.5.5 Fung (1978)

Fung's study (1978) on the strength of arc-spot welds was separated in three parts. The intent of the first series of tests was to establish a welding process that would produce arc-spot welds of consistent quality. The study showed that the welding machine setting was the most influential parameter. It also showed the importance of using the melting rate as a guide to obtain a proper machine setting. To achieve a proper setting the author suggests that a 11.4 mm (0.45 in.) nugget should remain attached to the hot rolled plate after the sheet has been separated by a peeling test. The study also noted that the welding process could blow holes in the sheet instead of properly fusing the sheet and the plate together if the machine setting is too hot. A 4.0 mm (5/32 in.) diameter E6010 electrode was used to produce the welds for all three test series.

The objective of the second series of tests was to determine the shear and tensile strength of arc-spot welds. Steel sheets of thicknesses varying from 0.79 mm. (0.031 in.) to 1.50 mm (0.059 in.) were welded to a 12.7 mm (½ in.) hot rolled plate. The authors reported that the majority of shear strength specimen failures occurred by tearing of the sheet in front of the weld. The observed shear strength of the specimens was then compared to the values predicted by the equations from the American Welding Standard (American Welding Society 1977). The average safety factor resulting from the comparison was equal to 3.2 with a standard deviation of 0.44. During the tensile strength tests the authors noted a peeling effect causing a non uniform stress distribution around the weld as the tensile force was applied. No attempt was made to correct this situation because the authors believed that this configuration represented typical uplift conditions for steel deck diaphragm connections. Failure of the tension specimens usually commenced with tearing of the sheet around the weld at the location nearest to the legs of the channel and then would spread along the contour of the weld. The observed tensile capacities of the specimens had a standard deviation varying from 12 to 18% depending on the thickness of sheets tested. The authors also noted that the ratio of mean shear capacity to mean tension capacity was reasonably constant.

The third series of tests investigated the effect of certain parameters on the strength of arc-spot welds. The results demonstrated that the plate thickness to sheet thickness ratio should be maintained over 2.5. The yield strength of the sheet steel proved to have little effect on the strength of the weld. This finding is contradictory to the American Welding Standard which predicts an increase in weld capacity as the sheet material strength increases. The author also concluded that increasing the size of the weld beyond ¾ in. will provide little gain in resistance. The series of tests also investigated how the presence of an air gap can affect the capacity of an arc-spot weld. It was found that an air gap will result in a decrease in both tension and shear capacity; the maximum tolerable air gap would appear to be 1/16 in.

1.5.6 Peuler (2002)

Peuler (2002) conducted a study on the inelastic arc-spot welded deck-to-frame connections. During the study, a total of 235 specimens were tested under monotonic shear, cyclic shear or seismic shear loading. The loading rate for the monotonic tests was equal to 0.5mm/minute. The testing program included specimens with three different types of welding washers and sheet steel thicknesses varying from 16 to 22 gauge of ASTM A653 material (Grade 230, F_y=230 MPa, F_u=310 MPa). A welding protocol was developed with the help of a certified welder to maximize the quality of the welds fabricated throughout the project. Weld dimensions were also taken for every specimen before and after failure to evaluate the penetration of each weld. A comparative study of four different electrode types was made during the study, E4310 (E6010), E4311 (E6011), (E6022) and E4918 (E7018). Peuler concluded that the E4311 electrode had better penetrating capacity than the E4310 electrode. Although the connections with washers did not exhibit a higher average resistance than the connections without washers, the connections with washers were able to carry post-ultimate loads at large displacements while the connections without washers lost most of their capacity at smaller displacements. During the study, all 3 major failure modes observed by Peköz and McGuire (1979) were reproduced. Only 4% of the specimens tested failed due to shear failure through the weld nugget. It was noted that this failure

mode is very brittle and must be avoided if the roof diaphragm is expected to act as an energy absorbing fuse. As a general conclusion, Peuler recommended that welding washers be used in seismic design to ensure the diaphragm will be able to maintain some resistance while sustaining inelastic deformations.

1.5.7 Easterling and Snow (2009)

Easterling and Snow (2009) oriented their study to determine a relationship between the strength of arc-spot welds and the arc time used to form the weld. The testing matrix used in the study encompassed three welding time categories; full-time, 2/3-time and 1/3-time. The average times required to form 15.9 (5/8 in.) and 19.1 (¾ in.) welds were 8.1 and 12.8 seconds respectively. Arc-spot welds of 15.9 mm (5/8 in.) and 19.1 mm (¾ in.) in single, double and four-layer configurations were tested with 16 gauge (1.52 mm), 18 gauge (1.21 mm), 20 gauge (0.91 mm) and 22 gauge (0.76 mm) steel sheets. All welds were fabricated usig a 1/8" diameter E6010 electrode. The welds were loaded in shear in a set-up based on the AISI TS-5-02 (AISI, 2002). The sheet steel material used was ASTM A653 Grade 33 galvanized. A benchmark time to fabricate a satisfactory weld was first established and designated as the full-time weld to be used for each configuration. To establish this time, several attempts were made at different current settings until sufficient penetration was obtained. Once the proper setting was determined, the remaining full-time, 2/3 time and 1/3 time welds specimens were fabricated. It was noted that the specimens that were fabricated with 2/3 time welds and 1/3 time welds had smaller diameters and therefore presented less strength than the specimens fabricated with full-time welds. It was also observed that the equations provided in the 2001 AISI Specification (AISI 2001) could adequately predict the strength of full-time, 2/3 time and 1/3 time welds if the visual diameter is used instead of the nominal diameter. The study suggests that arc spot welds can be adequately fabricated in single and double layers of sheet steel if the total thickness does not exceed 3.81 mm (0.15 in.). The study also reported welds with sufficient penetration could not be fabricated in four layers of sheet steel regardless of the total thickness. It must be noted that all these

observations were for welds fabricated with a E6010 type electrode. Finally, for full-time welds the measured shear strength was 1.31 times the predicted shear strength based on the 2001 AISI specification.

1.6 Design Standards

1.6.1 CSA S136 (2007)

In North America, the design specifications for cold-formed steel structures are provided by The American Iron and Steel Institute (AISI), in cooperation with Canadian Standards Association (CSA). These specifications for welded connections are valid if the thinnest connected part or the combined thickness of multiple sheets being connected is less than or equal to 3.81 mm. Appendix B of the specification contains provisions that are applicable only to Canada. Section E2.2a of Appendix B states that the maximum single sheet thickness shall be 2.0 mm and that the maximum aggregate sheet thickness of double sheets shall be 2.5 mm. Furthermore the specification also requires that the thickness of the underlying supporting member be at least 2.5 times the steel sheet thickness. In section E2.2.1 of the CSA S136, the nominal ultimate shear strength of an arc-spot weld connection P_n is the smaller of:

$$P_n = \frac{\pi d_{eff}^2}{4} 0.75 F_{xx} \qquad (1-2)$$

$For\ (d_a/t) \leq\ 0.815\sqrt{E/F_u}$:

$$P_n = 2.20 t d_a F_u \qquad (1-3)$$

$For\ 0.815\sqrt{E/F_u} < (d_a/t) < 1.397\sqrt{E/F_u}$:

$$P_n = 0.280\left[1 + 5.59\frac{\sqrt{E/F_u}}{d_a/t}\right] t d_a F_u \qquad (1-4)$$

$For\ (d_a/t) \geq\ 1.397\sqrt{E/F_u}$:

$$P_n = 1.40 t d_a F_u \qquad (1-5)$$

Where

$P_n = Nominal\ strength\ of\ arc\ spot\ weld$

$d_{vis} = Visible\ diameter\ of\ outer\ surface\ of\ arc\ spot\ weld$

$d_a = (d_{vis} - t)$

$= Average\ diam.of\ weld\ at\ mid\ thickness\ of\ t\ for\ max.of\ 4\ lapped\ sheets$

$d_{eff} = 0.7d_{vis} - 1.5t \leq 0.55\ d_{vis}$

$= Effective\ diameter\ of\ fused\ area\ at\ plane\ of\ maximum\ shear\ transfer$

$t = Total\ combined\ base\ steel\ thickness\ (exclusive\ of\ coatings)$

$F_{xx} = Tensile\ strength\ of\ electrode\ classification$

$F_u = Ultimate\ tensile\ strength\ of\ sheet\ steel$

$E = Young's\ modulus\ of\ sheet\ steel$

It is noted that the thickness t in the above equations is the total combined steel thickness of the sheets located above the plane of maximum shear transfer. In CSA S136, the minimum allowable effective diameter of a weld is 9.53 mm. Equation 1-2 was developed to predict the capacity of connections failing by shear through the welds. A shear factor of 0.75 was proposed by Struble et al. to account for the distribution of shear stress. This equation is equal to half of Equation 1-1 proposed by Struble et al. because it considers only one weld. Equations 1-3, 1-4, and 1-5 are associated with failure by tearing and buckling of the sheet. Equations 1-3 and 1-5 are lower and upper bounds whereas Equation 1-4 provides linear transition between the above two as a function of d_a/t. It is worth noting that Equations 1-3 to 1-5 gives values of bearing capacity that diminish when the thickness is reduced with respect to d_a (when d_a/t is increased) and that these values are lower than those permitted for bearing failure mode in structural steels (equal to 3.0 dtF_u in CSA-S6-01), the main reason being that bearing is associated to buckling in thin sheet steels.

When the shear plane is between two sheet steels of equal thickness, CSA S136 provides other equations in Section E.2.2.1.3 for the shear strength:

$$P_n = 1.65 t d_a F_u \qquad (1-5)$$

When using this equation, the following limits apply: $F_u \leq$ 407 MPa, ii) $F_{xx} > F_u$, and iii) 0.71 mm $\leq t \leq$ 1.61 mm. The same definition applies to t, i.e., the total steel thickness above the shear plane.

The CSA Specification in Section E.2.2.2 determines the ultimate tensile strength of an arc-spot weld connection as being the smaller of:

$$P_n = \frac{\pi d_e^2}{4} F_{xx} \qquad (1-6)$$

$$P_n = 0.8\left(F_u/F_y\right)^2 t d_a F_u \qquad (1-7)$$

For the case of multiple sheets, CSA 136 states that the strength is determined by taking the sum of the sheet thicknesses located above the supporting steel members, which may be different than the thickness used to determine the shear strength. Equation 1-6 considers a tensile failure of the weld while equation 1-7 considers tearing of the sheet along the contour of the weld. CSA 136 also specifies a 50% reduction in capacity for welds subject to eccentric loading and a 30% reduction welded connections in sidelap joints in deck systems. This 30% reduction in loading is applied to account for the reduction in capacity caused by a peeling effect observed in sidelap connections (see Section 1.5.4).

1.6.2 Steel Deck Institute (2004)

The SDI method for the design of steel deck diaphragms is explained in the SDI Design Manual published by the Steel Deck Institute (Luttrell 2004). The SDI method includes provisions to

determine the capacity of arc-spot welds to structural members for base metal thicknesses varying between 0.72 mm (0.0285 in.) and 1.61 mm (0.0635 in.). According to the SDI it is essential to obtain proper balance between welding time and electrode burn-off rate if sound quality welds are to be produced. For instance, it is recommended that burn-off rates are between 4 mm (0.15 in.) and 6 mm (0.25 in.) of electrode per second in typical E60XX or E70XX 4 mm (5/32 in.) electrodes. The time required per weld may vary between 3 to 6 seconds or more depending on the properties of parts being connected.

The SDI provides two equations to predict the shear strength of arc spot welds connecting a steel sheet to an underlying framing member, for welds produced without washers:

$$Q_f = 2.2tF_u(d_{vis} - t) \qquad (1-8)$$

Where

$t = \ Base\ metal\ thickness$

For welds produced with washers:

$$Q_f = 99t(1.33d_o + 0.3F_{xx}t) \qquad (1-9)$$

Where

$d_o = Hole\ diameter$

No indication is given in SDI whether these equations can be applied to multi-ply connections. SDI however indicates that within the diaphragm system, end laps may be staggered or on a continuous line without particular effect on the diaphragm strength. However, greater care must be exercised when making connections through multiple layers of deck at the panel corners on the end lap. When multiple panel layers must be penetrated the SDI Manual stipulates that the welding time must be slightly increased at these locations. In the case of sidelap or stitch welds,

the SDI does not recommend using material 0.0295 in. (0.75 mm) or thinner. According to the manual, the thinner the material, the more difficult it is to produce quality welds. The SDI states that welding such thin material is likely to produce holes, however if the perimeter is welded and if excellent nesting of the sheets exists therefore the capacity of sheet-to-sheet welds is found to be:

$$Q_s = 0.75\, Q_f \qquad (1-10)$$

The SDI does not provide any equations to determine the capacity of arc-spot welds in tension.

1.6.3 Manual of Stressed Skin Diaphragm Design (1982)

Davies and Bryan published a European manual in which they propose a method for the design of sheet steel diaphragms (1982). The design equations provided to determine the ultimate shear strength of arc-spot welds have been derived from the research done by Peköz and McGuire (1979). The nominal resistance of arc-spot welds subject to shear is found to be the lesser of:

$$F_p' = 1.4 t d_e \sigma_u \qquad if\ \ d_e/t < 11.6/\sqrt{\sigma_u} \qquad (1-11)$$

$$F_p' = \left[2.1 - \frac{d_e\sqrt{\sigma_u}}{16.3t}\right] t d_e \sigma_u \qquad if\ \ 11.6/\sqrt{\sigma_u} \le d_e/t \le 19.9/\sqrt{\sigma_u} \qquad (1-12)$$

$$F_p' = 0.9 t d_e \sigma_u \qquad if\ \ d_e/t > 19.9/\sqrt{\sigma_u} \qquad (1-13)$$

$$F_p' = 0.35(0.7 d_w - 1.5t)^2 \sigma_{uw} \qquad (1-14)$$

Where

$d_e = d_w - t = effective\ weld\ diameter$

$d_w = visible\ weld\ diameter$

$t = base\ sheet\ steel\ thickness$

$\sigma_u = ultimate\ tensile\ strength\ of\ sheet\ metal$

$\sigma_{uw} = \ nominal\ tensile\ strength\ of\ filler\ metal$

The manual includes the description of standard testing procedures to determine the tensile resistance of fasteners but no design equations are provided for the strength of arc-spot welds in tension. In section 6.10 of the Manual of Stressed Skin Diaphragm Design (1982), which discusses welded diaphragms, no limit on the thickness of sheet steel is imposed.

1.6.4 Eurocode (2001)

Eurocode (2001) states that the nominal shear resistance of a circular arc-spot weld shall be taken as:

$$F_{W,Rd} = \frac{\pi}{4} d_s^2 \times 0.625 F_{uw} \qquad (1-15)$$

$$F_{W,Rd} = 1.33 d_p \Sigma t F_u \qquad for\ d_p/\Sigma t \leq 24\varepsilon \qquad (1-16)$$

$$F_{W,Rd} = 0.17\left(d_p + 164\varepsilon\Sigma t\right)\Sigma t F_u \qquad for\ 24\varepsilon \leq d_p/\Sigma t \leq 41.5\varepsilon \qquad (1-17)$$

$$F_{W,Rd} = 0.84 d_p \Sigma t F_u \qquad for\ d_p/\Sigma t \geq 41.5\varepsilon \qquad (1-18)$$

Where

$d_s = 0.7 d_w - 1.5\Sigma t$

$d_s \leq 0.55 d_w$

$d_s = interface\ diameter\ of\ the\ arc\ spot\ weld$

$d_w = visible\ diameter\ of\ the\ arc\ spot\ weld$

$F_{uw} = minimum\ ultimate\ tensile\ strength\ of\ the\ welding\ electrodes$

$\varepsilon = \sqrt{235/F_u}$

Similar to the CSA S136 Specification, equation 1-15 relates to failure through the nugget of the weld while equations 1-16, 1-17 and 1-18 relate to failure of the sheet steel along the contour of

the weld. Equation 1-15 uses a shear factor of 0.625 which is lower than the shear factor of 0.75 used in Equation 1-2 from CSA S136.

1.7 Summary

A review of the literature available on arc-spot welds shows that past research has been undertaken to determine the resistance of arc-spot welds for simple configurations. Much of research has been focused on the shear capacity of arc-spot welds, whereas a limited number of studies have observed the tensile capacity of such connections. Only a few tests have been carried out on multi-overlap configurations that are representative of the loading conditions typically encountered in roof deck construction. Most research projects focused on welds with dimensions that vary from 12 to 18 mm which are common in practice. Much of the research that has been carried out indicated that the current design provisions in the CSA S136 Specification (2007) to determine the resistance of arc-spot welds are conservative. The current restrictions on the thickness of sheet steel for welded connections are based on the scope of previous test programs which was limited to 3.81 mm (2 x 1.91 mm). Furthermore the requirement that the thickness of the supporting steel be 2.5 times the steel sheet thickness was included in the CSA version of the specification to include the recommendations made by Fung (1978). Welding thick decks has become more and more common although the determination of the resistance of such connections remains unclear throughout the literature. Finally, few attempts have been made to verify what welding technique, if any, is suitable for the welding of thick decks in multi-overlap configurations.

CHAPTER 2. STUDY OF ROOF DECK DIAPHRAGMS

To understand the flow of forces that occurs in a roof deck diaphragm a typical one storey building is studied to illustrate the loads applied to fasteners in steel deck diaphragms. The layout of a typical building of a one-storey industrial building is shown in Figure 2.1. The lateral force resisting system of the building is composed of a roof deck diaphragm and vertical bracings along the perimeter of the building.

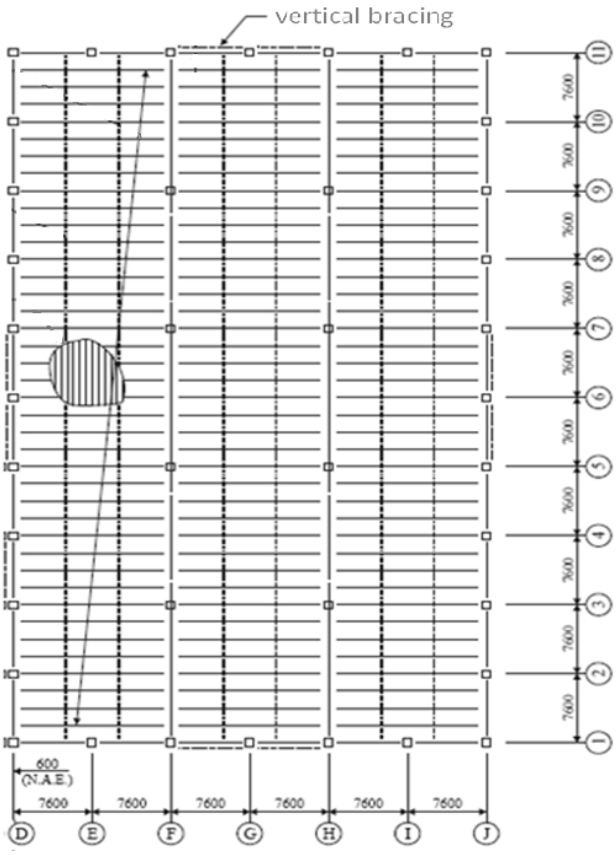

Figure 2.1 Typical layout of a one-storey industrial building

The NBCC 2005 recommends a capacity approach for the seismic design of such buildings; the diagonal bracing members are to be designed so that they exhibit ductile behaviour under seismic

solicitations and the steel deck must be designed to remain elastic under the loads generated when the diagonal bracing reaches its expected capacity. The roof deck profile must also be selected so it can sustain the gravity loads as well as wind uplift pressures as specified by the NBCC 2005.

The method proposed by the Steel Deck Institute (SDI) Design Manual (2004) is used to examine the flow of shear forces throughout the steel deck and establish the loads applied on fasteners. In order to determine the in-plane shear strength of a diaphragm the SDI method considers the shear strength of the connections and the out-of-plane buckling of the deck between horizontal framing members. The maximum load on a connection is determined using the equations provided in the SDI method for exterior panels, interior panels and corner fastener limitations. All equations are based on force equilibrium between applied diaphragm shear force and the forces in the fasteners. Figure 2.2 illustrates the free body diagram of a steel deck panel part of a roof deck diaphragm.

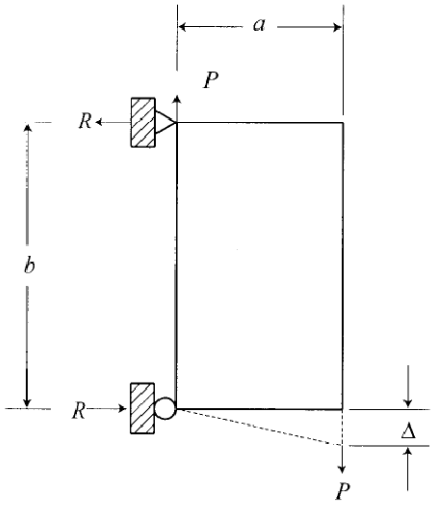

Figure 2.2 Free body diagram of roof deck diaphragm (SDI 2004)

Figure 2-3 illustrates the free body diagram of half a steel deck panel (across its width *w*) located at the edge of a building. The loads acting on the individual fasteners can be determined from equilibrium of the forces acting parallel to the length of the sheet panels.

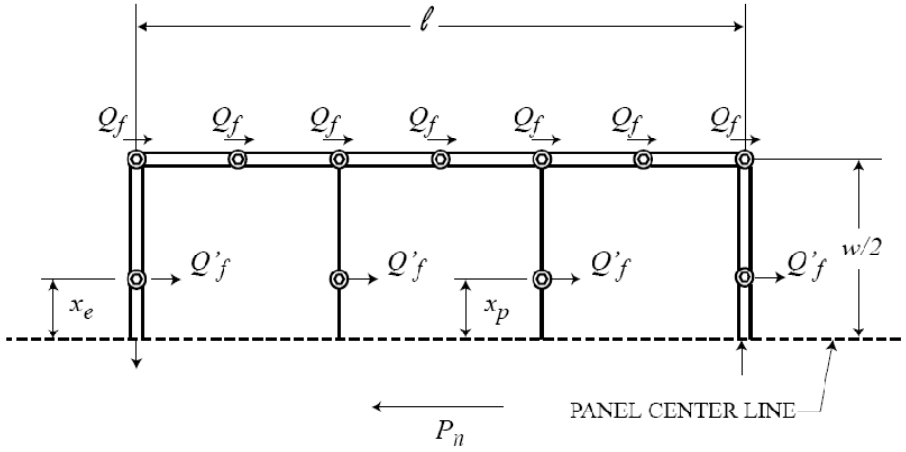

Figure 2.3 Free body diagram of steel deck panel located at perimeter (SDI 2004)

In accordance with the connection arrangement and end fastener spacing selected the load Q_f acting on the connector of an exterior panel can be derived from Eq.2.2-1 in the SDI Design Manual (2004):

$$Q_f = P_n/(2\alpha_1 + n_p \times \alpha_2 + n_e) \qquad (2-1)$$

where:

$\alpha_1 = end\ distribution\ factor$

$\alpha_2 = purlin\ distribution\ factor$

$n_e = number\ of\ edge\ connectors\ between\ cross\ supports$

$n_p = number\ of\ purlins\ excluding\ \ those\ located\ at\ ends\ or\ end\ laps$

$P_n = total\ force\ acting\ along\ the\ edge\ of\ the\ panel$

The connectors of exterior panels must transmit the force Q_f from the steel deck to the collector members located on the perimeters of the building. Along the edge of panels where sheets are lapped one over the other, arc-spot welds are fabricated through two thicknesses of steel deck to a collector member. This situation, illustrated in Figure 2.4, is reproduced in our testing program with the shear perimeter configuration. No tests were carried out with one thickness of steel sheets to reproduce the conditions found between the end laps along the perimeter.

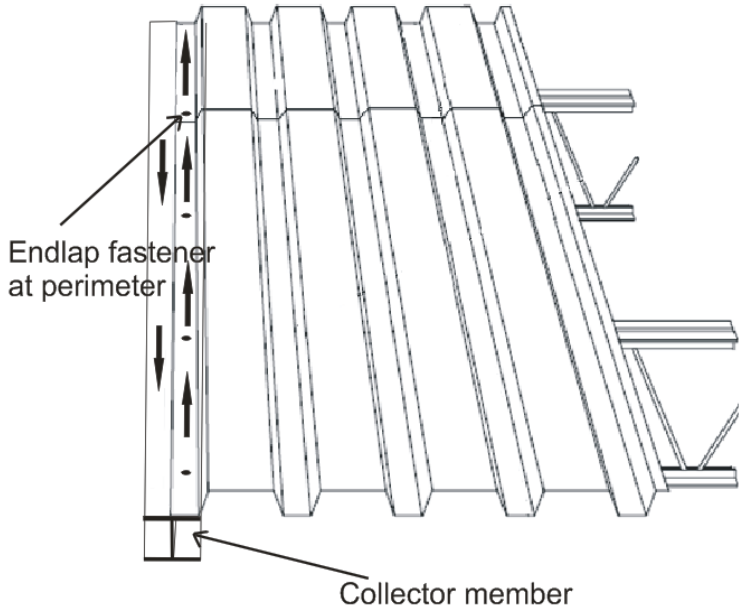

Figure 2.4 Schematic of shear flow at perimeter of building

The free body diagram of an interior steel deck panel is illustrated in Figure 2-5. The force transferred by sidelap fasteners (Q_s) must be considered and is typically expressed as a function of Q_f. At the corner of panels, the SDI specifies a reduction factor (λ) to account for the tendency of panel corners to distort. The resistance of corner fasteners are thereby limited to a lower value of $\lambda \times Q_f$.

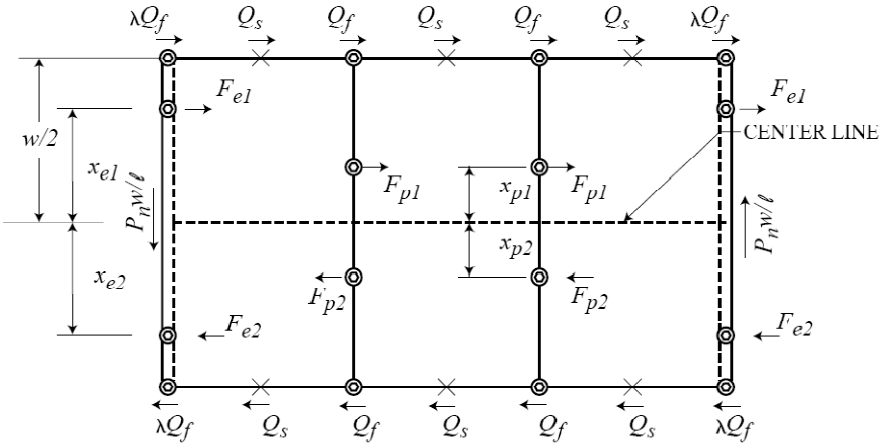

Figure 2.5 Free body diagram of interior deck panel (SDI 2004)

The maximum load Q_f on a sidelap connector located at an intermediate joist (or purlin) for an interior panel can be derived from Eq.2.2-4 specified by the SDI Design Manual (2004):

$$Q_f = P_n/(2A \times (\lambda - 1) + B) \qquad (2-2)$$

where

$$B = n_s \times \alpha_s + \frac{1}{w^2}(2 \times n_p \times \Sigma\alpha_p{}^2 + 4\Sigma\alpha_e{}^2)$$

$$\lambda = 1 - \frac{h \times l_v}{240\sqrt{t}} \geq 0.7$$

$h =$ *panel depth*

$l_v =$ *joist or purlin spacing*

$n_s =$ *number of stich connectors*

$n_p =$ *number of joists/purlins excluding those located at ends or end laps*

$P_n =$ *total force acting along the edge of the panel*

$A = 2$ *for double edge fasteners*

$= 1$ *for single edge fasteners*

As illustrated in Figure 2.6, the shear force (P) acting along the edge of a deck panel causes an equal and opposite reaction along the edge of the adjacent panel.

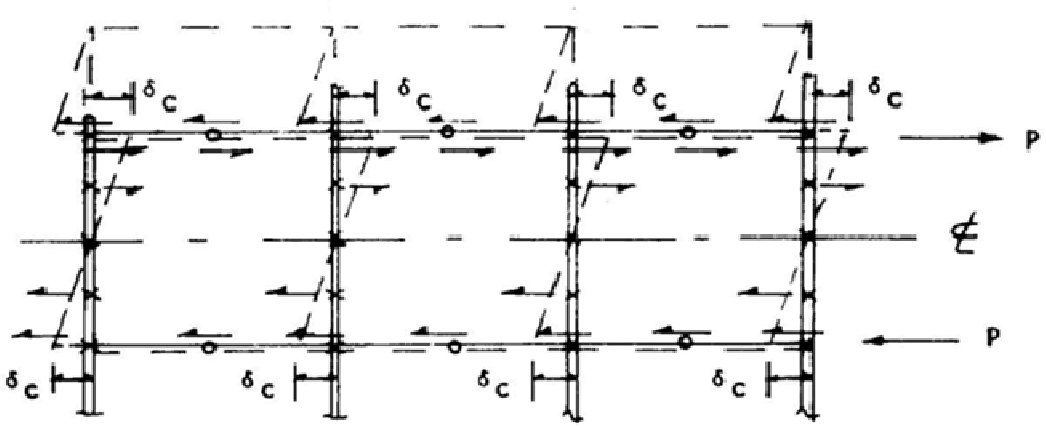

Figure 2.6 Schematic of shear flow in steel deck panel (SDI Manual 2004)

As illustrated in Figure 2-7, the force from one panel is transferred to the adjacent panel by the sidelap fasteners located along the edge of the deck panel. When arc-spot welds are used as sidelap fasteners the welds are fabricated through 2 layers of sheet steel. This situation is reproduced in the testing program by the 2-layer configuration where two steel sheets are welded together with an underlying hot rolled plate. During the testing the steel sheets are pulled in opposite directions to induce a longitudinal shear load parallel to the sidelap.

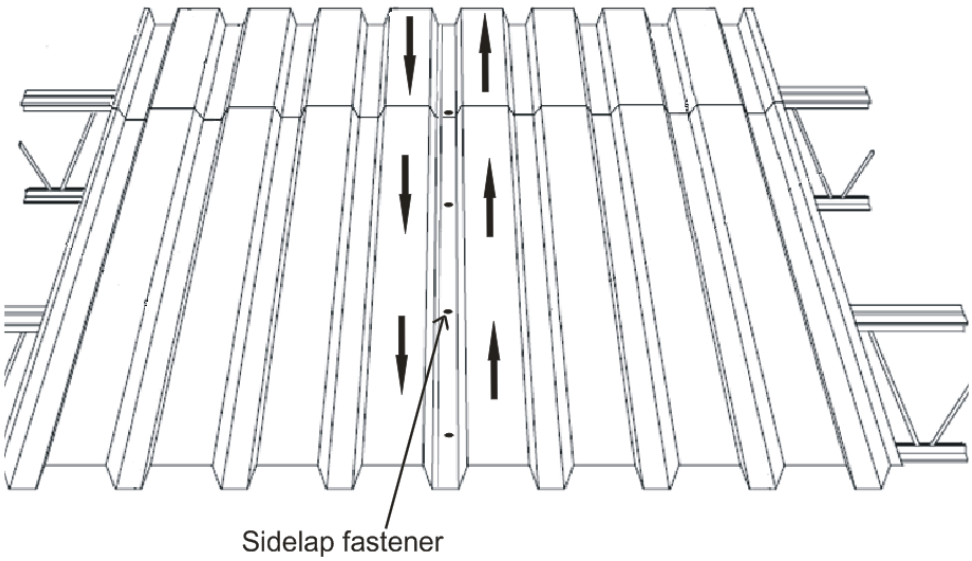

Figure 2.7 Schematic of shear flow at sidelap

At the corner of interior panels, 4 layers of steel sheets are overlapped above the underlying hot rolled steel. The arrangement of the sheets depends upon the installation sequence in the field. When sheets are installed at the end of each other first, the two top sheets from the next row of sheets will transfer the longitudinal shear force to the lower two sheets that were installed first. In that case, the shear plane in the weld is at mid-thickness of the four ply connection. This situation, illustrated in Figure 2-8a, is reproduced in the testing program by the 4-layer configuration where 4 steel sheets of varying thicknesses are welded to a hot rolled plate. When sheets are installed one next to each other first, Figure 2-8b, shear acting across the width of the sheets at end laps must also be transferred by the connection. For this installation sequences, that shear is transferred along two shear planes, between the sheets 1 and 2, from the top, and between sheets 3 and 4, again from the top. For the common case where comparable fastener spacing are used along the sidelap and end lap joints, the shear force along these two planes is lower than the shear transferred parallel to the sheet lengths between sheets 2 and 3 and, hence, represents a less critical condition.

The two shear forces, parallel and perpendicular to the sheets, coexist at the corner connections. However, in theory, there is no interaction between the two shear transfer mechanisms, i.e., the upper two sheets pushing against the weld in the direction parallel to the sheets do not produce shear between sheets 1 and 2 and between sheets 3 and 4, and the opposite holds for the shear transfer across the end lap in the orthogonal direction. In practice, since the sheet thickness is small compared to the weld diameter and because contact tension and bearing stresses between the sheets and the welds may not be uniformly distributed, the welds may be subjected to shear forces acting in the two orthogonal directions. This possibility was omitted in this test program.

If the sheets are installed side by side first during construction, the situation is inversed: the shear flow acting perpendicular the sheet width at end laps will cause maximum shear in the weld at mid-depth of the 4 plies, between sheets 2 and 3, which is the same case as the one that was considered for the test program.

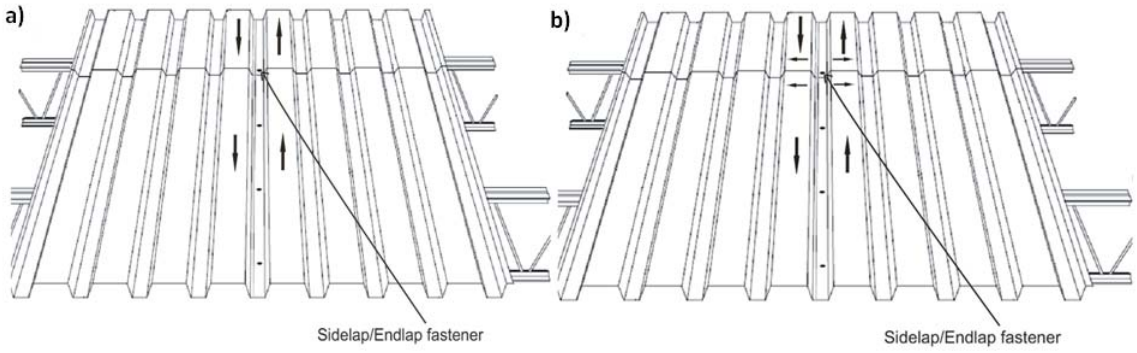

Figure 2.8 Schematic of shear flow at sidelap/endlap

According to the NBCC 2005 the fasteners of roof deck diaphragms must also resist tensile loads induced by internal and external wind pressure acting on the roof. In fact, Section 4.1.7 of NBCC 2005 specifies a method to determine the positive or negative wind pressure designers must

consider. When negative external pressure is applied along the surface of a roof deck diaphragm, the fasteners must resist tensile loads so the steel deck panels stay attached to the underlying structure. This external pressure acts on the roof membrane and is eventually transferred to the upper deck surface through the connectors and/or adhesive attaching the roof membrane and insulation to the deck. Internal positive pressure acting directly under the roof steel deck also adds to the effect of the external wind suction on the roof. Hence, both external and internal pressures tend to separate vertically the steel deck from the supporting steel members and all fasteners connecting the deck to the steel framework contributed to resisting these uplift forces. This load path was reproduced in the tension test setup that was used in this research.

At the edge of panels, where welds act as sidelap fasteners and are fabricated through two layers of sheet steel, the uplift forces are transferred by the steel sheets to the underlying structure through the weld. This situation is illustrated in Figure 2-9 and has been reproduced in the testing program with the 2-layer tension configuration where two steel sheets are welded to an underlying angle that is used to simulate the flange of an open web steel joist. During the test steel sheets are pulled upwards while the hot rolled angle is fixed.

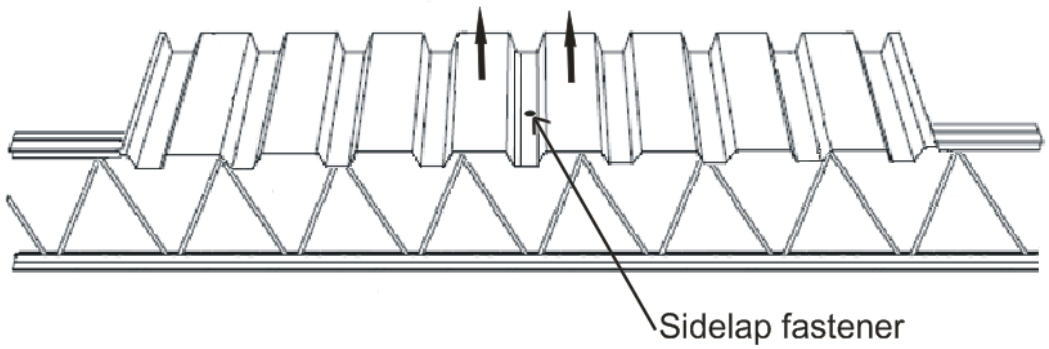

Figure 2.9 Schematic of tension forces acting on a sidelap fastener

At the locations where the endlap and sidelap occur simultaneously, the tension forces are transferred from the steel sheets to the underlying hot rolled plate by the welded connection

which is fabricated through four layers of steel sheets. This situation is illustrated in Figure 2-10 and will be reproduced in our testing program by the 4-layer tension configuration where four steel sheets are welded to an underlying hot rolled angle used to simulate the flange of an open web steel joist. Test were also performed with 1-ply connections to study the situation away from endlaps and sidelaps

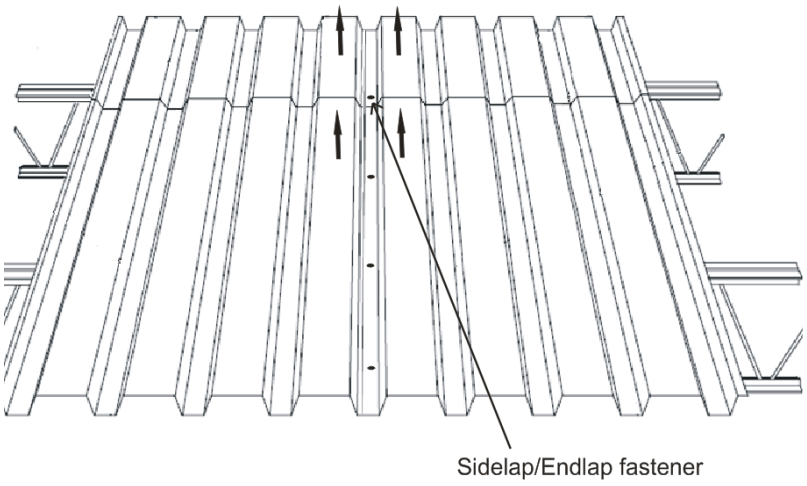

Figure 2.10 Schematic of tension forces acting on a sidelap/endlap fastener

CHAPTER 3. TESTING PROGRAM

3.1 Test set-up

The testing area in the laboratory consisted of a vertical steel frame built with two W-shape columns and top and bottom W-shape cross beams. An MTS tension/compression 250 kN actuator controlled by an MTS Flextest control system was vertically attached underneath the upper cross beam. The test setup and test specimens were mounted on and connected to the lower cross beam. The upper part of the test setup was connected to the lower end of the actuator load cell. At that end, the actuator was horizontally braced to prevent lateral and transversal movements. The test set-up for the shear strength test is illustrated in Figure 3-1 and 3-2. This setup is similar to the "Alternate-2 Lap-Joint Shear Test" illustrated in the AISI Manual of Cold-Formed Steel Design (2002) which includes two sets of hot rolled plates. Each set contains a set of 4 holes for 12.7 mm (½ in.) diameter A325 bolts used to attach the test specimen to the plates. One set of plates was anchored to reaction frame while the other was attached to the load cell which was then connected to the actuator. When the actuator was activated the force was transferred from the hot rolled plates to the steel sheets through the bolts. The force was then transferred between the sheets through the welded connection at the centre of the specimen. The L shaped hot rolled plate was guided to remain vertical by a stiffened guiding member that included brass plates to minimize friction. The L shaped design for the plates was used to minimize eccentricity in the system. One LVDT was bolted to two components of the shear jig in order to provide an accurate measure of the relative displacements between the steel sheets.

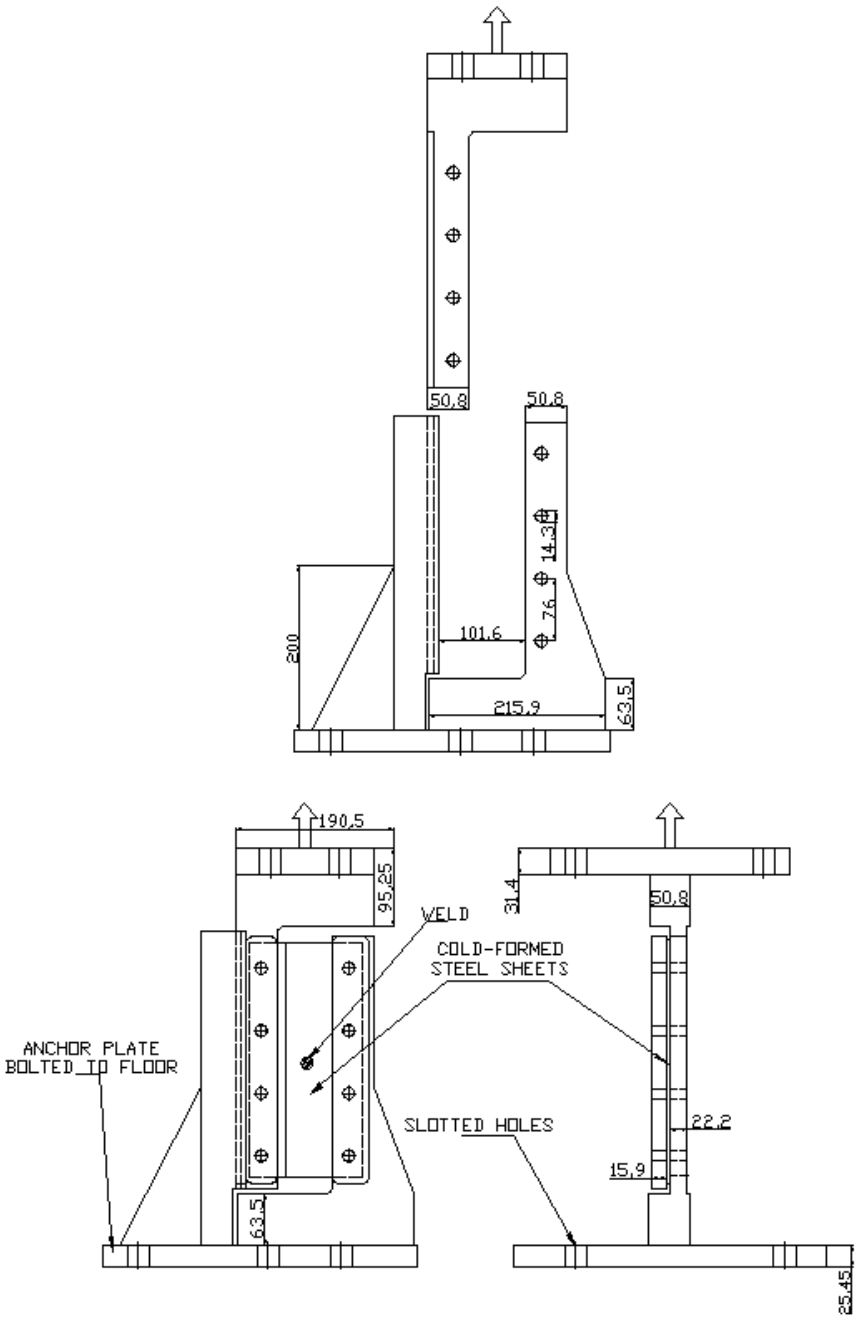

Figure 3.1 Schematic of shear jig

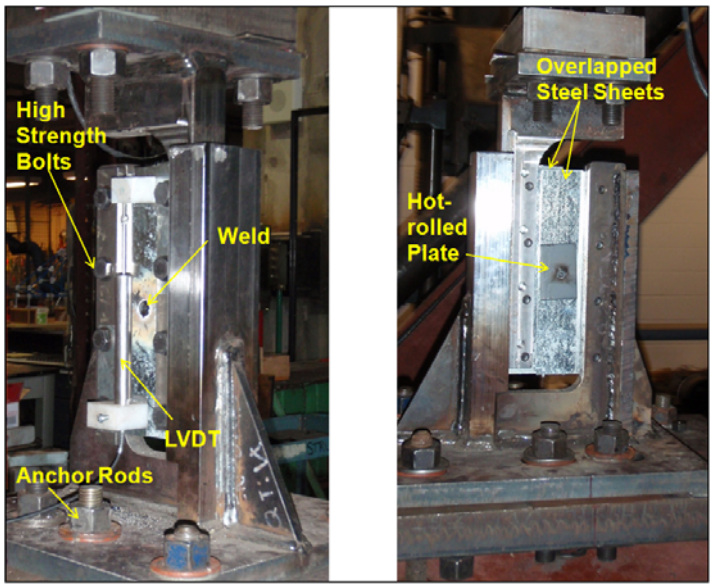

Figure 3.2 Shear test set-up

The set-up used to test the tension strength of the arc-spot welds was similar to the "Modified Standard Tension-Test Fixture" described in the AISI Manual of Cold-Formed Steel Design (2002) (Figure 3-3 and Figure 3-4). This type of set-up allows the influence of flexible support members (i.e. very thin joist chords) to be observed. The steel sheets were welded to a hot rolled steel angle to simulate an overlap connection typically found in steel deck diaphragms where the steel sheets are welded to steel joists. The angle, which represents the top chord of the joist, was connected to the base of the tension jig with two ¾ in. diameter A325 bolts. In turn, the tension jig was anchored to the lower beam of the reaction frame with four anchor rods. The upper part of the tension jig had two loading arms that came into contact underneath the steel sheets when the actuator was moved upward. The force was transferred to the test specimens by the loading arms. This configuration reproduced the effect of uplift wind pressure being transferred to the connection through the deck.An LVDT was bolted to the base of tension jig to measure the vertical deformation of the specimen.

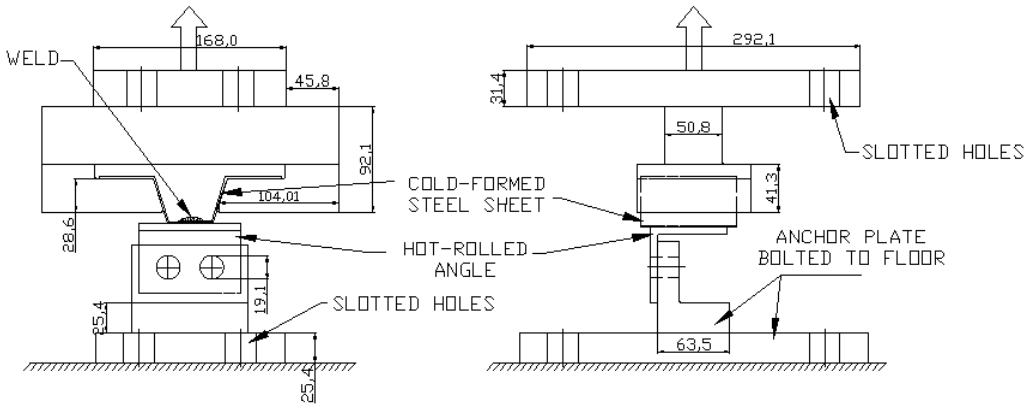

Figure 3.3 Schematic of tension jig.

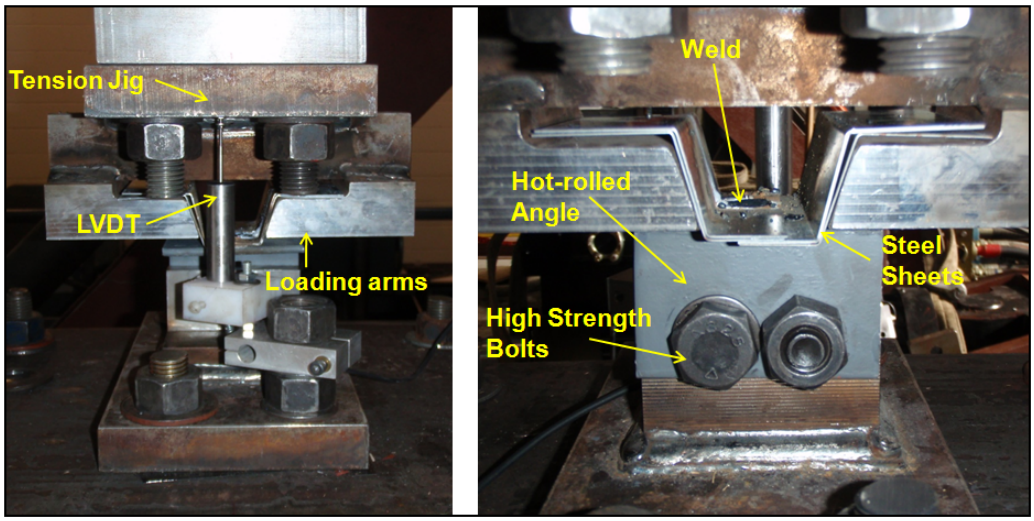

Figure 3.4 Tension test set-up

3.2 Test parameters

The testing program included 107 shear strength tests and 72 tension strength tests. A 1/8 in. diameter E6011 (E4311) electrode was used to fabricate all welds. The sheet steel material used was of ASTM A653 Gr.33 (nominal F_y = 230 MPa, nominal F_u = 310 MPa). The thicknesses of sheet steel tested were 16 (1.52 mm), 18 (1.21 mm), 20 (0.91 mm) and 22 gauge (0.76 mm). The physical properties of the four sheet steels were determined in accordance with the ASTM A370

(2009) procedure. The actual material properties of the steel sheet were determined according to the ASTM A370 Standard Test Methods and Definitions for MechanicalTesting of Steel Products using 50 mm gage length coupons. The average measured values from three coupon tests for each sheet thickness are given in Table 3-1. Detailed information can be found in Appendix H.

Table 3.1 Material properties for cold-formed steel sheets

Nominal sheet thickness (mm)	Overall sheet thickness (mm)	Base metal thickness (mm)	F_y (MPa)	F_u (MPa)	F_u/F_y	% Elongation
0.76	0.786	0.728	392	446	1.14	30.1
0.91	0.912	0.880	346	415	1.20	35.5
1.21	1.209	1.169	358	429	1.20	28.0
1.52	1.513	1.458	356	388	1.09	37.3

3.3 Test specimen configuration

The test specimens included in the testing program were fabricated using different sheet steel thicknesses (1.52, 1.21, 0.91 and 0.76 mm), underlying hot rolled steel thicknesses (6.4 and 3.2 mm), loading protocols (monotonic and cyclic) and sheet steel configurations.

3.3.1 Underlying plates and steel sheets

In the shear strength tests, an underlying hot rolled Grade 350W CSA G40.21 (2004) steel plate with a one-coat primer according to CISC/CPMA 2-75 specifications was provided for all test specimens in order to provide the welder with similar conditions as the ones typically encountered in the field. This plate represents the supporting joist chord or beam flange. During the testing program most shear specimens were fabricated with 51 mm x 76 mm x 6.4 mm (2 in. x 3 in x ¼ in.) underlying plates while others had 51 mm x 76 mm x 3.2 mm (2 in. x 3 in. x 1/8

in.) steel plates such that the effect of the thickness of the underlying material could be evaluated. All shear specimens were fabricate using steel sheets cut to 102 mm x 280 mm 4 in. x 11 in. sections with four pre drilled 14.3 mm holes used to connect the specimen to the shear jig. Another series of tests were carried out to study the behaviour of welds located at the building roof perimeter; the underlying plates used for these specimens were 102 mm x 280 mm x 6.4 mm (4 in. x 11 in x ¼ in.). Grade 350W CSA G40.21 (2004) steel plates with four pre drilled 14.3 holes. These holes were used to attach the underlying plate to the shear jig.

The underlying plates of the tension specimens were cut from angle shapes to model the top chord of a joist that is typically used as an underlying material in roof deck construction. The tension resistance specimens were composed of L63x63x6.4 mm (L2½ x 2½ x ¼ in.) angles or L63x63x3.2 mm (2½ x 2½ x 1/8 in.) angles made from grade 350W CSA G40.21 (2004) steel . Sheet steel sections used for most tension resistance specimens were cut and bent to model one half of one flute from a typical corrugated steel deck. A series of tension resistance tests were also performed with steel sheets cut and cold bent to model one flute from the common 38 mm deep x 914 mm wide trapezoidal steel deck profile with flutes spaced 152 mm o/c illustrated in Chapter 2.

3.3.2 Sheet steel configurations

Three sheet steel configurations were included in the shear strength tests. The 2-layer configuration was used to simulate a sidelap connection. Two steel sheets were welded to a hot rolled plate as illustrated in Figure 3-5 and 3-6. For this configuration, the shear plane was located between the two steel sheets.

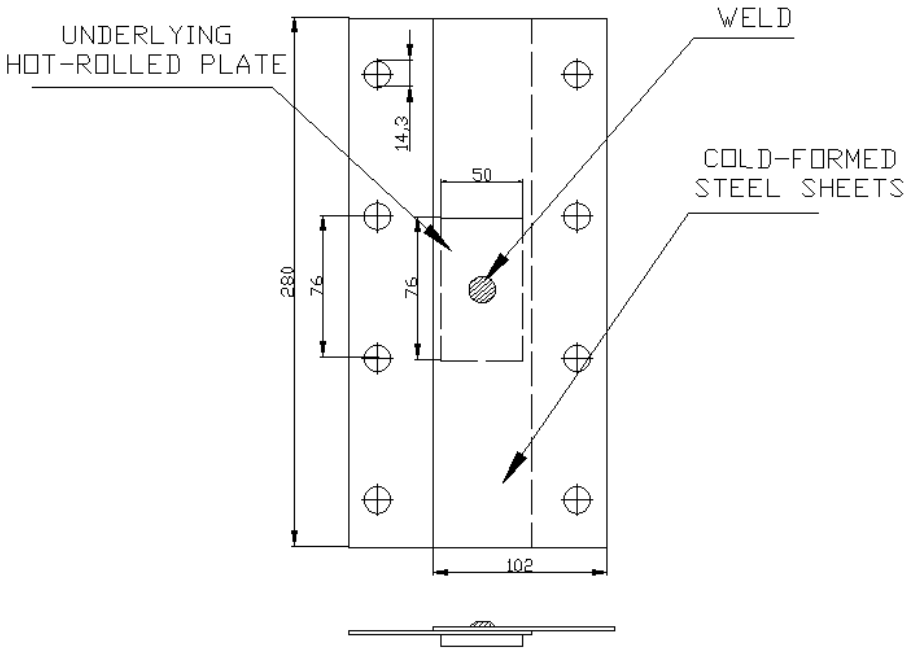

Figure 3.5 Schematic of 2-layer configuration

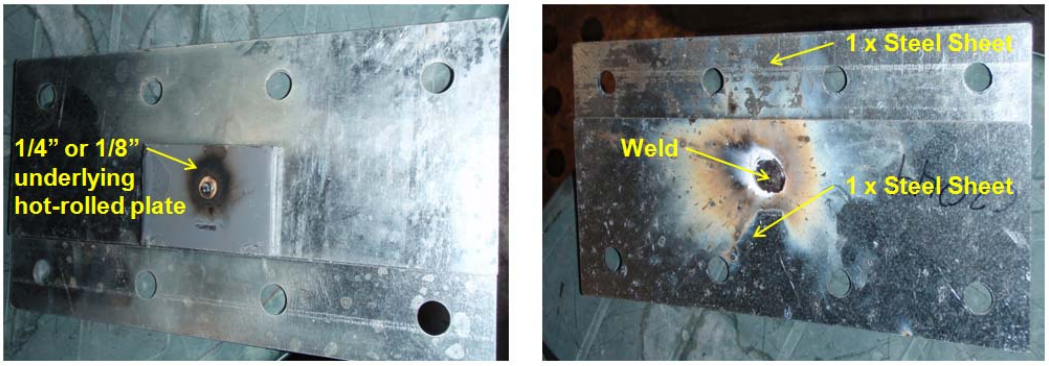

Figure 3.6 2-layer shear configuration

The 4-layer configuration was used to simulate the connection at the corner of deck panels where the sidelap and endlap occur simultaneously. Four steel sheets were welded to a hot rolled plate (Figure 3-7 and 3-8) and the shear plane was located between the steel sheets, as explained in Chapter 2.

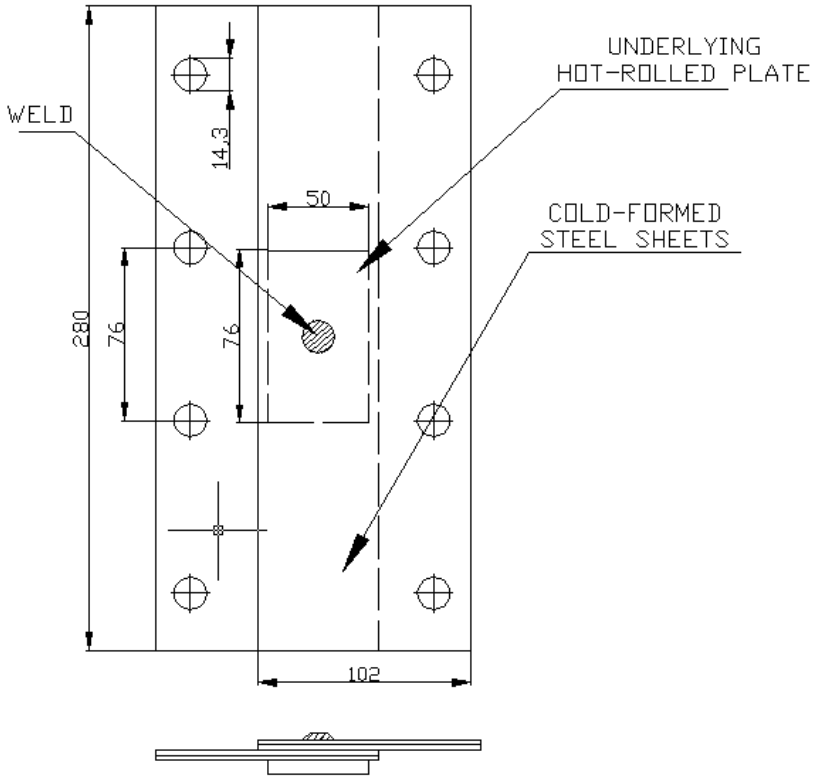

Figure 3.7 Schematic of 4-layer configuration

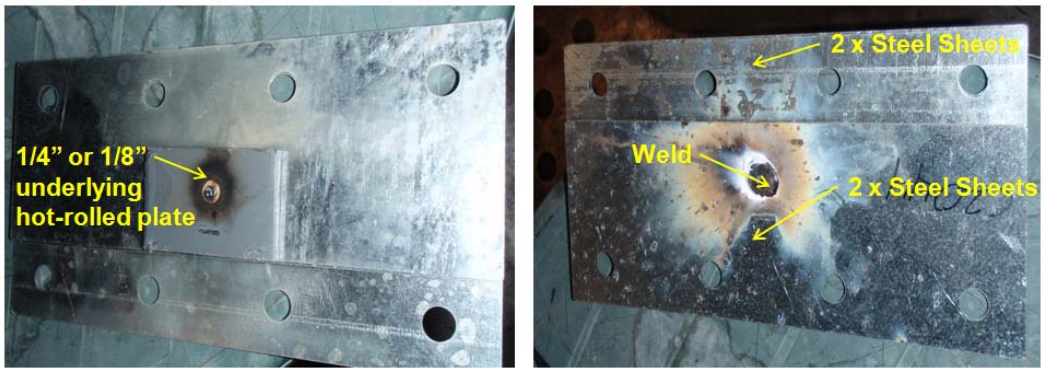

Figure 3.8 4-layer shear configuration

The perimeter configuration was a variant of the 2-layer configuration used to simulate the typical connections where end laps occur at the perimeter of buildings. In this case, two steel sheets were welded to a hot rolled plate (Figure 3-9 and 3-10) and the shear plane was located between the hot rolled plate and the steel sheets.

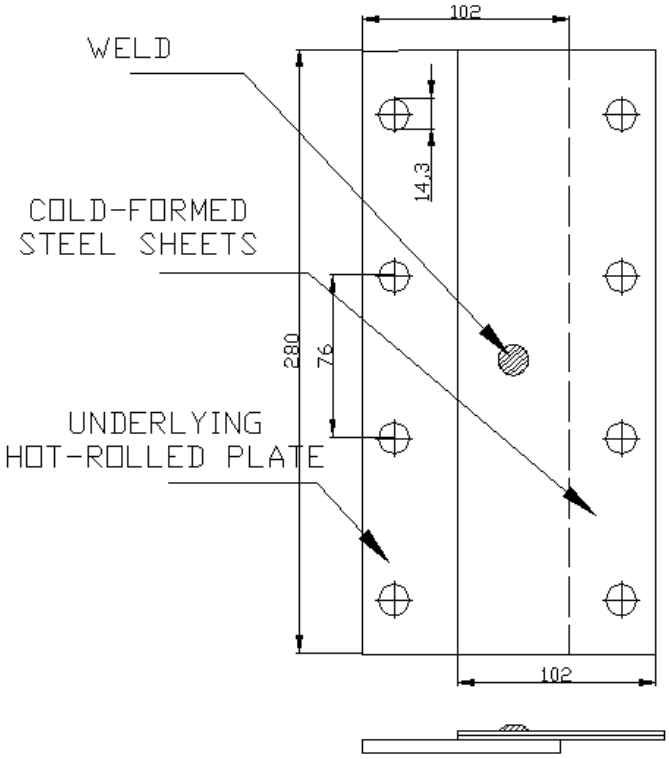

Figure 3.9 Schematic of perimeter configuration

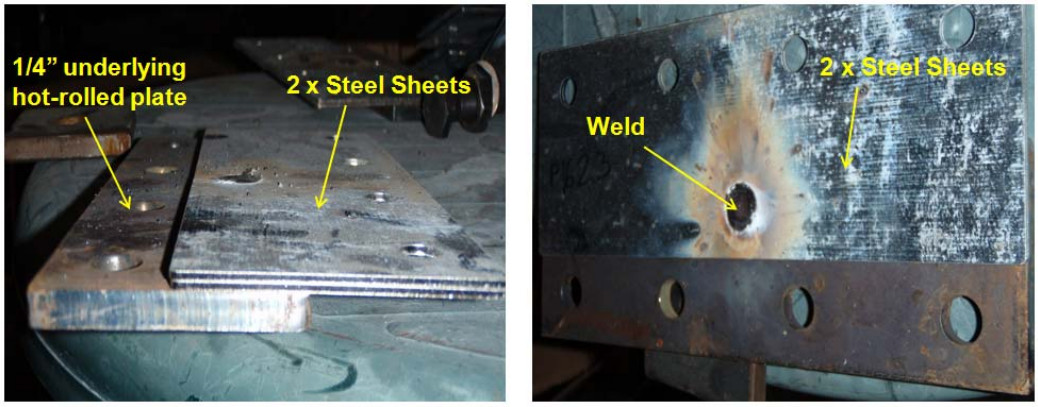

Figure 3.10 2-layer perimeter configuration

The tension strength tests comprised three configurations. The first was a 2-layer configuration (Figure 3-11 and 3-12) simulating sidelap connections away from end laps or end lap connections away from sidelaps. The second was a four ply configuration (Figure 3-13 and 3-14) simulating simultaneous sidelap and endlap connections at the corners of deck sheets. The third was a single layer (Figure 3-15) configuration with only one thickness of steel sheets to study the situations away from endlaps and sidelaps.

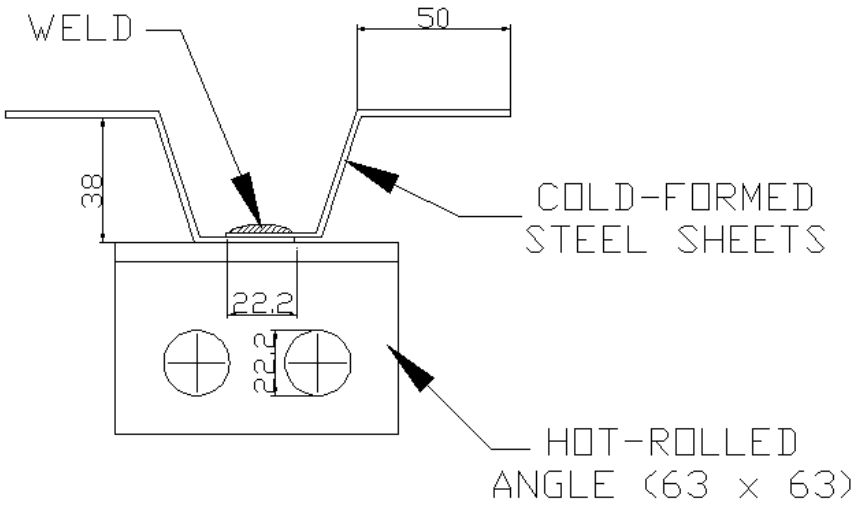

Figure 3.11 Schematic of 2-layer tension configuration give dimensions

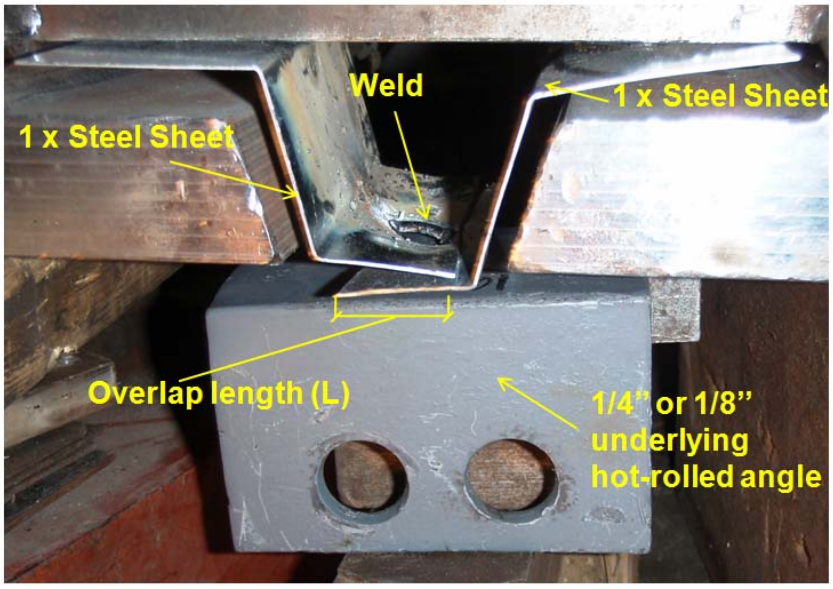

Figure 3.12 2-layer tension configuration

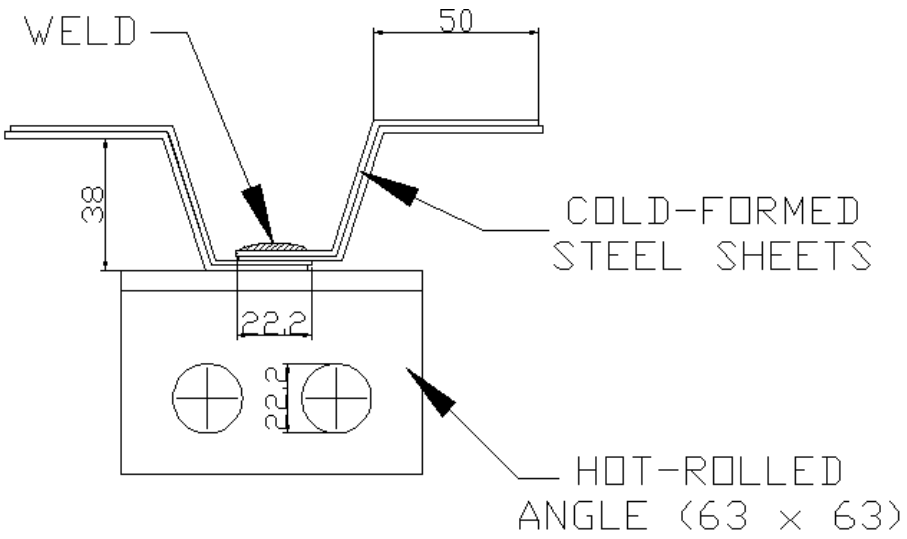

Figure 3.13 Schematic of 4-layer tension configuration

Figure 3.14 4-layer tension configuration

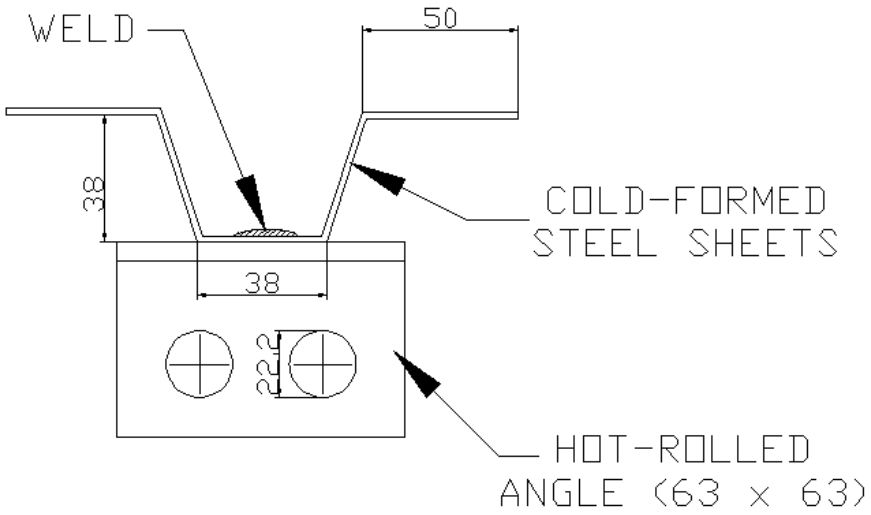

Figure 3.15 Schematic of 1-layer tension configuration

Each specimen can be identified with a tag formed by a unique series of letters and numbers, e.g. M1624T. The tag indicates the testing parameters specific to each specimen. The first symbol is a letter that designates the loading protocol; M= Monotonic Shear, C= Cyclic Shear, T=Monotonic Tension. The second and third symbols indicate the gauge (thickness) of the sheet steel; 22 = 22 gauge (0.76 mm), 20 = 20 gauge (0.91 mm), 18 = 18 gauge (1.21 mm), 16 = 16 gauge (1.52 mm). The fourth symbol indicates the configuration; 2 = 2 ply configuration, 4 = 4 ply configuration. The fifth symbol indicates the number of the specimen within a given series. The letter P is added at the end of the tag to denote the perimeter configuration while a letter T is added to the end of the tag to denote the specimens fabricated with either a 3.2 mm (1/8 in.) thick hot rolled plate or an angle.

Table 3-2 gives the test matrix for the entire test program. The number of specimens for each specimen configuration and steel sheet thickness is shown. In each case, the numbers are associated to letters that give the failure mode observed in the tests. These failure modes are described in Chapter 4.

Table 3.2 Test matrix and observed failure modes

Specimen No.	Sheet thickness (mm) / Gauge			
	0.76 / 22	0.91 / 20	1.21 / 18	1.52 / 16
Mxx2z	4T	4T	4T	4B
Mxx4z	2W+1T+1B	2W+1T+1B	4W	4W
Mxx2zP	2W+2T	1W+3T	4W	4W
Mxx2zT	4T	3T	4T	3W
Mxx4zT	2W+1T+1B	1W+1T+2B	3W	3W
Cxx2z	4T	4T	4T	4B
Cxx4z	1W+1T+2B	1W+1T+2B	3W	4W
Txx1z	3T	4T	4T	4T
Txx2z	4T	4T	4T	3W+1T
Txx4z	3T	1W+3T	1W+3T	3W
Txx2zT	5T	3T	3W	3T
Txx4zT	4T	1W+2T	3W	3W

3.3.3 Welding Protocol

The quality of an arc spot weld is largely dependent on the skill and experience of the welder. Selection of the proper electrode, current setting and proper welding technique are also necessary to fabricate arc spot welds of sound quality. To maximize the quality and uniformity of the welds throughout the study, great care was taken to elaborate a suitable welding protocol specific to the welding of multi-overlap configurations. In collaboration with welding engineer from Consultarc inc., Mr. Gil Trigo, and experienced certified welders, the key parameters affecting weld quality in multi-overlap configurations were identified as being; the electrode type, the current setting and the welding technique. E6011 (E4311) electrodes were selected because Peuler (2002) noted in his study on arc-spot welds, that these electrodes provided better penetration capacity than

other commonly used electrodes. Furthermore, the results reported by Easterling and Snow (2009) demonstrated that proper welds could difficulty be fabricated through multi-overlap configurations when using E6010 (E4310) electrodes. The main difference between the E6010 and E6011 electrodes is in the composition of the flux coating. While the core wire is made of the same material, the flux coating of the E6010 electrode is rich in cellulose and sodium while the E6011 electrode is rich in cellulose and potassium (CSA W48-06). Current settings were first based on the study by Easterling and Snow (2009) who reported that the current must be set high (200± A) in order to obtain sufficient penetration when attempting to weld multi overlap. Two welding sessions were organized to verify the quality of welds fabricated and to refine the welding procedure. Upon fabrication of the test specimens, the first hour was spent experimenting with different current settings and welding techniques to minimize the porosity of the welds and maximize the fused area between the steel sheets. When the current setting was set too high, excessive porosity in the welds was observed. When the current setting was too low, the welder encountered resistance when piercing through the sheets which resulted in insufficient penetration. The final parameters used for the fabrication of the test specimens were as follows:

- The weld shall be circular and have a visible diameter from 16 mm to 19 mm

- The electrode shall be 3.2 mm (1/8'' in.) diameter and meet E4311 (E6011) specifications

- Current shall be AC and set at 195 amps when welding 16 and 18 gauge steel sheets and 160 amps when welding 20 and 22 gauge steel sheets

The following welding technique was selected as it facilitated piercing through thicker sheets while minimizing porosity. Welding was done in the flat position. Once the arc was sparked, the electrode was pushed vertically through the material to drill through the sheets until proper fusion of the underlying hot rolled steel was obtained. The electrode was then gradually withdrawn with a circular motion to allow the hole to be filled with molten metal. The arc was then broken vertically.

For all test specimens, the time spent fabricating each weld was recorded. Table 3.3 provides the average welding times for specimens according to their sheet steel thickness. The results listed in Table 3.3 show that as the total thickness of sheet steel increases the amount of time necessary to fabricate the weld also increases.

Table 3.3 Average welding times recorded

Sheet Thickness (gauge)	Configuration (layers)	Total Thickness (mm)	Average Welding Time (s)
22	1	0.76	5.3
20	1	0.91	6.8
18	1	1.21	5.3
22	2	1.52	5.8
16	1	1.52	5.0
20	2	1.82	6.8
18	2	2.42	6.7
22	4	3.04	7.2
16	2	3.04	7.6
20	4	3.64	7.7
18	4	4.84	8.7
16	4	6.08	9.3

The SDI Manual (Lutrell 2004) suggests that ¾ in. (19 mm) welds should be fabricated in 3 to 6 seconds using 5/32 in. electrodes. Easterling and Snow (2009) noted that these limits may not be applicable when using 1/8 in. electrodes. The welding time results obtained during this testing program tend to be shorter than to the welding times obtained by Easterling and Snow. The average welding time observed for welds made through a single layer of sheet steel by Easterling and Snow is 33% longer than the average welding time measured during this study. Furthermore, for welds made through two layers of sheet steel, the average welding time reported by Easterling and Snow was 18% longer than in this research project. In conclusion, the results obtained during the study conducted by Easterling and Snow also suggest that the welding times should be increased when using 1/8 in. electrodes, especially when fabricating welds through multi-layer

configurations. The average welding time observed for welds fabricated with 6.4 mm thick underlying steel plates was 24% longer than the average time measured for welds fabricated with 3.2 mm thick underlying steel plates. These results indicate that the thicker underlying steel plate acts a greater heat sink which increases time required to fabricate the arc-spot weld.

3.3.4 Loading protocol

An MTS control system was used to impose displacements to the test specimens. As in Peuler (2002), input files were used to prescribe the motion and loading of the actuator. A monotonic loading protocol was used for all tension strength tests and 76 shear strength tests. The remaining 31 shear strength tests were carried out using a reversed cyclic loading protocol to simulate the loading typically encountered during an earthquake.

The rate of loading for all monotonic tests was 0.5 mm/minute. This rate of loading is in accordance with what has been used by Peuler (2002) and Rogers and Tremblay (2000). The monotonic tests were utilized to study the ultimate strength of the specimens. Before beginning the cyclic tests, the data from the monotonic shear tests were compiled to provide an estimate of the average ultimate shear strength ($P_{u\ avg.}$) for each connection configuration. A loading protocol specific to each configuration was then determined. Each cyclic loading protocol was composed of three different phases. The first phase, illustrated in Figure 3-16, included load controlled cycles used to simulate the expected demand on an arc-spot weld diaphragm connection during an earthquake. The typical behaviour of a specimen during the first phase of a cyclic test is illustrated in Figure 3-17.

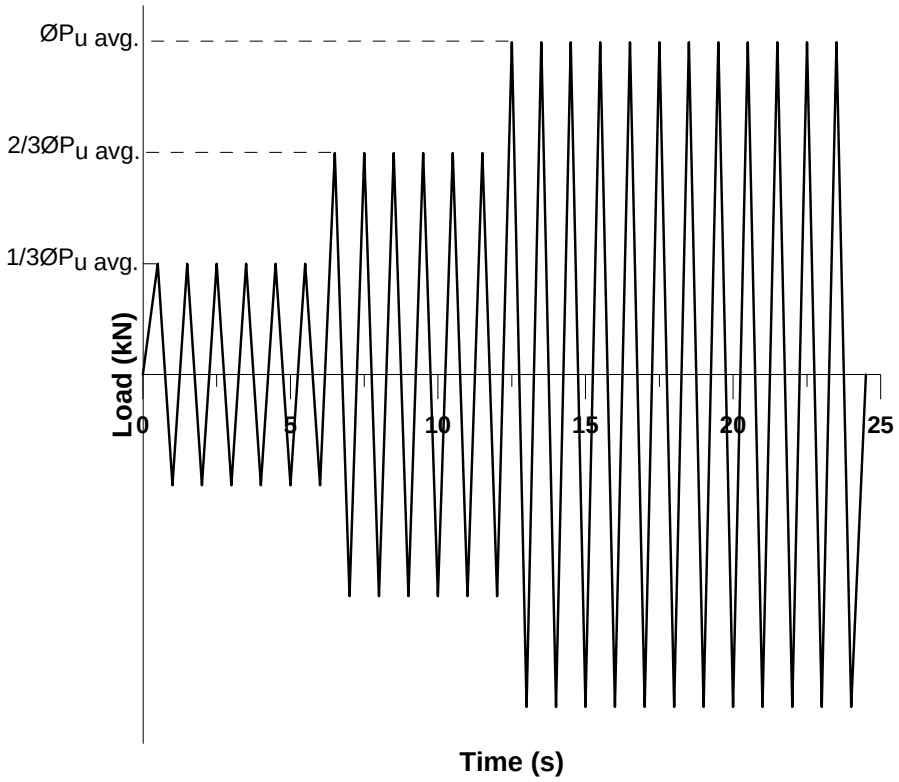

Figure 3.16 Phase 1 of cyclic loading protocol.

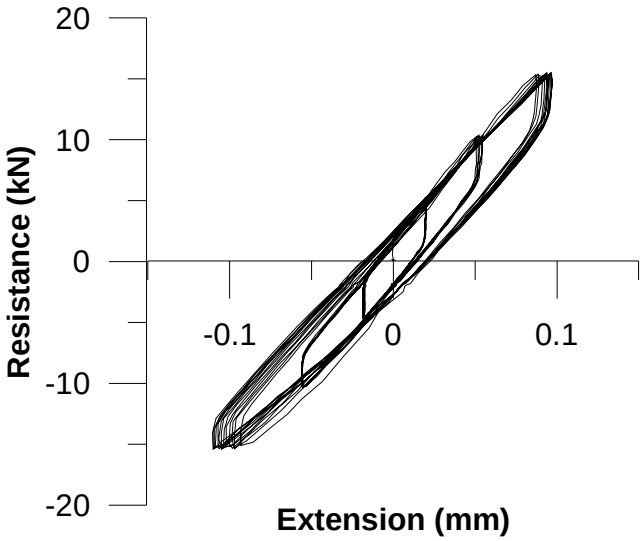

Figure 3.17 Behaviour of specimen during phase 1 of cyclic test (Specimen No.SC1841).

All cycles during this phase had a frequency of 1 Hz, representing the fundamental period of a typical low-rise steel building with flexible steel roof deck diaphragm (Tremblay and Rogers 2005). The resistance levels used for the tests were a function of the specimen factored measured resistance, i.e., ϕ x $P_{u\ avg}$ where ϕ is the resistance factor given by the CSA S136 Specification. As ϕ varies according to the failure mode the ϕ value used for each test was the ϕ value corresponding to the predicted failure mode For specimens where the predicted failure mode is weld failure ϕ = 0.5. For specimens where the predicted failure mode is sheet failure the ϕ value depends on which of equation 1-3, 1-4 or 1-5 governs their specific failure mode. The corresponding resistance factors are ϕ= 0.6, 0.45 and 0.4 respectively. Six cycles were first carried out at 1/3 x $\phi P_{u\ avg.}$ followed by six cycles at 2/3 x $\phi P_{u\ avg.}$. These cycles were used to simulate the 10 to 12 s stage at the beginning of an earthquake during which a fraction of the maximum loads are imposed. This first stage is typically followed by a 10 to 15 s stage where the maximum loads are imposed. To simulate this second stage 12 cycles were carried out at the specimen factored measured ultimate resistance ($\phi P_{u\ avg.}$). The second phase included one displacement controlled cycle where the specimen was loaded at a rate of 0.5 mm/minute, past its

ultimate load (P_u) until it reached its failure point (0.8 x P_u). The load was then reversed until the failure point in the opposite direction was reached. Figure 3-18 shows the resistance *vs.* deformation relationship of a specimen during phase two of a cyclic test.

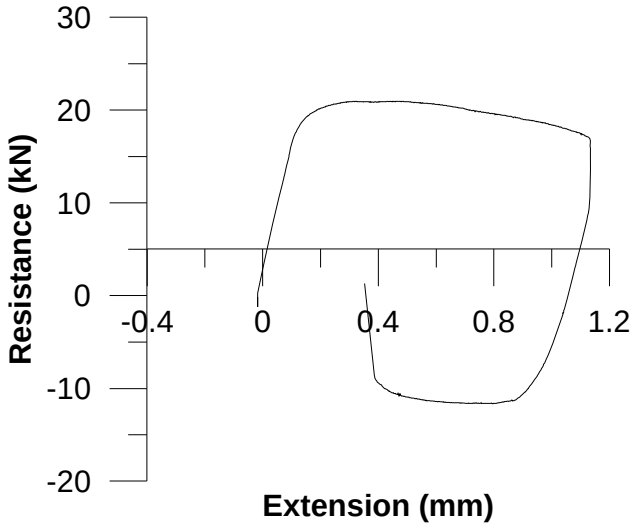

Figure 3.18 Behaviour of specimen during phase 2 of cyclic test (Specimen No.SC1842).

The third phase, shown in Figure 3-19 consisted of six displacement controlled cycles at a frequency of 1.0 Hz. Two cycles were completed with 2 mm, 4 mm and 6.4 mm amplitudes. This phase was used to observe the ductility of the specimens in the post peak region. The resistance *vs.* deformation relationship of a specimen during phase 3 of a cyclic test is illustrated in Figure 3-20.

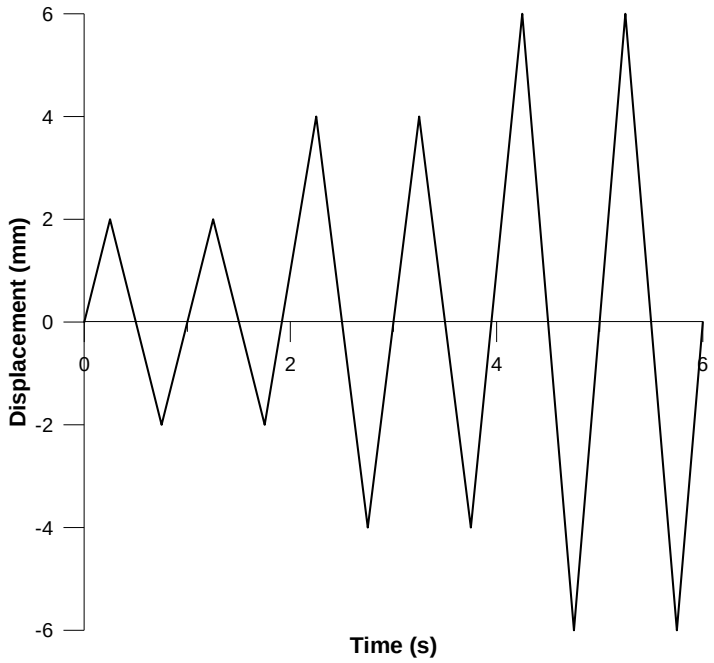

Figure 3.19 Phase 3 of cyclic loading protocol.

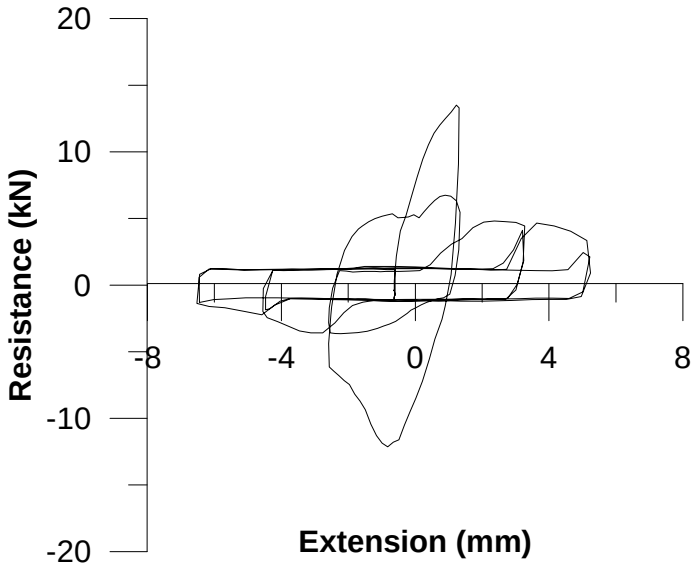

Figure 3.20 Behaviour of specimen during phase 3 of cyclic test (Specimen No. SC2242).

CHAPTER 4. RESULTS AND ANALYSIS

4.1 Failure modes

The failure modes for all specimens described in this section are reported in Appendix C. Appendices E, F, and G contain all load-deformation curves measured in the tests.

4.1.1 Shear failure modes

Three different failure modes were encountered during the shear strength tests: weld shear failure (W), sheet tearing failure (T) and sheet bearing failure (B). These failure modes are reported in Table 3-2 for each connection configuration and sheet thickness. Details can be found in Appendix C. The weld shear failure illustrated in Figure 4-1 is characterized by shear fracture of the specimen through the weld nugget. As illustrated in Figure 4-2, a sudden loss in resistance occurring at small displacements, and overall brittle behaviour are associated with this failure mode. Weld shear occurs mainly for the configurations that have a low weld diameter to total thickness ratio (d/t). When the effective diameter is relatively small compared to the thickness of the sheet steel plate the critical load causing failure through the weld plane is reached before the sheet steel plate can exhibit significant deformations.

Figure 4.1 Shear test specimen after weld shear failure (Specimen No. SM2021P)

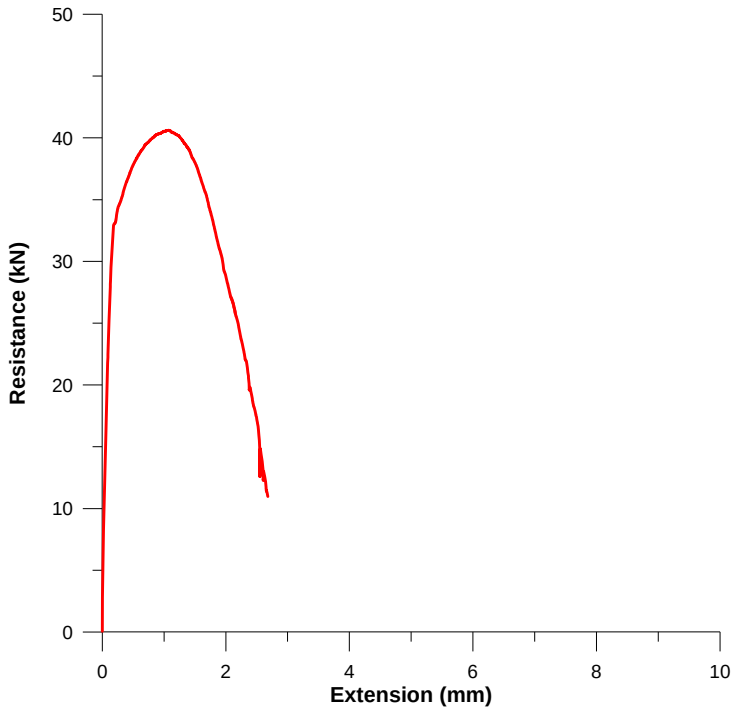

Figure 4.2 Typical specimen behaviour during weld shear failure (Specimen No. SM2021P)

As illustrated in Figure 4-3, when sheet tearing occurs, the failure initiates along the contour weld on the tension side of the weld with the tear typically spreading on a line perpendicular to the

applied load. Out of plane deformations then occur in the sheet steel on the compression side of the weld. This failure mode occurs when the d/t ratio is high. The resistance of the connection decreases in a gradual manner once the ultimate capacity has been reached as shown in Figure 4-4.

Figure 4.3 Shear test specimen after sheet tearing failure (Specimen No. SM2222P)

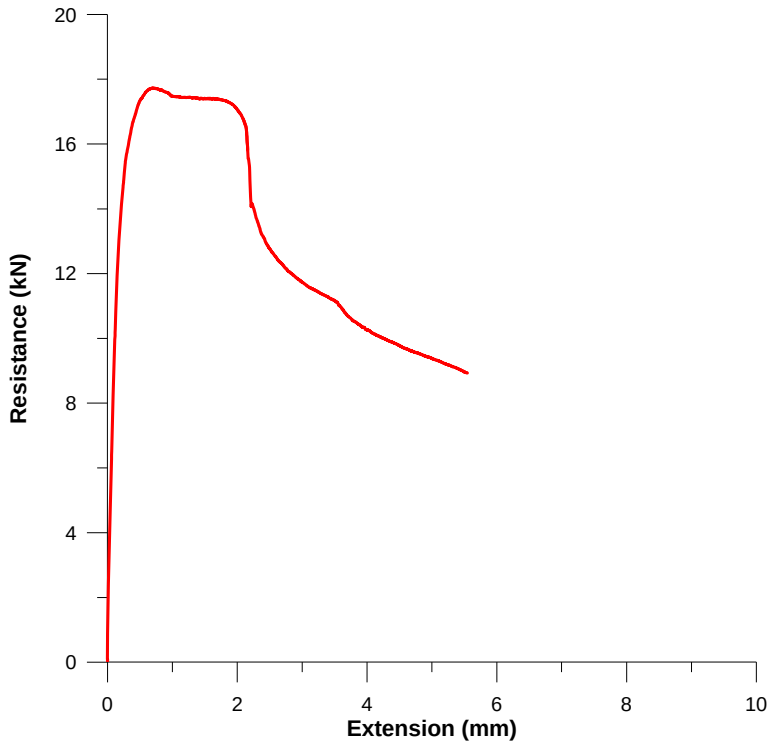

Figure 4.4 Typical specimen behaviour during sheet tearing failure (Specimen No. SM2222P)

Sheet bearing failure, illustrated in Figure 4-5 is characterized by a ductile failure that occurs through piling of the sheet steel in front of the weld nugget and by shearing of the sheet around the contour of the weld on lines parallel to the applied load. Relatively large displacements are associated with this failure mode. As observed in Figure 4-6, once the ultimate load has been reached the load decreases gradually. After the ultimate load there are several plateaus where the load increases slightly before decreasing again, this type of behaviour for typical of bearing failure modes.

Figure 4.5 Shear test specimen after sheet bearing failure (Specimen No. SM2241)

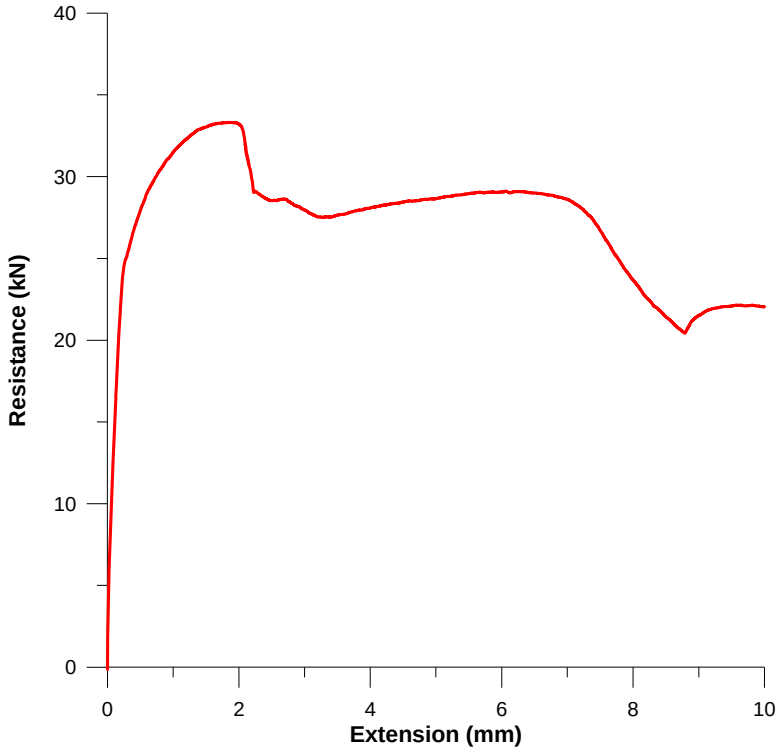

Figure 4.6 Typical specimen behaviour during sheet bearing failure (Specimen No. SM1623)

4.1.2 Tension failure modes

During tension strength tests two failure modes were encountered; weld failure (W) and sheet tearing failure (T). The weld failure occurred for configurations with low d/t ratios. As illustrated in Figure 4-7, this brittle failure mode occurs through the effective diameter of the weld. Relatively small displacements are associated with this failure mode as shown in Figure 4-8.

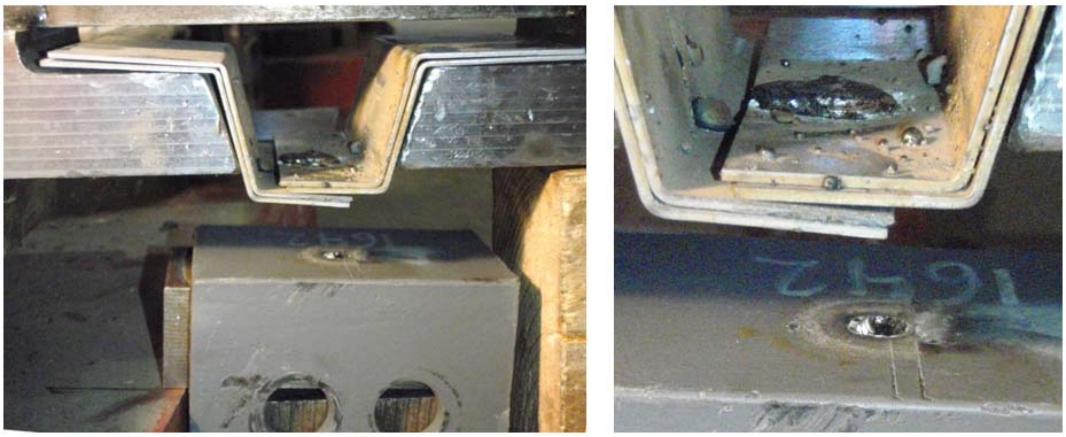

Figure 4.7 Tension test specimen after weld failure (Specimen No. T1642)

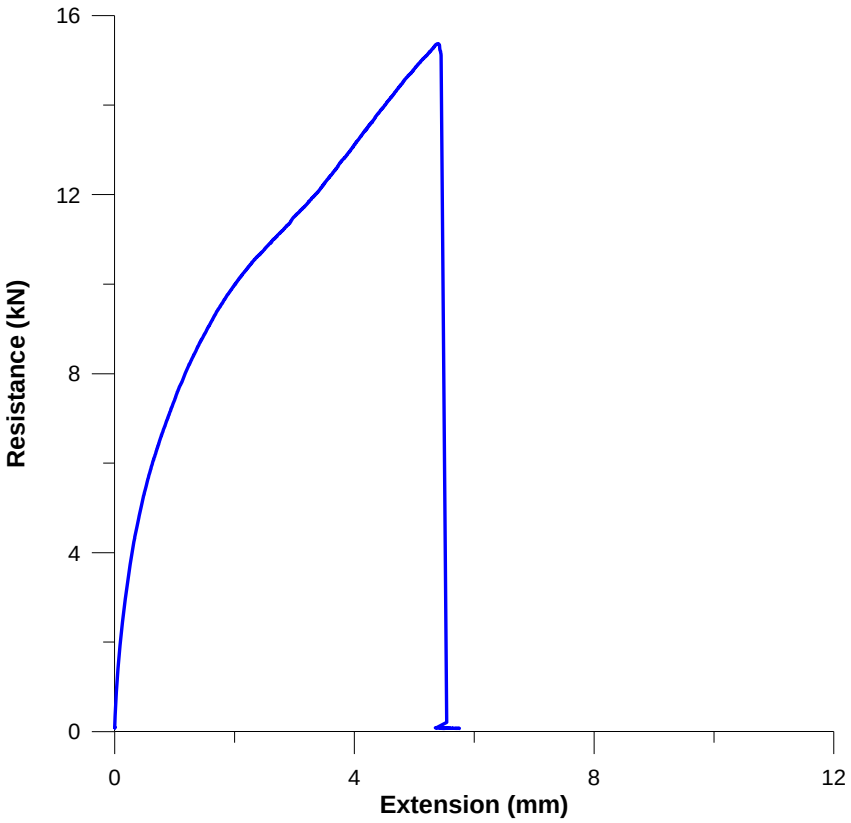

Figure 4.8 Typical tension specimen behaviour during weld failure (Specimen No.T1642)

The sheet tearing failure mode, shown on Figure 4-9, is characterized by tearing of the sheet steel along the contour of the weld. A peeling effect caused by the geometry of the overlap connection causes stress concentrations at the contour of the weld. As illustrated in Figure 4-10, during sheet tearing failure, gradual decrease in resistance occurs once the ultimate resistance has been reached.

Figure 4.9 Tension test specimen after sheet tearing failure (Specimen No. T1822)

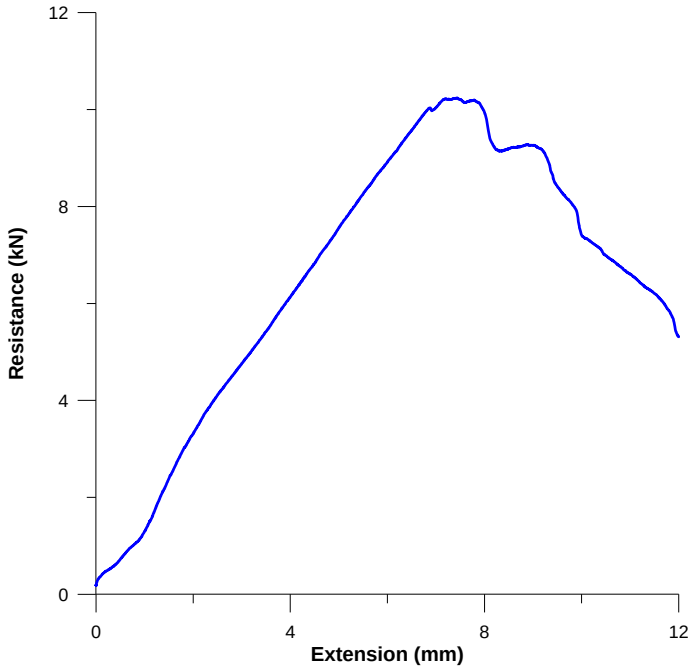

Figure 4.10 Typical tension specimen behaviour during sheet tearing failure (Specimen No.T1824)

4.2 Effective Weld diameter

An arc spot weld is fabricated by pushing the electrode through the sheet steel layers until proper penetration into the underlying hot rolled steel plate (joist chord or beam flange) is obtained. The cross-section of the weld nugget typically has a conical shape, with the diameter of the weld decreasing with the distance from the underlying material. As illustrated in Figure 4-11, the effective weld diameter (d_{eff}) is measured along the shear plane of the weld while the visual weld diameter (d_{vis}) is measured at the visible surface of the weld. In the case illustrated in Figure 4-11, the shear plane is located at the interface between the cold-formed steel sheets and the hot rolled steel. With the 2-layer and 4-layer shear specimens, the shear plane is located at the mid-thickness of the steel sheets.

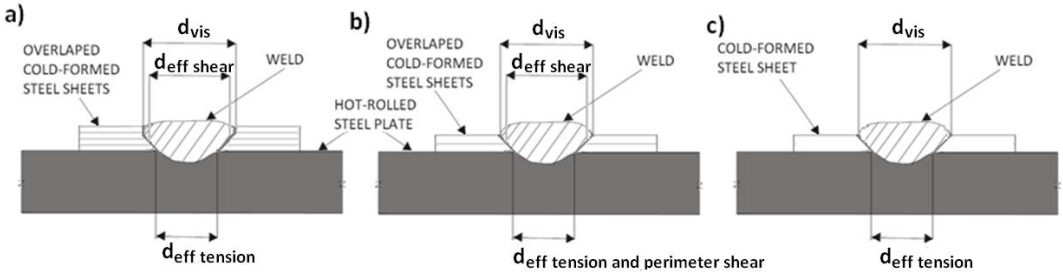

Figure 4.11 Schematic of cross-section showing visible and effective weld diameters for: a) Four-ply connection in shear and tension; b) Two-ply connections in shear and tension; and c) Single-ply connection in tension.

As the total thickness of sheet steel increases the difference between the visual diameter and the effective diameter also increases. The CSA S136 (2007) specifies the resistance of an arc spot weld as a function of its effective diameter. Because it is impossible for a designer to see or specify the effective weld diameter, Peköz & McGuire developed an equation, also found as Equation E2.2.1-5 in the CSA S136, to relate the effective weld diameter to the visible weld diameter [Eq 4-1];

$$d_{eff} = 0.7d_{vis} - 1.5t \leq 0.55d_{vis} \qquad (4-1)$$

where t is the total thickness of the cold-formed steel sheets.

This equation was developed by Peköz and McGuire who indicated that the weld area obtained with d_{eff} from Equation 4-1 provides an accurate estimate of the net effective area of welds which contain substantial pitting and porosity. This equation has previously been found to be quite conservative as the effective weld diameter measured by Peuler (2002) was on average 50% higher than the effective weld diameters predicted by Equation 4-1 for welds fabricated without washers. More recently, Easterling and Snow (2009) measured effective weld diameters that were on average 30% higher than those calculated using equation 4-1. It must be noted that the values published by Peuler and those published by Easterling and Snow do not include any reduction to account for the porosity recorded during their respective studies. As part of this research project, prior to testing the visible diameter of each weld was recorded. It was also possible to measure with a vernier calliper the effective weld diameter of specimens that experienced weld failure. After failure, the average of two diameter measurements taken in perpendicular directions was used to calculate a gross effective weld area. These measurements were taken along the failure plain of the weld. A measure of pitting and porosity was recorded with the vernier calliper and deducted from the effective gross weld area to calculate the effective net weld area (A_{ne}). The effective net weld area was used to calculate the effective weld diameter with the following equation;

$$d_{eff} = \sqrt{4A_{ne}/\pi} \qquad (4-2)$$

Details of these calculations are reported in Appendix B. A plot of the data recorded from the shear and tension specimens of this testing program and the data reported from previous studies by Peuler (2002) and Easterling and Snow (2009) is provided in Figure 4-12. The data from Peuler was categorized according to the type of electrode used; only specimens fabricated without welding washers were plotted. Only the specimens with full-time welds were plotted for the study by Easterling and Snow because of the observation that the time taken to fabricate the weld influences the effective weld diameter.

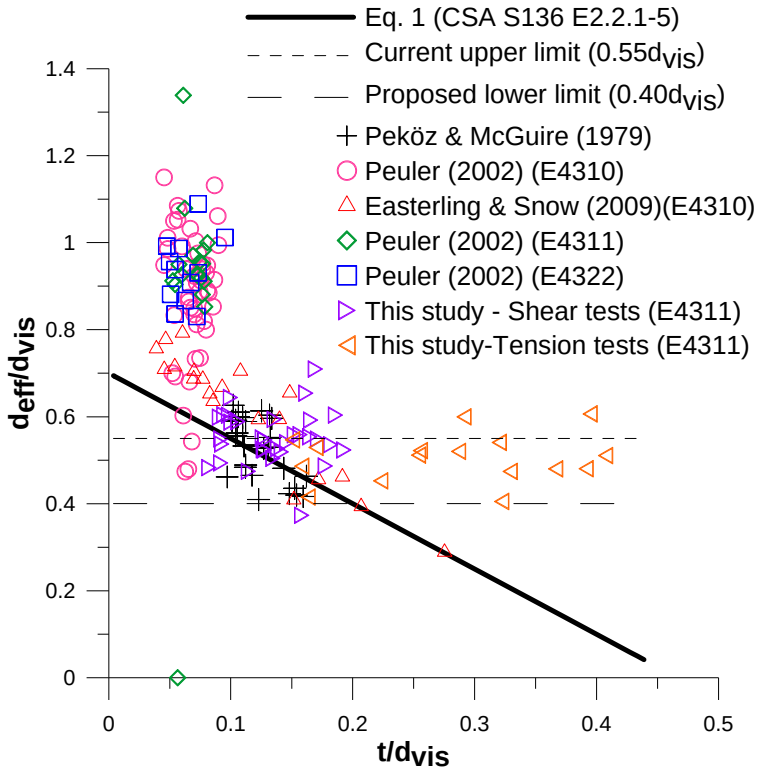

Figure 4.12 Effective weld diameter results

The results obtained during this study support that Equation E2.2.1-5 accurately predicts the effective weld diameter for the t/d range where tests had previously been carried out. As this study investigated thick sheets with multi-overlap configurations, the results provided data in a t/d range where few tests had previously been done. Figure 4.12 shows that Equation E2.2.1-5 becomes overly conservative as t/d increases. The results suggest that a lower limit should be added to Equation E2.2.1-5 to read:

$$d_{eff} = 0.7d_{vis} - 1.5t \quad ,with\ 0.4d_{vis} \leq d_{eff} \leq 0.55d_{vis} \qquad (4-3)$$

This lower limit should be applied only if welds are fabricated with a proper welding procedure using an E4311 (E6011) penetrating electrode as discussed in Section 3.3. In Fig. 4-12, it is also noted that the results from the other studies indicate that the upper limit of 0.55 d_{vis} is

conservative for low t/d_{vis} ratios. This limit could eventually be also revisited but this aspect is not examined herein.

4.3 Shear resistance results

4.3.1 Monotonic shear resistance results

The testing program included the measurement of the shear resistance of 76 under monotonically increasing load. The geometry and resistance values for each specimen are tabulated in Appendix A, B and C. Diagrams illustrating the load vs. deformation relationship of each test can be found in Appendix E.

4.3.1.1 Specimens with 6.4 mm thick underlying steel plates

Figure 4-13 shows the average shear resistance of 2-layer specimens per cold-formed steel sheet thickness. For 2-layer specimens with 16 gauge (1.52 mm) sheets, the underlying plate thickness to sheet steel thickness ratio was equal to 2.1 which is lower than the minimum requirement of 2.5 found in CSA S136. The results show that the measured shear resistance of the specimens consistently increases as the steel sheet thickness increases. The measured visible weld diameter did not vary with regard to the steel sheet thickness.

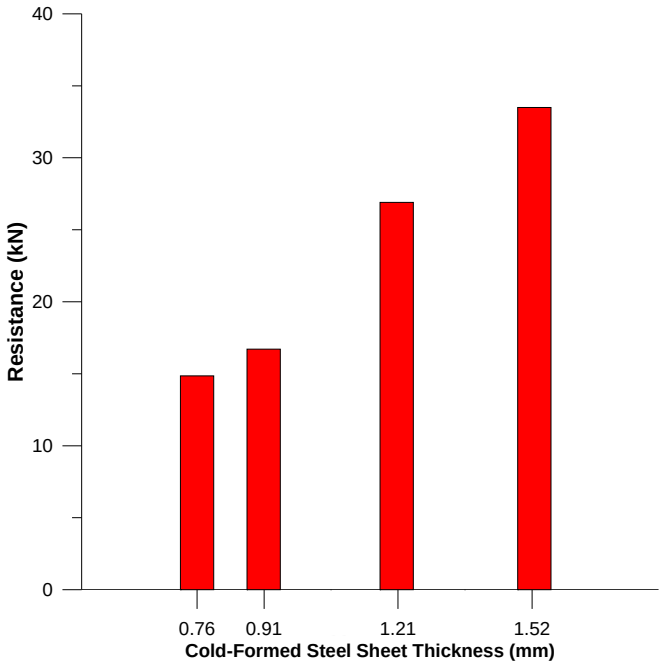

Figure 4.13 Average shear resistance of 2-layer specimens with 6.4mm underlying plate

The 2-layer specimens with 18 (1.21mm), 20 (0.91 mm) and 22 gauge (0.76 mm) sheet steel all failed by tearing of the steel sheet perpendicular to the applied load. These test specimens also exhibited out of plane warping on the compression side of the weld. The specimens with 16 gauge (1.52 mm) steel sheets failed due to sheet bearing failure (see Section 3.1.1). This failure is characterized by tearing of the sheet along the perimeter of the weld followed by ploughing of the weld nugget through the steel sheets. Tearing of the steel sheets occurred on lines parallel to the applied load.

The 4-layer configuration was used to test 16 specimens and gain insight into the behaviour of welds at locations where an end lap and a sidelap occur simultaneously. All 4-layer specimens present an underlying plate to sheet steel thickness ratio that is lower than the minimum requirement of 2.5 from CSA S136. Figure 4-14 illustrates that the average shear resistance of 4-layer specimens increases as the thickness of the steel sheets increases.

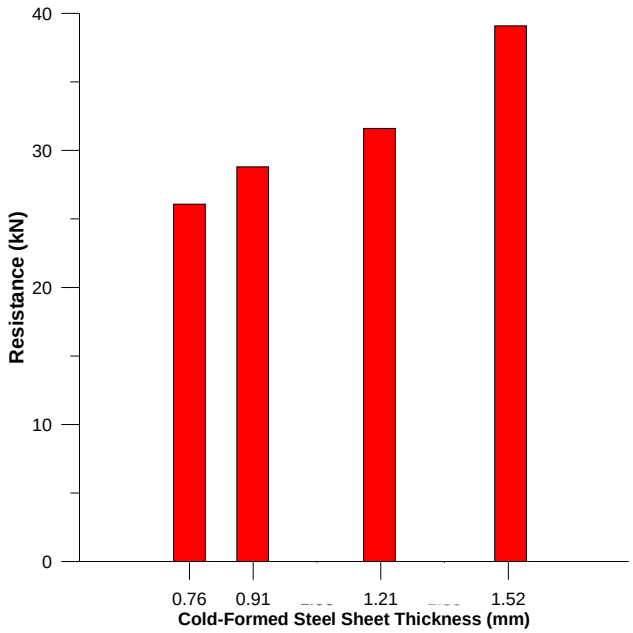

Figure 4.14 Average shear resistance of 4-layer specimens with 6.4mm thick underlying plate

Figure 4-14 also shows that the average resistance of the 4-layer specimens is higher than that of the 2-layer specimens with the same sheet steel thickness. The recorded average visible weld diameters are equal for 2-layer and 4-layer specimens. The 4-layer specimens with 16 (1.52 mm) and 18 (1.21 mm) gauge steel sheets all failed in a brittle manner by shearing through weld nugget. Figure 4-14 indicates that the 16 gauge specimens have a higher average resistance than the 18 gauge (1.21 mm) specimens even though the weld shear failure is a function of the effective weld area and not a function of the sheet thickness. In fact, the strength of the 16 gauge specimens should be less as the effective weld area should be smaller. The higher observed strength is caused by the fact that the measured average effective weld area of the 16 gauge (1.52 mm) specimens was on average 15 percent larger than the measured average effective weld area of the 18 gauge (1.21 mm) specimens. Two specimens fabricated with 18 gauge steel sheets had significant pitting and porosity therefore reducing the average effective weld area recorded where as no specimens fabricated with 16 gauge steel sheets showed significant pitting and porosity. The specimens with 20 (0.91 mm) and 22 (0.76 mm) gauge steel sheets failed in various modes

including plate tearing, plate bearing and weld shear, although plate bearing was the most common failure mode.

The testing program also included 16 specimens that were configured to represent a diaphragm perimeter connection. This configuration reproduces the loading condition that occurs at an end lap along the perimeter of a building. In this case, the weld must transfer the applied load from the two steel sheets to the 6.4 mm thick underlying hot-rolled steel plate. Figure 4-15 shows that for the specimens with 16 (1.52 mm) and 18 gauge (1.21 mm) steel sheets that are governed by weld shear failure, the thickness of the sheet steel does not influence the shear resistance of the specimens. Although it is expected that the effective weld area of the 16 gauge specimens should be smaller, the average measured effective weld area of the 16 gauge (1.52 mm) specimens is 7% higher than that of the 18 gauge (1.21 mm) specimens which explains the higher average resistance of the 16 gauge (1.52 mm) specimens. The average measured visible diameter was 4% larger for the 16 gauge (1.52 mm) specimens than for the 18 gauge (1.21 mm) specimens which can explain the slight difference in average measured effective weld area.

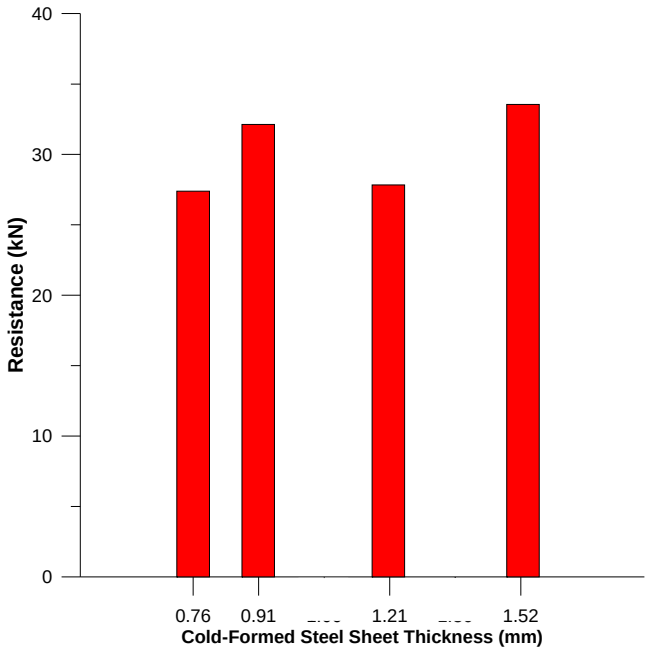

Figure 4.15 Average shear resistance of specimens in perimeter configuration with 6.4 mm thick underlying plate

4.3.1.2 Specimens with 3.2 mm thick underlying steel plates

The study also included 28 shear specimens comprised of an underlying plate thickness of 3 mm. The data recorded from these tests was used to investigate the effect of the underlying plate thickness on the shear strength of specimens with multi-overlap configurations. All specimens fabricated with a 3.2 mm thick underlying plate have an underlying plate to sheet steel thickness ratio that is lower than the minimum requirement from CSA S136. A series of tests were carried out with 2-layer and 4-layer configurations for each sheet metal thickness: 16 (1.52 mm), 18 (1.21 mm), 20 (0.91 mm) and 22 (0.76 mm) gauge. A total of 14 specimens were tested with a 2-layer configuration where the weld must transfer the applied load between the two steel sheets. The average measured visible diameter was equal for all steel sheet thicknesses. Similar to what was found for specimens with an underlying plate thickness of 6.4 mm, Figure 4-16 demonstrates that the average shear resistance of 2-layer specimens increases as the sheet thickness increases.

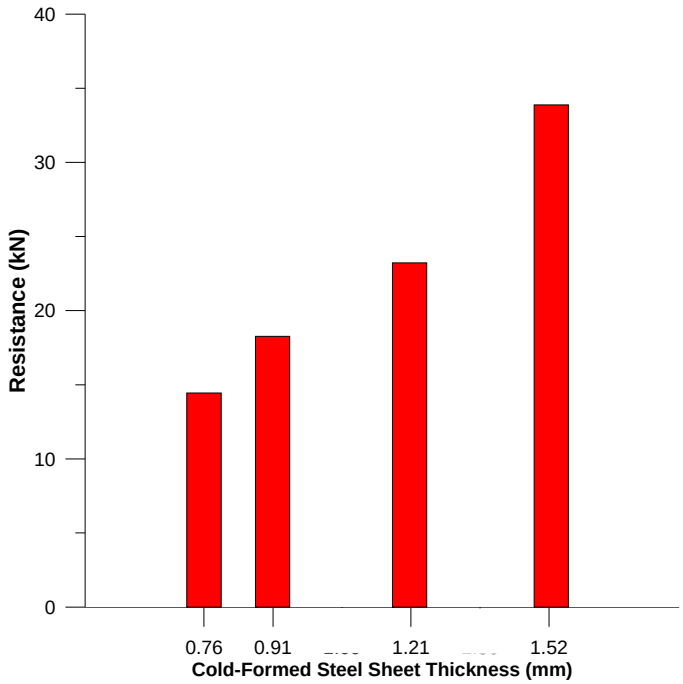

Figure 4.16 Average shear resistance of 2-layer specimens with 3.2mm thick underlying plate

As for the specimens with thicker underlying steel plates, the specimens with 18 (1.21 mm), 20 (0.91 mm) and 22 (0.76 mm) gauge steel sheets failed due to sheet tearing perpendicular to the applied load. The specimens with 16 gauge (1.52 mm) steel sheets failed due to weld shear through the weld nugget. These results suggest that the failure mode is not influenced by the thickness of the underlying steel plate within the scope of the plate thicknesses included in the test matrix. Moreover, Figure 4-17 shows that the underlying steel plate has no significant effect on the shear resistance. The average resistance of 2-layer specimens with an underlying plate thickness of 3 mm is similar to the average resistance of 2-layer specimens with an underlying plate thickness of 6.4 mm. Therefore, it can be concluded that the resistance of welds fabricated with multi-overlap configurations is not a function of the underlying plate thickness.

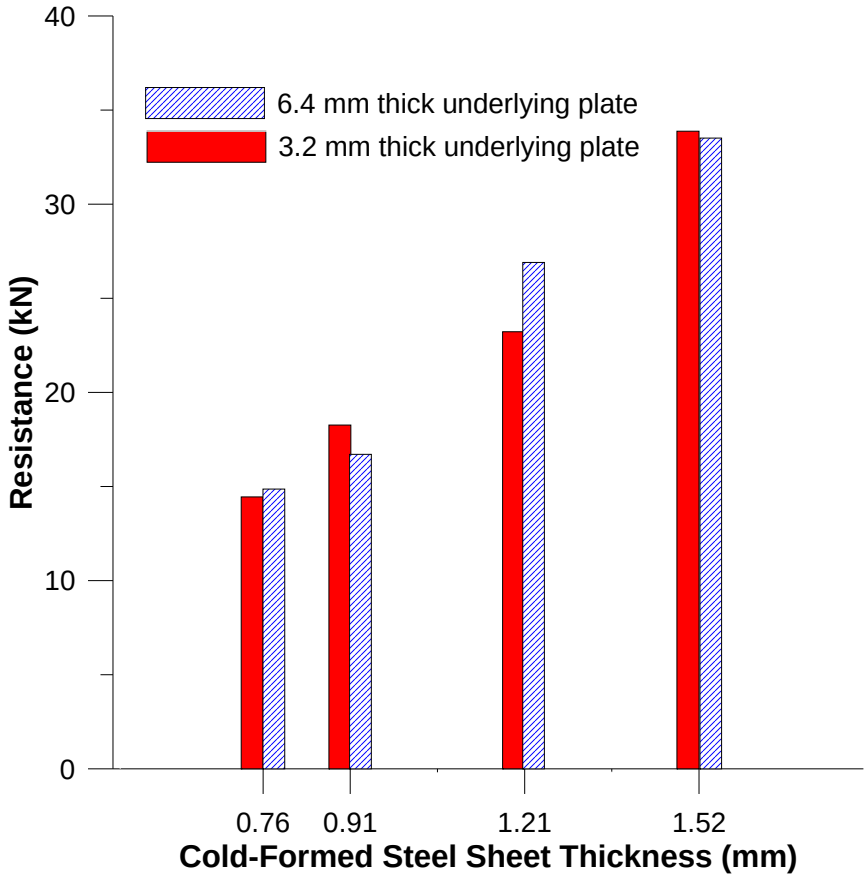

Figure 4.17 Average shear resistance of 2-layer specimens with 3.2mm and 6.4mm underlying plate thickness

A total of 14 specimens configured with 3 mm thick underlying plates and 4-layers of sheet steel were tested. The weld, in this case, is used to transfer the shear force from the two upper steel sheets to the two lower steel sheets. The results illustrated in Figure 4-18 show that the resistance of the specimens does not consistently increase as the thickness of the steel sheet plates increases. This is related to the failure mode engaged by the specimens. In fact, the specimens with 16 (1.52 mm) and 18 gauge (1.21 mm) steel sheets failed due to weld shear therefore their resistance is a function of the effective weld area and not a function of the steel sheet thickness. The resistance of the 16 (1.52 mm) and 18 gauge (1.21 mm) specimens are relatively equal as illustrated in

Figure 4-18 as the average measured effective weld area of the 16 gauge (1.52 mm) specimens is only 1% larger than the average measured effective weld area of the 18 gauge (1.21 mm) specimens. This can be explained as there was only a 1% difference in average measured visible weld diameter between the 16 gauge (1.52 mm) and 18 gauge (1.21 mm) specimens. The average resistance of the 20 (0.91 mm) and 22 gauge (0.76 mm) specimens is governed by various failure modes such as plate tearing perpendicular to the applied load and plate bearing that are a function of the steel sheet thickness.

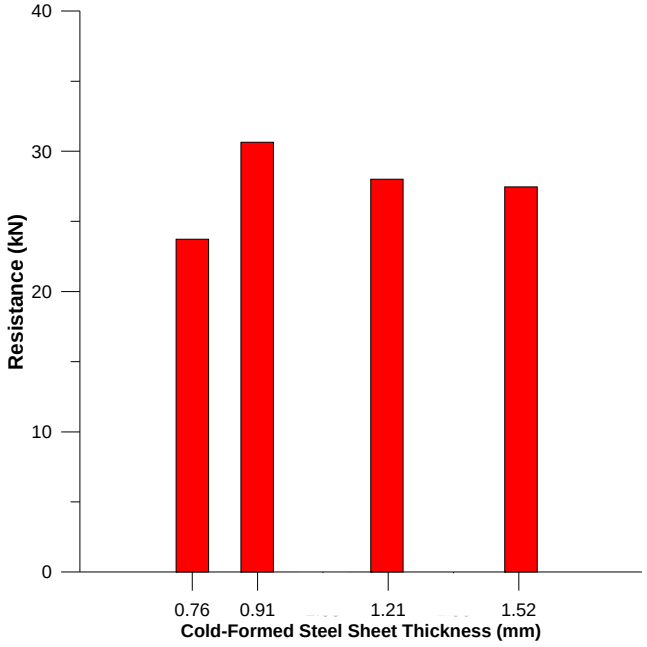

Figure 4.18 Average shear resistance of 4-layer specimens with 3.2mm thick underlying plate

Figure 4-19 compares the average shear resistance of the 4-layer specimens fabricated with 3.2 mm thick underlying plates to 4-layer specimens fabricated with 6.4 mm underlying plate. The results show that in most cases, the resistance of the specimen does not vary substantially when the thickness of the underlying material is changed. However, for the particular case of the 4-layer specimens fabricated with 16 gauge (1.52mm) material and 3.2 mm thick underlying plates, the average measured shear resistance is 32 percent lower than the average measured shear

resistance of the 4-layer specimens with 6.4 mm thick underlying plates. The measured effective weld area was 28% lower for specimens fabricated with 3.2 mm thick underlying plates. This difference is mainly due to the average measured visible diameter which is 13% lower for specimens fabricated with 3.2 mm thick underlying plates. As the average recorded welding time was 41% shorter for specimens with 3.2 mm thick underlying plates the smaller weld dimensions were to be expected. These results show that when the ratio of underlying material to total sheet steel thickness is lower than 0.5 (3.2/4 x 1.52 ≈ 0.5), the welder may experience more difficulty producing welds with consistent effective weld diameters, which can result in reduced connection strength as was seen in this study. These findings indicate that the requirement found in section E2.2a of CSA S136 where the minimum ratio of underlying material to total sheet steel thickness is 2.5 could be lowered. As mentioned in section 3.3 of this report, this is perhaps because the thicker underlying plate acts as a better heat sink.

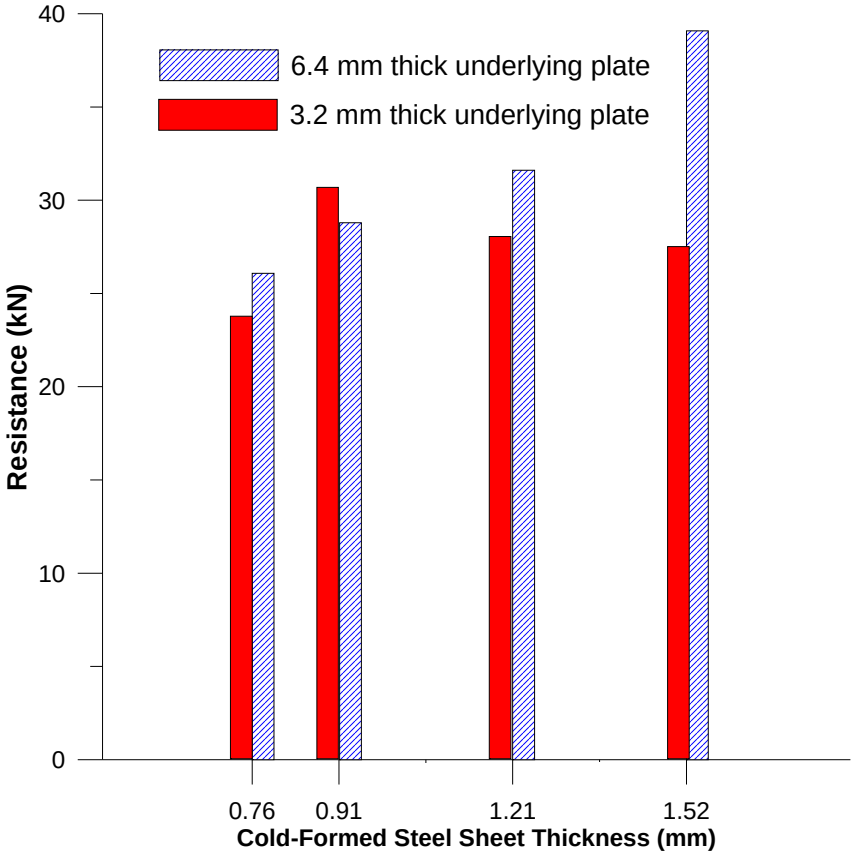

Figure 4.19 Average shear resistance of 4-layer specimens with 3.2mm and 6.4mm underlying plate thickness

4.3.2 Reversed cyclic shear resistance results

The research program also included a series of reversed cyclic shear resistance tests which were performed with 2-layer and 4-layer configurations having an underlying plate thickness of 6.4 mm. The 31 cyclic shear tests each consisted of three separate phases that are detailed in the Section 2.3.4 of this document. The geometry and resistance values for each specimen are tabulated in Appendix A, B and C. The diagrams associated with each cyclic shear resistance test are provided in Appendix F.

4.3.2.1 Phase 1 results

The first phase of the reversed cyclic test consisted of a series of load controlled cycles. The 6 first load controlled cycles were completed at a level equal to one third of the design factored resistance. These cycles were followed by 6 cycles at a level equal to two thirds of the design factored resistance and 12 cycles at a level equal to the design factored resistance as defined by CSA S136. The results shown in Appendix F, show that all specimens but one (Specimen No. SC1644) exhibited stable nearly elastic response up to and including in the cycles at the factored shear resistance level. This indicates that the resistance factors specified by CSA S136 are sufficiently conservative.

4.3.2.2 Phase 2 results

During the second phase of the reversed cyclic test, the specimen was loaded with a monotonically increasing load until failure occurred. The loading direction was then reversed and the specimen was loaded until failure occurred in the opposite direction. This particular phase of the cyclic resistance test was used to verify the ultimate resistance of specimens after having sustained several loading cycles at the factored design load level. The deformation, resistance and failure mode was recorded for each specimen and tabulated in Appendix A, B and C. During the cyclic tests, the measured shear resistance of a specimen is considered to be the maximum load sustained before the loading direction is reversed. The average measured resistance of the 2-layer specimens during phase 2 of the cyclic resistance tests is illustrated in Figure 4-20. The results demonstrate that even after sustaining several loading cycles at the design load level, the resistance of the 2-layer specimens is similar to the resistance of the 2-layer specimens measured during the monotonic shear resistance tests. In fact, the average ultimate shear resistance of the 2-layer specimens during phase 2 of the cyclic tests is only 6% lower than the resistance of the 2-layer specimens under monotonic loading.

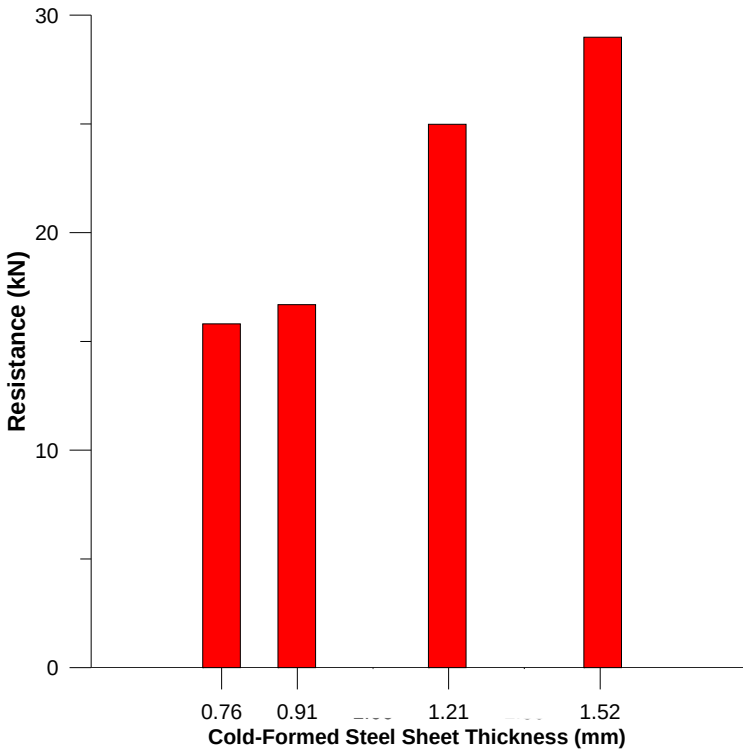

Figure 4.20 Average shear resistance of 2-layer specimens with 6.4mm underlying plate thickness during cyclic tests

During the cyclic tests, plate tearing perpendicular to the loading direction was the failure mode recorded for the 2-layer specimens fabricated with 18 (1.21 mm), 20 (0.91 mm) and 22 (0.76 mm) gauge steel sheets. The failure mode recorded for the 2-layer specimens with 16 gauge (1.52 mm) steel sheets was plate bearing during which plate tearing occurs along lines parallel to the loading direction. These failure modes are the same as those observed during the monotonic shear resistance tests.

A total of 16 cyclic shear tests were carried with 4-layer specimens. Figure 4-21 illustrates the average measured shear resistance of the 4-layer specimens recorded during phase 2 of the cyclic tests. The average measured shear resistance for all 4-layer specimens during phase 2 of the

cyclic shear resistance tests is 7% lower than the average shear resistance for all 4-layer specimens measured during the monotonic shear resistance tests.

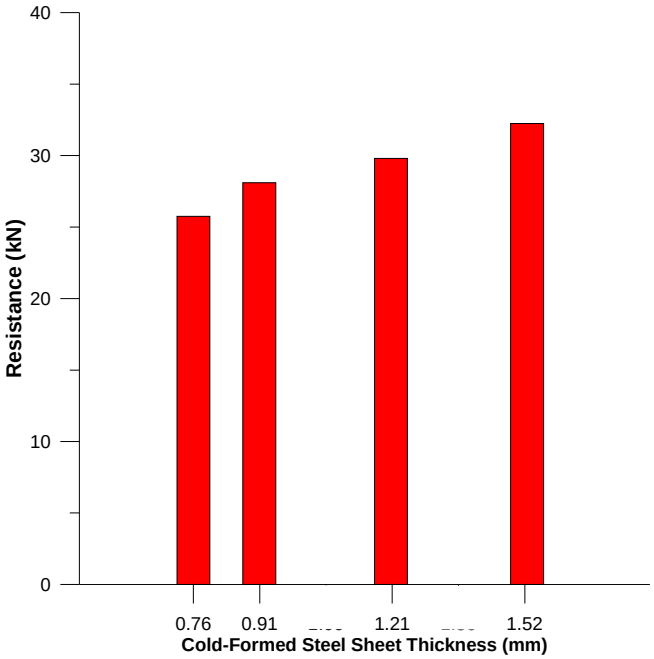

Figure 4.21 Average shear resistance of 4-layer specimens with 6.4mm underlying plate thickness during cyclic tests

As was the case during the monotonic shear resistance tests, the weld shear failure mode governed for the 4-layer specimens with 16 (1.52 mm) and 18 gauge (1.21 mm) steel sheets. All three failure modes were observed for the 4-layer specimens with 20 (0.91 mm) and 22 gauge (0.76 mm) steel sheets. For the 2 and 4-layer configurations, differences between specimens were observed in the post-peak region and for the remaining of the tests according to the failure mode: when sheet bearing mode was engaged the specimens could exhibit significant ductility, i.e., maintaining most of their capacity upon load reversal in phase 2. This difference can be seen in Fig. 4.22, with the behaviour of the specimen illustrated in Fig.4.22a being more ductile than the one illustrated in Fig.4-22b. During the load reversal of phase II, the ductile specimens (bearing

failure mode) could develop, on average, 74% of the peak capacity reached in the previous half-cycle. For the other specimens, that percentage reduces to 66%.

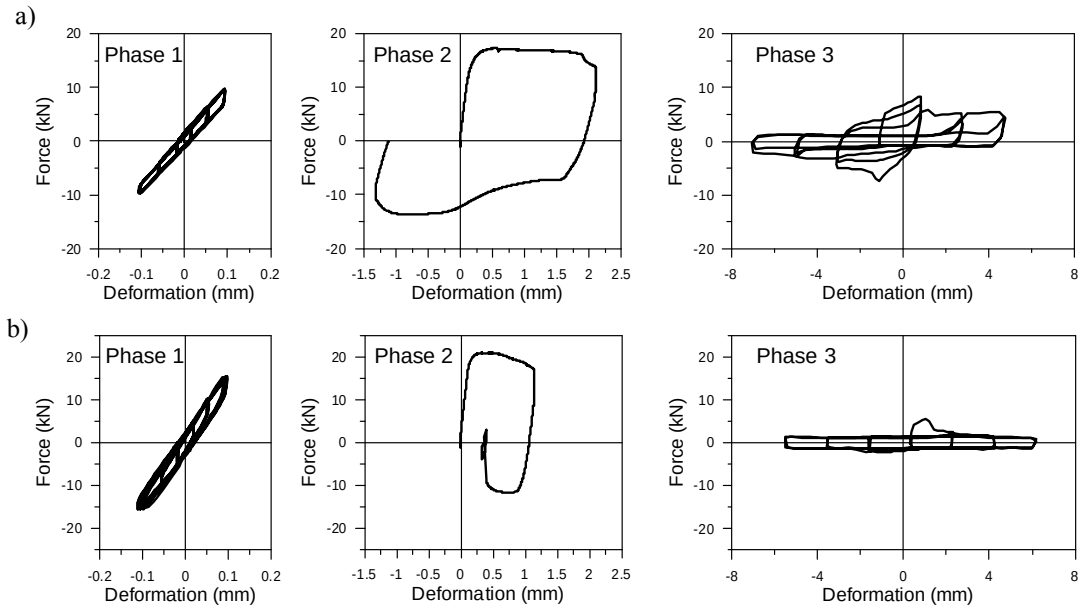

Figure 4.22 Cyclic load-deformation response of two-layer shear specimens: a) No. SC2021; b) No. SC1841

4.3.2.3 Phase 3 results

The third phase of the cyclic shear resistance tests consisted of a series of displacement controlled cycles. The amplitude of the two first cycles was 2 mm; this was followed by two cycles at 4 mm and two more cycles at 6 mm. The goal of this phase was to observe the behaviour of the specimens when large displacements were imposed after failure of the connection had occurred. The results show that the specimens were able to sustain such large displacements while still providing some resistance only if failure was due to sheet bearing. When the connections failed due to sheet tearing perpendicular to the applied load, the specimen would exhibit some resistance during the first two cycles before definite rupture occurred. When specimens failed due

to shearing through the weld nugget, no significant resistance was recorded during the post-failure displacement controlled cycles.

4.3.3 Analysis of shear resistance equations from CSA S136

The results of the 76 shear specimens are used to validate the CSA S136 equations. The results of the shear test under cyclic loading are discussed next. The tests resistance of multi-overlap specimens is governed by different factors according to their failure mode. For specimens with a failure mode related to weld fracture, the resistance of the specimen is governed by the effective diameter of the weld. When the failure mode is related to sheet failure, the thickness of the steel sheets above the plane of maximum shear, and the visible weld diameter influence the resistance of the specimen. As discussed previously, the thickness of the underlying plate does not influence the resistance of the weld although it may influence the fabrication parameters for the weld during the fabrication.

When considering the 33 shear specimens where weld failure occurred, the comparison of the measured effective weld diameter with the values predicted by Equation E2.2.1-5 from CSA S136 yielded an average measured-to-predicted ratio of 1.13 with a coefficient of variation of 0.15 (Appendix D). Equation E2.2.1-5 then accurately predicts the effective weld diameter for the range of t/d_{vis} ratio corresponding to the shear specimens ($0.06 < t/d_{vis} < 0.2$). The predicted values were calculated using the measured weld diameter and the nominal electrode strength. It is important to note that for sidelap specimens the shear plane is located at the mid-thickness of the combined steel sheets; that is, the design thickness (t_d) used to compute the predicted values was equal to one half of the total thickness (t) typically used. For specimens with a perimeter configuration, the design thickness (t_d) used to compute the predicted values was equal to the total thickness (t) because the shear plane of this configuration is located between the steel sheets and the underlying steel plate as explained in Chapter 3 of this report. Equation E2.2.1-1 of CSA S136 (2007) was used to evaluate the resistance of the connection specimens with regard to the weld shear failure mode. Using, the nominal tensile strength of the weld metal (F_{xx} = 430 MPa)

and the effective weld diameter measured during the tests, the average measured-to-predicted resistance ratio for the shear specimens that failed due to weld fracture is 1.42 with a coefficient of variation of 0.15. This trend is similar to that obtained by Peköz and McGuire who reported an average test-to-predicted ratio of 1.22 with a coefficient of variation of 0.30 for similar tests. Equation E2.2.1-1 is plotted in Fig. 4.23 along with the data recorded during the experimental program and the data reported by Peköz and McGuire.

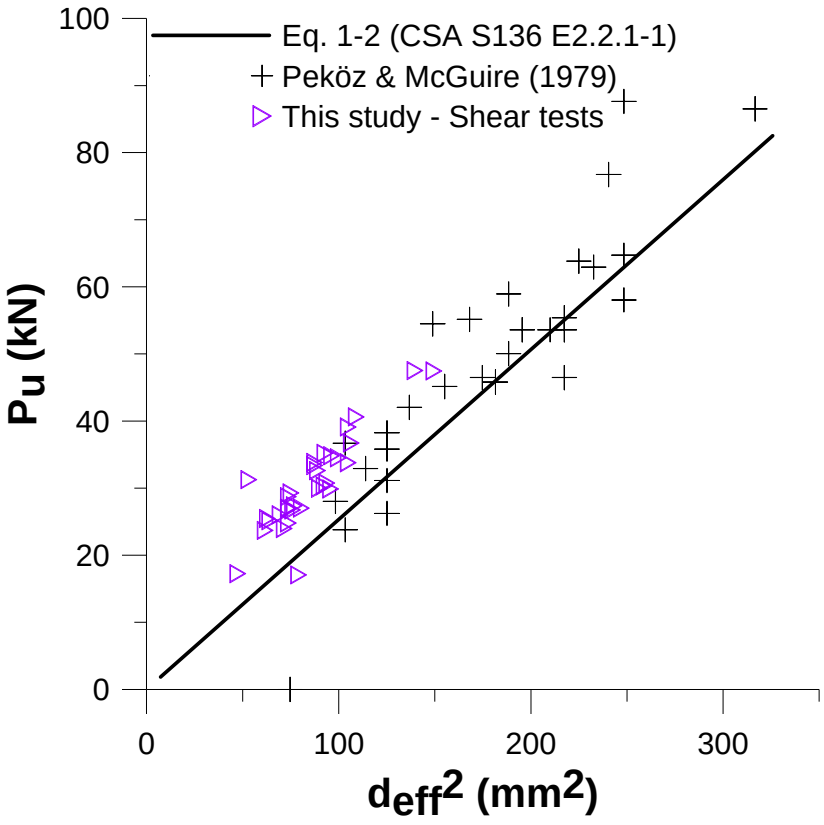

Figure 4.23 Plot of E2.2.1-1 and available data

The comparison shows that Equation E2.2.1-1 consistently under-predicts the shear capacity of welded conditions for the range of d_{eff} examined. This is likely caused by the difference between

the actual and nominal values of the tensile strength of the weld metal. It is difficult to measure the actual tensile strength of the weld metal in test specimens as it can vary significantly over the weld failure plane. This property was not measured in this test program. Anecdotal information, however, has shown that the actual tensile strength of virgin electrodes can be as much as 30% higher than the nominal value. The results show that Equation E2.2.1-1 can safely be used to determine the shear resistance for arc spot weld failures in multi-overlap configurations.

The ultimate resistance measured for specimens that failed due sheet failure was compared with the values predicted by Equations E2.2.1-2 to E2.2.1-4. Of all monotonic shear specimens, 35 were governed by Equation E2.2.1-2 because $(d_a/t) \leq 0.815\sqrt{E/F_u}$. Figure 4-24 presents a plot of Equations E2.2.1-2 to E2.2.1-4 from CSA S136 (2007) with the results recorded from the 35 specimens whose predicted resistance was governed by Equation E2.2.1-2 according to their d_a/t ratio. The data reported by Peköz and McGuire (1979) and Easterling (2009) are also presented in Figure 4-24.

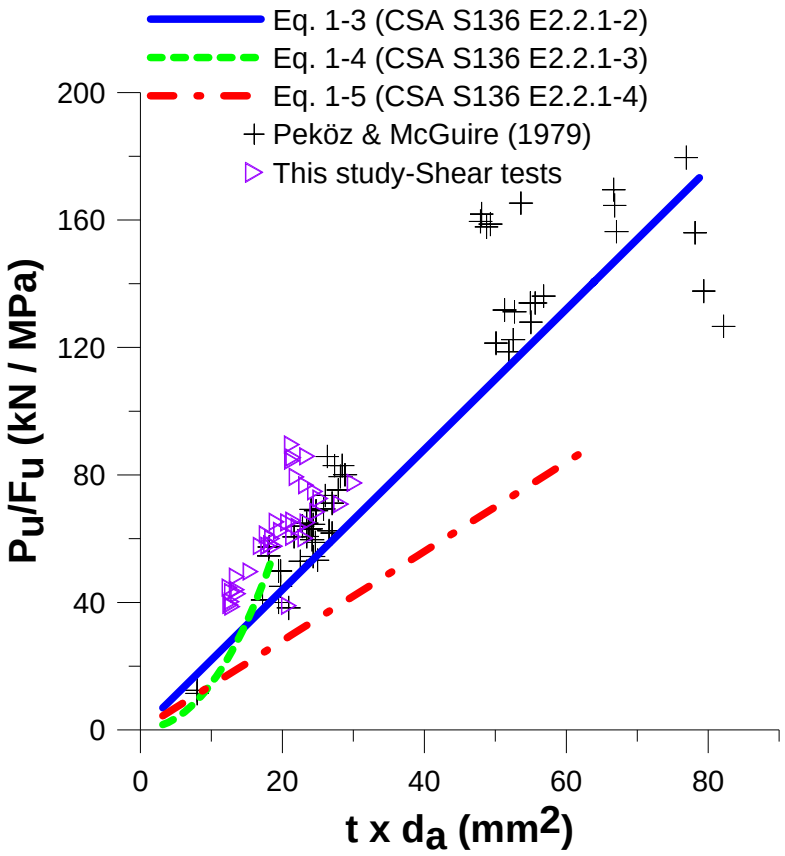

Figure 4.24 Plot of available data governed by E2.2.1-2 according to d_a/t

A trend can be observed where the measured resistance values are generally higher than the predicted resistance values. The average measured-to-predicted resistance ratio was 1.44 with a coefficient of variation of 0.14 (Appendix D) for this group of specimens during this experimental program. Likewise, Peköz and McGuire (1979) reported an average measured-to-predicted resistance ratio of 1.15 with a coefficient of variation of 0.17 while Easterling and Snow reported a ratio of 1.28 with a coefficient of variation of 0.09 for specimens where $(d_a/t) \leq 0.815\sqrt{E/F_u}$. The difference between the three ratios recorded may be attributed to the differences in weld quality. Although this data was not recorded, some specimens may not have efficient connectivity along the entire perimeter of the weld which would inevitably lower

the resistance of the specimen. When analysing the data collected during this experimental program the best fit formula was found to be:

$For\ (d_a/t) \leq\ 0.815\sqrt{E/F_u}$:

$$P_u = 2.40td_aF_u \qquad (4-4)$$

This new proposed equation was analyzed in accordance with Section F.1 of CSA S136 (2007) which specifies the statistical treatment to determine the structural performance for limit states design. When comparing the data obtained during this testing program with Equation 4-4, the average measured-to-predicted ratio was 1.32 with a coefficient of variation of 0.14 (Appendix D). When using these values, the minimum required reliability index of 4.0 can be attained with a resistance factor $\phi = 0.6$.

A total of 8 specimens were governed by Equation E2.2.1-3 because $0.815\sqrt{E/F_u} < (d_a/t) < 1.397\sqrt{E/F_u}$. The average measured-to-predicted resistance ratio for specimens governed by equation E2.2.1-3 was 1.58 with a coefficient of variation of 0.04 (Appendix D). The data measured in this study and the data reported by Peköz and McGuire are compared to the predicted values in Figure 4-25.

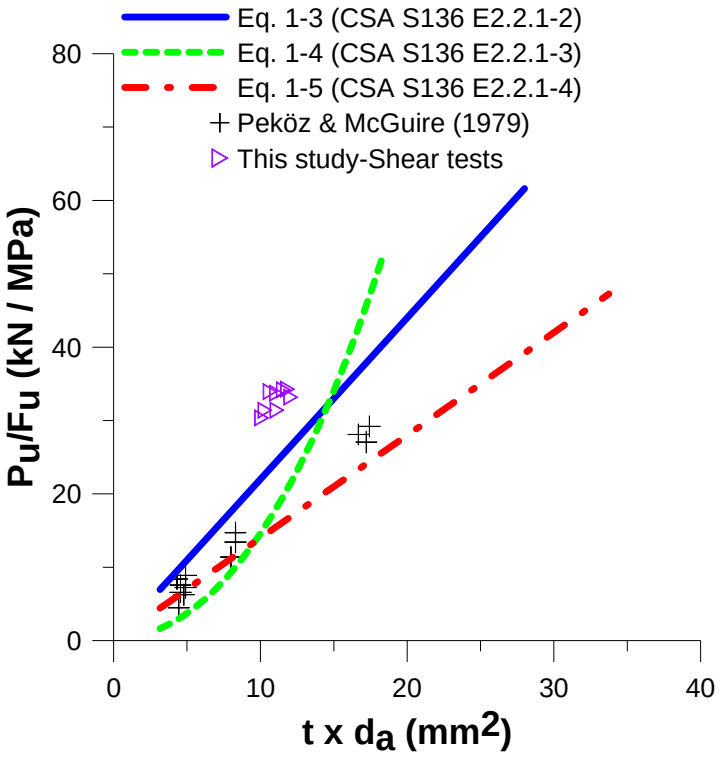

Figure 4.25 Plot of available data governed by E2.2.1-3 according to d_a/t

Equation E2.2.1-3 generally underestimates the resistance values of the specimens tested during this experimental program. However, too few specimens were governed by this equation during the testing program to warrant the modification of the current CSA S136 equation. Further research targeting this specific range of specimens should however be carried out to validate the accuracy of Equation E2.2.1-3. Finally the results recorded during the study suggest that Equations E2.2.1-3 can safely be used to predict the shear resistance of specimens with multi-overlap configurations where $0.815\sqrt{E/F_u} < (d_a/t) < 1.397\sqrt{E/F_u}$. Of all the specimens tested during this experimental program, none presented a d_a/t ratio indicating that Equation E2.2.1-4 would govern. As no new data was gathered during this study no suggestions can be made towards Equation E2.2.1-4.

4.4 Tension resistance results

The tensile resistance of 72 specimens was evaluated during the testing program. Each tension specimen was loaded with a monotonically increasing load and the resistance, deformation and failure mode were recorded. The geometry and resistance values for each specimen are tabulated in Appendix A, B and C. Diagrams illustrating the load *vs.* deformation relationship of each test can be found in Appendix H.

4.4.1 Specimens with 6.4 mm thick underlying angles

The testing program included 30 tensile resistance tests for 2-layer and 4-layer configurations welded to a 6.4 mm thick underlying angle. The results for the 2-layer specimens, illustrated in Figure 4-26, show that the resistance of the specimens increases as the thickness of the steel sheets increases. This can be explained because all 2-layer specimens with a 6.4 mm thick underlying angle failed due to sheet tearing along the contour of the weld. Therefore, the resistance of all 2-layer specimens is function of the steel sheet thickness. For 2-layer specimens with 16 gauge (1.52 mm) sheets the underlying plate to sheet steel thickness ratio was lower than the minimum specified by CSA S136.

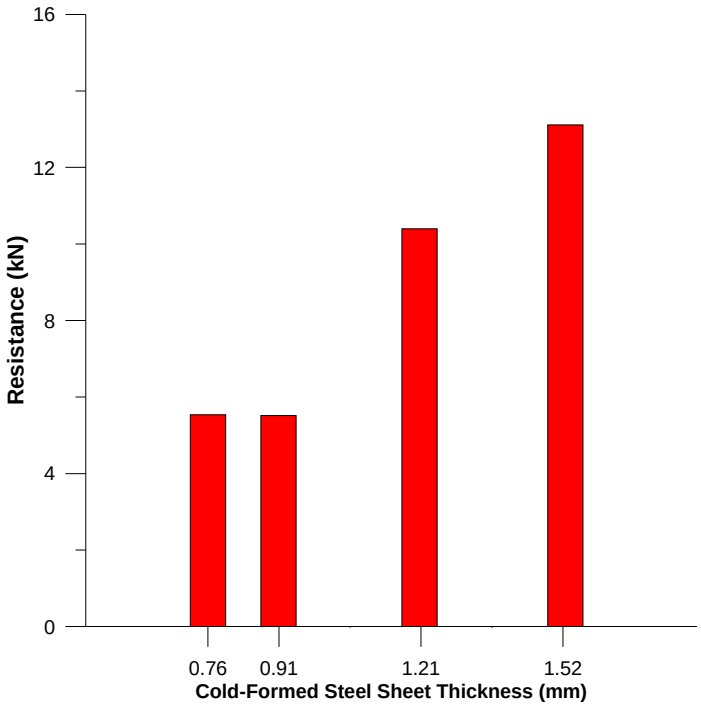

Figure 4.26 Average tensile resistance of 2-layer specimens with 6.4 mm thick underlying angles

The 4-layer specimens fabricated with 18 (1.21 mm), 20 (0.91 mm) and 22 (0.76 mm) gauge steel sheets all failed due to sheet tearing along the contour of the weld. For the specimens with 16 gauge (1.52 mm) steel sheets, the failure occurred by weld fracture through the weld nugget. All 4-layer specimens presented an underlying plate to steel sheet thickness ratio that was lower than the minimum requirement from CSA S136. The average measured resistances of 4-layer specimens fabricated with 6.4 mm thick underlying angles are illustrated in Figure 4-27. The results indicate that when sheet tearing failure is the controlling limit state, the resistance of the specimens increase as the thickness of the sheet steel increases.

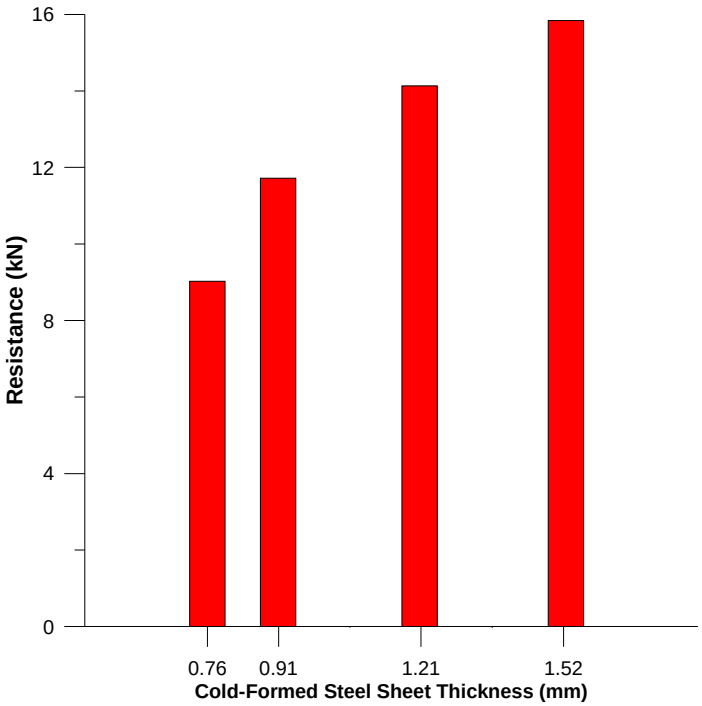

Figure 4.27 Average tensile resistance of 4-layer specimens with 6.4mm thick underlying angles

A total of 15 1-layer specimens were also tested to verify the tension capacity of arc-spot welds fabricated through a single layer of sheet steel. All 1-layer specimens failed due to sheet tearing around the contour of the weld. The average resistance of the specimens according to the sheet steel thickness is illustrated in Figure 4-28.

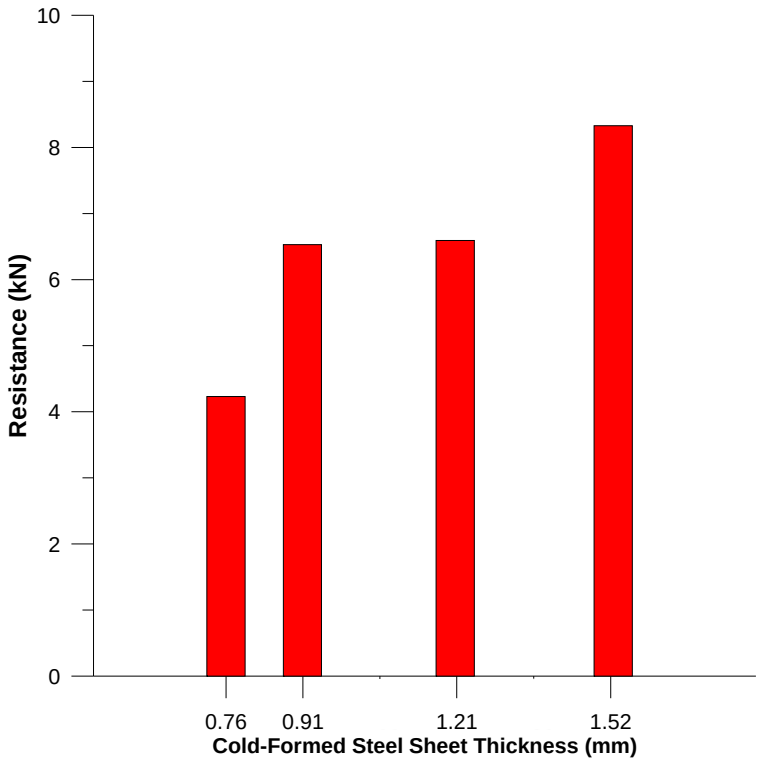

Figure 4.28 Average tensile resistance of 1-layer specimens with 6.4 mm underlying angles

The results show that the average tensile resistance of the 1-layer specimens increases as the sheet steel thickness increases.

4.4.2 Specimens with 3.2 mm thick underlying angles

The testing program also included a series of tests performed on specimens with 3 mm thick underlying angles to verify the effect of thinner framing elements on the tensile resistance. A total of 27 tests were completed with 2-layer and 4-layer configurations. All specimens fabricated with 3.2 mm thick underlying plates presented an underlying plate to sheet steel thickness ratio that was lower than the minimum specified in CSA S136. Similar to what was observed for specimens with 6.4 mm thick underlying angles, the results for the 2-layer specimens with 3.2 mm thick underlying plates, illustrated in Figure 4-30, show that the resistance of the specimens

increases as the thickness of the steel sheets increases. The results of the 2-ply specimens with 6.4 mm thick underlying steel angles and the 2-ply specimens with 3.2 mm thick underlying steel angles are compared in Figure 4-31. The diagram shows that for specimens with 16 (1.52 mm) and 18 (1.21 mm) gauge steel sheets, a decrease in resistance is observed when 3.2 mm thick underlying angles are used. This is likely caused by the rotation of the angle support due to the applied load. As the applied load increases the 3 mm thick underlying angle tends to deform as illustrated in Figure 4-29 causing stress concentrations along the perimeter of the weld thereby reducing the tension resistance of the arc spot weld. Such deformations did not occur with the 6.4 mm thick underlying angles.

Figure 4.29 Deformation of 3.2 mm thick angle under applied load

Moreover, for 16 (1.52 mm) and 18 (1.21 mm) gauge specimens fabricated with 3.2 mm thick underlying angles the average measured visible weld diameter is 17% smaller and the average welding times is 23 % shorter than for specimens fabricated with thicker underlying angles.

These results are in accordance with what was found during the shear resistance testing and are likely because the thicker underlying angle acts as a better heat sink than the thinner underlying angle.

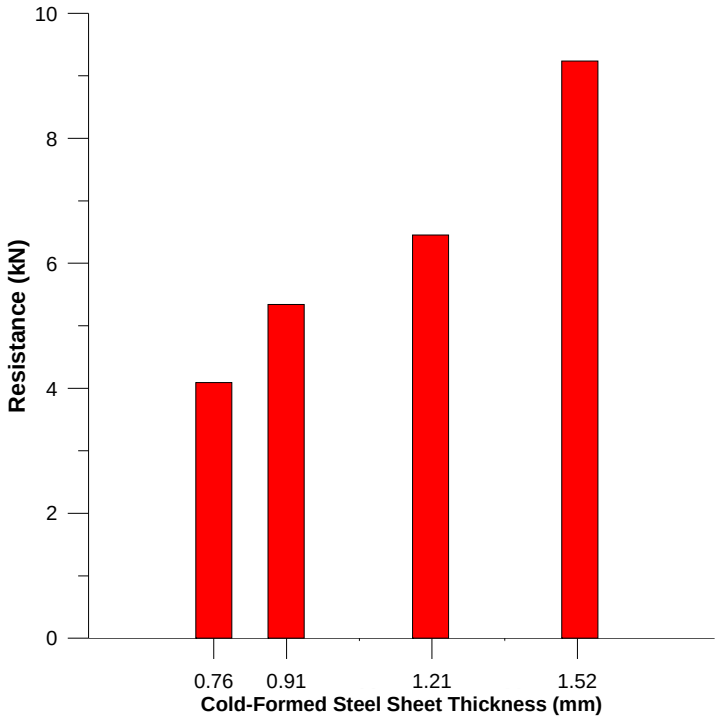

Figure 4.30 Average tensile resistance of 2-layer specimens with 3.2 mm thick underlying angles

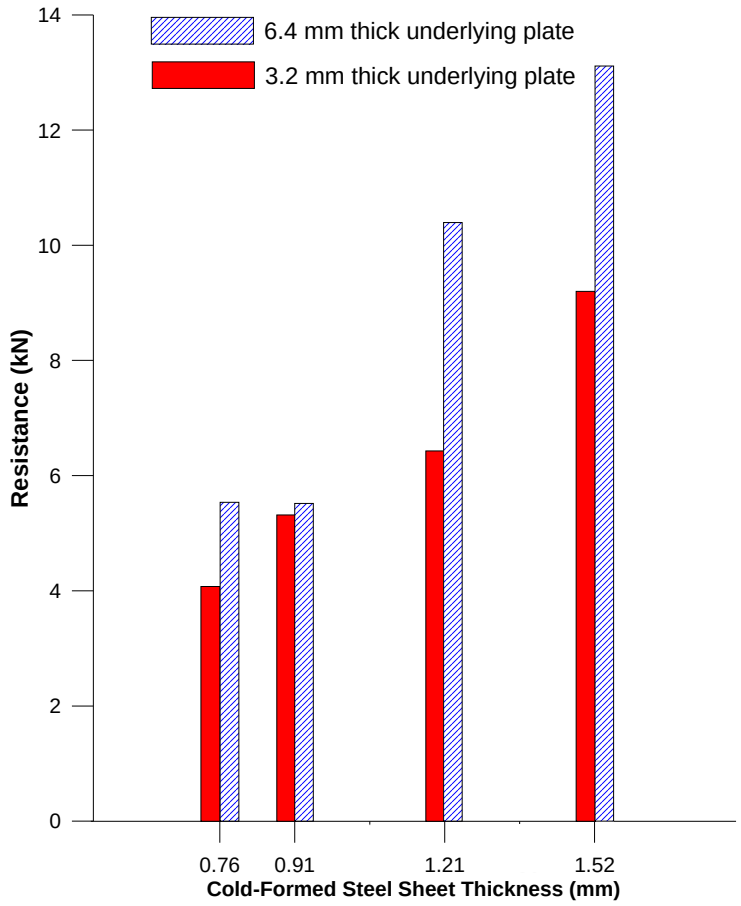

Figure 4.31 Average tensile resistance of 2-layer specimens with 3.2 mm and 6.4 mm thick underlying angles

Figure 4-32 shows the average tensile resistance of the 4-layer specimens with 3.2 mm thick underlying steel angles. It can be observed that the resistance increases as the sheet steel thickness increases for specimens with 20 (0.91 mm) and 22 (0.76 mm) gauge steel sheets which failed due to sheet tearing along the contour of the weld. For specimens with 16 (1.52 mm) and 18 (1.21 mm) gauge steel sheets that failed due to weld failure, the resistance is not a function of the sheet steel thickness but a function of the effective weld area. The average measured effective weld area of specimens with 18 gauge (1.21 mm) steel sheets was 25% higher than the effective weld area of specimens with 16 gauge steel sheets which explains the higher resistance of the

specimens with 18 gauge (1.21 mm) steel sheets. These results are in accordance with the results obtained during the shear resistance tests and provide more evidence that welder may experience difficulty producing quality welds through 4 layers of 16 gauge (1.52 mm) steel sheets if the underlying angle does not provide an adequate heat sink because it is too thin. The difference in average measured resistance of 4-layer specimens fabricated with 3.2 mm and 6.4 mm thick underlying angles is represented in Figure 4-33. As was the case with the 2-layer specimens, a decrease in resistance can be observed for the specimens with 3.2 mm thick underlying steel angles when compared to the specimens with 6.4 mm thick underlying steel angles. This is likely caused by the stress concentrations around the contour of the weld originating from large deformations of the thinner underlying angles and because the thicker underlying angles act as a better heat sink, which facilitates better quality and larger arc-spot welds. These results suggest that the underlying steel thickness should be thick enough to avoid large deformations of the supporting member. For most applications, ass demonstrated in this study, an underlying plate thickness of 6.4mm is sufficient to avoid these large deformations.

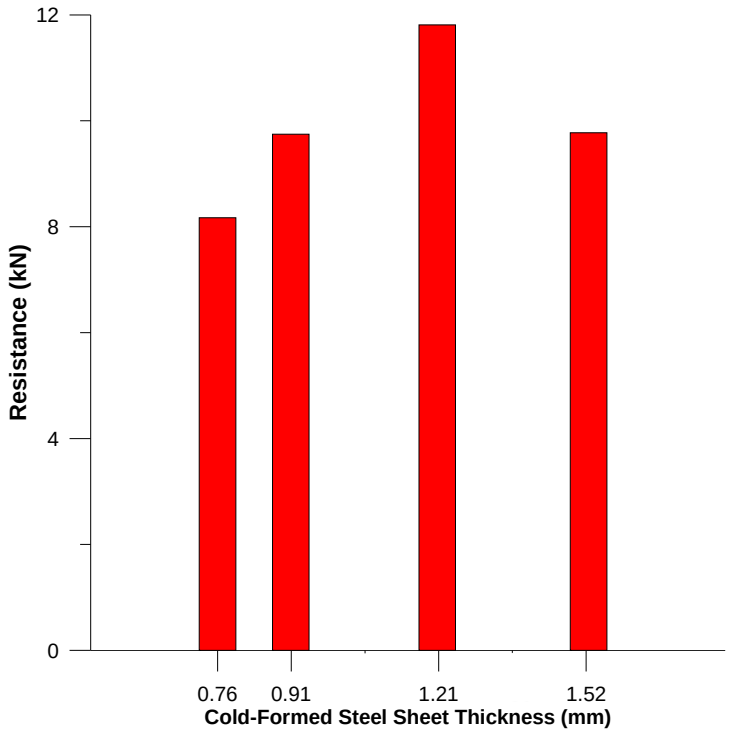

Figure 4.32 Average tensile resistance of 4-layer specimens with 3.2mm thick underlying angles

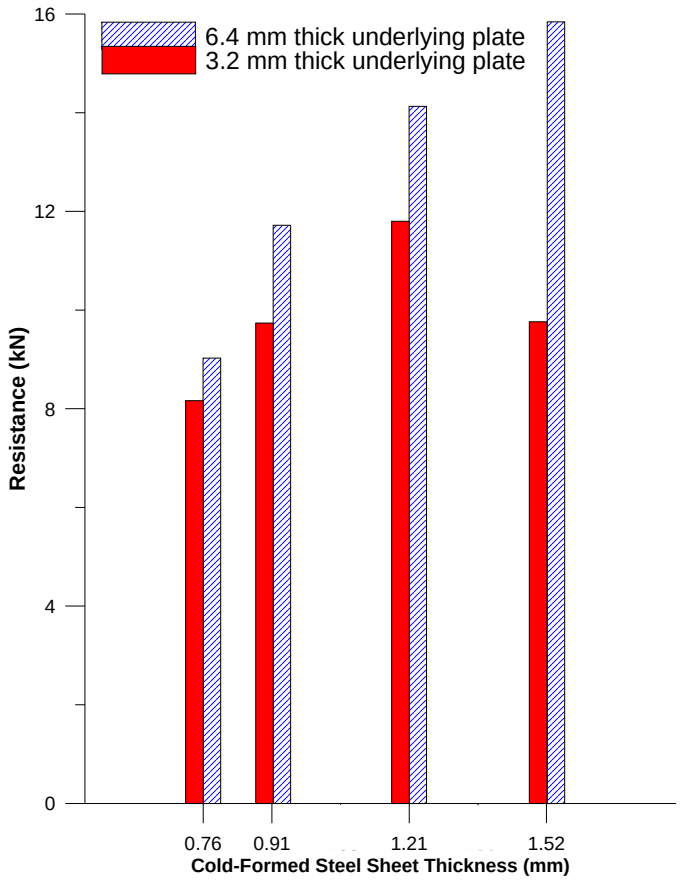

Figure 4.33 Average tensile resistance of 4-layer specimens with 3.2mm and 6.4mm thick underlying angles

4.4.3 Analysis of tension resistance equations from CSA S136

Section E2.2.2 of CSA S136 (2007) is used by designers to determine the tensile resistance of arc-spot welds. As was the case for the shear resistance of these welds a distinction was made between the specimens that failed due to weld fracture and those that suffered from sheet failure. During the experimental program a total of 40 tension specimens with 2-layer and 4-layer configurations failed due to sheet failure. Equation E2.2.2-2 of CSA S136 (2007) predicts the tensile resistance of specimens when sheet failure is involved. Section E2.2.2 also specifies that

the tensile resistance of arc-spot welds fabricated in sidelap configurations should be reduced by 30%. Figure 4-33 illustrates Equation E2.2.2-2 with and without the 30% reduction in capacity. The results obtained during the testing program are also plotted in Figure 4-34.

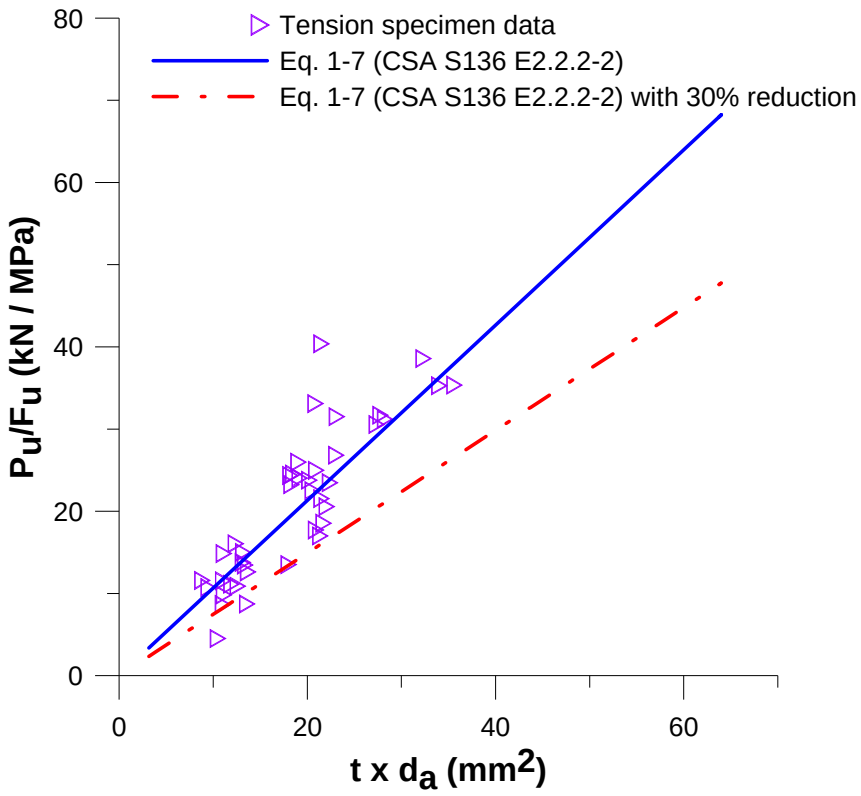

Figure 4.34 Plot of Eq. E2.2.2-2 with tension specimens that failed due to sheet tearing

The average measured-to-predicted resistance ratio was equal to 1.67 with a coefficient of variation of 0.28 (Appendix D) when the measured values were compared with the reduced resistance values specified in Section E2.2.2 of CSA S136 (2007). The measured visible weld diameter, actual yield and ultimate tensile strength and the measured thickness (Table 3-1) were used to determine the predicted values. It must also be noted that for sidelap configurations the thickness (t) used in Equation E2.2.2-2 was equal to half of the total thickness as failure always occurs at the mid-thickness of the steel sheets. This approach was also used by LaBoube and Yu

(1991) and should be specified in CSA S136 . The measured-to-predicted ratios recorded during this study are greater than those recorded by LaBoube and Yu . This is likely because the resistance of the lapped specimens tested by LaBoube and Yu varied according to the unstiffened flange length provided for the specimen which was sometimes very small compared to the visible weld diameter as explained in Section 1.5 of this text. During this study, the unstiffened flange length was greater than the visible weld diameter for all specimens which can explain the higher resistance values measured. The results from this research suggest that the 30% reduction in resistance specified in Section E2.2.2 of CSA S136 (2007) should not apply to Equation E2.2.2-2. Moreover, to produce sound welds, the unstiffened flange length provided should be greater than or equal to the visible weld diameter (Section 1.5). When compared with Equation E2.2.2-2 (not reduced) the average measured-to-predicted ratio of the specimens tested during this study was 1.17 with a coefficient of variation of 0.28 (Appendix D). According to theses values and the statistical treatment specified by Section F.1 of CSA S136 (2007), the resistance factor must be lowered from 0.5 to 0.38.

Equation E2.2.2-1 of CSA S136 (2007) is used to determine the tensile resistance of arc-spot welds when weld failure is involved. During the testing program, a total of 16 tension specimens failed due to weld fracture. The resistance of such specimens is related to the effective weld diameter of each specimen. Figure 4-34 contains a plot of Equation E2.2.2-1 a reduced resistance equation where Equation E2.2.2-1 is reduced by 30%. The results obtained during the testing program and the data reported by LaBoube and Yu are also shown. The resistance values obtained from the tested specimens are plotted twice, once with the effective weld diameter measured during the tests and once with the effective weld diameter calculated using Equation 4-3. In both cases, the thickness (t) used to determine the effective weld diameter is equal to the total thickness of sheet steel from the specimen because the failure plane is located between the steel sheets and the underlying steel angle.

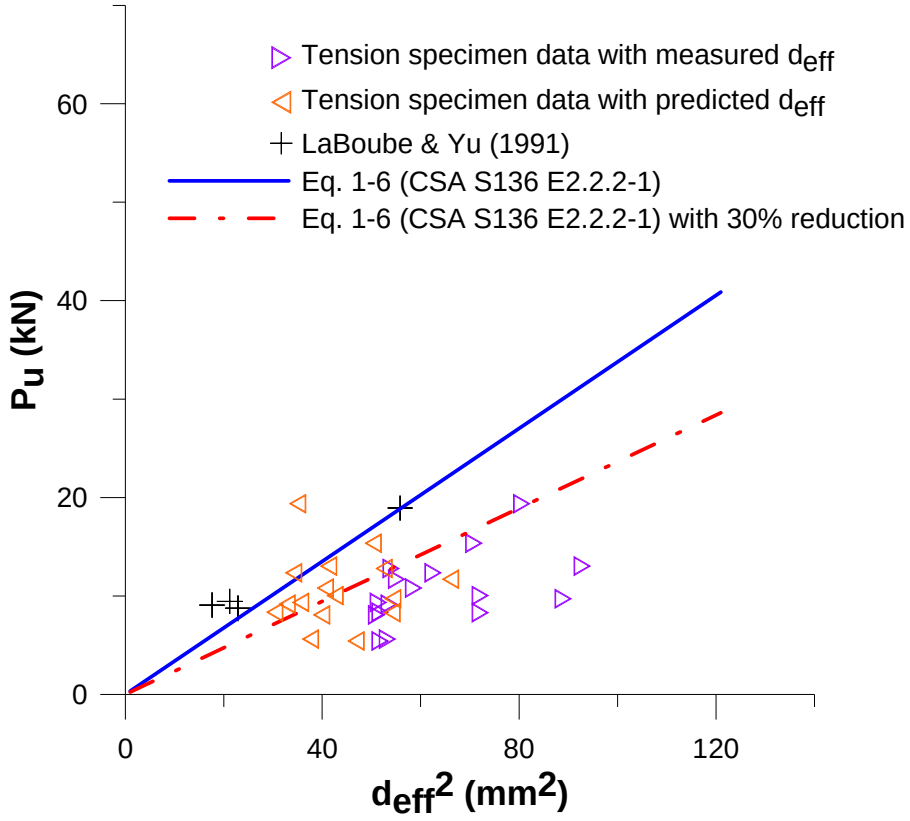

Figure 4.35 Plot of Eq. E2.2.2-1 with data available for specimens that failed due to weld fracture

Figure 4.35 shows that the best fit is obtained when using Equation 4.3 to predict the effective weld diameter. The average measured-to-predicted ratio was equal to 0.75 when using the measured effective weld diameter. When applying a 30% reduction, that ratio increases to 1.08 with a coefficient of variation of 0.27 when the effective weld diameters are determined using Equation 3. This suggests that the 30% reduction in resistance should be maintained when determining the tensile resistance related to weld failure. This 30% reduction in resistance should also be applied to welds that are not fabricated in multi-overlap configurations because there is no evidence that the multi-overlap configuration reduces the capacity of welds when tensile weld failure is involved. For simplicity equation E2.2.2-1 should be modified to:

$$P_n = \frac{\pi d_e^2}{4} 0.7 F_{xx} \qquad (4-5)$$

This equation should apply to all arc-spot welds without considering the sheet steel configuration. When the statistical treatment of Equation 4-5 is carried out according to Section F.1 of CSA S136 using the measured-to-predicted ratio of 1.08 and the coefficient of variation of 0.27 then the resistance factor must be lowered to 0.31 to attain the required reliability index of 4.0.

CHAPTER 5. CONCLUSION AND RECOMMENDATIONS

The results of the 179 tests permitted the evaluation of various aspects of arc-spot welds fabricated in multi-overlap configurations. The first objective of this research was to determine a welding procedure to consistently produce quality arc-spot welds through several layers of thick steel sheets. Through several welding sessions it was determined that there are three important factors that must be controlled to provide quality arc-spot welds in multi-overlap configurations; type of electrode (E6011), high current setting (±200 Amps) and proper welding technique. It must also be noted that during the study welds were fabricated in conditions where the gap between the sheets was essentially zero. Earlier studies (Fung 1978) have shown that gaps between sheets can have an adverse effect on the resistance of arc spot welds. The arc time required to fabricate each weld was recorded during the experimental program. The results show that the amount of time necessary to fabricate the weld increases as the total thickness of sheet steel increases because the weld must pierce through more material before depositing the weld metal. The results obtained during this study support those obtained by Easterling and Snow (2009) that suggest welding times recommended by the SDI Manual (2004) of 3 to 6 seconds to fabricate 19 mm welds should be increased when using 1/8 in. electrodes especially for welds fabricated with multi-overlap configurations. Moreover, the results indicate that more time is required to fabricate welds with thicker underlying steel plate because the thicker steel plates act as a greater heat sink.

As part of this research project, the visible diameter of each weld was recorded prior to testing. It was also possible to measure the net effective weld diameter of specimens that experienced weld failure. These results were compared with the net effective weld diameter values predicted by Equation E2.2.1-5 from CSA S136. The comparison showed that when the thickness as the total thickness of sheet steel increases Equation E2.2.1-5 becomes excessively conservative. The results demonstrate that a lower limit for the net effective weld diameter should be imposed in

order to improve the precision of Equation E2.2.1-5 when E4311 (E6011) electrodes are used in combination with the welding procedure suggested in this report.

The results of the 76 shear specimens that were tested under monotonic loading indicated that the resistance of multi-overlap specimens is governed by different factors according to their failure mode. When the specimen are governed by failure mode related to sheet failure the total thickness of the steel sheets and the average weld diameter influence the resistance of the specimen. For specimens that are governed by a failure mode related to weld fracture, the resistance of the specimen is governed by the effective diameter of the weld. The results also show that the thickness of the underlying plate does not influence the resistance of the weld although it may influence the fabrication parameters for the weld during the fabrication. These results confirm what had previously been observed by Peköz and McGuire (1979) in single layer configurations. Tests also showed that the minimum ratio for the underlying material to total sheet thickness could be lowered from 2.5 to 0.5.

The results from the 31 reversed cyclic shear specimens provided insight on the behaviour of welds under dynamic loading. The second phase of the reversed cyclic tests showed that the resistance of the specimens was not affected by the loading cycles sustained during the first phase (Figure 3-15). The average resistance of the reversed cyclic specimens was only 7% lower than the average resistance of the monotonic shear specimens. The third phase of the reversed cyclic tests demonstrated that when the sheet bearing failure mode was engaged the specimens could exhibit significant ductility. The specimens that were governed by other failure modes showed little ductility upon failure.

The data obtained during the shear resistance tests enabled the evaluation of Section E2.2.1 of CSA S136 which specifies the shear resistance of arc-spot welds. The results showed that equation E2.2.1-2 was generally conservative. These results are similar to those published by Peköz and McGuire (1979). When analysing the data collected during this experimental program the best fit formula was found to be:

$$P_n = 2.40 t d_a F_u \qquad For\ (d_a/t) \leq 0.815\sqrt{E/F_u} \qquad (4-4)$$

Similarly to what was found for the shear resistance of arc-spot welds, the results from the 72 tension specimens demonstrated that different factors influenced the tensile resistance of multi-overlap specimens according to their failure mode. The results showed that when the tension specimens are governed by sheet failure, the total thickness of sheet steel and the average weld diameter influence the tension resistance. When the specimens were governed by weld fracture, the results demonstrated the effective weld diameter influenced the tension resistance. The results also indicated that the thickness of the underlying plate can influence the resistance of the specimens. In fact, if the loading causes deformations in the support, these deformations may create stress concentrations that can adversely affect the resistance of the specimen. The deformation of the support can be avoided by using hot rolled angle supports with a minimum thickness of 6.4 mm.

The data obtained during the tension resistance tests were used to evaluate Section E2.2.2 of CSA S136 (2007) which specifies the tension resistance of arc-spot welds. When tension weld failure governs, the results indicate that the 30% reduction in capacity specified by Section E2.2.2 for arc-spot welds for sidelap connections should also be applied to all connections, including connections made of single sheets, because there is no evidence to suggest that the multi-overlap configuration influences the resistance of specimens governed by this failure mode. A resistance factor $\phi = 0.31$ is proposed when applying this 30% reduction. The results also suggest that the 30% reduction in tension capacity specified by Section E2.2.2 for arc-spot welds made with multi-overlap configurations should not apply when the failure mode of the specimen is related to sheet failure.

REFERENCES

AISI (2002). *Cold-formed Steel Design Manual*, American Iron and Steel Institute, Washington DC

ASTM (2009). *ASTM A370: Standard Test Methods and Definitions for Mechanical Testing of Steel Products, West Conshohocken, PA.*

AWS (1989), AWS D1.3-89, *Structural Welding Code – Sheet Steel*, Miami, FL.

AWS (1977), AWS D1.3-77, *Specification for Welding Sheet Steel in Structures*, Miami, FL.

CSA (2006), CSA W48-06, *Filler Metals and Allied Materials for Metal Arc Weldingl*, Toronto, ON, Canada.

CSA (2004), CSA-G40.20-04/G40.21-04, *General Requirements for Rolled or Welded Structural Quality Steel*, Toronto, ON, Canada.

CSA (2001), *CAN/CSA-S16-01, Limit States Design of Steel Structures*, Canadian Standards Association, Toronto, ON, Canada.

CSA, (2007), *CSA-S136-07, North American Specification for the Design of Cold-Formed Steel Structural Members*, Canadian Standards Association, Toronto, ON, Canada.

CISC. (1975), *CISC/CPMA Standard. CISC/CPMA Standard 2-75, A Quick-drying Primer for Use on Structural Steel,* Canadian Institute of Steel Construction (CISC), Toronto, ON.

Davies, J.M., and Bryan, E.R. (1982), *Manual of Stressed Skin Diaphragm Design*, John Wiley & Sons Inc., N.Y., US.

Easterling, W.S., and Snow, G.L. (2009), *Strength of Arc-spot Welds Made in Single and Multiple Steel Sheets*, Research Report No. CE/VPI-ST-08/02, Virginia Polytechnic Institute and State University, Blacksburg, Va, US.

European Committee for Standardisation, Eurocode 3 (2001), *Design of Steel Structures, Part 1.3 General rules, Supplementary Rules for Cold Formed Thin Gauge Members and Sheeting*, Brussels, Belgium.

Fung, C. (1978). *Strength of Arc-Spot Weld in Sheet Steel Construction*, Final Report on CSICC Industry Research Project 175, Westeel-Rosco, Ltd., Canada.

LaBoube, R.A., and Yu, W.W. (1991), *Tensile Strength of Welded Connections*, Final Report, Civil Engineering Studies 91-3, University of Missouri-Rolla, Rolla, Mo, US.

Luttrell, L.D. (2004), *Diaphragm Design Manual*, Third Edition, Steel Deck Institute (SDI). Fox River Grove, IL.

NRCC (2005), *National Building Code of Canada 2005*,12th ed., National Research Council of Canada, Ottawa, ON, Canada.

Peköz, T., and McGuire, W. (1979), *Welding of Sheet Steel*, Report SG-79-2, American Iron and Steel Institute, Washington, DC.

Peuler, M., (2002), *Inelastic response of arc-spot welded deck-to-frame connections for steel roof deck diaphragms*, Master's Degree Project Report, Department of Civil Engineering and Applied Mechanics, McGill University, Montreal, QC, Canada.

Rogers, C.A., and Tremblay, R. (2000), *Inelastic Seismic Response of Frame and Side-lap Fasteners for Steel Roof Decks*, Research Report No. EPM/CGS-2000-09, Department of Civil, Geological and Mining Engineering, École Polytechnique, Montreal, QC, Canada.

Rogers, C. and Tremblay, R. (2009), "Impact of diaphragm behaviour on the seismic design of low-rise steel buildings," *Eng. J., AISC*. (in press)

SANZ (1996). *AS/NZS 4600 – Cold Formed Steel Structures*, Standards Australia / Standards New Zealand, Sydney, NWS, Australia.

Struble, J.W., Peköz, T., and McGuire, W. (1978), *Tests on Puddle Weld Connections*, Department of Structural Engineering, Cornell University, Ithaca, NY.

Tremblay, R., and Rogers, C. (2005), "Impact of Capacity Design Provisions and Period Limitations on the Seismic Design of Low-Rise Steel Buildings," *Int. J. of Steel Structures*, Vol. 5, No. 1, pp. 1-22.

Yarnell, R.S., and Peköz, T. (1973), *Tests on Field Weld Puddle and Fillet Welded Connections*, Department of Structural Engineering, Cornell University, Ithaca, NY.

APPENDIX A. COLD-FORMED STEEL SHEET DATA

Appendix A contains the dimension and properties of the cold formed steel sheets for all specimens. A detailed explanation on the cold formed steel sheet data is provided in Section 3.2. The design thickness (t_d) is the sheet steel thickness above the shear plane (Section 3.3)

Table A.1 Cold formed steel sheet data for shear specimens (6.4 mm plates)

Specimen		Cold Formed Sheet Data						
Name	Configuration	Nominal Sheet Thickness (mm)	Measured Sheet Thickness (mm)	# of sheets	Total Thickness (t) (mm)	Design Thickness (t_d) (mm)	Measured F_y (MPa)	Measured F_u (MPa)
SM1621	2-layer	1.52	1.46	2	2.92	1.46	356.4	388.1
SM1622	2-layer	1.52	1.46	2	2.92	1.46	356.4	388.1
SM1623	2-layer	1.52	1.46	2	2.92	1.46	356.4	388.1
SM1624	2-layer	1.52	1.46	2	2.92	1.46	356.4	388.1
SM1641	4-layer	1.52	1.46	4	5.84	2.92	356.4	388.1
SM1642	4-layer	1.52	1.46	4	5.84	2.92	356.4	388.1
SM1643	4-layer	1.52	1.46	4	5.84	2.92	356.4	388.1
SM1644	4-layer	1.52	1.46	4	5.84	2.92	356.4	388.1
SM1821	2-layer	1.21	1.17	2	2.34	1.17	357.7	428.5
SM1822	2-layer	1.21	1.17	2	2.34	1.17	357.7	428.5
SM1823	2-layer	1.21	1.17	2	2.34	1.17	357.7	428.5
SM1824	2-layer	1.21	1.17	2	2.34	1.17	357.7	428.5
SM1841	4-layer	1.21	1.17	4	4.68	2.34	357.7	428.5
SM1842	4-layer	1.21	1.17	4	4.68	2.34	357.7	428.5
SM1843	4-layer	1.21	1.17	4	4.68	2.34	357.7	428.5
SM1844	4-layer	1.21	1.17	4	4.68	2.34	357.7	428.5
SM2021	2-layer	0.91	0.88	2	1.76	0.88	345.6	415.3
SM2022	2-layer	0.91	0.88	2	1.76	0.88	345.6	415.3
SM2023	2-layer	0.91	0.88	2	1.76	0.88	345.6	415.3
SM2024	2-layer	0.91	0.88	2	1.76	0.88	345.6	415.3
SM2041	4-layer	0.91	0.88	4	3.52	1.76	345.6	415.3
SM2042	4-layer	0.91	0.88	4	3.52	1.76	345.6	415.3
SM2043	4-layer	0.91	0.88	4	3.52	1.76	345.6	415.3
SM2044	4-layer	0.91	0.88	4	3.52	1.76	345.6	415.3
SM2221	2-layer	0.76	0.73	2	1.46	0.73	391.8	446.4
SM2222	2-layer	0.76	0.73	2	1.46	0.73	391.8	446.4
SM2223	2-layer	0.76	0.73	2	1.46	0.73	391.8	446.4
SM2224	2-layer	0.76	0.73	2	1.46	0.73	391.8	446.4
SM2241	4-layer	0.76	0.73	4	2.92	1.46	391.8	446.4
SM2242	4-layer	0.76	0.73	4	2.92	1.46	391.8	446.4

Table A.1 Cold formed sheet steel data for shear specimens (6.4 mm plates) – Cont.

Specimen		Cold Formed Sheet Data						
Name	Configuration	Nominal Sheet Thickness (mm)	Measured Sheet Thickness (mm)	# of sheets	Total Thickness (t) (mm)	Design Thickness (t_d) (mm)	Measured F_y (MPa)	Measured F_u (MPa)
SM2243	4-layer	0.76	0.73	4	2.92	1.46	391.8	446.4
SM2244	4-layer	0.76	0.73	4	2.92	1.46	391.8	446.4
SM1621P	Perimeter	1.52	1.46	2	2.92	2.92	356.4	388.1
SM1622P	Perimeter	1.52	1.46	2	2.92	2.92	356.4	388.1
SM1623P	Perimeter	1.52	1.46	2	2.92	2.92	356.4	388.1
SM1624P	Perimeter	1.52	1.46	2	2.92	2.92	356.4	388.1
SM1821P	Perimeter	1.21	1.17	2	2.34	2.34	357.7	428.5
SM1822P	Perimeter	1.21	1.17	2	2.34	2.34	357.7	428.5
SM1823P	Perimeter	1.21	1.17	2	2.34	2.34	357.7	428.5
SM1824P	Perimeter	1.21	1.17	2	2.34	2.34	357.7	428.5
SM2021P	Perimeter	0.91	0.88	2	1.76	1.76	345.6	415.3
SM2022P	Perimeter	0.91	0.88	2	1.76	1.76	345.6	415.3
SM2023P	Perimeter	0.91	0.88	2	1.76	1.76	345.6	415.3
SM2024P	Perimeter	0.91	0.88	2	1.76	1.76	345.6	415.3
SM2221P	Perimeter	0.76	0.73	2	1.46	1.46	391.8	446.4
SM2222P	Perimeter	0.76	0.73	2	1.46	1.46	391.8	446.4
SM2223P	Perimeter	0.76	0.73	2	1.46	1.46	391.8	446.4
SM2224P	Perimeter	0.76	0.73	2	1.46	1.46	391.8	446.4

Table A.2 Cold formed sheet data for shear specimens with 3.2 mm thick plates

Specimen		Cold Formed Sheet Data						
Name	Configuration	Nominal Sheet Thickness (mm)	Measured Sheet Thickness (mm)	# of sheets	Total Thickness (t) (mm)	Design Thickness (t_d) (mm)	Measured F_y (MPa)	Measured F_u (MPa)
SM1621T	2-layer	1.52	1.46	2	2.92	1.46	356.4	388.1
SM1622T	2-layer	1.52	1.46	2	2.92	1.46	356.4	388.1
SM1623T	2-layer	1.52	1.46	2	2.92	1.46	356.4	388.1
SM1641T	4-layer	1.52	1.46	4	5.84	2.92	356.4	388.1
SM1642T	4-layer	1.52	1.46	4	5.84	2.92	356.4	388.1
SM1643T	4-layer	1.52	1.46	4	5.84	2.92	356.4	388.1
SM1821T	2-layer	1.21	1.17	2	2.34	1.17	357.7	428.5
SM1822T	2-layer	1.21	1.17	2	2.34	1.17	357.7	428.5
SM1823T	2-layer	1.21	1.17	2	2.34	1.17	357.7	428.5
SM1824T	2-layer	1.21	1.17	2	2.34	1.17	357.7	428.5
SM1841T	4-layer	1.21	1.17	4	4.68	2.34	357.7	428.5

Table A.2 Cold formed sheet data for shear specimens with 3.2 mm thick plates-Cont.

Specimen		Cold Formed Sheet Data						
Name	Configuration	Nominal Sheet Thickness (mm)	Measured Sheet Thickness (mm)	# of sheets	Total Thickness (t) (mm)	Design Thickness (t_d) (mm)	Measured F_y (MPa)	Measured F_u (MPa)
SM1842T	4-layer	1.21	1.17	4	4.68	2.34	357.7	428.5
SM1843T	4-layer	1.21	1.17	4	4.68	2.34	357.7	428.5
SM2021T	2-layer	0.91	0.88	2	1.76	0.88	345.6	415.3
SM2022T	2-layer	0.91	0.88	2	1.76	0.88	345.6	415.3
SM2023T	2-layer	0.91	0.88	2	1.76	0.88	345.6	415.3
SM2041T	4-layer	0.91	0.88	4	3.52	1.76	345.6	415.3
SM2042T	4-layer	0.91	0.88	4	3.52	1.76	345.6	415.3
SM2043T	4-layer	0.91	0.88	4	3.52	1.76	345.6	415.3
SM2044T	4-layer	0.91	0.88	4	3.52	1.76	345.6	415.3
SM2221T	2-layer	0.76	0.73	2	1.46	0.73	391.8	446.4
SM2222T	2-layer	0.76	0.73	2	1.46	0.73	391.8	446.4
SM2223T	2-layer	0.76	0.73	2	1.46	0.73	391.8	446.4
SM2224T	2-layer	0.76	0.73	2	1.46	0.73	391.8	446.4
SM2241T	4-layer	0.76	0.73	4	2.92	1.46	391.8	446.4
SM2242T	4-layer	0.76	0.73	4	2.92	1.46	391.8	446.4
SM2243T	4-layer	0.76	0.73	4	2.92	1.46	391.8	446.4
SM2244T	4-layer	0.76	0.73	4	2.92	1.46	391.8	446.4

Table A.3 Cold formed sheet data for tension specimens with 6.4 mm angles

Specimen		Cold Formed Sheet Data						
Name	Configuration	Nominal Sheet Thickness (mm)	Measured Sheet Thickness (mm)	# of sheets	Total Thickness (t) (mm)	Design Thickness (t_d) (mm)	Measured F_y (MPa)	Measured F_u (MPa)
T1611	1-layer	1.52	1.46	1	1.46	1.46	356.4	388.1
T1612	1-layer	1.52	1.46	1	1.46	1.46	356.4	388.1
T1613	1-layer	1.52	1.46	1	1.46	1.46	356.4	388.1
T1614	1-layer	1.52	1.46	1	1.46	1.46	356.4	388.1
T1621	2-layer	1.52	1.46	2	2.92	2.92	356.4	388.1
T1622	2-layer	1.52	1.46	2	2.92	2.92	356.4	388.1
T1623	2-layer	1.52	1.46	2	2.92	2.92	356.4	388.1
T1624	2-layer	1.52	1.46	2	2.92	2.92	356.4	388.1
T1641	4-layer	1.52	1.46	4	5.84	5.84	356.4	388.1
T1642	4-layer	1.52	1.46	4	5.84	5.84	356.4	388.1
T1643	4-layer	1.52	1.46	4	5.84	5.84	356.4	388.1
T1811	1-layer	1.21	1.17	1	1.17	1.17	357.7	428.5

Table A.3 Cold formed sheet data for tension specimens (6.4 mm angles) -Cont.

Specimen		Cold Formed Sheet Data						
Name	Configuration	Nominal Sheet Thickness (mm)	Measured Sheet Thickness (mm)	# of sheets	Total Thickness (t) (mm)	Design Thickness (t_d) (mm)	Measured F_y (MPa)	Measured F_u (MPa)
T1812	1-layer	1.21	1.17	1	1.17	1.17	357.7	428.5
T1813	1-layer	1.21	1.17	1	1.17	1.17	357.7	428.5
T1814	1-layer	1.21	1.17	1	1.17	1.17	357.7	428.5
T1821	2-layer	1.21	1.17	2	2.34	2.34	357.7	428.5
T1822	2-layer	1.21	1.17	2	2.34	2.34	357.7	428.5
T1823	2-layer	1.21	1.17	2	2.34	2.34	357.7	428.5
T1824	2-layer	1.21	1.17	2	2.34	2.34	357.7	428.5
T1841	4-layer	1.21	1.17	4	4.68	4.68	357.7	428.5
T1842	4-layer	1.21	1.17	4	4.68	4.68	357.7	428.5
T1843	4-layer	1.21	1.17	4	4.68	4.68	357.7	428.5
T1844	4-layer	1.21	1.17	4	4.68	4.68	357.7	428.5
T2011	1-layer	0.91	0.88	1	0.88	0.88	345.6	415.3
T2012	1-layer	0.91	0.88	1	0.88	0.88	345.6	415.3
T2013	1-layer	0.91	0.88	1	0.88	0.88	345.6	415.3
T2014	1-layer	0.91	0.88	1	0.88	0.88	345.6	415.3
T2021	2-layer	0.91	0.88	2	1.76	1.76	345.6	415.3
T2022	2-layer	0.91	0.88	2	1.76	1.76	345.6	415.3
T2023	2-layer	0.91	0.88	2	1.76	1.76	345.6	415.3
T2041	4-layer	0.91	0.88	4	3.52	3.52	345.6	415.3
T2042	4-layer	0.91	0.88	4	3.52	3.52	345.6	415.3
T2043	4-layer	0.91	0.88	4	3.52	3.52	345.6	415.3
T2044	4-layer	0.91	0.88	4	3.52	3.52	345.6	415.3
T2211	1-layer	0.76	0.73	1	0.73	0.73	391.8	446.4
T2212	1-layer	0.76	0.73	1	0.73	0.73	391.8	446.4
T2213	1-layer	0.76	0.73	1	0.73	0.73	391.8	446.4
T2221	2-layer	0.76	0.73	2	1.46	1.46	391.8	446.4
T2222	2-layer	0.76	0.73	2	1.46	1.46	391.8	446.4
T2223	2-layer	0.76	0.73	2	1.46	1.46	391.8	446.4
T2224	2-layer	0.76	0.73	2	1.46	1.46	391.8	446.4
T2241	4-layer	0.76	0.73	4	2.92	2.92	391.8	446.4
T2242	4-layer	0.76	0.73	4	2.92	2.92	391.8	446.4
T2243	4-layer	0.76	0.73	4	2.92	2.92	391.8	446.4

Table A.4 Cold formed sheet data for tension specimens (3.2 mm angles)

Specimen		Cold Formed Sheet Data						
Name	Configuration	Nominal Sheet Thickness (mm)	Measured Sheet Thickness (mm)	# of sheets	Total Thickness (t) (mm)	Design Thickness (t_d) (mm)	Measured F_y (MPa)	Measured F_u (MPa)
T1621T	2-layer	1.52	1.46	2	2.92	2.92	356.4	388.1
T1622T	2-layer	1.52	1.46	2	2.92	2.92	356.4	388.1
T1623T	2-layer	1.52	1.46	2	2.92	2.92	356.4	388.1
T1641T	4-layer	1.52	1.46	4	5.84	5.84	356.4	388.1
T1642T	4-layer	1.52	1.46	4	5.84	5.84	356.4	388.1
T1643T	4-layer	1.52	1.46	4	5.84	5.84	356.4	388.1
T1821T	2-layer	1.21	1.17	2	2.34	2.34	357.7	428.5
T1822T	2-layer	1.21	1.17	2	2.34	2.34	357.7	428.5
T1823T	2-layer	1.21	1.17	2	2.34	2.34	357.7	428.5
T1841T	4-layer	1.21	1.17	4	4.68	4.68	357.7	428.5
T1842T	4-layer	1.21	1.17	4	4.68	4.68	357.7	428.5
T1843T	4-layer	1.21	1.17	4	4.68	4.68	357.7	428.5
T2021T	2-layer	0.91	0.88	2	1.76	1.76	345.6	415.3
T2022T	2-layer	0.91	0.88	2	1.76	1.76	345.6	415.3
T2023T	2-layer	0.91	0.88	2	1.76	1.76	345.6	415.3
T2041T	4-layer	0.91	0.88	4	3.52	3.52	345.6	415.3
T2042T	4-layer	0.91	0.88	4	3.52	3.52	345.6	415.3
T2043T	4-layer	0.91	0.88	4	3.52	3.52	345.6	415.3
T2221T	2-layer	0.76	0.73	2	1.46	1.46	391.8	446.4
T2222T	2-layer	0.76	0.73	2	1.46	1.46	391.8	446.4
T2223T	2-layer	0.76	0.73	2	1.46	1.46	391.8	446.4
T2224T	2-layer	0.76	0.73	2	1.46	1.46	391.8	446.4
T2225T	2-layer	0.76	0.73	2	1.46	1.46	391.8	446.4
T2241T	4-layer	0.76	0.73	4	2.92	2.92	391.8	446.4
T2242T	4-layer	0.76	0.73	4	2.92	2.92	391.8	446.4
T2243T	4-layer	0.76	0.73	4	2.92	2.92	391.8	446.4
T2244T	4-layer	0.76	0.73	4	2.92	2.92	391.8	446.4

Table A.5 Cold formed sheet data for cyclic shear specimens (6.4 mm plates)

Specimen		Cold Formed Sheet Data						
Name	Configuration	Nominal Sheet Thickness (mm)	Measured Sheet Thickness (mm)	# of sheets	Total Thickness (t) (mm)	Design Thickness (t_d) (mm)	Measured F_y (MPa)	Measured F_u (MPa)
SC1621	2-layer	1.52	1.46	2	2.92	1.46	356.4	388.1
SC1622	2-layer	1.52	1.46	2	2.92	1.46	356.4	388.1
SC1623	2-layer	1.52	1.46	2	2.92	1.46	356.4	388.1
SC1624	2-layer	1.52	1.46	2	2.92	1.46	356.4	388.1
SC1641	4-layer	1.52	1.46	4	5.84	2.92	356.4	388.1
SC1642	4-layer	1.52	1.46	4	5.84	2.92	356.4	388.1
SC1643	4-layer	1.52	1.46	4	5.84	2.92	356.4	388.1
SC1644	4-layer	1.52	1.46	4	5.84	2.92	356.4	388.1
SC1821	2-layer	1.21	1.17	2	2.34	1.17	357.7	428.5
SC1822	2-layer	1.21	1.17	2	2.34	1.17	357.7	428.5
SC1823	2-layer	1.21	1.17	2	2.34	1.17	357.7	428.5
SC1824	2-layer	1.21	1.17	2	2.34	1.17	357.7	428.5
SC1841	4-layer	1.21	1.17	4	4.68	2.34	357.7	428.5
SC1842	4-layer	1.21	1.17	4	4.68	2.34	357.7	428.5
SC1843	4-layer	1.21	1.17	4	4.68	2.34	357.7	428.5
SC2021	2-layer	0.91	0.88	2	1.76	0.88	345.6	415.3
SC2022	2-layer	0.91	0.88	2	1.76	0.88	345.6	415.3
SC2023	2-layer	0.91	0.88	2	1.76	0.88	345.6	415.3
SC2024	2-layer	0.91	0.88	2	1.76	0.88	345.6	415.3
SC2041	4-layer	0.91	0.88	4	3.52	1.76	345.6	415.3
SC2042	4-layer	0.91	0.88	4	3.52	1.76	345.6	415.3
SC2043	4-layer	0.91	0.88	4	3.52	1.76	345.6	415.3
SC2044	4-layer	0.91	0.88	4	3.52	1.76	345.6	415.3
SC2221	2-layer	0.76	0.73	2	1.46	0.73	391.8	446.4
SC2222	2-layer	0.76	0.73	2	1.46	0.73	391.8	446.4
SC2223	2-layer	0.76	0.73	2	1.46	0.73	391.8	446.4
SC2224	2-layer	0.76	0.73	2	1.46	0.73	391.8	446.4
SC2241	4-layer	0.76	0.73	4	2.92	1.46	391.8	446.4
SC2242	4-layer	0.76	0.73	4	2.92	1.46	391.8	446.4
SC2243	4-layer	0.76	0.73	4	2.92	1.46	391.8	446.4
SC2244	4-layer	0.76	0.73	4	2.92	1.46	391.8	446.4

APPENDIX B. WELD DATA

Appendix B contains the measured and calculated weld dimensions for all specimens. A detailed explanation on the weld data is provided in section 4.2. Measured effective weld diameters are provided only for specimens that failed due to weld failure.

Table B.1 Weld data for shear specimens with 6.4 mm thick plates

Specimen		Weld data			
Name	Configuration	Measured visible diam. (d_{vis}) (mm)	Calculated average diam. (d_a) (mm)	Calculated effective diam. (d_{eff}) (mm)	Measured effective diam. (d_{eff}) (mm)
SM1621	2-layer	17.0	15.5	9.3	N/A
SM1622	2-layer	17.0	15.5	9.3	N/A
SM1623	2-layer	18.4	16.9	10.1	N/A
SM1624	2-layer	17.1	15.6	9.4	N/A
SM1641	4-layer	17.1	14.1	7.6	9.4
SM1642	4-layer	17.6	14.7	8.0	10.4
SM1643	4-layer	17.7	14.8	8.0	9.8
SM1644	4-layer	18.1	15.2	8.3	11.8
SM1821	2-layer	18.1	16.9	10.0	N/A
SM1822	2-layer	17.6	16.4	9.7	N/A
SM1823	2-layer	16.9	15.7	9.3	N/A
SM1824	2-layer	19.0	17.8	10.4	N/A
SM1841	4-layer	18.3	15.9	9.3	10.0
SM1842	4-layer	18.5	16.1	9.4	9.7
SM1843	4-layer	17.4	15.0	8.7	8.8
SM1844	4-layer	18.6	16.2	9.5	10.2
SM2021	2-layer	15.6	14.7	8.6	N/A
SM2022	2-layer	15.5	14.6	8.5	N/A
SM2023	2-layer	16.5	15.6	9.1	N/A
SM2024	2-layer	15.3	14.4	8.4	N/A
SM2041	4-layer	15.9	14.2	8.5	N/A
SM2042	4-layer	16.3	14.6	8.8	N/A
SM2043	4-layer	16.6	14.9	9.0	9.8
SM2044	4-layer	16.3	14.5	8.8	N/A
SM2221	2-layer	16.0	15.2	8.8	N/A
SM2222	2-layer	17.0	16.2	9.3	N/A
SM2223	2-layer	17.3	16.5	9.5	N/A
SM2224	2-layer	16.6	15.8	9.1	N/A
SM2241	4-layer	15.4	13.9	8.5	N/A
SM2242	4-layer	17.6	16.1	9.7	N/A
SM2243	4-layer	15.9	14.5	8.8	7.9
SM2244	4-layer	14.8	13.3	8.1	N/A

Table B.1 Weld data for shear specimens with 6.4 mm thick plates-Cont.

Specimen		Weld data			
Name	Configuration	Measured visible diam. (d_{vis}) (mm)	Calculated average diam. (d_a) (mm)	Calculated effective diam. (d_{eff}) (mm)	Measured effective diam. (d_{eff}) (mm)
SM1621P	Perimeter	19.5	16.6	9.3	12.1
SM1622P	Perimeter	18.5	15.5	8.5	6.9
SM1623P	Perimeter	17.2	14.3	7.7	12.2
SM1624P	Perimeter	16.4	13.5	7.1	8.0
SM1821P	Perimeter	16.9	14.6	8.3	8.9
SM1822P	Perimeter	18.4	16.0	9.3	9.6
SM1823P	Perimeter	16.5	14.2	8.1	8.6
SM1824P	Perimeter	17.3	14.9	8.6	10.2
SM2021P	Perimeter	17.6	15.8	9.7	10.3
SM2022P	Perimeter	18.9	18.0	10.4	N/A
SM2023P	Perimeter	16.2	15.3	8.9	N/A
SM2024P	Perimeter	17.8	16.9	9.8	N/A
SM2221P	Perimeter	14.9	13.4	8.2	9.0
SM2222P	Perimeter	16.7	15.3	9.2	N/A
SM2223P	Perimeter	16.2	14.7	8.9	N/A
SM2224P	Perimeter	17.8	16.3	9.8	8.6

Table B.2 Weld data for shear specimens with 3.2 mm thick plates

Specimen		Weld data			
Name	Configuration	Measured visible diam. (d_{vis}) (mm)	Calculated average diam. (d_a) (mm)	Calculated effective diam. (d_{eff}) (mm)	Measured effective diam. (d_{eff}) (mm)
SM1621T	2-layer	14.6	13.2	8.1	9.4
SM1622T	2-layer	16.1	14.6	8.8	9.6
SM1623T	2-layer	15.5	14.0	8.5	9.4
SM1641T	4-layer	15.2	12.2	6.2	7.9
SM1642T	4-layer	15.7	12.8	6.6	9.5
SM1643T	4-layer	16.0	13.1	6.8	8.6
SM1821T	2-layer	16.4	15.2	9.0	N/A
SM1822T	2-layer	12.8	11.6	7.0	N/A
SM1823T	2-layer	15.7	14.5	8.6	N/A
SM1824T	2-layer	14.4	13.3	7.9	N/A
SM1841T	4-layer	15.4	13.0	7.3	8.6
SM1842T	4-layer	14.9	12.6	6.9	8.3
SM1843T	4-layer	16.0	13.7	7.7	8.7
SM2021T	2-layer	15.5	14.7	8.5	N/A

Table B.2 Weld data for shear specimens with 3.2 mm thick plates-Cont.

Specimen		Weld data			
Name	Configuration	Measured visible diam. (d_{vis}) (mm)	Calculated average diam. (d_a) (mm)	Calculated effective diam. (d_{eff}) (mm)	Measured effective diam. (d_{eff}) (mm)
SM2022T	2-layer	16.3	15.4	9.0	N/A
SM2023T	2-layer	15.2	14.3	8.3	N/A
SM2041T	4-layer	15.4	13.6	8.1	N/A
SM2042T	4-layer	15.6	13.8	8.3	N/A
SM2043T	4-layer	15.4	13.6	8.1	7.3
SM2044T	4-layer	15.7	14.0	8.4	N/A
SM2221T	2-layer	15.9	15.2	8.8	N/A
SM2222T	2-layer	14.8	14.1	8.2	N/A
SM2223T	2-layer	14.5	13.8	8.0	N/A
SM2224T	2-layer	15.3	14.6	8.4	N/A
SM2241T	4-layer	15.8	14.3	8.7	8.5
SM2242T	4-layer	15.8	14.3	8.7	N/A
SM2243T	4-layer	15.9	14.4	8.7	8.7
SM2244T	4-layer	15.1	13.7	8.3	N/A

Table B.3 Weld data for tension specimens with 6.4 mm thick angles

Specimen		Weld data			
Name	Configuration	Measured visible diam. (d_{vis}) (mm)	Calculated average diam. (d_a) (mm)	Calculated effective diam. (d_{eff}) (mm)	Measured effective diam. (d_{eff}) (mm)
T1611	1-layer	15.2	14.5	8.4	N/A
T1612	1-layer	15.6	14.8	8.6	N/A
T1613	1-layer	13.7	13.0	7.4	N/A
T1614	1-layer	15.4	14.6	8.5	N/A
T1621	2-layer	15.8	14.3	6.7	N/A
T1622	2-layer	16.2	14.7	7.0	N/A
T1623	2-layer	17.9	16.4	8.1	7.4
T1624	2-layer	17.3	15.9	7.7	N/A
T1641	4-layer	18.1	15.2	3.9	7.3
T1642	4-layer	17.7	14.8	3.7	8.4
T1643	4-layer	14.8	11.9	1.6	9.0
T1811	1-layer	15.5	14.9	8.5	N/A
T1812	1-layer	15.1	14.5	8.3	N/A
T1813	1-layer	15.1	14.5	8.3	N/A
T1814	1-layer	14.8	14.2	8.1	N/A
T1821	2-layer	17.5	16.3	8.7	N/A

Table B.3 Weld data for tension specimens with 6.4 mm thick angles-Cont.

Specimen		Weld data			
Name	Configuration	Measured visible diam. (d_{vis}) (mm)	Calculated average diam. (d_a) (mm)	Calculated effective diam. (d_{eff}) (mm)	Measured effective diam. (d_{eff}) (mm)
T1822	2-layer	17.6	16.4	8.8	N/A
T1823	2-layer	16.8	15.7	8.3	N/A
T1824	2-layer	18.5	17.3	9.4	N/A
T1841	4-layer	18.4	16.1	5.9	9.4
T1842	4-layer	16.2	13.8	4.3	N/A
T1843	4-layer	17.6	15.2	5.3	N/A
T1844	4-layer	16.9	14.5	4.8	N/A
T2011	1-layer	14.1	13.6	7.7	N/A
T2012	1-layer	16.0	15.6	8.8	N/A
T2013	1-layer	17.3	16.9	9.5	N/A
T2014	1-layer	14.9	14.5	8.2	N/A
T2021	2-layer	15.8	15.0	8.4	N/A
T2022	2-layer	16.4	15.6	8.9	N/A
T2023	2-layer	16.1	15.2	8.6	N/A
T2041	4-layer	17.5	15.8	7.0	N/A
T2042	4-layer	17.8	16.1	7.2	N/A
T2043	4-layer	15.8	14.0	5.8	7.1
T2044	4-layer	17.3	15.6	6.8	N/A
T2211	1-layer	14.4	14.0	7.9	N/A
T2212	1-layer	14.9	14.5	8.2	N/A
T2213	1-layer	13.6	13.2	7.5	N/A
T2221	2-layer	15.9	15.1	8.7	N/A
T2222	2-layer	17.1	16.4	9.4	N/A
T2223	2-layer	17.7	17.0	9.7	N/A
T2224	2-layer	18.0	17.3	9.9	N/A
T2241	4-layer	16.2	14.7	7.0	N/A
T2242	4-layer	16.6	15.1	7.2	N/A
T2243	4-layer	16.3	14.9	7.1	N/A

Table B.4 Weld data for tension specimens with 3.2mm thick angles

Specimen		Weld data			
Name	Configuration	Measured visible diam. (d_{vis}) (mm)	Calculated average diam. (d_a) (mm)	Calculated effective diam. (d_{eff}) (mm)	Measured effective diam. (d_{eff}) (mm)
T1621T	2-layer	14.1	12.7	5.5	N/A
T1622T	2-layer	13.9	12.5	5.4	N/A
T1623T	2-layer	15.6	14.1	6.5	N/A
T1641T	4-layer	14.9	12.0	1.7	7.2
T1642T	4-layer	15.9	13.0	2.4	7.7
T1643T	4-layer	14.3	11.4	1.3	7.3
T1821T	2-layer	13.8	12.6	6.1	7.3
T1822T	2-layer	14.8	13.6	6.8	7.2
T1823T	2-layer	15.5	14.4	7.4	8.5
T1841T	4-layer	16.1	13.7	4.2	9.6
T1842T	4-layer	16.3	14.0	4.4	8.5
T1843T	4-layer	14.6	12.3	3.2	7.9
T2021T	2-layer	13.5	12.6	6.8	N/A
T2022T	2-layer	15.9	15.0	8.5	N/
T2023T	2-layer	16.3	15.5	8.8	N/A
T2041T	4-layer	13.8	12.0	4.4	7.2
T2042T	4-layer	14.9	13.1	5.1	N/A
T2043T	4-layer	14.5	12.7	4.9	N/A
T2221T	2-layer	15.8	15.1	8.7	N/A
T2222T	2-layer	15.1	14.4	8.3	N/A
T2223T	2-layer	16.0	15.3	8.8	N/A
T2224T	2-layer	12.8	12.1	6.8	N/A
T2225T	2-layer	13.8	13.0	7.4	N/A
T2241T	4-layer	15.8	14.3	6.7	N/A
T2242T	4-layer	16.1	14.6	6.9	N/A
T2243T	4-layer	15.8	14.4	6.7	N/A
T2244T	4-layer	13.8	12.3	5.3	N/A

Table B.5 Weld data for cyclic shear specimens with 6.4mm thick plates

Specimen		Weld data			
Name	Configuration	Measured visible diam. (d) (mm)	Calculated average diam. (d_a) (mm)	Calculated effective diam. (d_{ec}) (mm)	Measured effective diam. (d_e) (mm)
SC1621	2-layer	14.6	13.2	8.1	N/A
SC1622	2-layer	16.1	14.6	8.8	N/A
SC1623	2-layer	15.5	14.0	8.5	N/A
SC1624	2-layer	15.2	13.7	8.3	N/A
SC1641	4-layer	15.7	12.8	6.6	10.2
SC1642	4-layer	16.0	13.1	6.8	9.7
SC1643	4-layer	16.4	14.0	7.9	8.9
SC1644	4-layer	12.8	10.4	5.4	8.1
SC1821	2-layer	15.7	14.5	8.6	N/A
SC1822	2-layer	14.4	13.3	7.9	N/A
SC1823	2-layer	15.4	13.0	7.3	N/A
SC1824	2-layer	14.9	12.6	6.9	N/A
SC1841	4-layer	16.0	11.4	4.2	10.2
SC1842	4-layer	15.5	13.8	8.2	10.2
SC1843	4-layer	16.3	14.5	8.8	9.5
SC2021	2-layer	15.2	14.3	8.3	N/A
SC2022	2-layer	15.4	14.4	8.4	N/A
SC2023	2-layer	15.6	14.7	8.6	N/A
SC2024	2-layer	15.4	14.5	8.5	N/A
SC2041	4-layer	15.7	14.0	8.4	N/A
SC2042	4-layer	15.9	14.5	8.8	N/A
SC2043	4-layer	14.8	13.4	8.2	8.4
SC2044	4-layer	14.5	13.1	8.0	N/A
SC2221	2-layer	15.3	14.6	8.4	N/A
SC2222	2-layer	15.8	15.0	8.7	N/A
SC2223	2-layer	15.8	15.1	8.7	N/A
SC2224	2-layer	15.9	15.2	8.7	N/A
SC2241	4-layer	15.1	13.7	8.3	N/A
SC2242	4-layer	17.0	15.5	7.5	N/A
SC2243	4-layer	17.0	15.5	7.5	11.6
SC2244	4-layer	18.4	16.9	8.5	N/A

APPENDIX C. RESISTANCE RESULTS

For specimens where the effective weld diameter was measured, the shear weld failure resistance was predicted by Equation 1-2 using the nominal tensile strength of the weld metal. The shear sheet failure resistance was predicted with Equations 1-3 to 1-5 according to the proper d_a/t ratio limits using the measured visible diameter, sheet thickness, yield strength and tensile strength of the specimen. The tension weld failure resistance was predicted by Equation 1-6 for specimens where the effective weld diameter was recorded using the nominal tensile strength of the weld metal. The tension sheet failure resistance was predicted with Equation 1-7 using the measured visible diameter, sheet thickness, yield strength and tensile strength of the specimen.

Table C.1 Resistance results for shear specimens with 6.4mm thick plates

Specimen Name	Weld Failure CSA S136 E2.2.1-1 (kN)	d_a/t	Sheet Failure CSA S136 E2.2.1-2 (kN)	Sheet Failure CSA S136 E2.2.1-3 (kN)	Sheet Failure CSA S136 E2.2.1-4 (kN)	Predicted Resist. P_n (kN)	Predicted Failure Mode	Recorded Failure Mode	Measured Resist. P_u (kN)
SM1621	--	10.6	19.3	--	--	19.3	Sheet	Sheet Bearing	32.8
SM1622	--	10.6	19.3	--	--	19.3	Sheet	Sheet Bearing	34.8
SM1623	--	11.6	21.1	--	--	21.1	Sheet	Sheet Bearing	33.3
SM1624	--	10.7	19.5	--	--	19.5	Sheet	Sheet Bearing	33.2
SM1641	22.2	4.8	35.2	--	--	22.2	Weld	Weld Shear	33.4
SM1642	27.6	5.0	36.7	--	--	27.6	Weld	Weld Shear	40.6
SM1643	24.4	5.1	36.9	--	--	24.4	Weld	Weld Shear	34.8
SM1644	35.4	5.2	37.8	--	--	35.4	Weld	Weld Shear	47.5
SM1821	--	14.5	18.7	--	--	18.7	Sheet	Sheet Tear	26.8
SM1822	--	14.0	18.1	--	--	18.1	Sheet	Sheet Tear	28.0
SM1823	--	13.4	17.4	--	--	17.4	Sheet	Sheet Tear	25.0
SM1824	--	15.2	19.6	--	--	19.6	Sheet	Sheet Tear	27.9
SM1841	25.3	6.8	35.2	--	--	25.3	Weld	Weld Shear	34.5
SM1842	23.8	6.9	35.6	--	--	23.8	Weld	Weld Shear	30.8
SM1843	19.5	6.4	33.2	--	--	19.5	Weld	Weld Shear	27.4
SM1844	26.6	6.9	35.8	--	--	26.6	Weld	Weld Shear	33.8
SM2021	--	16.7	11.8	--	--	11.8	Sheet	Sheet Tear	16.1
SM2022	--	16.6	11.7	--	--	11.7	Sheet	Sheet Tear	16.7
SM2023	--	17.8	12.6	--	--	12.6	Sheet	Sheet Tear	17.7

Table C.1 Resistance results for shear specimens with 6.4 mm thick plates-Cont.

Specimen Name	Weld Failure CSA S136 E2.2.1-1 (kN)	d_a/t	Sheet Failure CSA S136 E2.2.1-2 (kN)	Sheet Failure CSA S136 E2.2.1-3 (kN)	Sheet Failure CSA S136 E2.2.1-4 (kN)	Predicted Resist. P_n (kN)	Predicted Failure Mode	Recorded Failure Mode	Measured Resist. P_u (kN)
SM2024	--	16.4	11.6	--	--	11.6	Sheet	Sheet Tear	16.3
SM2041	--	8.0	22.8	--	--	22.8	Sheet	Sheet Tear	28.4
SM2042	--	8.3	23.5	--	--	23.5	Sheet	Sheet Bearing	31.9
SM2043	24.3	8.4	23.9	--	--	23.9	Sheet	Weld Shear	29.9
SM2044	--	8.3	23.4	--	--	23.4	Sheet	Sheet Bearing	25.0
SM2221	--	20.9	--	9.3	--	9.3	Sheet	Sheet Tear	14.0
SM2222	--	22.2	--	9.4	--	9.4	Sheet	Sheet Tear	15.3
SM2223	--	22.6	--	9.4	--	9.4	Sheet	Sheet Tear	14.8
SM2224	--	21.7	--	9.3	--	9.3	Sheet	Sheet Tear	15.3
SM2241	--	9.5	20.0	--	--	20.0	Sheet	Sheet Bearing	25.8
SM2242	--	11.0	23.1	--	--	23.1	Sheet	Sheet Tear	29.1
SM2243	15.6	9.9	20.7	--	--	15.6	Weld	Weld Shear	23.7
SM2244	--	9.1	19.1	--	--	19.1	Sheet	Weld Plow	25.8
SM1621P	37.1	12.3	25.8	--	--	25.8	Sheet	Weld Shear	44.3
SM1622P	12.0	11.6	24.4	--	--	12.0	Weld	Weld Shear	17.3
SM1623P	37.9	10.8	22.6	--	--	22.6	Sheet	Weld Shear	47.5
SM1624P	16.2	10.3	21.5	--	--	16.2	Weld	Weld Shear	25.1
SM1821P	20.0	8.6	24.4	--	--	20.0	Weld	Weld Shear	17.1
SM1822P	23.4	9.4	26.7	--	--	23.4	Weld	Weld Shear	30.3
SM1823P	18.7	8.4	23.8	--	--	18.7	Weld	Weld Shear	24.8
SM1824P	26.6	8.8	24.9	--	--	24.9	Sheet	Weld Shear	39.1
SM2021P	27.0	6.5	33.6	--	--	27.0	Weld	Weld Shear	36.7
SM2022P	--	15.2	19.6	--	--	19.6	Sheet	Sheet Tear	32.2
SM2023P	--	12.8	16.5	--	--	16.5	Sheet	Sheet Tear	30.2
SM2024P	--	14.2	18.4	--	--	18.4	Sheet	Sheet Tear	29.4
SM2221P	20.4	4.1	29.8	--	--	20.4	Weld	Weld Shear	27.0
SM2222P	--	4.7	34.4	--	--	34.4	Sheet	Sheet Tear	28.5
SM2223P	--	4.5	33.1	--	--	33.1	Sheet	Sheet Tear	27.0
SM2224P	18.7	5.1	37.1	--	--	18.7	Weld	Weld Shear	27.0

Table C.2 Resistance results for shear specimens with 3.2 mm thick plates

Specimen Name	Weld Failure CSA S136 E2.2.2-1 (kN)	d_a/t	Sheet Failure CSA S136 E2.2.1-2 (kN)	Sheet Failure CSA S136 E2.2.1-3 (kN)	Sheet Failure CSA S136 E2.2.1-4 (kN)	Predicted Resist. P_n (kN)	Predicted Failure Mode	Recorded Failure Mode	Measured Resist. P_u (kN)
SM1621T	22.5	9.0	16.4	--	--	16.4	Sheet	Weld Shear	32.6
SM1622T	23.5	10.0	18.2	--	--	18.2	Sheet	Weld Shear	35.2
SM1623T	22.2	9.6	17.5	--	--	17.5	Sheet	Weld Shear	33.8
SM1641T	15.9	4.2	30.5	--	--	15.9	Weld	Weld Shear	25.5
SM1642T	22.8	4.4	31.9	--	--	22.8	Weld	Weld Shear	30.0
SM1643T	18.7	4.5	32.7	--	--	18.7	Weld	Weld Shear	26.9
SM1821T	--	13.0	16.8	--	--	16.8	Sheet	Sheet Tear	26.3
SM1822T	--	9.9	12.8	--	--	12.8	Sheet	Sheet Tear	20.6
SM1823T	--	12.4	16.0	--	--	16.0	Sheet	Sheet Tear	24.7
SM1824T	--	11.3	14.6	--	--	14.6	Sheet	Sheet Tear	21.3
SM1841T	18.7	2.3	47.2	--	--	18.7	Weld	Weld Shear	28.7
SM1842T	17.6	2.2	45.2	--	--	17.6	Weld	Weld Shear	26.0
SM1843T	19.0	2.4	50.1	--	--	19.0	Weld	Weld Shear	29.3
SM2021T	--	16.6	11.8	--	--	11.8	Sheet	Sheet Tear	18.0
SM2022T	--	17.5	12.4	--	--	12.4	Sheet	Sheet Tear	18.3
SM2023T	--	16.2	11.5	--	--	11.5	Sheet	Sheet Tear	18.6
SM2041T	--	7.4	22.5	--	--	22.5	Sheet	Sheet Bearing	27.3
SM2042T	--	7.6	22.9	--	--	22.9	Sheet	Sheet Bearing	33.0
SM2043T	13.5	7.5	22.5	--	--	13.5	Weld	Weld Shear	31.3
SM2044T	--	7.9	22.5	--	--	22.5	Sheet	Sheet Tear	31.1
SM2221T	--	20.8	--	9.3	--	9.3	Sheet	Sheet Tear	15.1
SM2222T	--	19.3	--	9.2	--	9.2	Sheet	Sheet Tear	14.0
SM2223T	--	18.9	--	9.1	--	9.1	Sheet	Sheet Tear	13.6
SM2224T	--	20.0	--	9.2	--	9.2	Sheet	Sheet Tear	15.2
SM2241T	18.1	9.8	20.5	--	--	18.1	Weld	Weld Shear	24.0
SM2242T	--	9.8	20.5	--	--	20.5	Sheet	Sheet Tear	17.4
SM2243T	19.3	9.9	20.7	--	--	19.3	Weld	Weld Shear	26.8
SM2244T	--	9.4	19.6	--	--	19.6	Sheet	Sheet Bearing	26.8

Table C.3 Resistance results for tension specimens with 6.4mm thick angles

Specimen Name	Weld Failure CSA S136 Eq. E2.2.2-1 (kN)	Sheet Failure CSA S136 Eq. E2.2.2-2 (kN)	Reduced Design Resistance for Lapped Joints P_n (kN)	Predicted Failure Mode	Recorded Failure Mode	Measured Resistance (kN)
T1611	--	7.8	5.4	Sheet	Sheet	7.6
T1612	--	8.0	5.6	Sheet	Sheet	9.0
T1613	--	7.0	4.9	Sheet	Sheet	7.0
T1614	--	7.9	5.5	Sheet	Sheet	9.7
T1621	--	6.7	4.7	Sheet	Sheet	12.9
T1622	--	6.9	4.9	Sheet	Sheet	15.7
T1623	18.6	8.8	6.2	Sheet	Weld Failure	11.7
T1624	--	7.5	5.2	Sheet	Sheet	12.2
T1641	18.2	16.3	11.4	Sheet	Weld Failure	12.8
T1642	23.9	15.9	11.2	Sheet	Weld Failure	15.4
T1643	27.2	12.8	8.9	Sheet	Weld Failure	19.4
T1811	--	8.6	6.0	Sheet	Sheet	8.6
T1812	--	8.4	5.8	Sheet	Sheet	5.7
T1813	--	8.4	5.9	Sheet	Sheet	7.6
T1814	--	8.2	5.7	Sheet	Sheet	4.4
T1821	--	8.2	5.7	Sheet	Sheet	11.1
T1822	--	8.3	5.8	Sheet	Sheet	10.3
T1823	--	7.9	5.5	Sheet	Sheet	10.0
T1824	--	8.7	6.1	Sheet	Sheet	10.2
T1841	30.0	18.5	13.0	Sheet	Weld Failure	9.7
T1842	--	13.9	9.7	Sheet	Sheet	16.5
T1843	--	15.3	10.7	Sheet	Sheet	15.2
T1844	--	14.6	10.3	Sheet	Sheet	15.1
T2011	--	5.8	4.0	Sheet	Sheet	7.0
T2012	--	6.6	4.6	Sheet	Sheet	6.7
T2013	--	7.1	5.0	Sheet	Sheet	6.3
T2014	--	6.1	4.3	Sheet	Sheet	6.1
T2021	--	5.5	3.9	Sheet	Sheet	5.7
T2022	--	5.8	4.0	Sheet	Sheet	5.2
T2023	--	5.6	3.9	Sheet	Sheet	5.6
T2041	--	11.7	8.2	Sheet	Sheet	13.2
T2042	--	11.9	8.3	Sheet	Sheet	13.0
T2043	17.2	11.8	8.3	Sheet	Weld Failure	8.1
T2044	--	11.5	8.0	Sheet	Sheet	12.7
T2211	--	4.7	3.3	Sheet	Sheet	4.0
T2212	--	4.9	3.4	Sheet	Sheet	4.6
T2213	--	4.5	3.1	Sheet	Sheet	4.1

Table C.3 Resistance results for tension specimens with 6.4mm thick angles – Cont.

Specimen Name	Weld Failure CSA S136 Eq. E2.2.2-1 (kN)	Sheet Failure CSA S136 Eq. E2.2.2-2 (kN)	Reduced Design Resistance for Lapped Joints P_n (kN)	Predicted Failure Mode	Recorded Failure Mode	Measured Resistance (kN)
T2221	--	4.5	3.1	Sheet	Sheet	5.2
T2222	--	4.8	3.4	Sheet	Sheet	5.0
T2223	--	5.0	3.5	Sheet	Sheet	7.2
T2224	--	5.1	3.6	Sheet	Sheet	4.9
T2241	--	8.7	6.1	Sheet	Sheet	9.6
T2242	--	9.0	6.3	Sheet	Sheet	9.2
T2243	--	8.8	6.2	Sheet	Sheet	8.3

Table C.4 Resistance results for tension specimens with 3.2mm thick angles

Specimen Name	Weld Failure CSA S136 Eq. E2.2.2-1 (kN)	Sheet Failure CSA S136 Eq. E2.2.2-2 (kN)	Reduced Design Resistance for Lapped Joints P_n (kN)	Predicted Failure Mode	Recorded Failure Mode	Measured Resistance (kN)
T1621T	--	6.0	4.2	Sheet	Sheet	9.5
T1622T	--	5.9	4.1	Sheet	Sheet	9.5
T1623T	--	6.6	4.6	Sheet	Sheet	8.7
T1641T	17.4	12.9	9.0	Sheet	Weld Failure	9.3
T1642T	19.8	14.0	9.8	Sheet	Weld Failure	10.8
T1643T	18.1	12.3	8.6	Sheet	Weld Failure	9.2
T1821T	18.0	7.3	5.1	Sheet	Weld Failure	5.6
T1822T	17.5	7.8	5.5	Sheet	Weld Failure	5.4
T1823T	24.3	8.3	5.8	Sheet	Weld Failure	8.3
T1841T	31.3	15.8	11.1	Sheet	Weld Failure	13.0
T1842T	24.3	16.1	11.3	Sheet	Weld Failure	10.0
T1843T	21.1	14.1	9.9	Sheet	Weld Failure	12.4
T2021T	--	4.7	3.3	Sheet	Sheet	6.2
T2022T	--	5.5	3.9	Sheet	Sheet	6.2
T2023T	--	5.7	4.0	Sheet	Sheet	3.6
T2041T	17.5	10.1	7.1	Sheet	Weld Failure	8.4
T2042T	--	9.7	6.8	Sheet	Sheet	11.1
T2043T	--	9.4	6.6	Sheet	Sheet	9.8
T2221T	--	4.5	3.1	Sheet	Sheet	3.9
T2222T	--	4.3	3.0	Sheet	Sheet	2.0
T2223T	--	4.5	3.2	Sheet	Sheet	4.4
T2224T	--	3.6	2.5	Sheet	Sheet	5.2
T2225T	--	3.9	2.7	Sheet	Sheet	4.8
T2241T	--	8.5	5.9	Sheet	Sheet	7.9
T2242T	--	8.7	6.1	Sheet	Sheet	7.6
T2243T	--	8.5	5.9	Sheet	Sheet	11.2
T2244T	--	7.3	5.1	Sheet	Sheet	6.0

Table C.5 Resistance results for cyclic shear specimens with 6.4mm thick plates

Specimen Name	Sheet Failure CSA S136 E2.2.1-2 (kN)	Sheet Failure CSA S136 E2.2.1-3 (kN)	Sheet Failure CSA S136 E2.2.1-4 (kN)	Predicted Resist. P_n (kN)	Predicted Failure Mode	Recorded Failure Mode	Measured Resist. P_u (kN)
SC1621	20.6	--	--	20.6	Sheet	Sheet Bearing	27.6
SC1622	19.8	--	--	19.8	Sheet	Sheet Bearing	29.2
SC1623	20.5	--	--	20.5	Sheet	Sheet Bearing	26.6
SC1624	21.7	--	--	21.7	Sheet	Sheet Bearing	32.5
SC1641	42.3	--	--	25.6	Weld	Weld Shear	41.6
SC1642	40.2	--	--	23.1	Weld	Weld Shear	34.0
SC1643	38.1	--	--	19.7	Weld	Weld Shear	37.1
SC1644	40.4	--	--	16.4	Weld	Weld Shear	16.4
SC1821	16.5	--	--	16.5	Sheet	Sheet Tear	22.4
SC1822	18.0	--	--	18.0	Sheet	Sheet Tear	26.0
SC1823	18.5	--	--	18.5	Sheet	Sheet Tear	25.1
SC1824	18.8	--	--	18.8	Sheet	Sheet Tear	26.5
SC1841	34.0	--	--	25.7	Weld	Weld Shear	21.0
SC1842	35.9	--	--	26.0	Weld	Weld Shear	31.7
SC1843	37.9	--	--	22.1	Weld	Weld Shear	36.8
SC2021	--	13.7	--	13.7	Sheet	Sheet Tear	17.3
SC2022	--	13.6	--	13.6	Sheet	Sheet Tear	16.4
SC2023	12.8	--	--	12.8	Sheet	Sheet Tear	16.6
SC2024	12.9	--	--	12.9	Sheet	Sheet Tear	16.4
SC2041	20.8	--	--	20.8	Sheet	Sheet Tear	27.1
SC2042	21.1	--	--	21.1	Sheet	Sheet Bearing	29.3
SC2043	21.6	--	--	17.5	Weld	Weld Shear	25.6
SC2044	21.0	--	--	21.0	Sheet	Sheet Bearing	30.5
SC2221	--	10.2	--	10.2	Sheet	Sheet Tear	16.2
SC2222	--	10.2	--	10.2	Sheet	Sheet Tear	15.1
SC2223	--	10.0	--	10.0	Sheet	Sheet Tear	14.7
SC2224	--	10.1	--	10.1	Sheet	Sheet Tear	17.2
SC2241	22.8	--	--	22.8	Sheet	Sheet Bearing	27.6
SC2242	23.6	--	--	23.6	Sheet	Sheet Tear	26.7
SC2243	23.0	--	--	23.0	Sheet	Weld Shear	21.2
SC2244	22.7	--	--	22.7	Sheet	Sheet Bearing	26.4

APPENDIX D. MEASURED-TO-PREDICTED RESULTS

Appendix D provides the list of measured-to-predicted results used in Chapter 4 of this text for the analysis of the CSA S136 (2007) design standards.

Table D.1 Measured-to-predicted results for effective weld diameters (shear spec.)

Specimen		Weld Data		
Name	Configuration	Predicted effective diam. CSA S136 E2.2.1-5 (d_{effc}) (mm)	Measured effective diam. (d_{eff}) (mm)	Measured to predicted ratio (d_{effc} / d_{eff})
SM1621P	Perimeter	9.3	12.1	1.3
SM1622P	Perimeter	8.5	6.9	0.8
SM1623P	Perimeter	7.7	12.2	1.6
SM1624P	Perimeter	7.1	8.0	1.1
SM1821P	Perimeter	8.3	8.9	1.1
SM1822P	Perimeter	9.3	9.6	1.0
SM1823P	Perimeter	8.1	8.6	1.1
SM1824P	Perimeter	8.6	10.2	1.2
SM2021P	Perimeter	9.7	10.3	1.1
SM2221P	Perimeter	8.2	9.0	1.1
SM2224P	Perimeter	9.8	8.6	0.9
SM1621T	2-layer	8.1	9.4	1.2
SM1622T	2-layer	8.8	9.6	1.1
SM1623T	2-layer	8.5	9.4	1.1
SM2241T	4-layer	8.7	8.5	1.0
SM2243T	4-layer	8.7	8.7	1.0
SM2243	4-layer	8.8	7.9	0.9
SM2043T	4-layer	8.1	7.3	0.9
SM2043	4-layer	9.0	9.8	1.1
SM1841T	4-layer	7.3	8.6	1.2
SM1842T	4-layer	6.9	8.3	1.2
SM1843T	4-layer	7.7	8.7	1.1
SM1841	4-layer	9.3	10.0	1.1
SM1842	4-layer	9.4	9.7	1.0
SM1843	4-layer	8.7	8.8	1.0
SM1844	4-layer	9.5	10.2	1.1
SM1641T	4-layer	6.2	7.9	1.3
SM1642T	4-layer	6.6	9.5	1.4
SM1643T	4-layer	6.8	8.6	1.3
SM1641	4-layer	7.6	9.4	1.2
SM1642	4-layer	8.0	10.4	1.3
SM1643	4-layer	8.0	9.8	1.2
SM1644	4-layer	8.3	11.8	1.4

Table D.2 Measured-to-predicted results for shear specimens governed by E2.2.1-1

Specimen		Predicted Resist. P_n CSA S136 E2.2.1-1 (kN)	Measured Resist. P_u (kN)	Measured to predicted ratio P_u/P_n (kN)
Name	Configuration			
SM1621P	Perimeter	37.1	44.3	1.20
SM1622P	Perimeter	12.0	17.3	1.44
SM1623P	Perimeter	37.9	47.5	1.25
SM1624P	Perimeter	16.2	25.1	1.55
SM1821P	Perimeter	20.0	17.1	0.85
SM1822P	Perimeter	23.4	30.3	1.30
SM1823P	Perimeter	18.7	24.8	1.33
SM1824P	Perimeter	26.6	39.1	1.47
SM2021P	Perimeter	27.0	36.7	1.36
SM2221P	Perimeter	20.4	27.0	1.32
SM2224P	Perimeter	18.7	27.0	1.45
SM1621T	2-layer	22.5	32.6	1.45
SM1622T	2-layer	23.5	35.2	1.50
SM1623T	2-layer	22.2	33.8	1.53
SM2241T	4-layer	18.1	24.0	1.32
SM2243T	4-layer	19.3	26.8	1.39
SM2243	4-layer	15.6	23.7	1.52
SM2043T	4-layer	13.5	31.3	2.32
SM2043	4-layer	24.3	29.9	1.23
SM1841T	4-layer	18.7	28.7	1.54
SM1842T	4-layer	17.6	26.0	1.48
SM1843T	4-layer	19.0	29.3	1.54
SM1841	4-layer	25.3	34.5	1.37
SM1842	4-layer	23.8	30.8	1.29
SM1843	4-layer	19.5	27.4	1.40
SM1844	4-layer	26.6	33.8	1.27
SM1641T	4-layer	15.9	25.5	1.60
SM1642T	4-layer	22.8	30.0	1.32
SM1643T	4-layer	18.7	26.9	1.44
SM1641	4-layer	22.2	33.4	1.51
SM1642	4-layer	27.6	40.6	1.47
SM1643	4-layer	24.4	34.8	1.43
SM1644	4-layer	35.4	47.5	1.34

Table D.3 Measured-to-predicted results for shear specimens governed by E2.2.1-2

Specimen		Predicted Resist. P_n CSA S136 E2.2.1-2 (kN)	Measured Resist. P_u (kN)	Measured to predicted ratio P_u/P_n (kN)
Name	Configuration			
SM2022P	Perimeter	27.6	32.2	1.17
SM2023P	Perimeter	23.2	30.2	1.30
SM2024P	Perimeter	25.8	29.4	1.14
SM2222P	Perimeter	21.9	28.5	1.30
SM2223P	Perimeter	21.1	27.0	1.28
SM1821T	2-layer	16.8	26.3	1.57
SM1822T	2-layer	12.8	20.6	1.61
SM1823T	2-layer	16.0	24.7	1.55
SM1824T	2-layer	14.6	21.3	1.45
SM2021T	2-layer	11.8	18.0	1.53
SM2022T	2-layer	12.4	18.3	1.47
SM2023T	2-layer	11.5	18.6	1.62
SM2044T	4-layer	22.5	31.1	1.38
SM2242T	4-layer	20.5	17.4	0.85
SM1821	2-layer	18.7	26.8	1.43
SM1822	2-layer	18.1	28.0	1.55
SM1823	2-layer	17.4	25.0	1.44
SM1824	2-layer	19.6	27.9	1.42
SM2021	2-layer	11.8	16.1	1.36
SM2022	2-layer	11.7	16.7	1.42
SM2023	2-layer	12.6	17.7	1.41
SM2024	2-layer	11.6	16.3	1.41
SM2041	4-layer	22.8	28.4	1.25
SM2242	4-layer	23.1	29.1	1.26
SM2041T	4-layer	19.7	27.3	1.39
SM2042T	4-layer	20.1	33.0	1.64
SM2244T	4-layer	18.2	26.8	1.47
SM1621	2-layer	18.2	32.8	1.80
SM1622	2-layer	18.2	34.8	1.91
SM1623	2-layer	20.1	33.3	1.66
SM1624	2-layer	18.4	33.2	1.80
SM2042	4-layer	21.3	31.9	1.50
SM2044	4-layer	21.2	25.0	1.18
SM2241	4-layer	18.6	25.8	1.38
SM2244	4-layer	17.7	25.8	1.46

Table D.4 Measured-to-predicted results for shear specimens governed by Eq. 4-1

Specimen		Predicted Resist. P_n Equation 4-1 (kN)	Measured Resist. P_u (kN)	Measured to predicted ratio P_u/P_n (kN)
Name	Configuration			
SM2022P	Perimeter	30.1	32.2	1.07
SM2023P	Perimeter	25.3	30.2	1.19
SM2024P	Perimeter	28.2	29.4	1.04
SM2222P	Perimeter	23.9	28.5	1.19
SM2223P	Perimeter	23.0	27.0	1.17
SM1821T	2-layer	18.3	26.3	1.44
SM1822T	2-layer	14.0	20.6	1.47
SM1823T	2-layer	17.4	24.7	1.42
SM1824T	2-layer	16.0	21.3	1.33
SM2021T	2-layer	12.9	18.0	1.40
SM2022T	2-layer	13.5	18.3	1.35
SM2023T	2-layer	12.5	18.6	1.48
SM2044T	4-layer	24.5	31.1	1.27
SM2242T	4-layer	22.4	17.4	0.78
SM1821	2-layer	20.4	26.8	1.31
SM1822	2-layer	19.7	28.0	1.42
SM1823	2-layer	18.9	25.0	1.32
SM1824	2-layer	21.4	27.9	1.30
SM2021	2-layer	12.9	16.1	1.25
SM2022	2-layer	12.8	16.7	1.31
SM2023	2-layer	13.7	17.7	1.29
SM2024	2-layer	12.6	16.3	1.29
SM2041	4-layer	24.8	28.4	1.15
SM2242	4-layer	25.2	29.1	1.15
SM2041T	4-layer	21.5	27.3	1.27
SM2042T	4-layer	21.9	33.0	1.50
SM2244T	4-layer	19.9	26.8	1.35
SM1621	2-layer	19.9	32.8	1.65
SM1622	2-layer	19.9	34.8	1.75
SM1623	2-layer	21.9	33.3	1.52
SM1624	2-layer	20.1	33.2	1.65
SM2042	4-layer	23.3	31.9	1.37
SM2044	4-layer	23.2	25.0	1.08
SM2241	4-layer	20.3	25.8	1.27
SM2244	4-layer	19.3	25.8	1.34

Table D.5 Measured-to-predicted results for shear specimens governed by E2.2.1-3

Specimen		Predicted Resist. P_n CSA S136 E2.2.1-3 (kN)	Measured Resist. P_u (kN)	Measured to predicted ratio P_u/P_n (kN)
Name	Configuration			
SM2221T	2-layer	9.3	15.1	1.62
SM2222T	2-layer	9.2	14.0	1.53
SM2223T	2-layer	9.1	13.6	1.48
SM2224T	2-layer	9.2	15.2	1.64
SM2221	2-layer	9.3	14.0	1.51
SM2222	2-layer	9.4	15.3	1.63
SM2223	2-layer	9.4	14.8	1.58
SM2224	2-layer	9.3	15.3	1.64

Table D.6 Measured-to-predicted results for tension specimens governed by E2.2.2-1

Specimen		Predicted Resist. P_n CSA S136 E2.2.2-1 (kN)	Reduced Predicted Resist. $0.7*P_n$ CSA S136 E2.2.2-1 (kN)	Measured Resist. P_u (kN)	Measured to predicted ratio P_u/P_n (kN)	Measured to reduced predicted ratio $P_u/(0.7*P_n)$ (kN)
Name	Configuration					
T1641T	4-layer	12.0	8.4	9.3	0.78	1.11
T1642T	4-layer	13.7	9.6	10.8	0.79	1.13
T1643T	4-layer	11.1	7.8	9.2	0.83	1.18
T1821T	2-layer	12.7	8.9	5.6	0.44	0.63
T1822T	2-layer	15.8	11.1	5.4	0.34	0.49
T1823T	2-layer	18.3	12.8	8.3	0.45	0.65
T1841T	4-layer	13.9	9.8	13.0	0.94	1.34
T1842T	4-layer	14.4	10.1	10.0	0.70	1.00
T1843T	4-layer	11.5	8.1	12.4	1.07	1.53
T2041T	4-layer	10.3	7.2	8.4	0.81	1.16
T1623	2-layer	22.3	15.6	11.7	0.52	0.75
T1641	4-layer	17.8	12.4	12.8	0.72	1.03
T1642	4-layer	17.0	11.9	15.4	0.90	1.29
T1643	4-layer	11.8	8.3	19.4	1.64	2.34
T1841	4-layer	18.4	12.8	9.7	0.53	0.76
T2043	4-layer	13.5	9.4	8.1	0.60	0.86

Table D.7 Measured-to-predicted results for tension specimens governed by E2.2.2-2

Specimen Name	Specimen Configuration	Predicted Resist. P_n CSA S136 E2.2.2-2 (kN)	Reduced Predicted Resist. $0.7*P_n$ CSA S136 E2.2.2-2 (kN)	Measured Resist. P_u (kN)	Measured to predicted ratio P_u/P_n (kN)	Measured to reduced predicted ratio $P_u/(0.7*P_n)$ (kN)
T1621T	2-layer	6.0	4.2	9.5	1.60	2.28
T1622T	2-layer	5.9	4.1	9.5	1.61	2.30
T1623T	2-layer	6.6	4.6	8.7	1.32	1.88
T2021T	2-layer	4.7	3.3	6.2	1.32	1.89
T2022T	2-layer	5.5	3.9	6.2	1.13	1.61
T2023T	2-layer	5.7	4.0	3.6	0.63	0.91
T2042T	4-layer	9.7	6.8	11.1	1.15	1.64
T2043T	4-layer	9.4	6.6	9.8	1.04	1.48
T2221T	2-layer	4.5	3.1	3.9	0.87	1.24
T2222T	2-layer	4.3	3.0	2.0	0.47	0.68
T2223T	2-layer	4.5	3.2	4.4	0.97	1.39
T2224T	2-layer	3.6	2.5	5.2	1.44	2.06
T2225T	2-layer	3.9	2.7	4.8	1.24	1.77
T2241T	4-layer	8.5	5.9	7.9	0.93	1.33
T2242T	4-layer	8.7	6.1	7.6	0.88	1.25
T2243T	4-layer	8.5	5.9	11.2	1.31	1.87
T2244T	4-layer	7.3	5.1	6.0	0.82	1.18
T1621	2-layer	6.7	4.7	12.9	1.91	2.73
T1622	2-layer	6.9	4.9	15.7	2.26	3.23
T1624	2-layer	7.5	5.2	12.2	1.64	2.34
T1821	2-layer	8.2	5.7	11.1	1.36	1.94
T1822	2-layer	8.3	5.8	10.3	1.25	1.78
T1823	2-layer	7.9	5.5	10.0	1.26	1.80
T1824	2-layer	8.7	6.1	10.2	1.17	1.67
T1842	4-layer	13.9	9.7	16.5	1.19	1.70
T1843	4-layer	15.3	10.7	15.2	0.99	1.41
T1844	4-layer	14.6	10.3	15.1	1.03	1.48
T2021	2-layer	5.5	3.9	5.7	1.04	1.48
T2022	2-layer	5.8	4.0	5.2	0.91	1.30
T2023	2-layer	5.6	3.9	5.6	0.99	1.42
T2041	4-layer	11.7	8.2	13.2	1.13	1.61
T2042	4-layer	11.9	8.3	13.0	1.09	1.56
T2044	4-layer	11.5	8.0	12.7	1.10	1.58
T2221	2-layer	4.5	3.1	5.2	1.15	1.64
T2222	2-layer	4.8	3.4	5.0	1.03	1.47
T2223	2-layer	5.0	3.5	7.2	1.43	2.04
T2224	2-layer	5.1	3.6	4.9	0.95	1.36
T2241	4-layer	8.7	6.1	9.6	1.10	1.58
T2242	4-layer	9.0	6.3	9.2	1.03	1.47
T2243	4-layer	8.8	6.2	8.3	0.94	1.34

APPENDIX E. LOAD VS. DEFORMATION PLOTS OF MONOTONIC SHEAR SPECIMENS

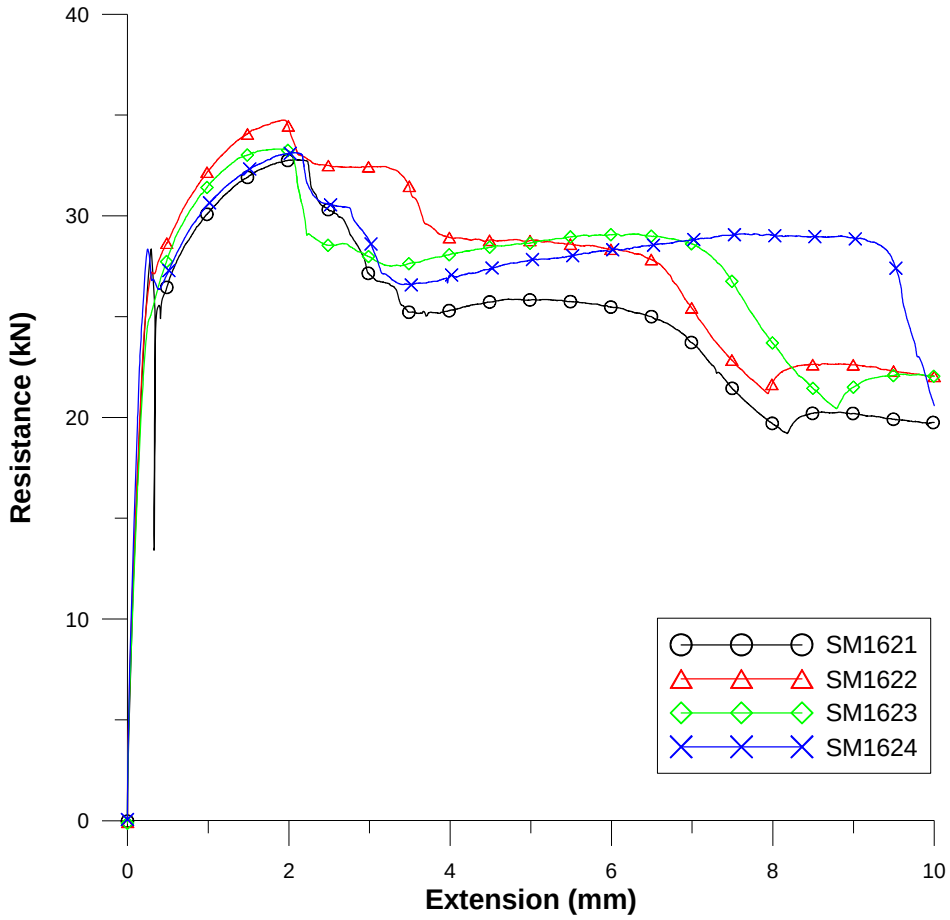

Figure E.1 : 2-layer shear specimens with 1.52 mm sheets and 6.4 mm plate

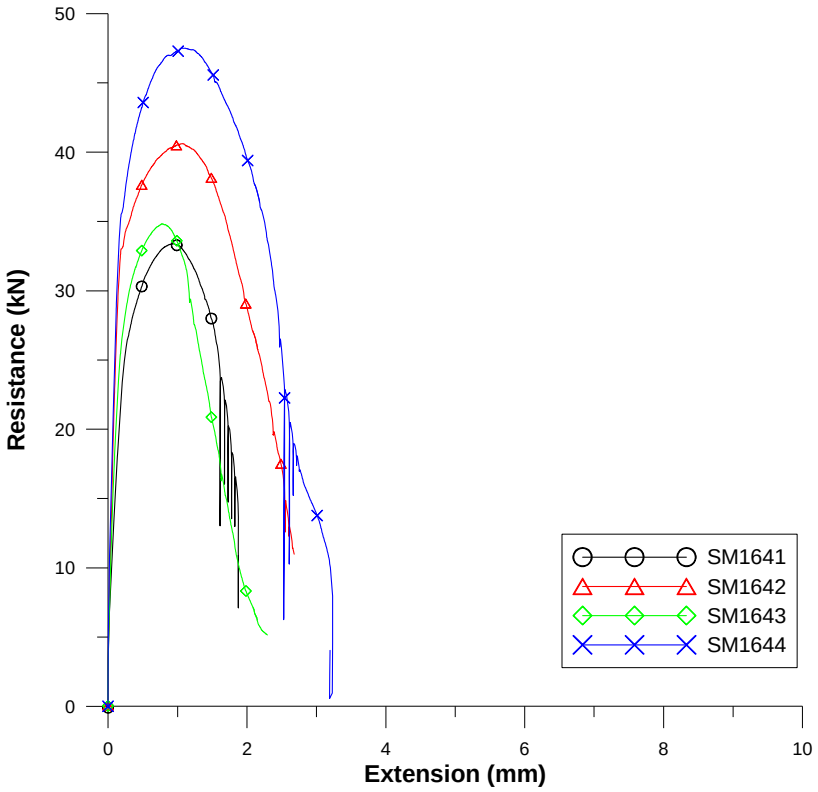

Figure E.2 : 4-layer shear specimens with 1.52 mm sheets and 6.4 mm plate

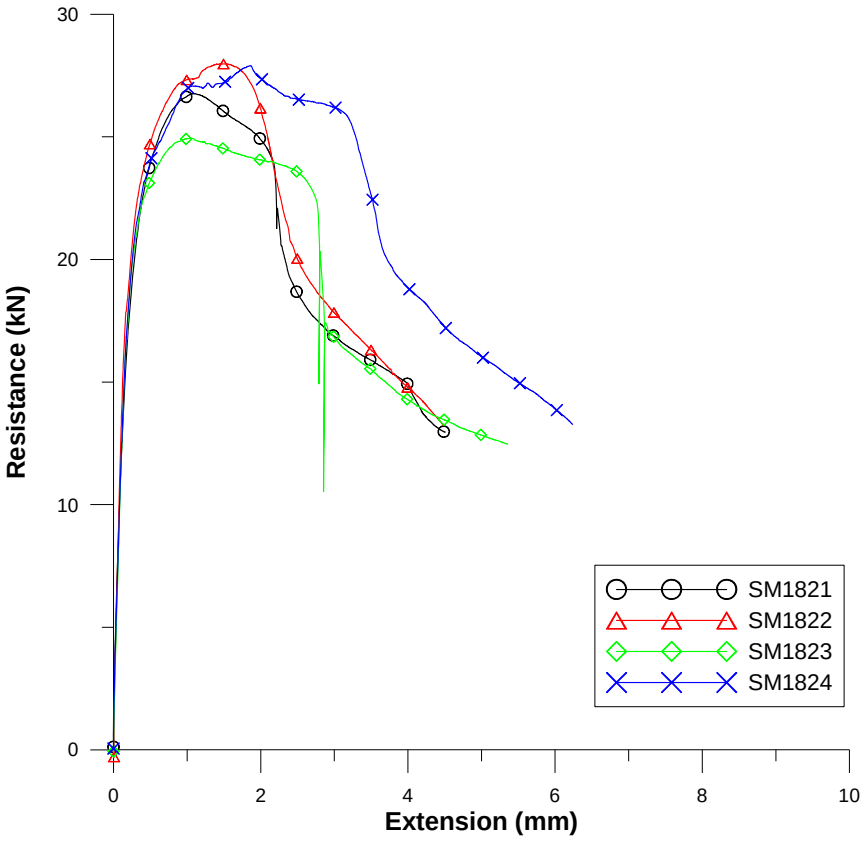

Figure E.3 : 2-layer shear specimens with 1.21 mm sheets and 6.4 mm plate

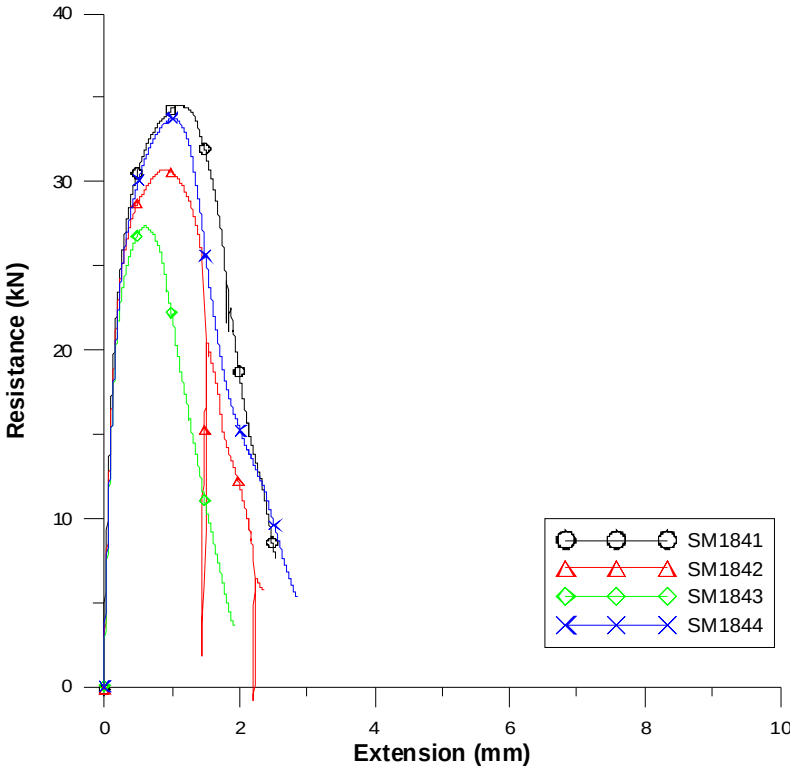

Figure E.4 : 4-layer shear specimens with 1.21 mm sheets and 6.4 mm plate

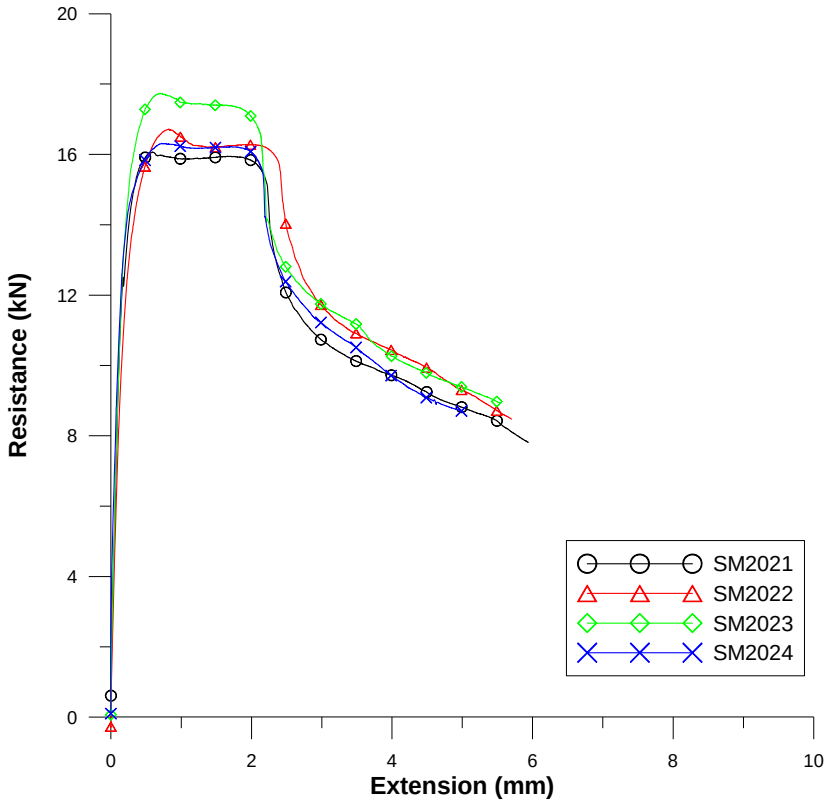

Figure E.5 : 2-layer shear specimens with 0.91 mm sheets and 6.4 mm plate

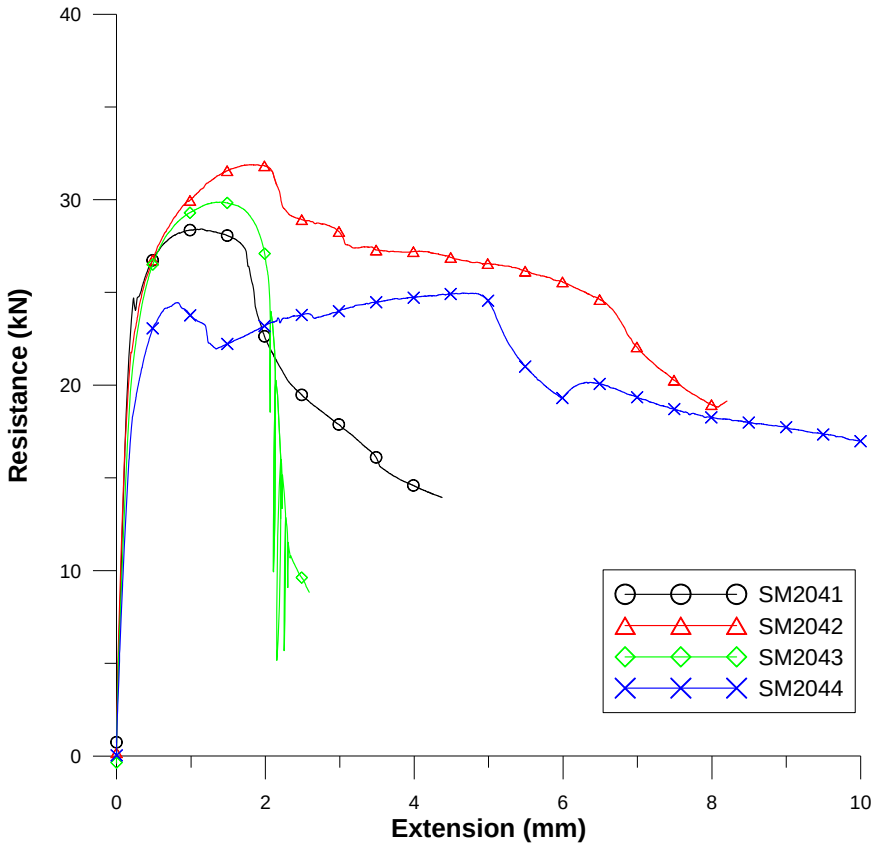

Figure E.6 4-layer shear specimens with 0.91 mm sheets and 6.4 mm plate

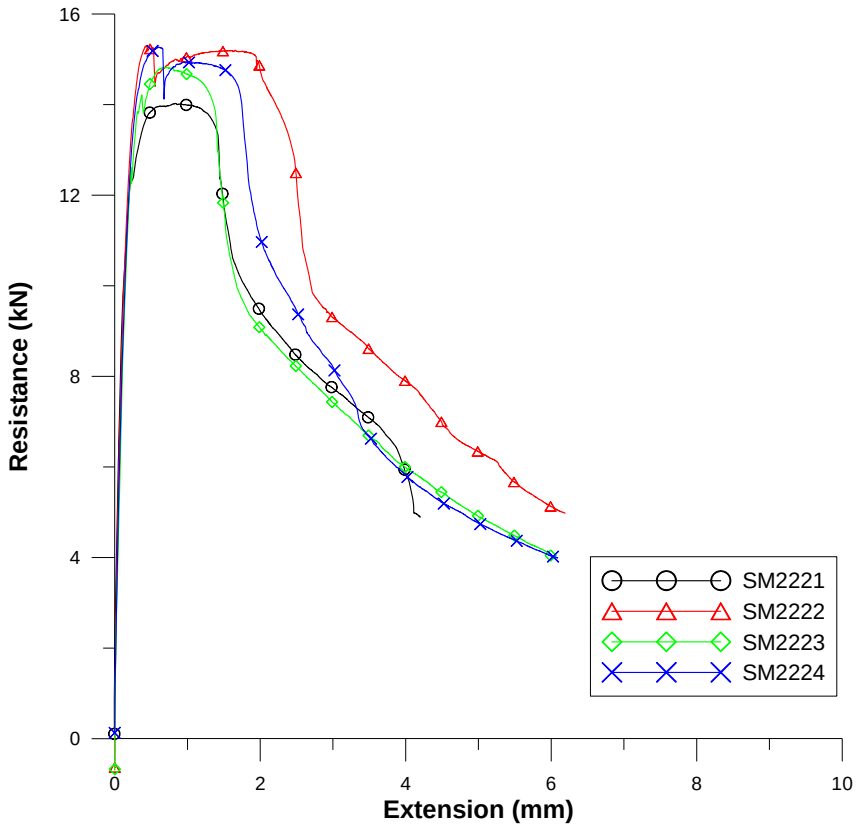

Figure E.7 2-layer shear specimens with 0.76 mm sheets and 6.4 mm plate

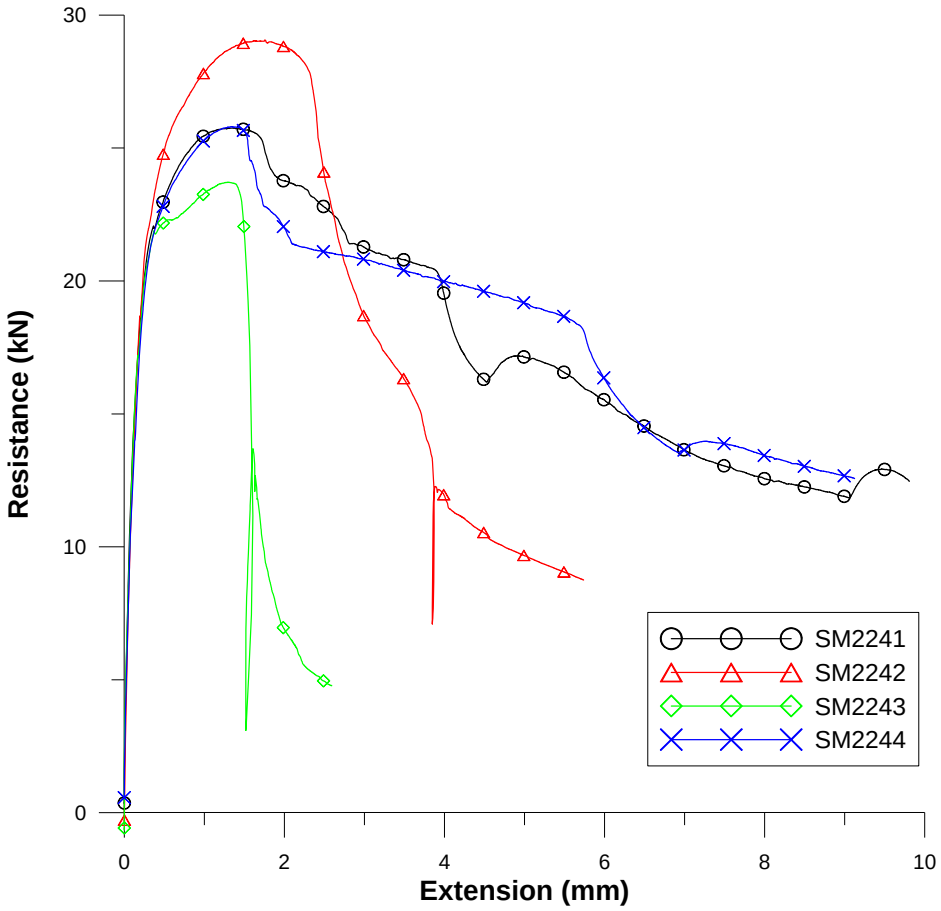

Figure E.8 4-layer shear specimens with 0.76 mm sheets and 6.4 mm plate

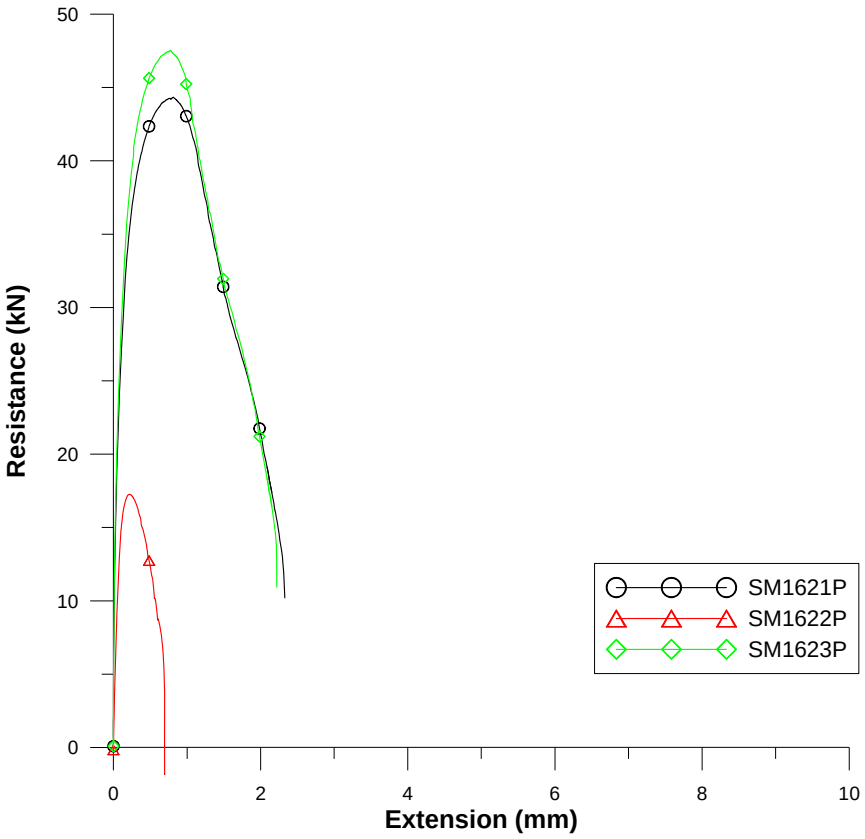

Figure E.9 Perimeter shear specimens with 1.52 mm sheets and 6.4 mm plate

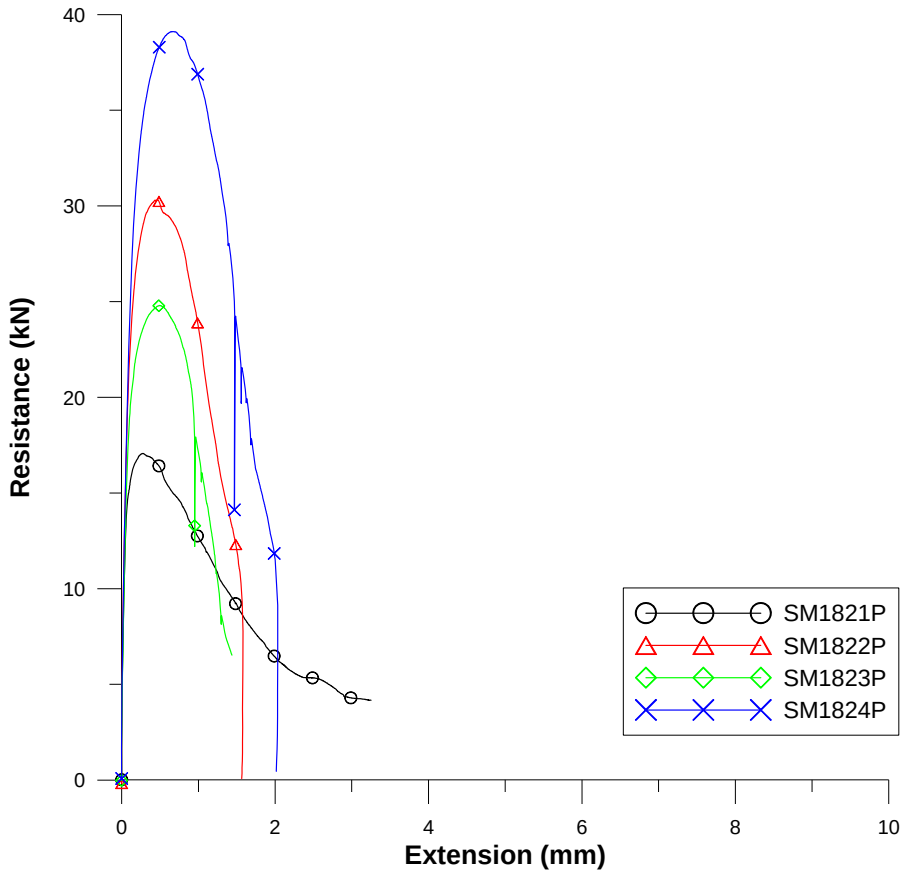

Figure E.10 Perimeter shear specimens with 1.21 mm sheets and 6.4 mm plate

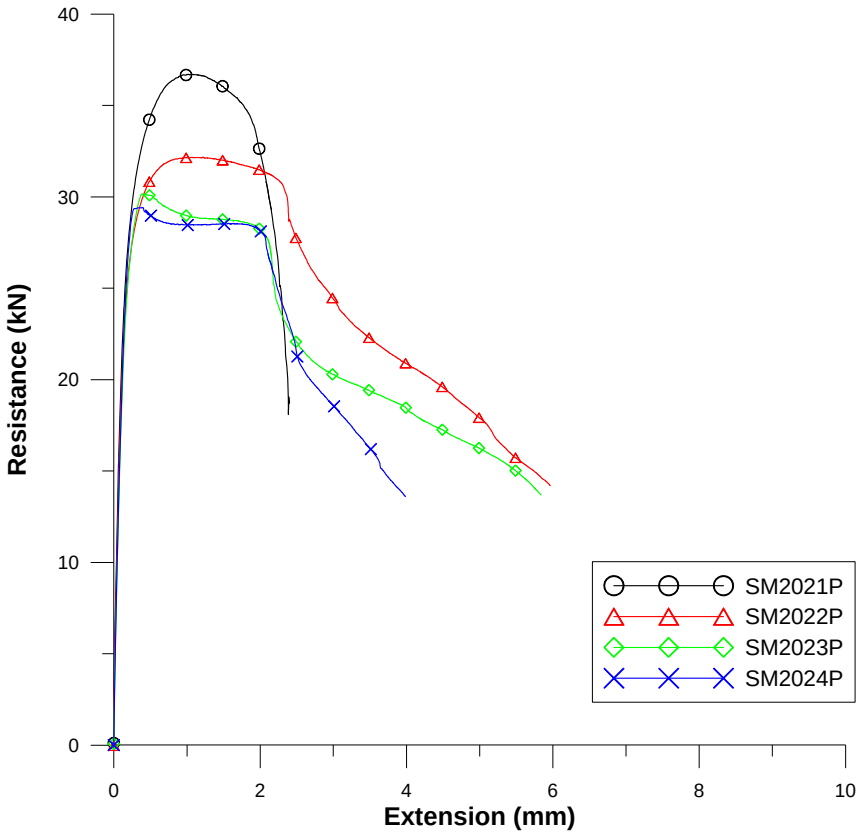

Figure E.11 Perimeter shear specimens with 0.91 mm sheets and 6.4 mm plate

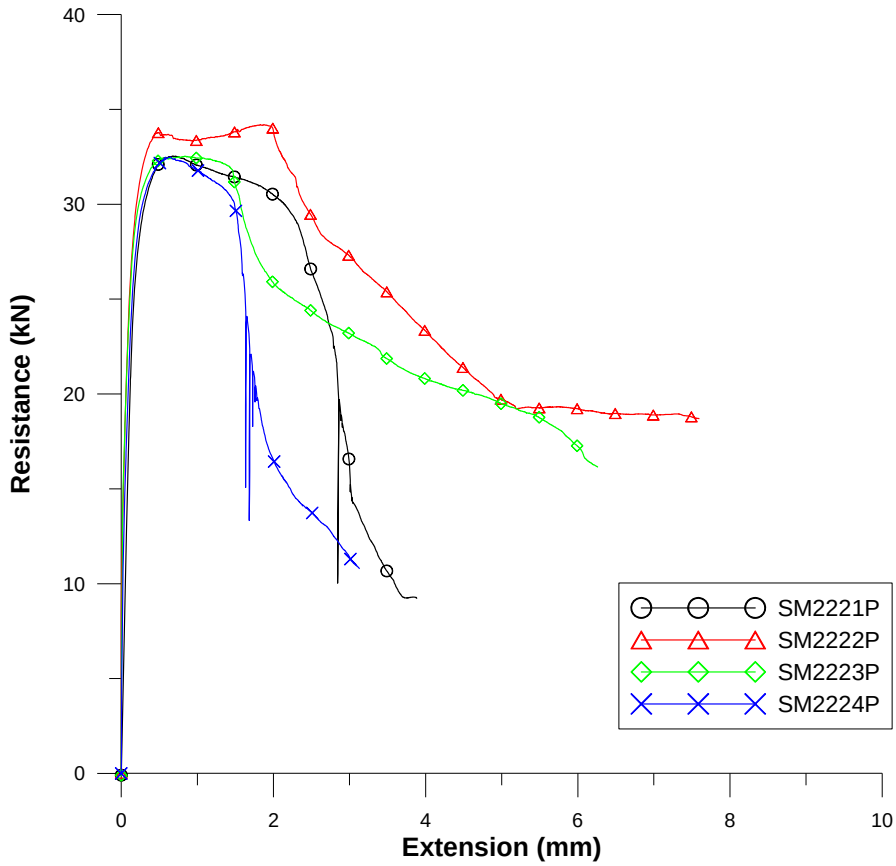

Figure E.12 Perimeter shear specimens with 0.76 mm sheets and 6.4 mm plate

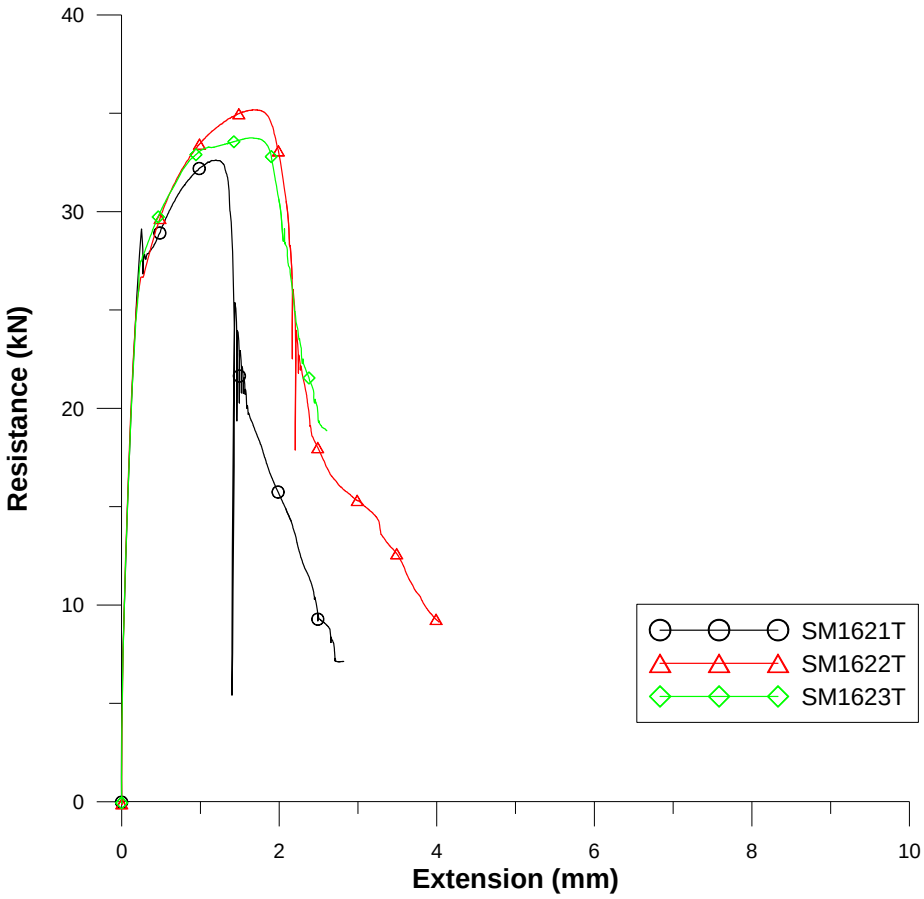

Figure E.13 2-layer shear specimens with 1.52 mm sheets and 3.2 mm plate

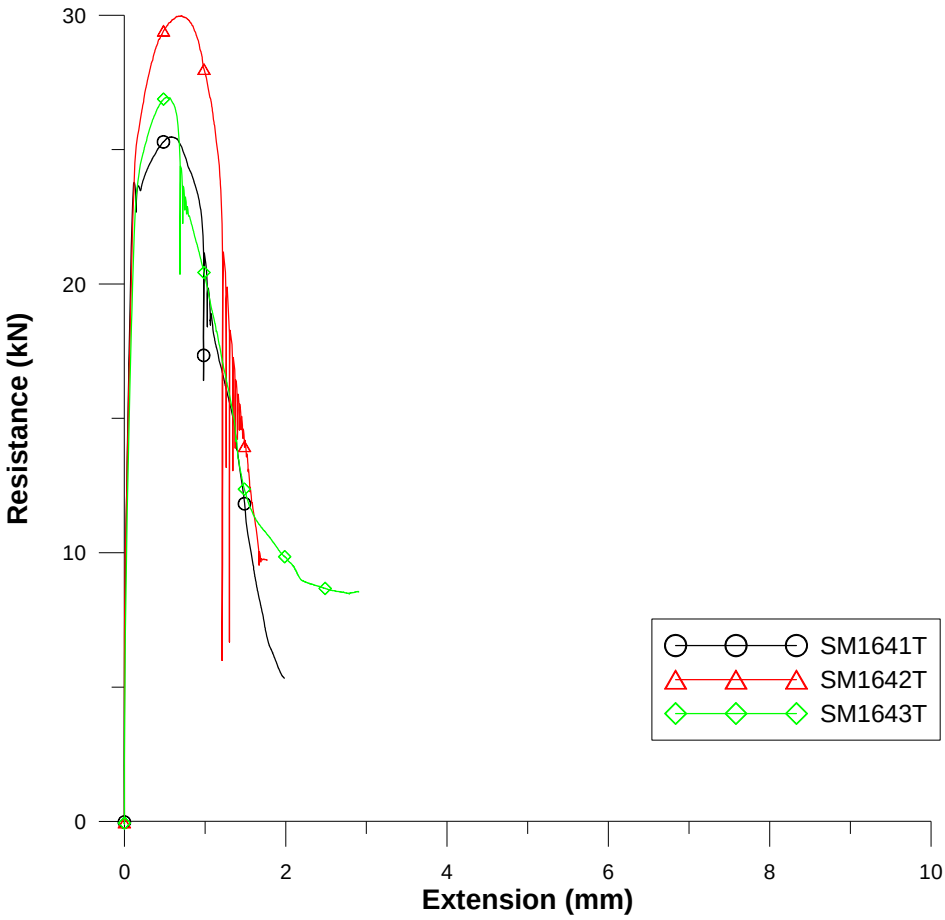

Figure E.14 2-layer shear specimens with 1.21 mm sheets and 3.2 mm plate

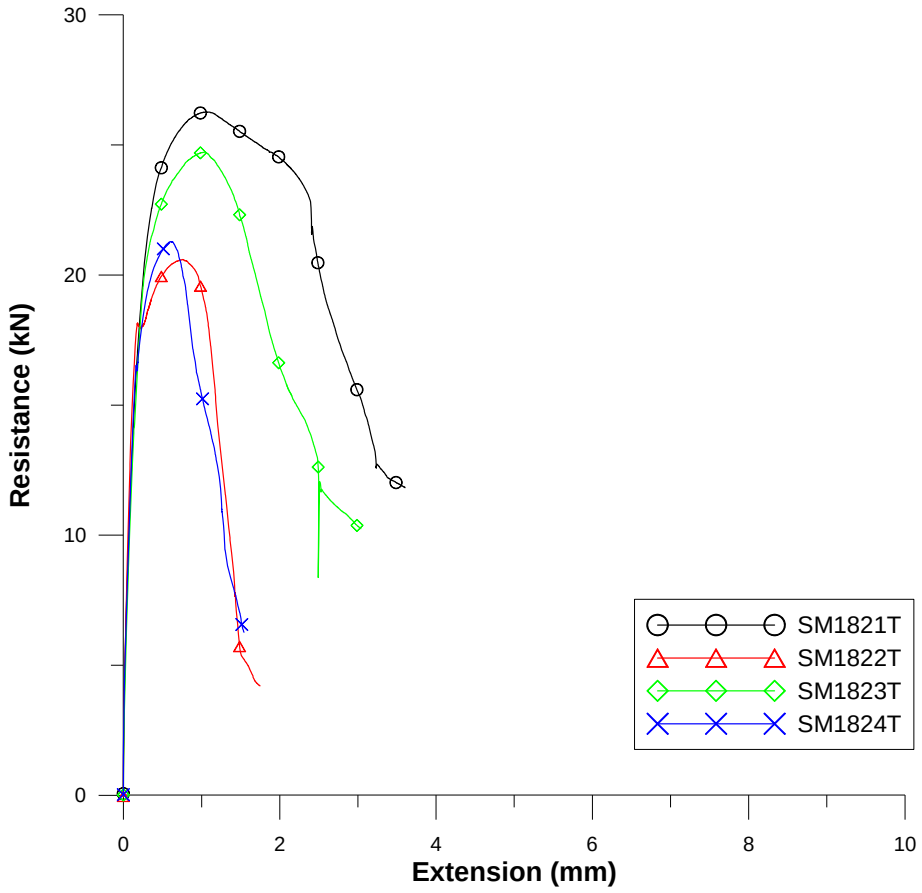

Figure E.15 4-layer shear specimens with 1.52 mm sheets and 3.2 mm plate

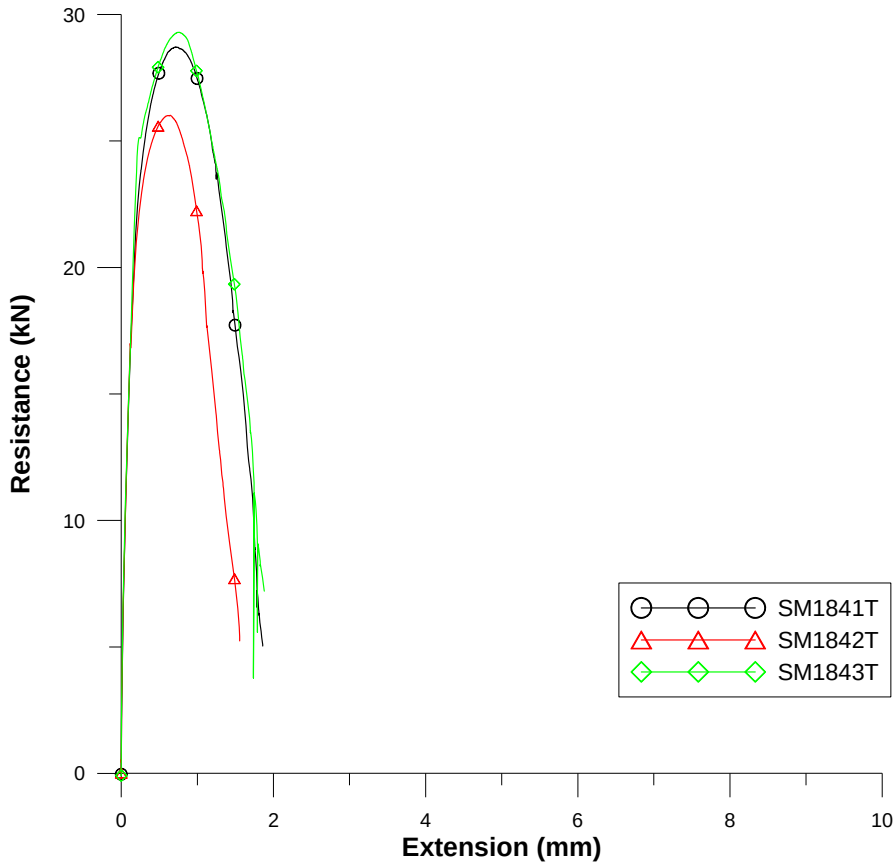

Figure E.16 4-layer shear specimens with 1.21 mm sheets and 3.2 mm plate

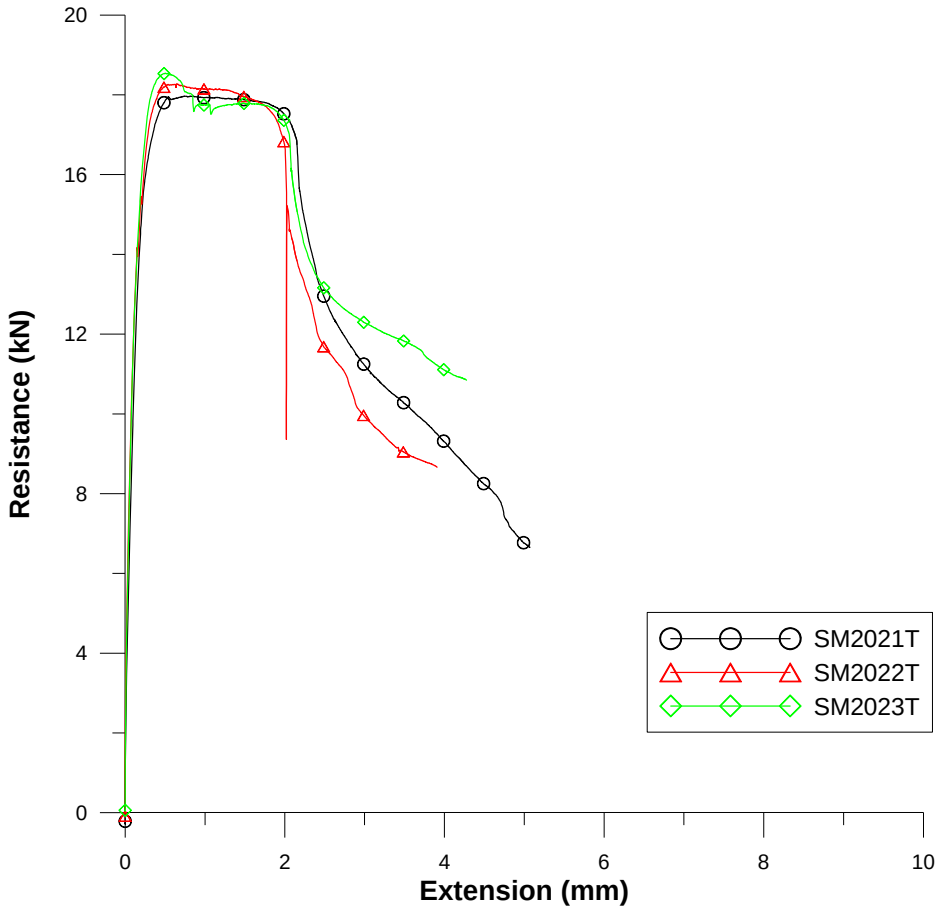

Figure E.17 2-layer shear specimens with 0.91 mm sheets and 3.2 mm plate

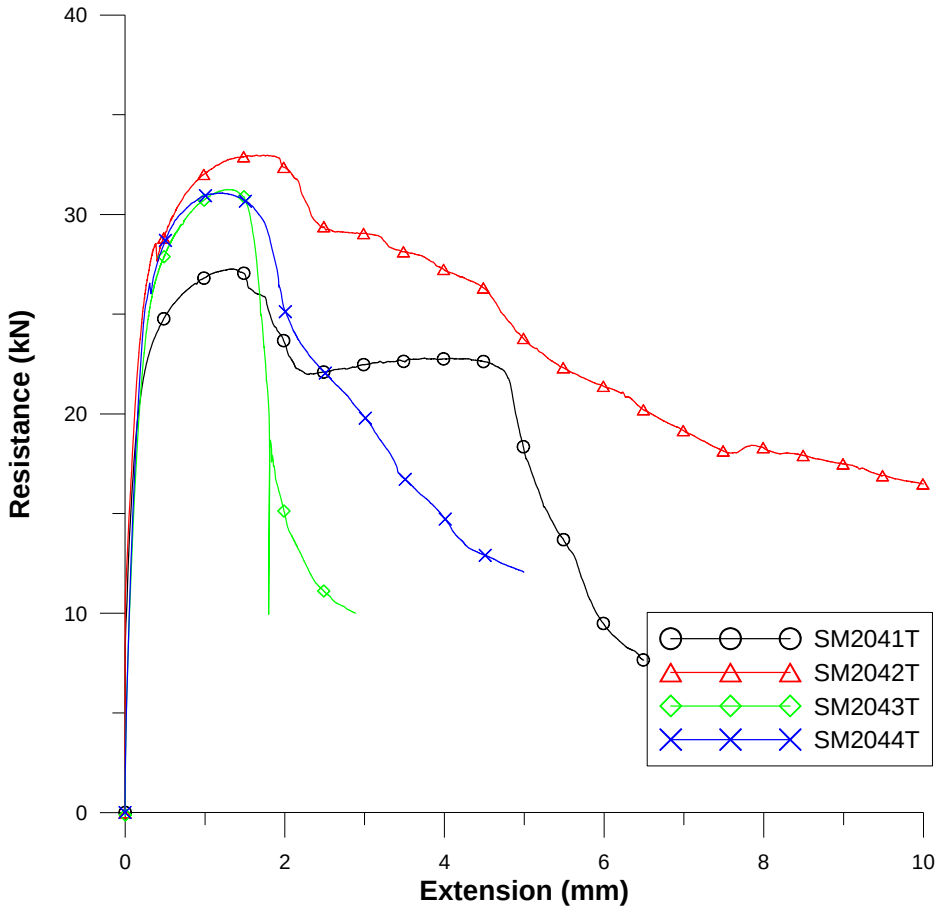

Figure E.18 4-layer shear specimens with 0.91 mm sheets and 3.2 mm plate

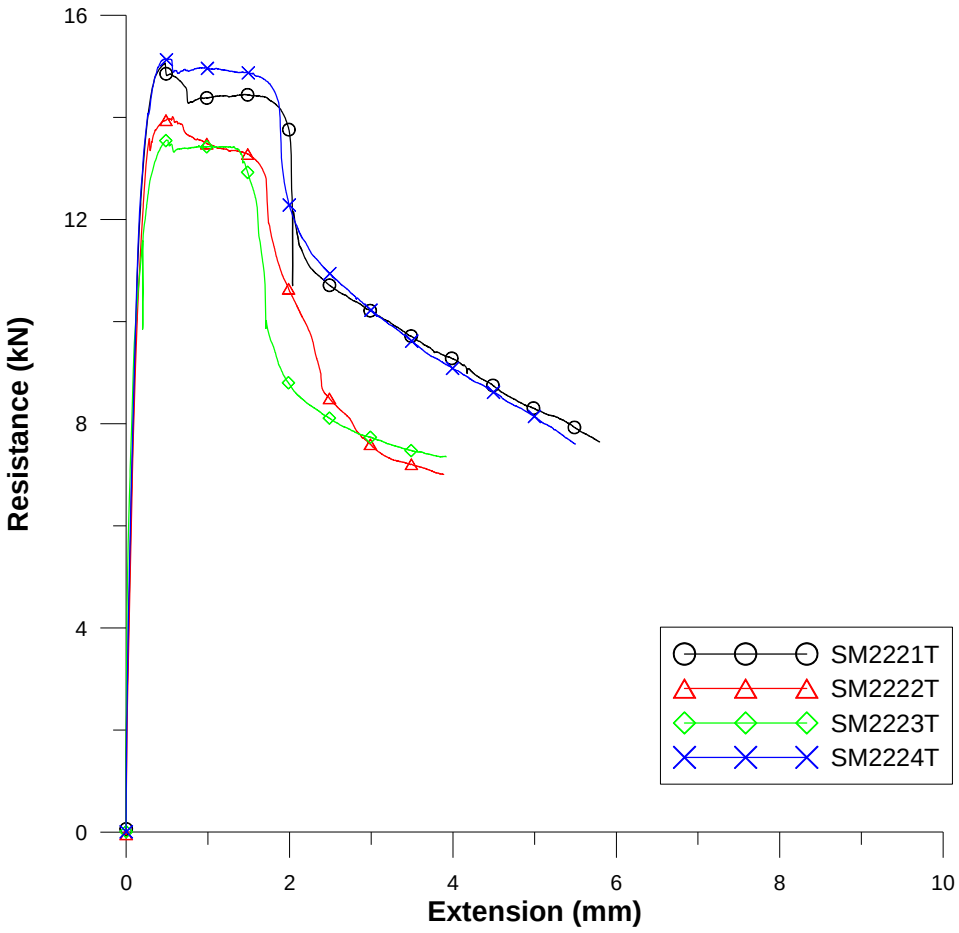

Figure E.19 2-layer shear specimens with 0.76 mm sheets and 3.2 mm plate

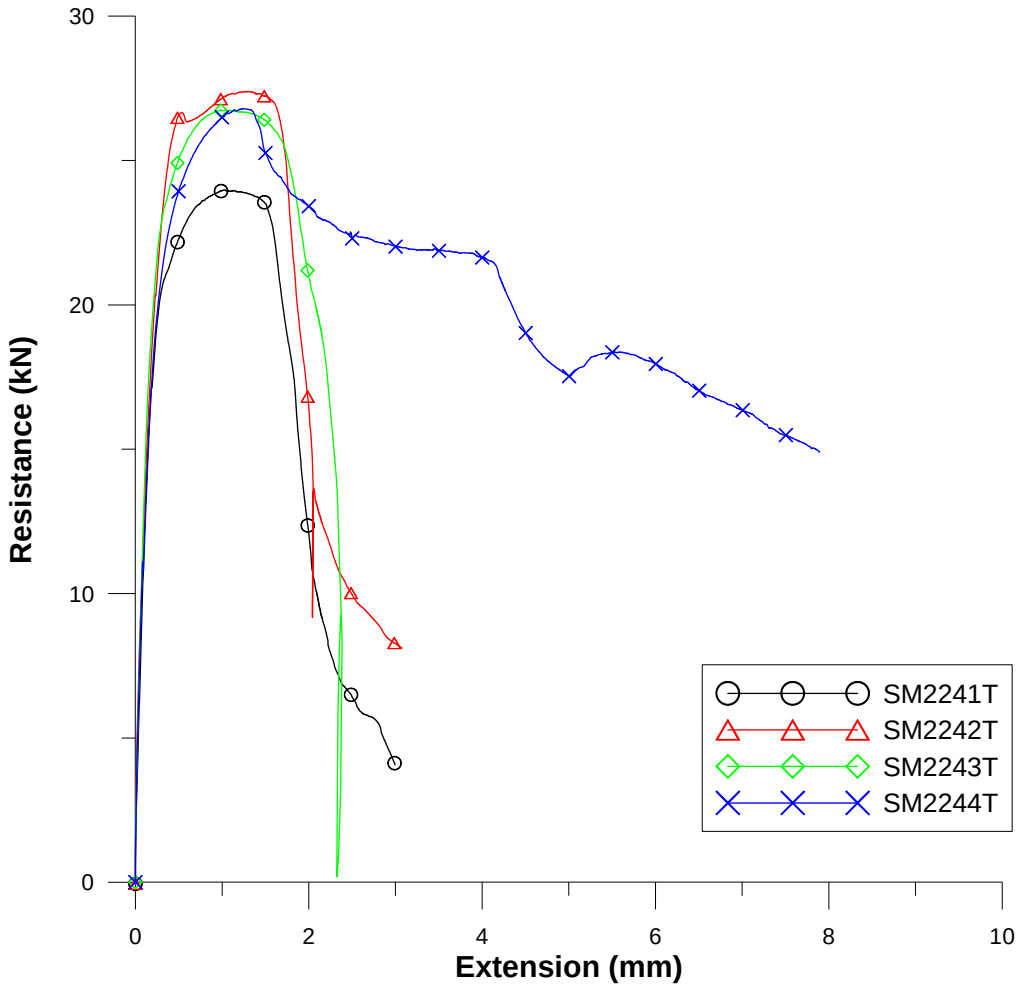

Figure E.20 4-layer shear specimens with 0.76 mm sheets and 3.2 mm plate

APPENDIX F. LOAD VS. DEFORMATION PLOTS OF REVERSED CYCLIC SHEAR SPECIMENS

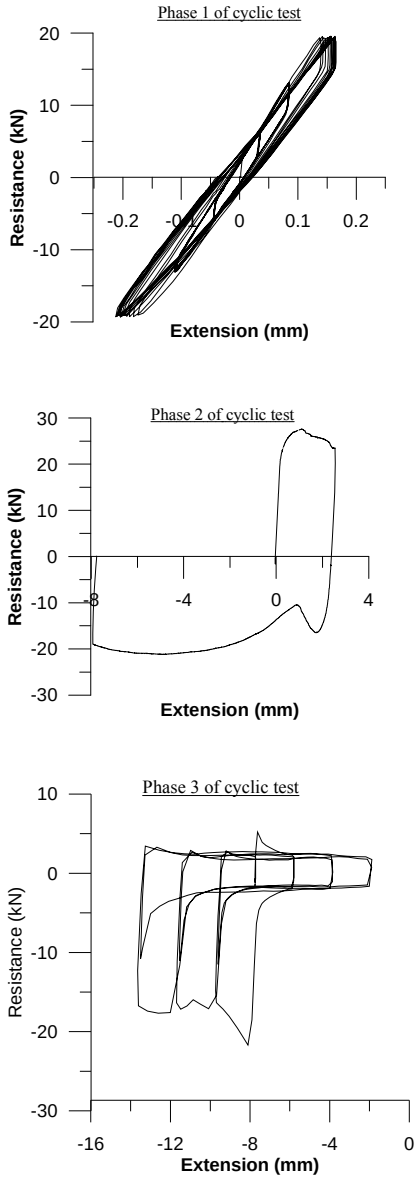

Figure F.1 2-layer shear specimen with 1.52 mm sheets and 6.4 mm plate (SC1621)

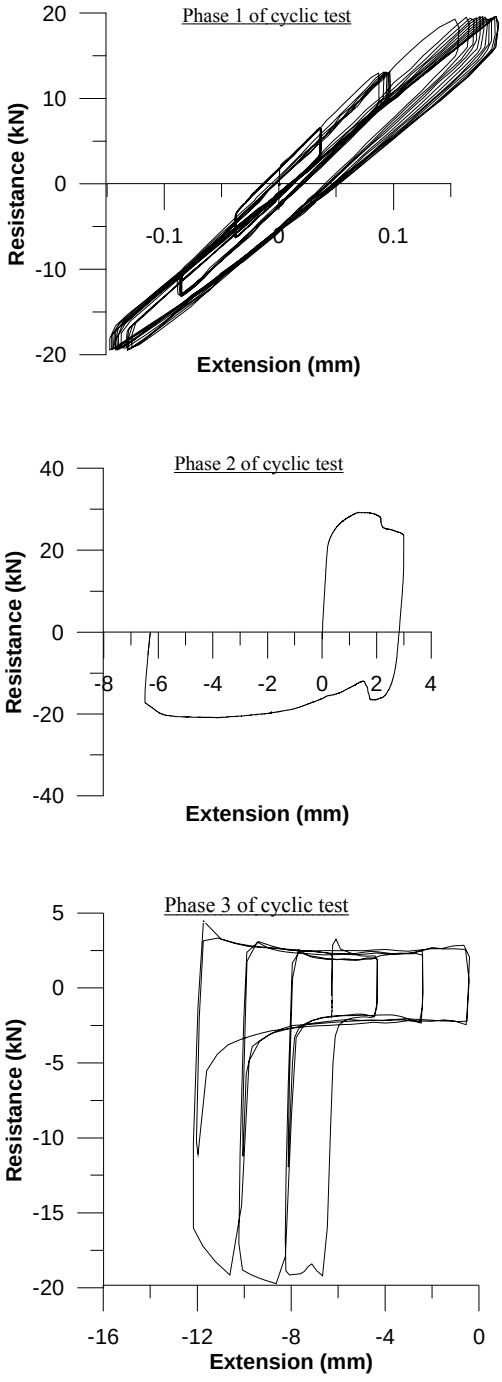

Figure F.2 2-layer shear specimen with 1.52 mm sheets and 6.4 mm plate (SC1622)

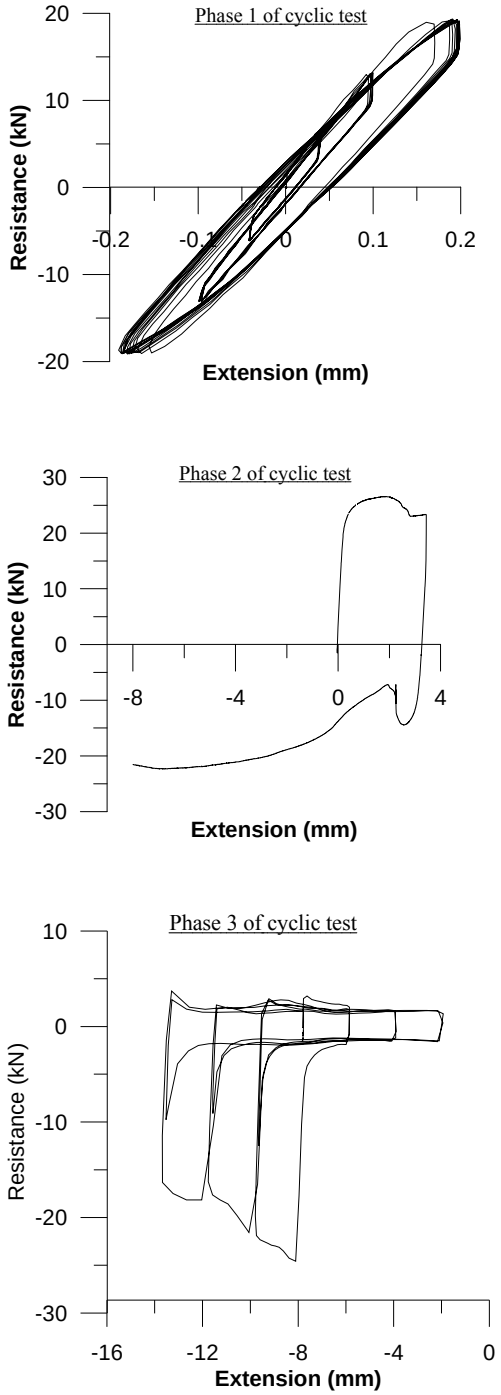

Figure F.3 2-layer shear specimen with 1.52 mm sheets and 6.4 mm plate (SC1623)

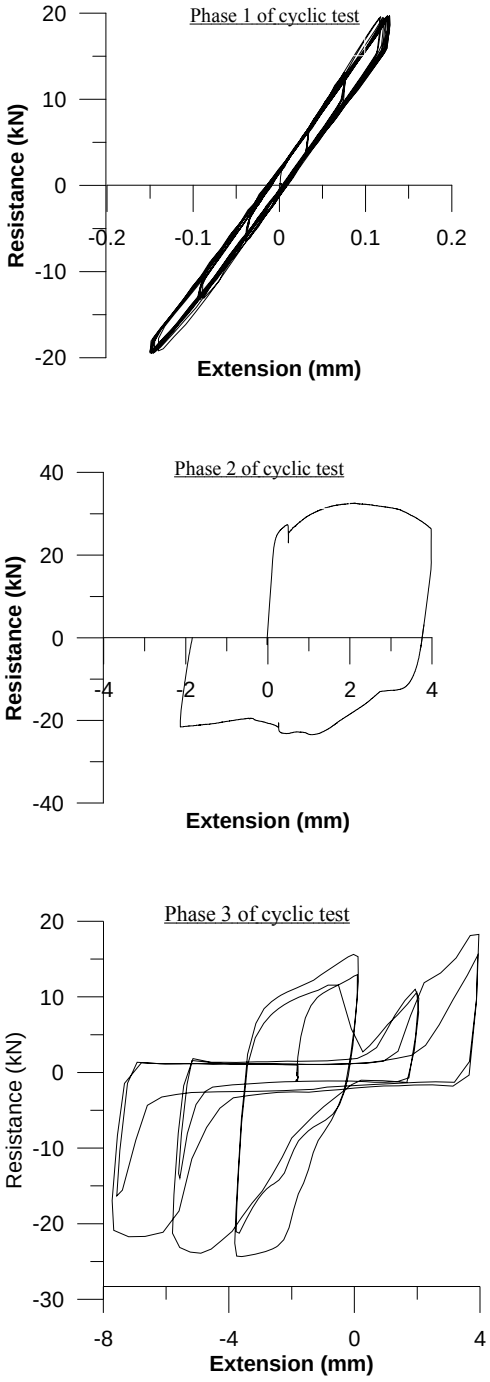

Figure F.4 2-layer shear specimen with 1.52 mm sheets and 6.4 mm plate (SC1624)

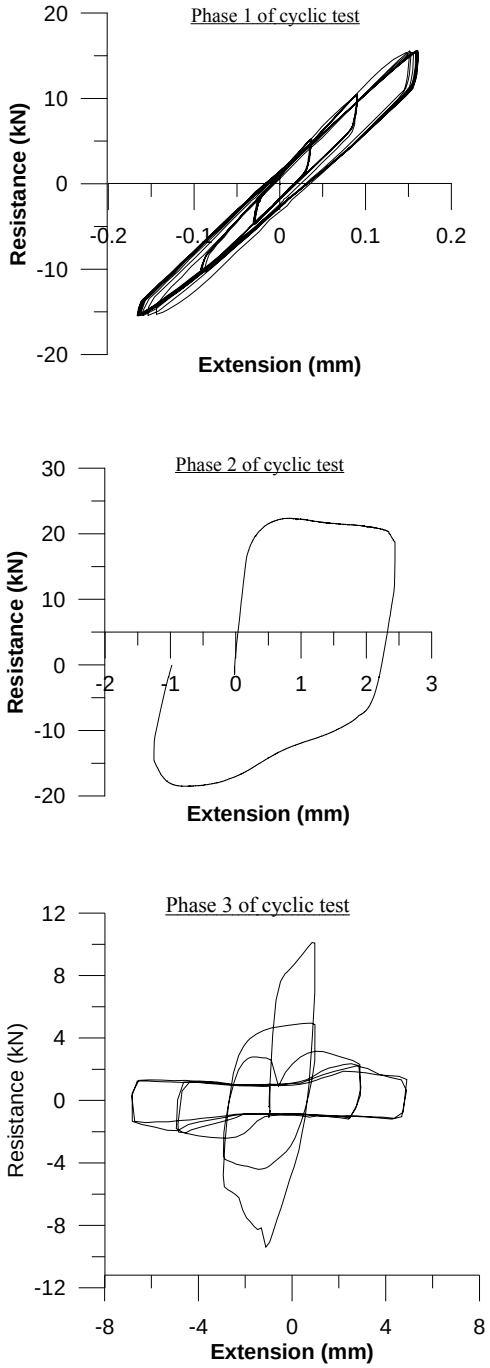

Figure F.5 2-layer shear specimen with 1.21 mm sheets and 6.4 mm plate (SC1821)

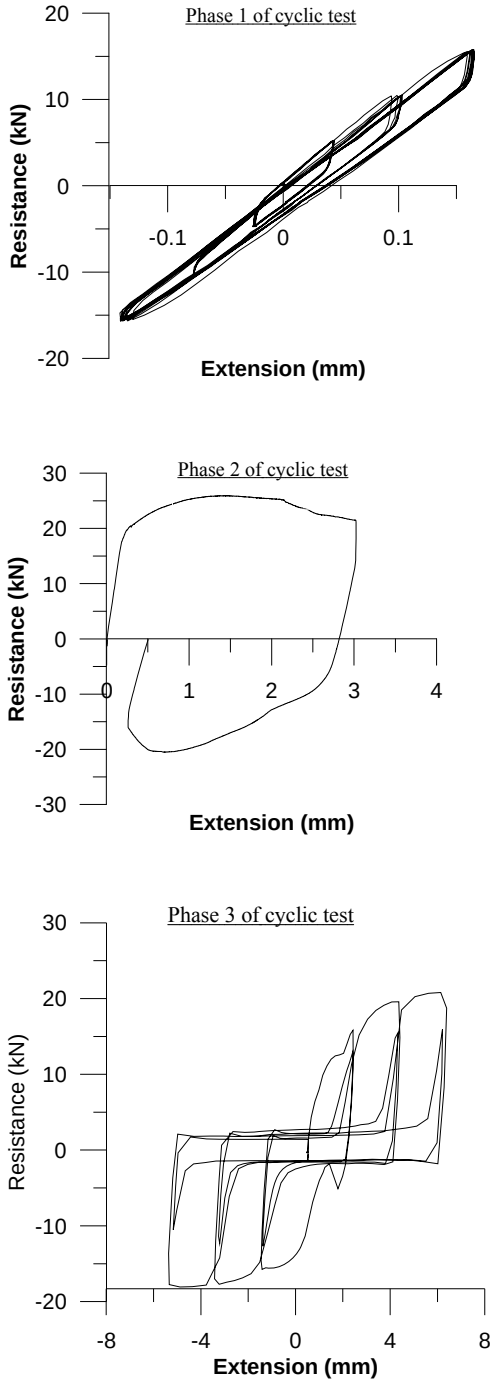

Figure F.6 2-layer shear specimen with 1.21 mm sheets and 6.4 mm plate (SC1822)

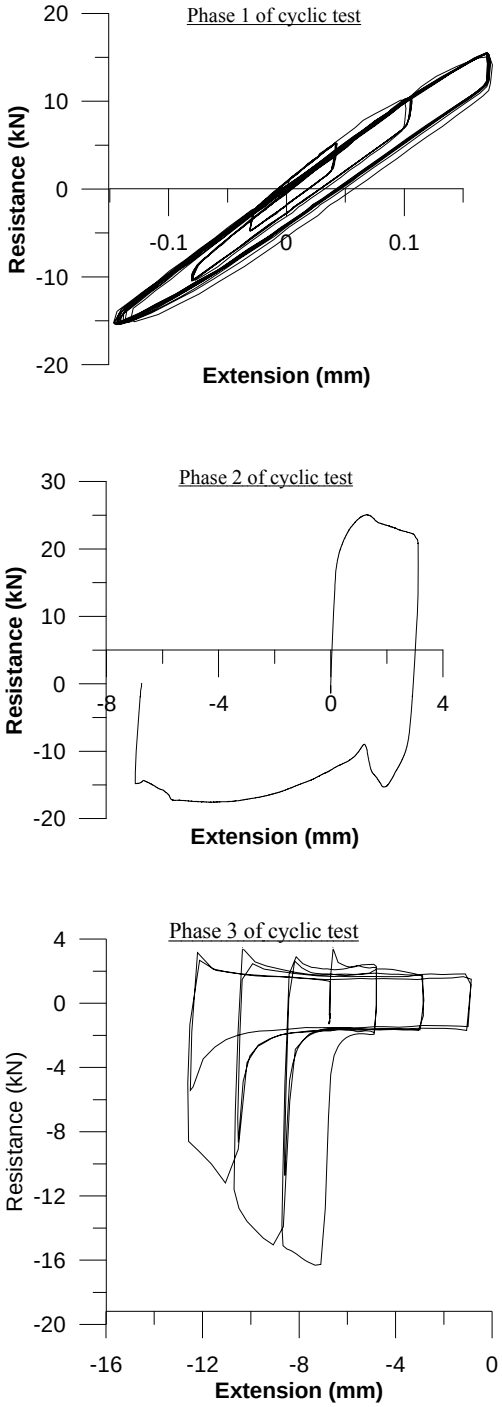

Figure F.7 2-layer shear specimen with 1.21 mm sheets and 6.4 mm plate (SC1823)

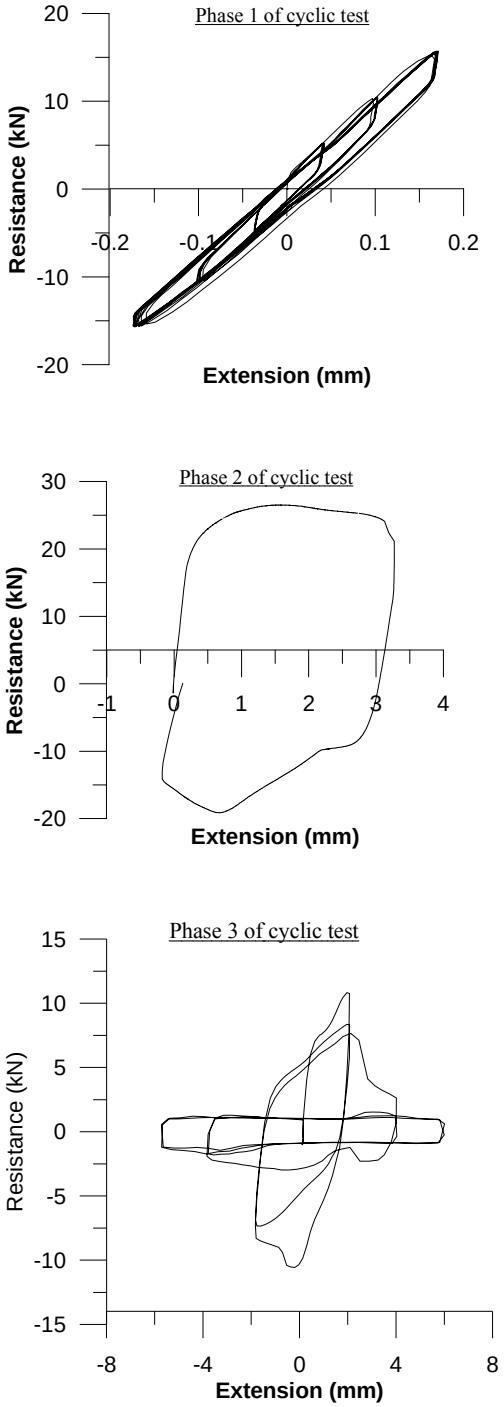

Figure F.8 2-layer shear specimen with 1.21 mm sheets and 6.4 mm plate (SC1824)

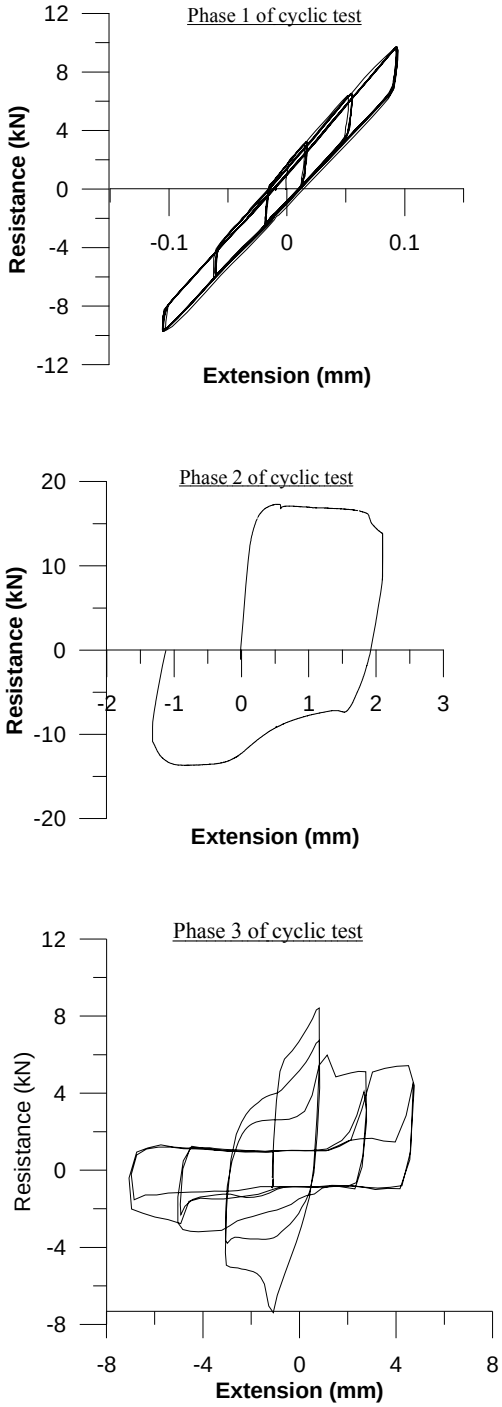

Figure F.9 2-layer shear specimen with 0.91 mm sheets and 6.4 mm plate (SC2021)

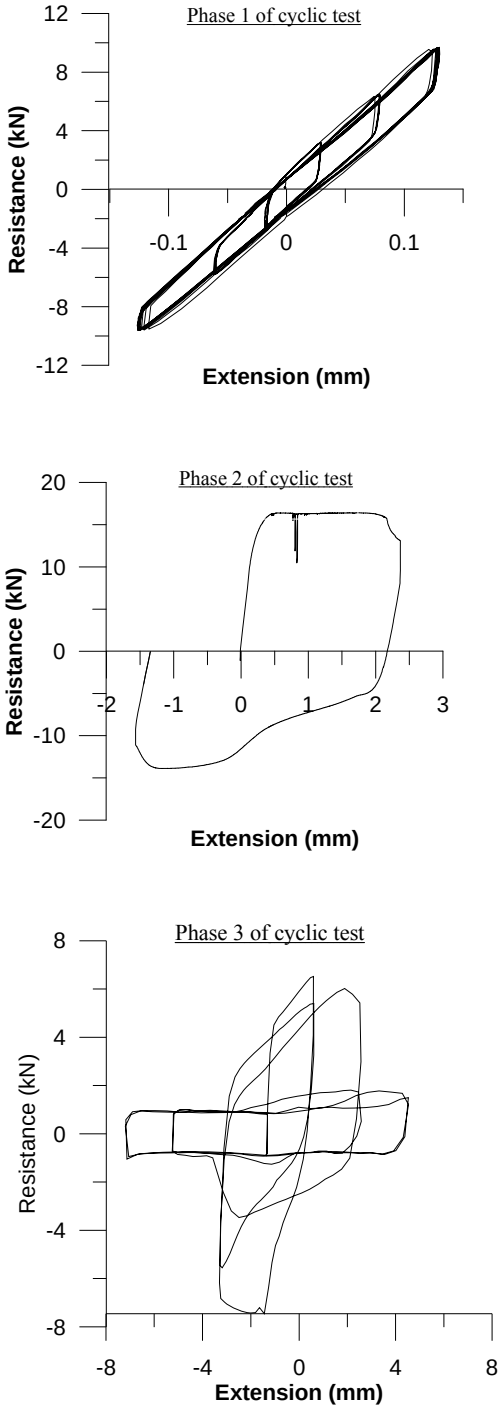

Figure F.10 2-layer shear specimen with 0.91 mm sheets and 6.4 mm plate (SC2022)

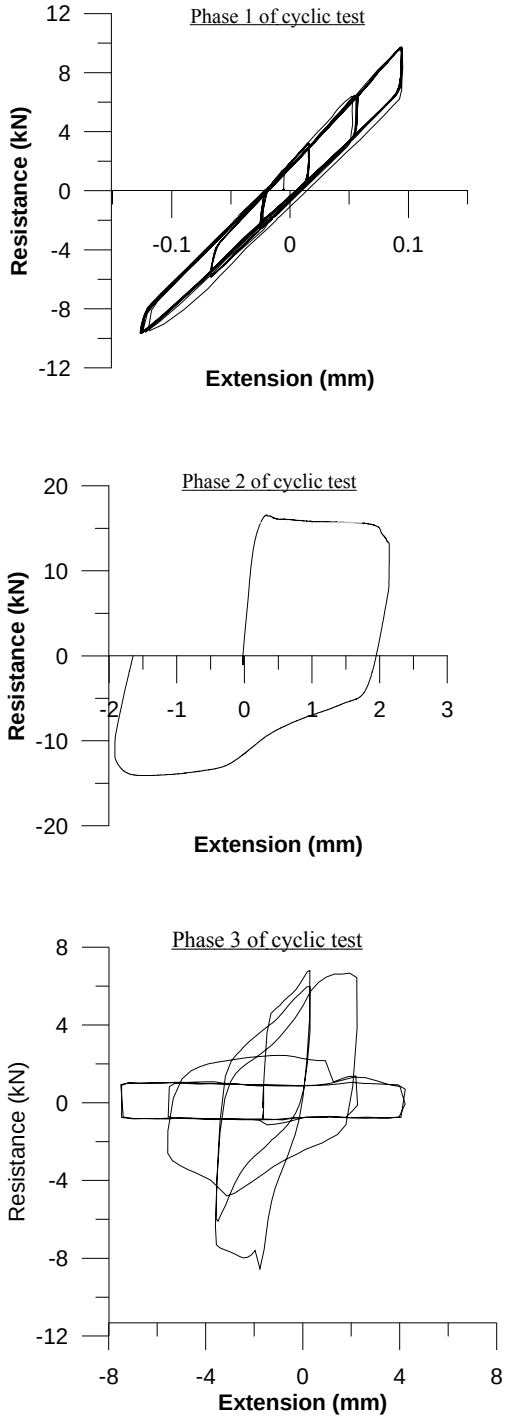

Figure F.11 2-layer shear specimen with 0.91 mm sheets and 6.4 mm plate (SC2023)

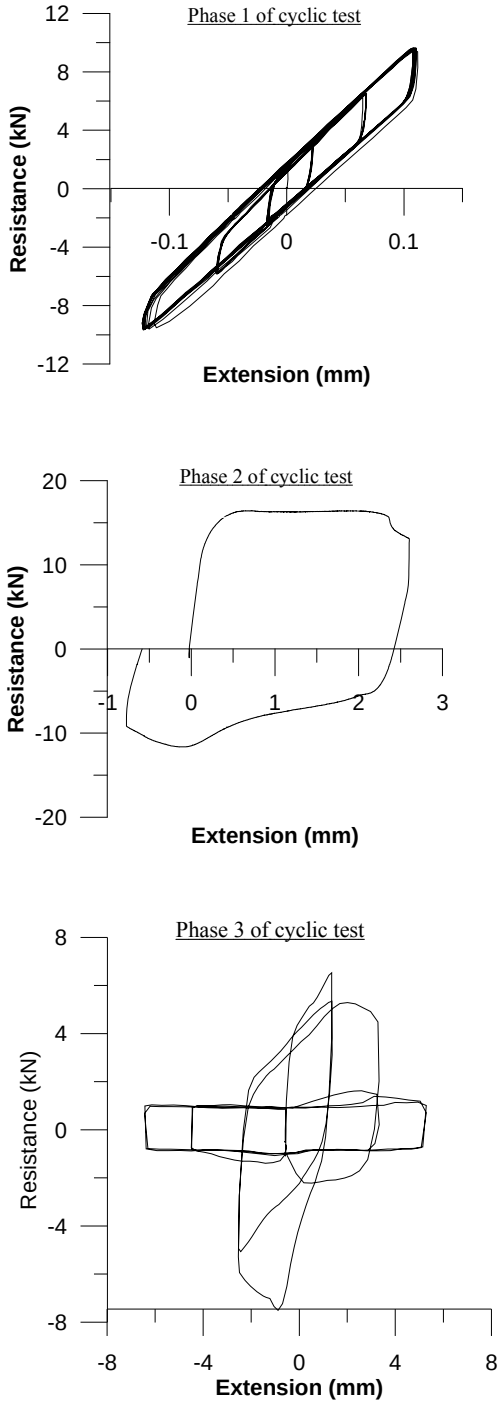

Figure F.12 2-layer shear specimen with 0.91 mm sheets and 6.4 mm plate (SC2024)

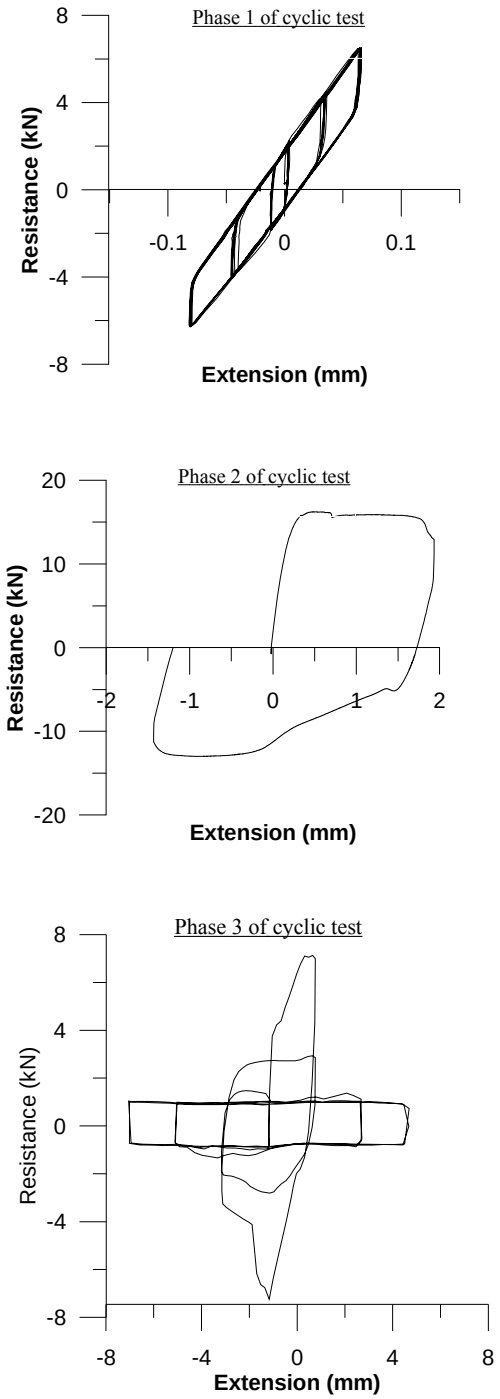

Figure F.13 2-layer shear specimen with 0.76 mm sheets and 6.4 mm plate (SC2221)

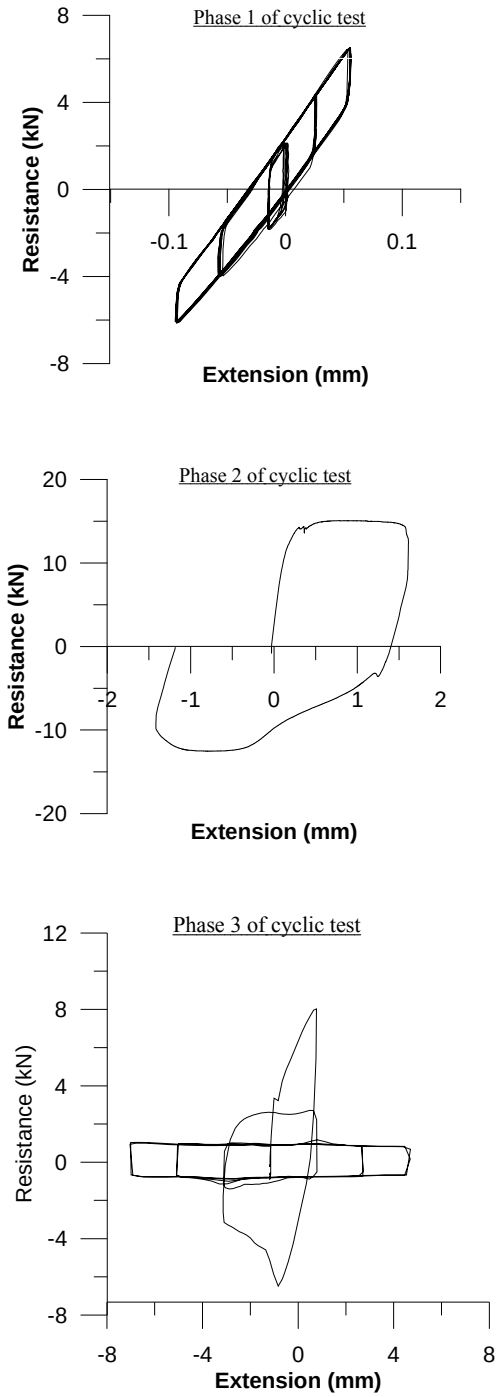

Figure F.14 2-layer shear specimen with 0.76 mm sheets and 6.4 mm plate (SC2222)

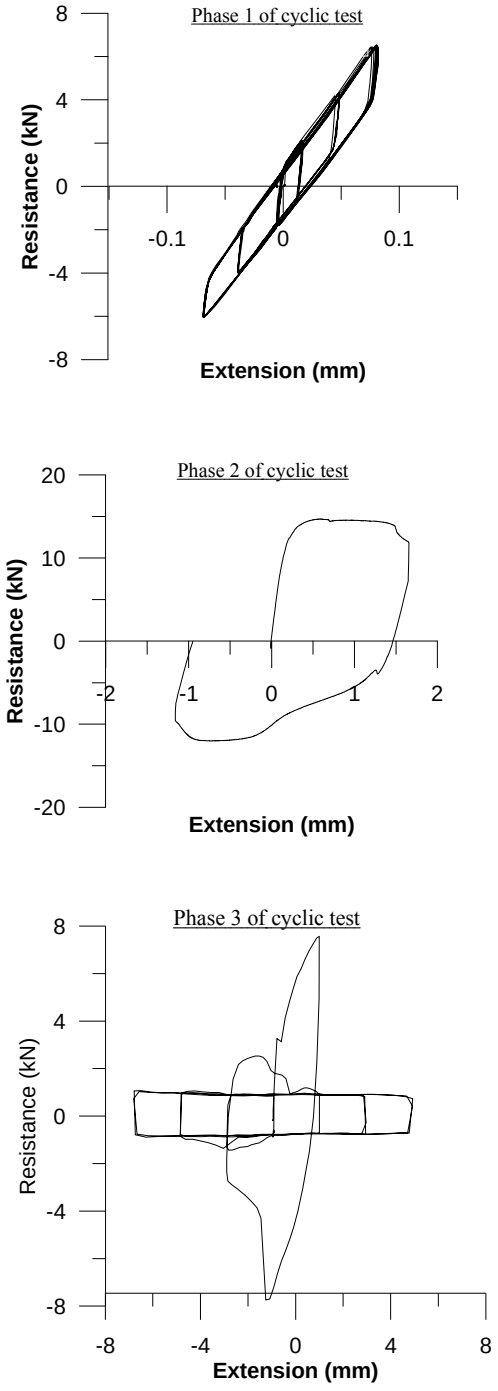

Figure F.15 2-layer shear specimen with 0.76 mm sheets and 6.4 mm plate (SC2223)

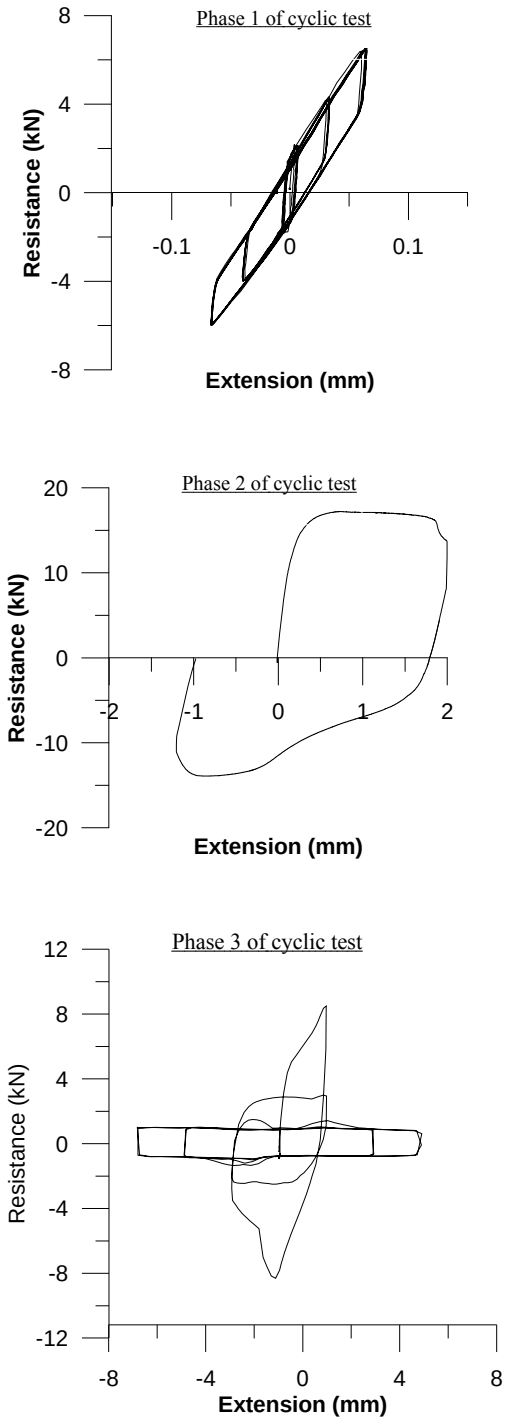

Figure F.16 2-layer shear specimen with 0.76 mm sheets and 6.4 mm plate (SC2224)

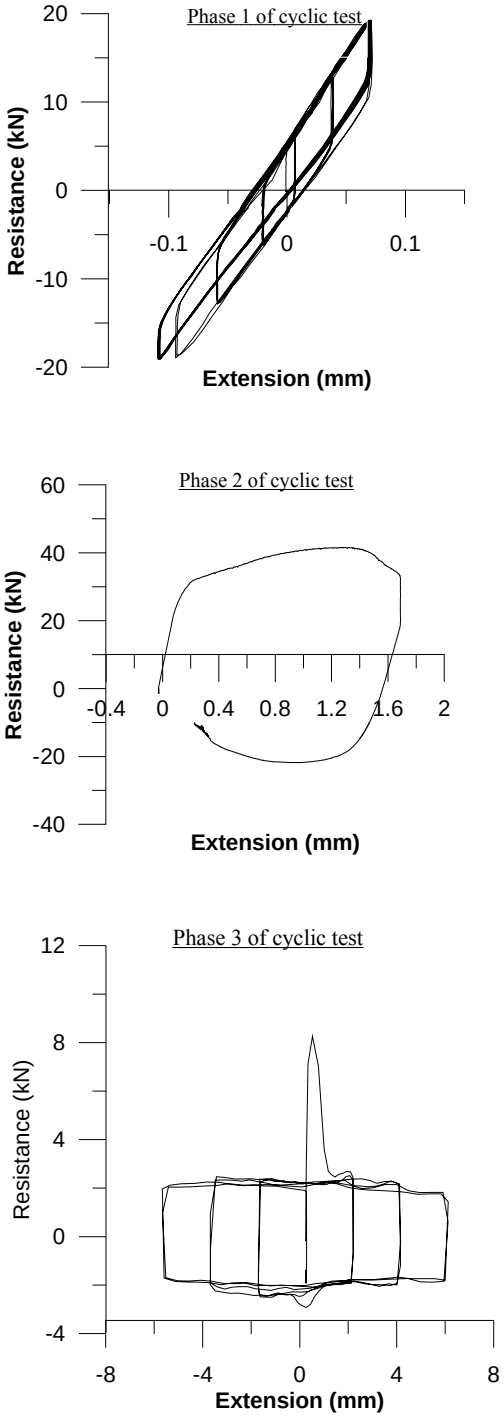

Figure F.17 4-layer shear specimen with 1.52 mm sheets and 6.4 mm plate (SC1641)

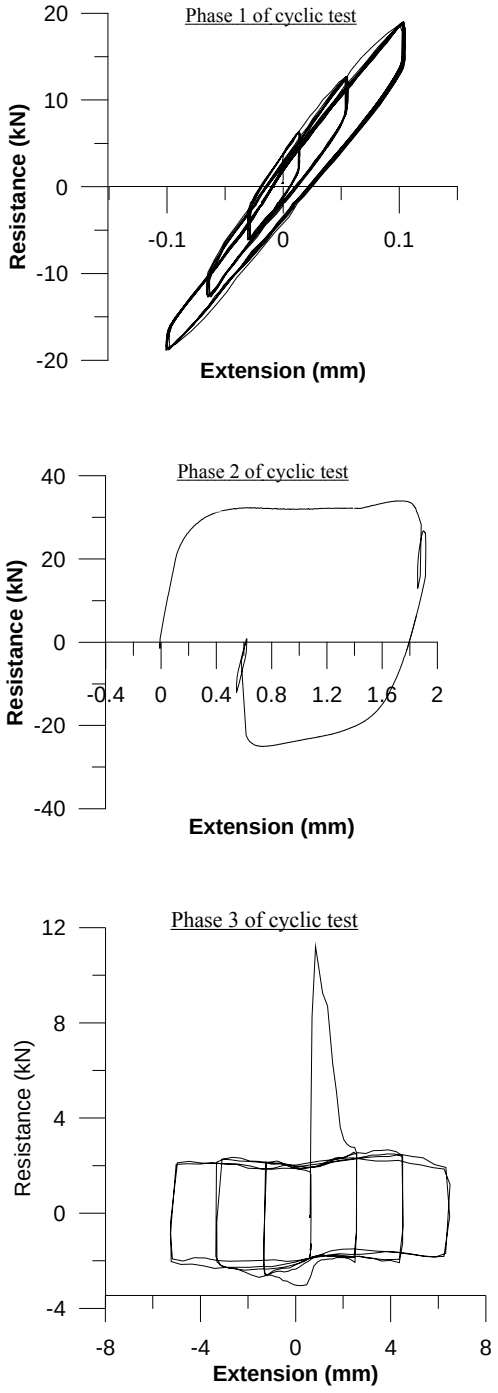

Figure F.18 4-layer shear specimen with 1.52 mm sheets and 6.4 mm plate (SC1642)

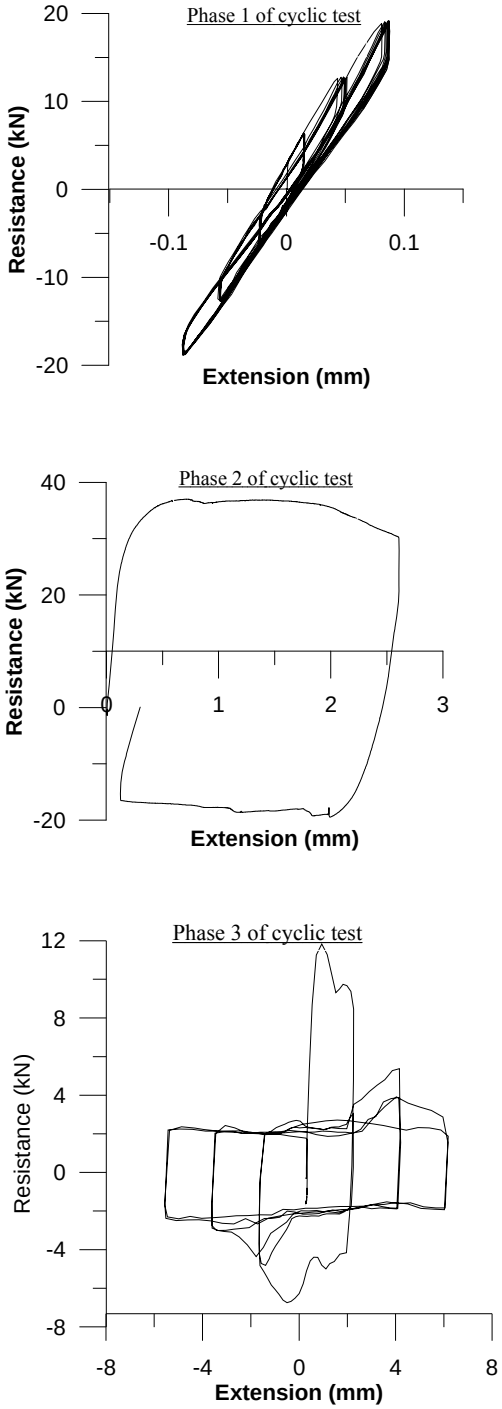

Figure F.19 4-layer shear specimen with 1.52 mm sheets and 6.4 mm plate (SC1643)

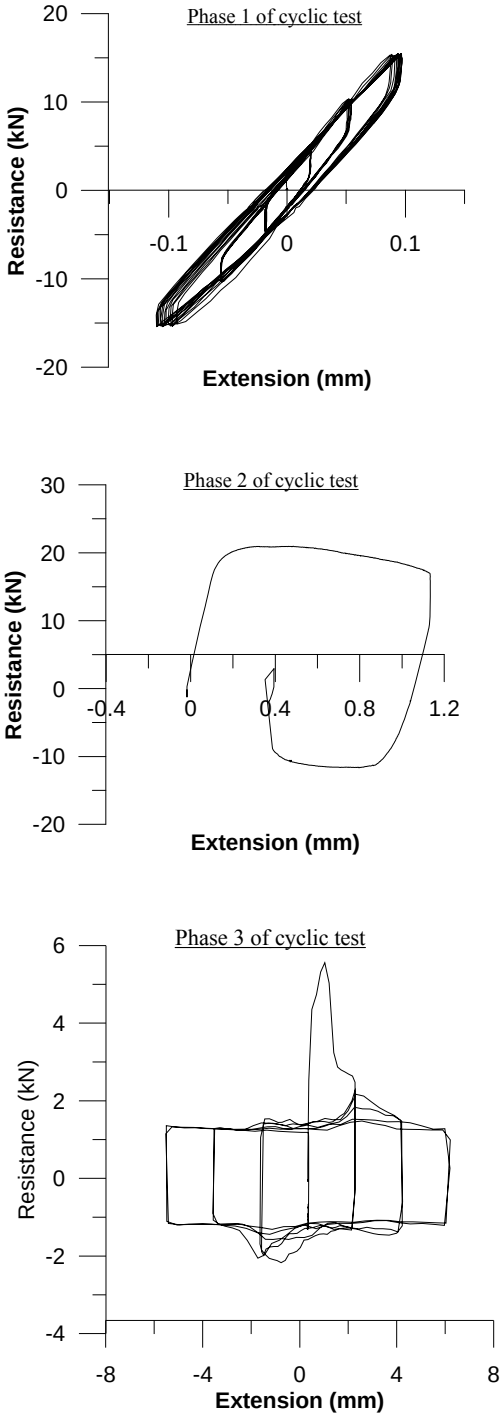

Figure F.20 4-layer shear specimen with 1.21 mm sheets and 6.4 mm plate (SC1841)

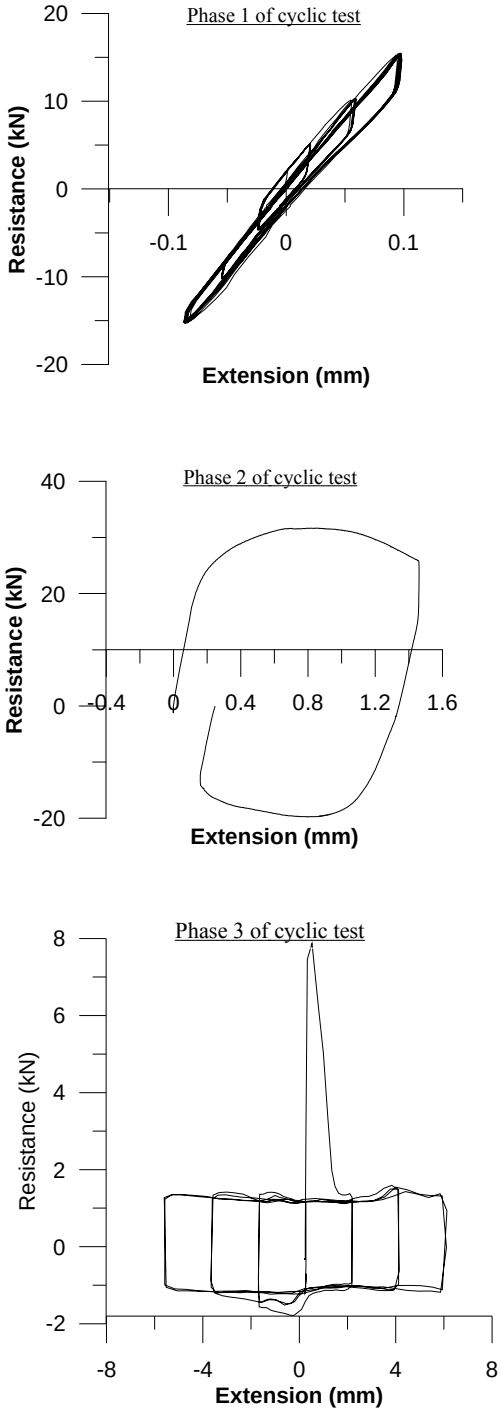

Figure F.21 4-layer shear specimen with 1.21 mm sheets and 6.4 mm plate (SC1842)

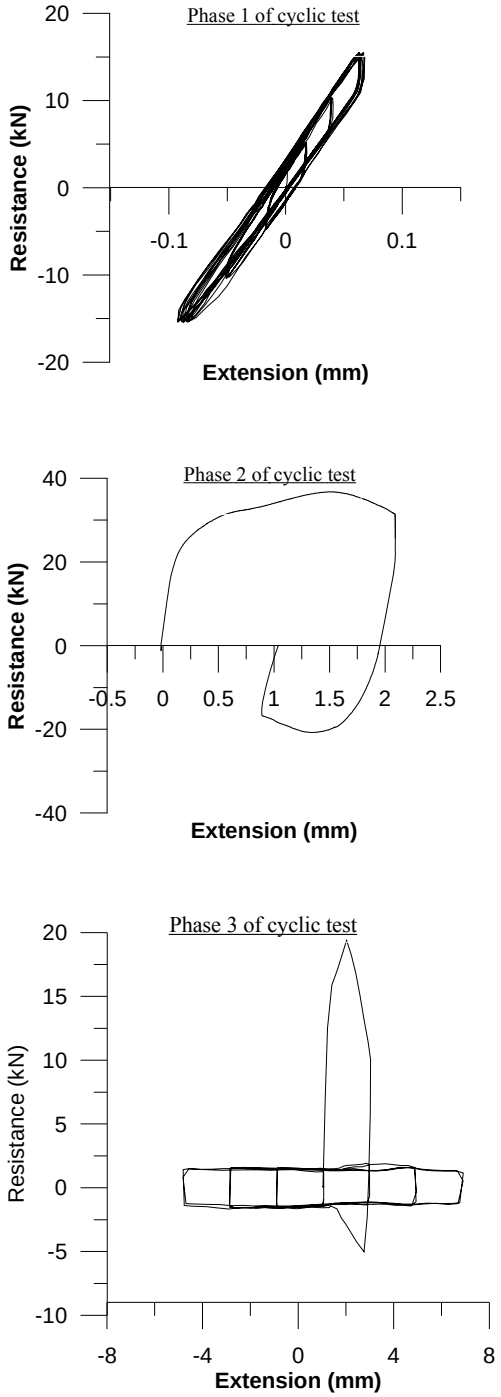

Figure F.22 4-layer shear specimen with 1.21 mm sheets and 6.4 mm plate (SC1843)

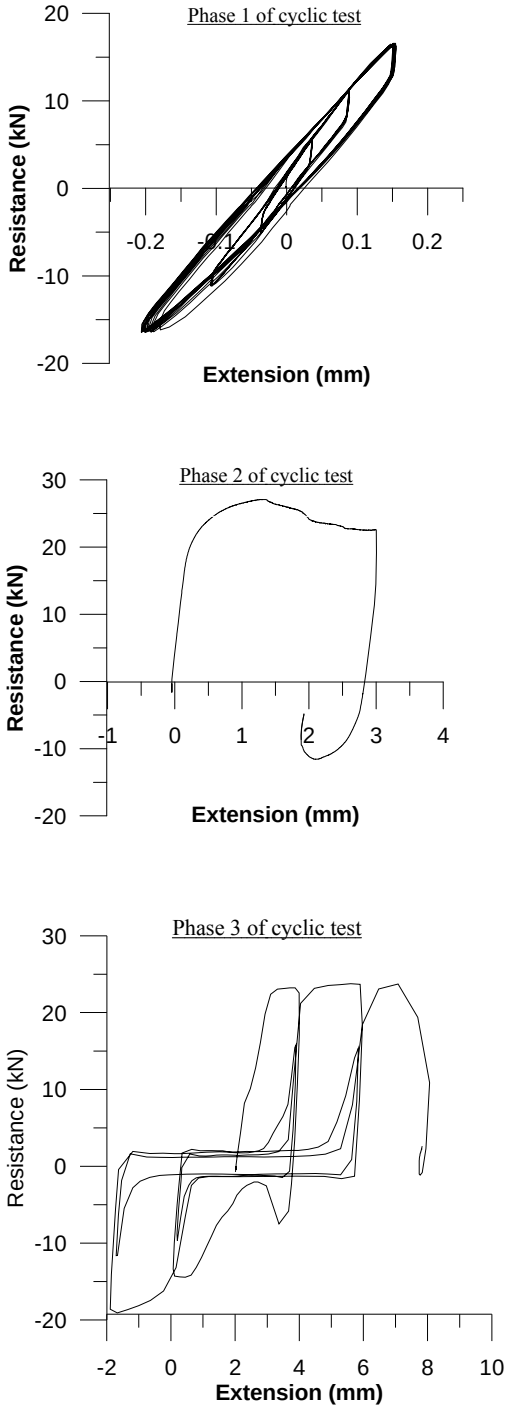

Figure F.23 4-layer shear specimen with 0.91 mm sheets and 6.4 mm plate (SC2041)

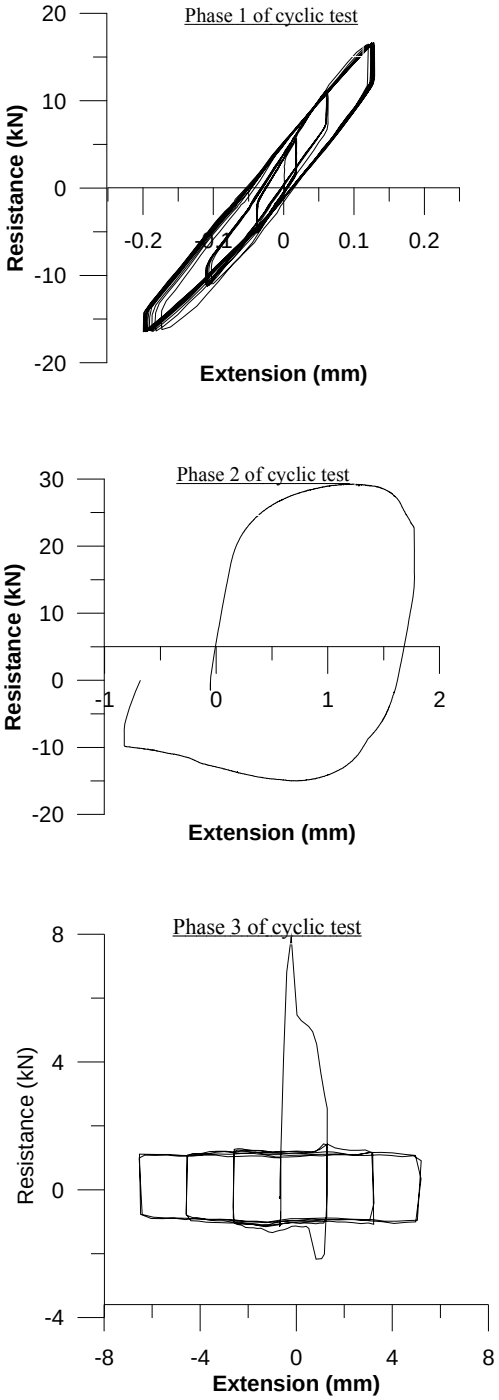

Figure F.24 4-layer shear specimen with 0.91 mm sheets and 6.4 mm plate (SC2042)

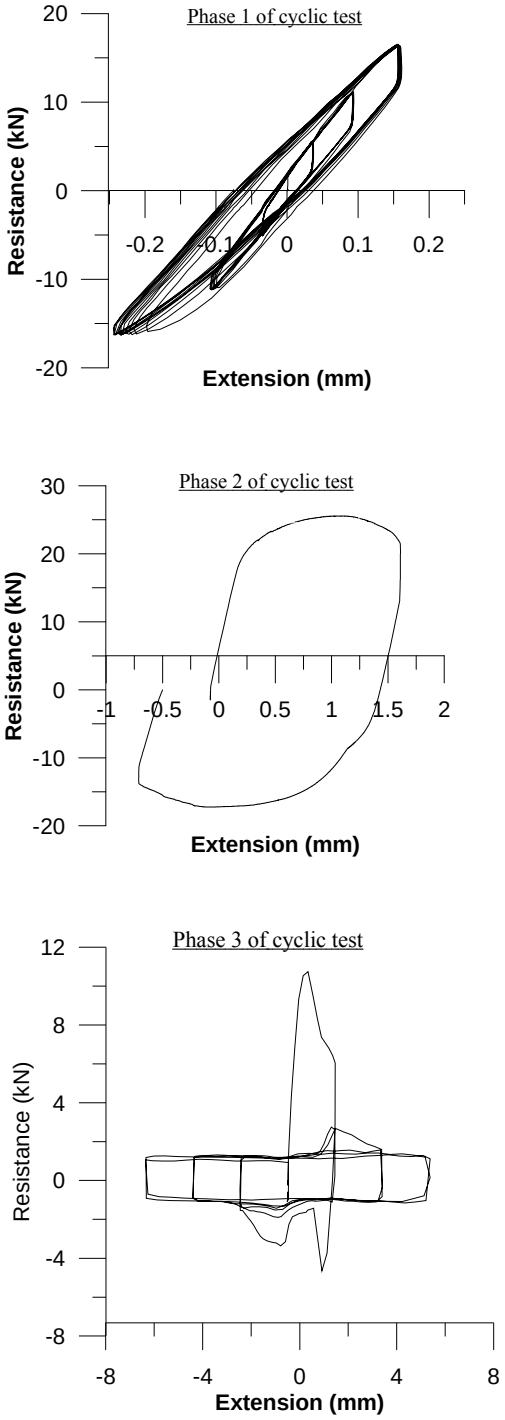

Figure F.25 4-layer shear specimen with 0.91 mm sheets and 6.4 mm plate (SC2043)

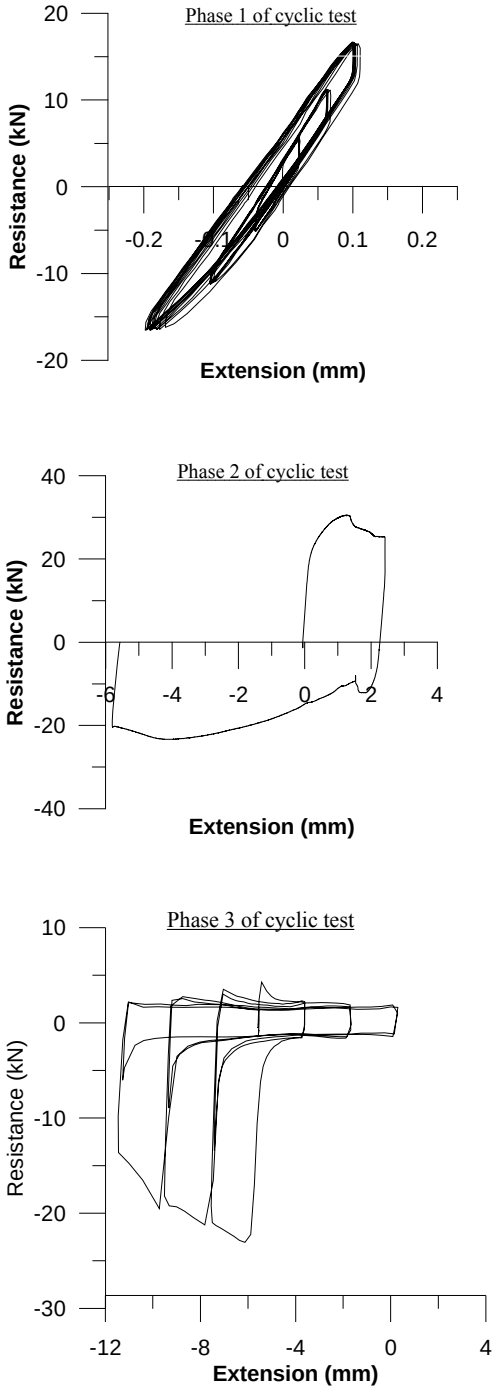

Figure F.26 4-layer shear specimen with 0.91 mm sheets and 6.4 mm plate (SC2044)

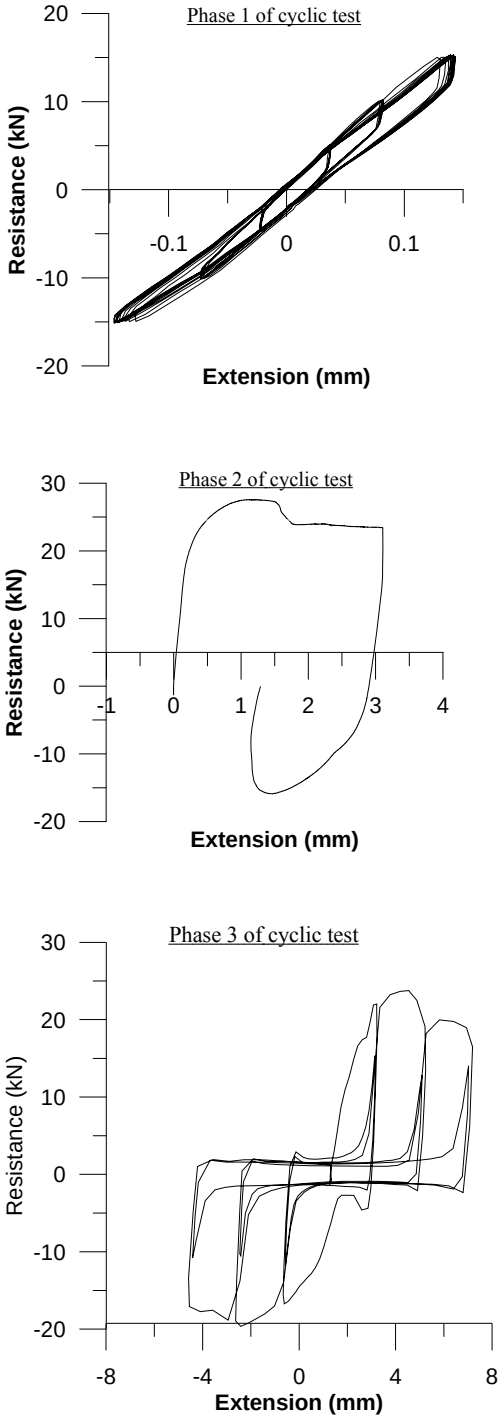

Figure F.27 4-layer shear specimen with 0.76 mm sheets and 6.4 mm plate (SC2241)

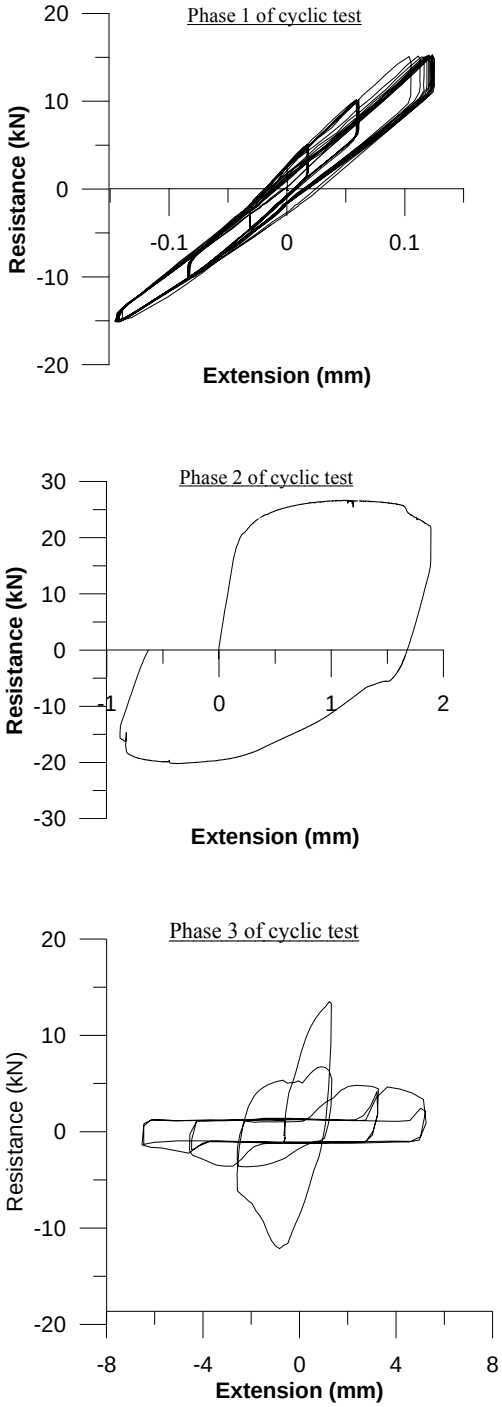

Figure F.28 4-layer shear specimen with 0.76 mm sheets and 6.4 mm plate (SC2242)

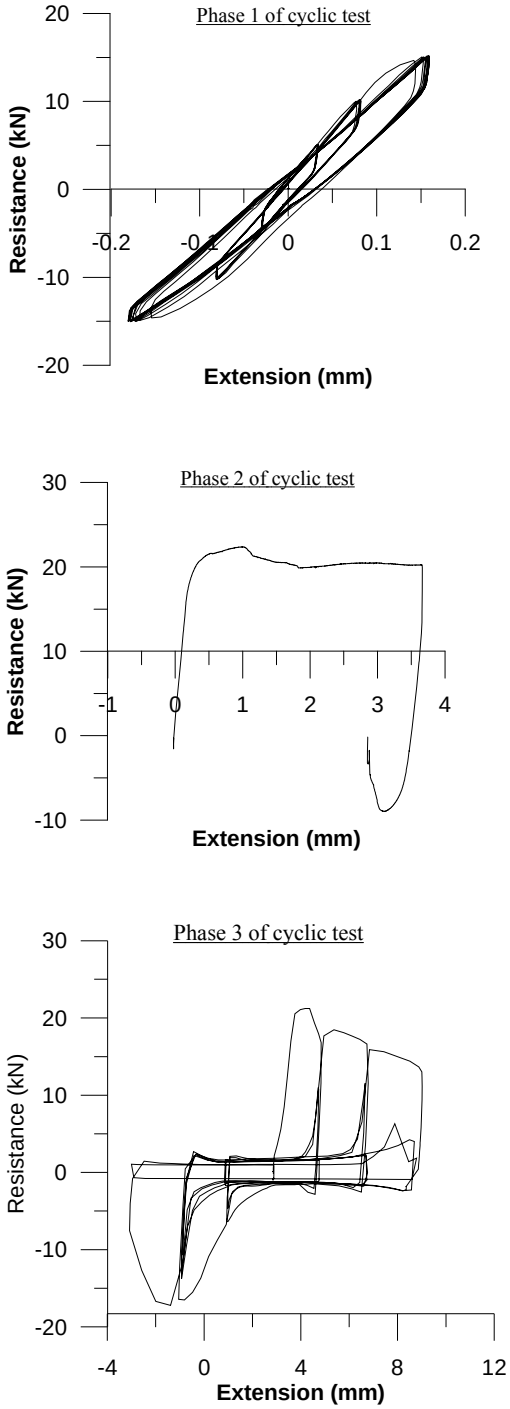

Figure F.29 4-layer shear specimen with 0.76 mm sheets and 6.4 mm plate (SC2243)

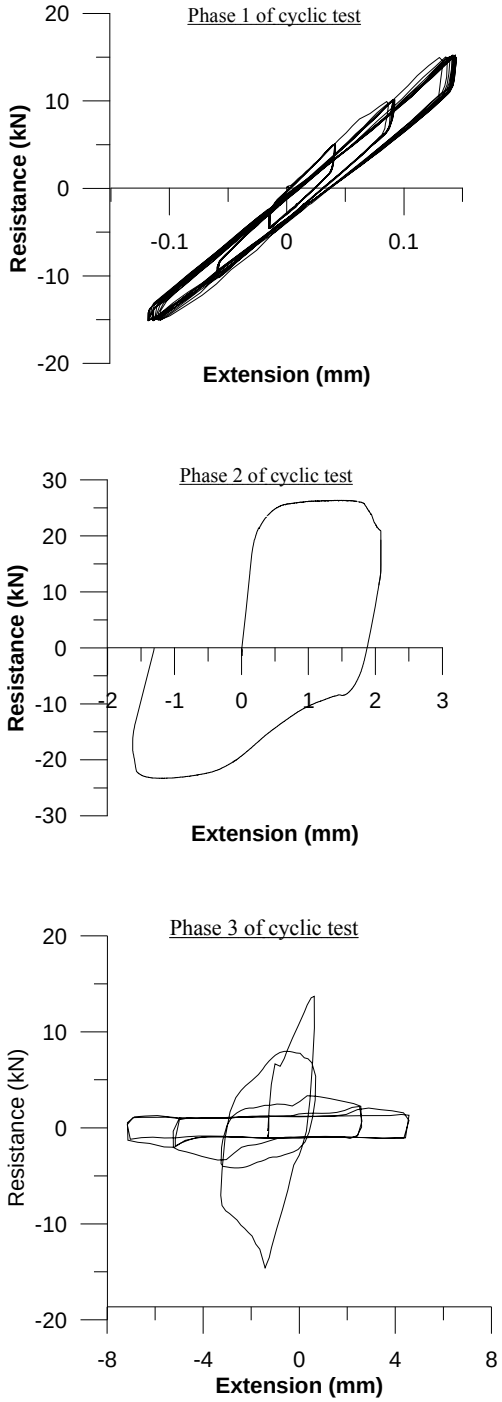

Figure F.30 4-layer shear specimen with 0.76 mm sheets and 6.4 mm plate (SC2244)

APPENDIX G. LOAD VS. DEFORMATION PLOTS OF MONOTONIC TENSION SPECIMENS

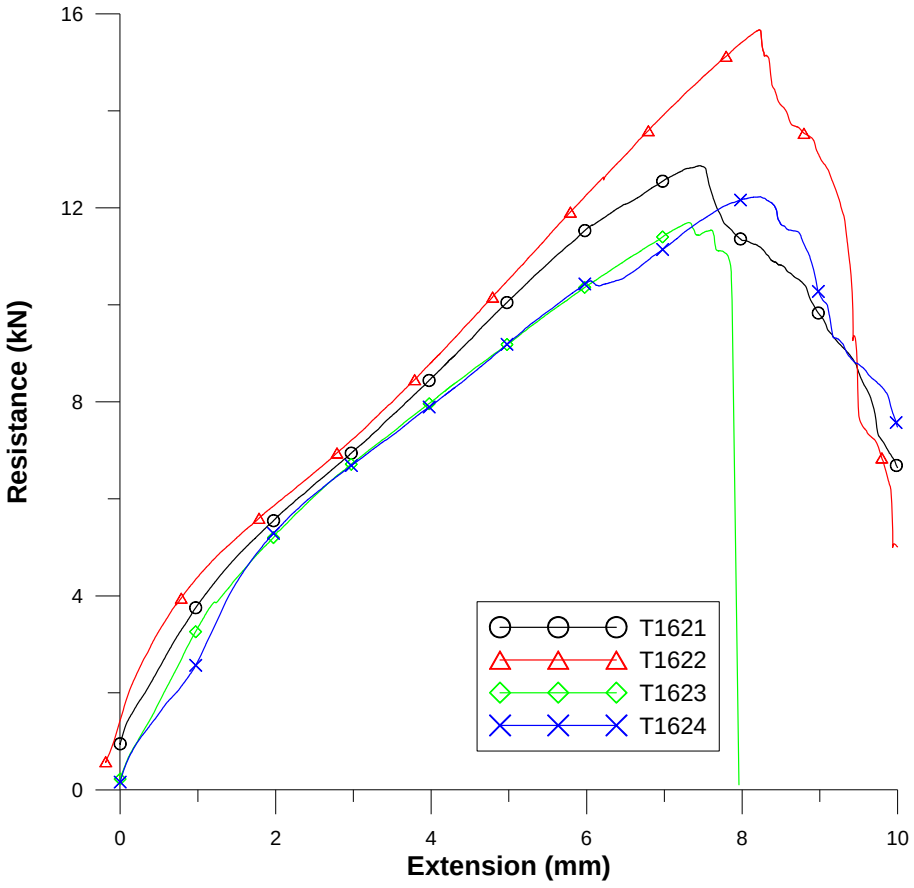

Figure G.1 2-layer tension specimens with 1.52 mm sheets and 6.4 mm angle

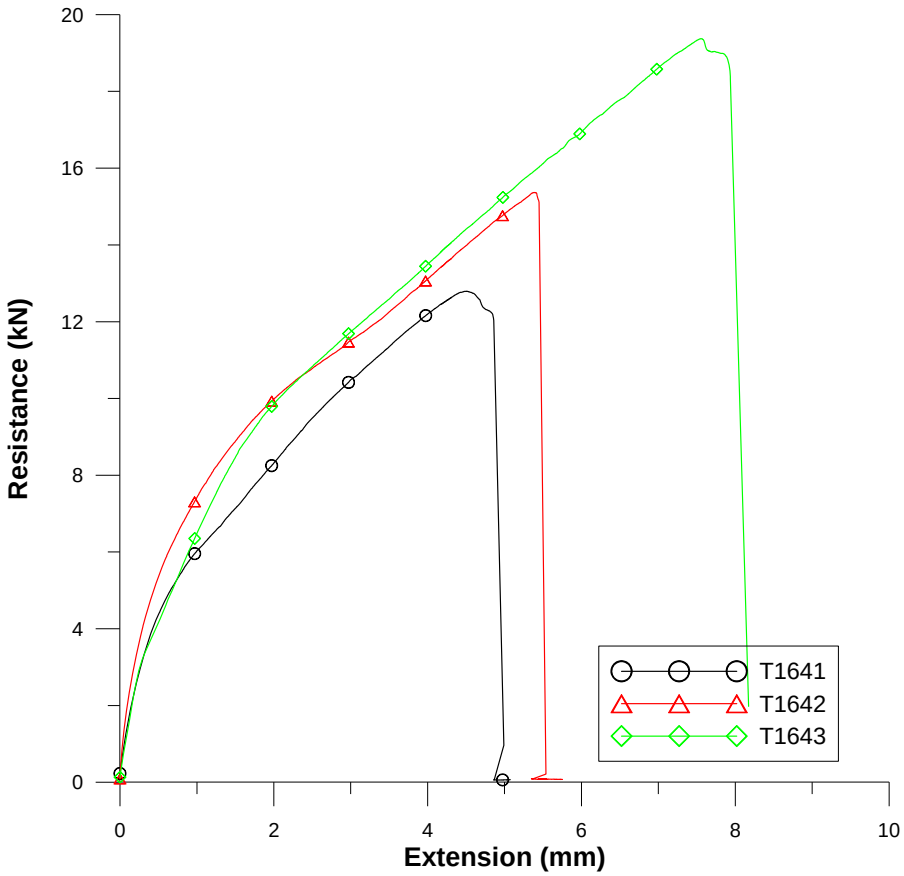

Figure G.2 4-layer tension specimens with 1.52 mm sheets and 6.4 mm angle

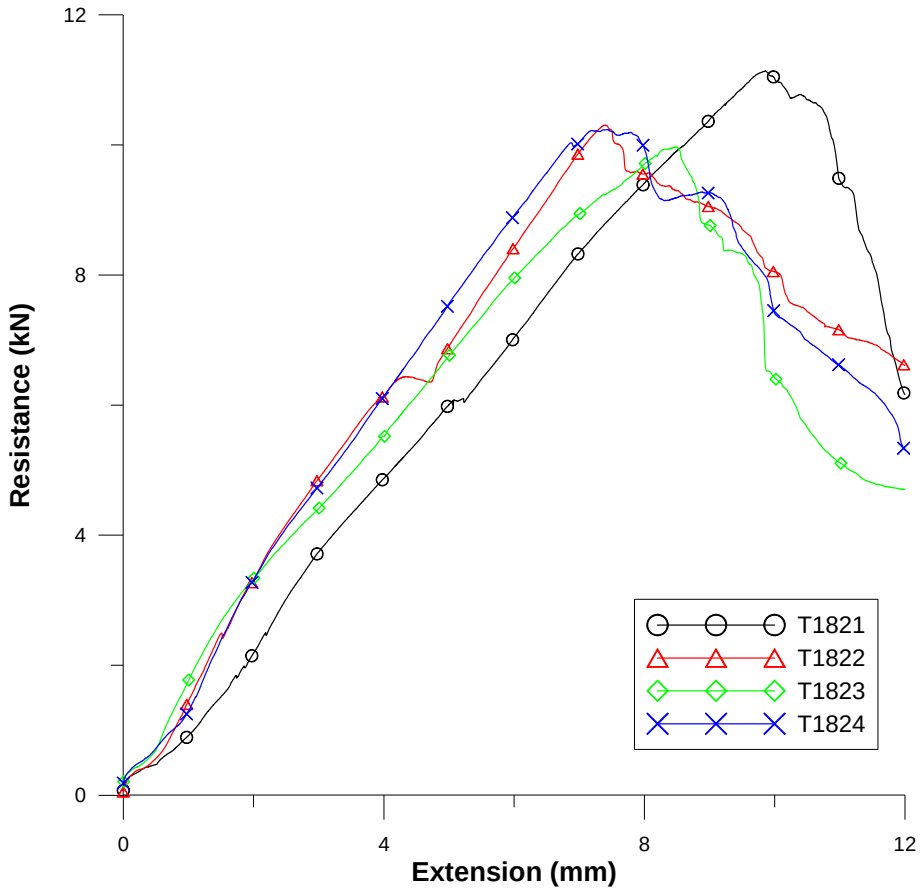

Figure G.3 2-layer tension specimens with 1.21 mm sheets and 6.4 mm angle

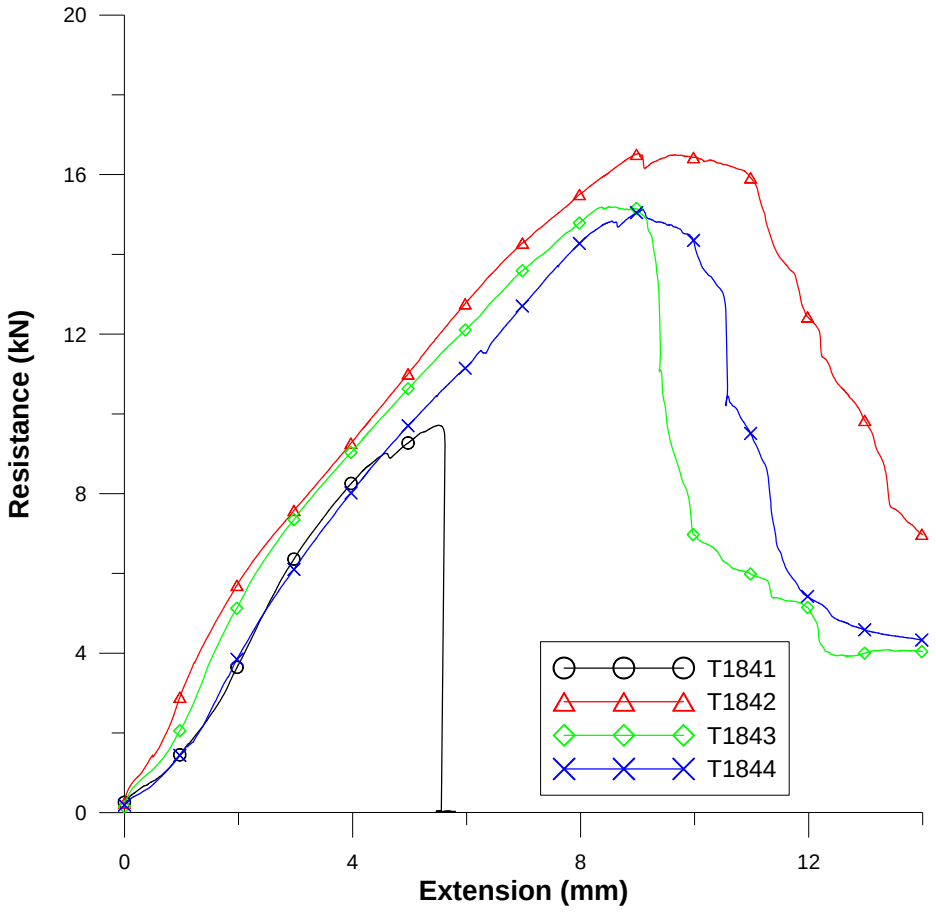

Figure G.4 4-layer tension specimens with 1.21 mm sheets and 6.4 mm angle

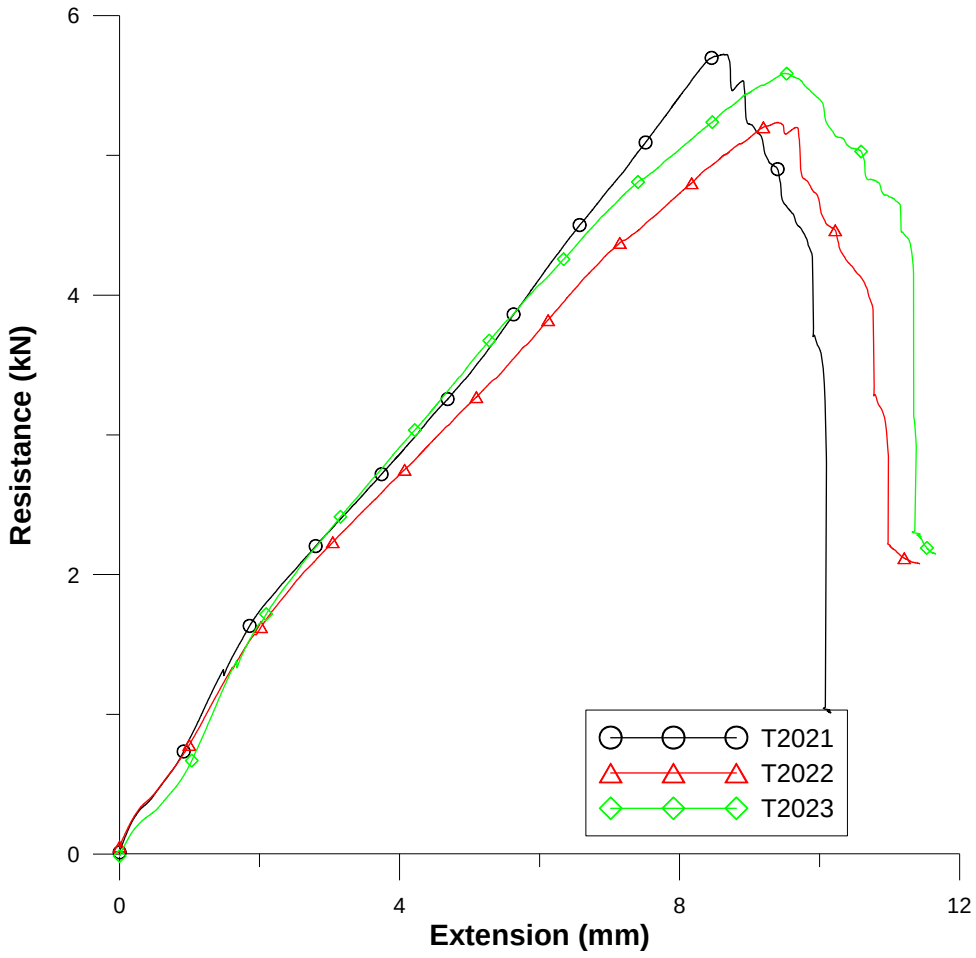

Figure G.5 2-layer tension specimens with 0.91 mm sheets and 6.4 mm angle

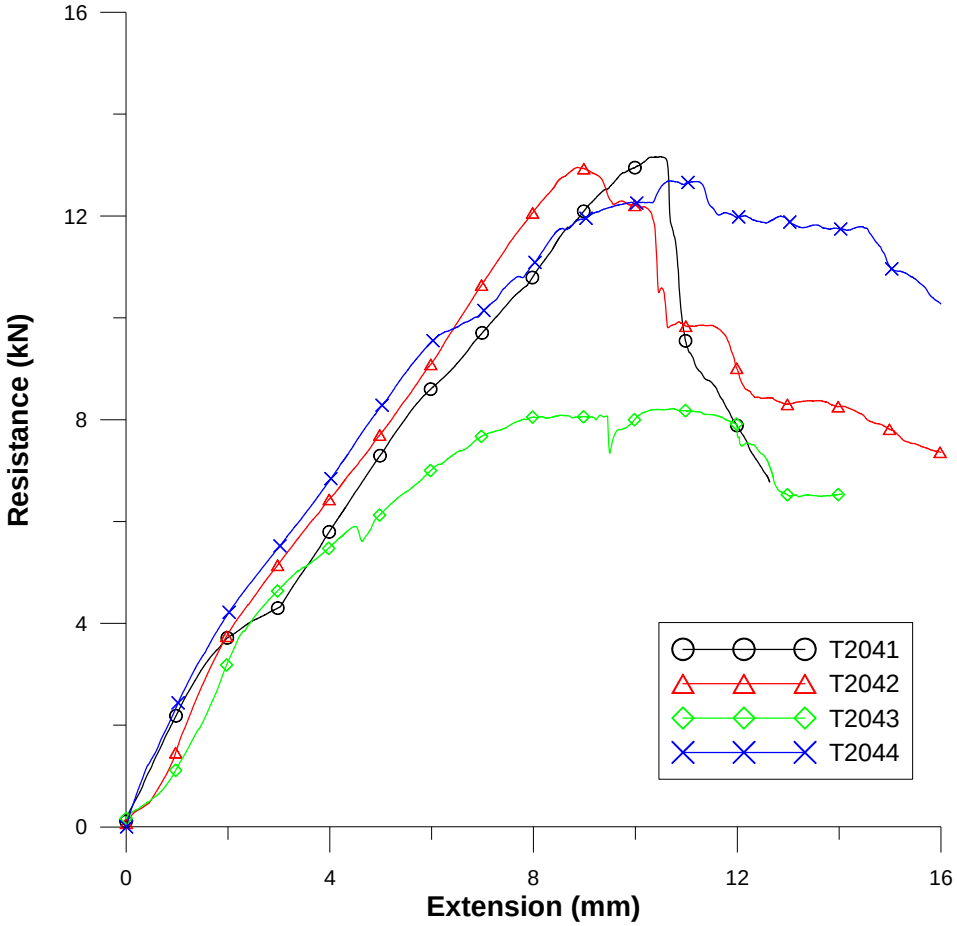

Figure G.6 4-layer tension specimens with 0.91 mm sheets and 6.4 mm angle

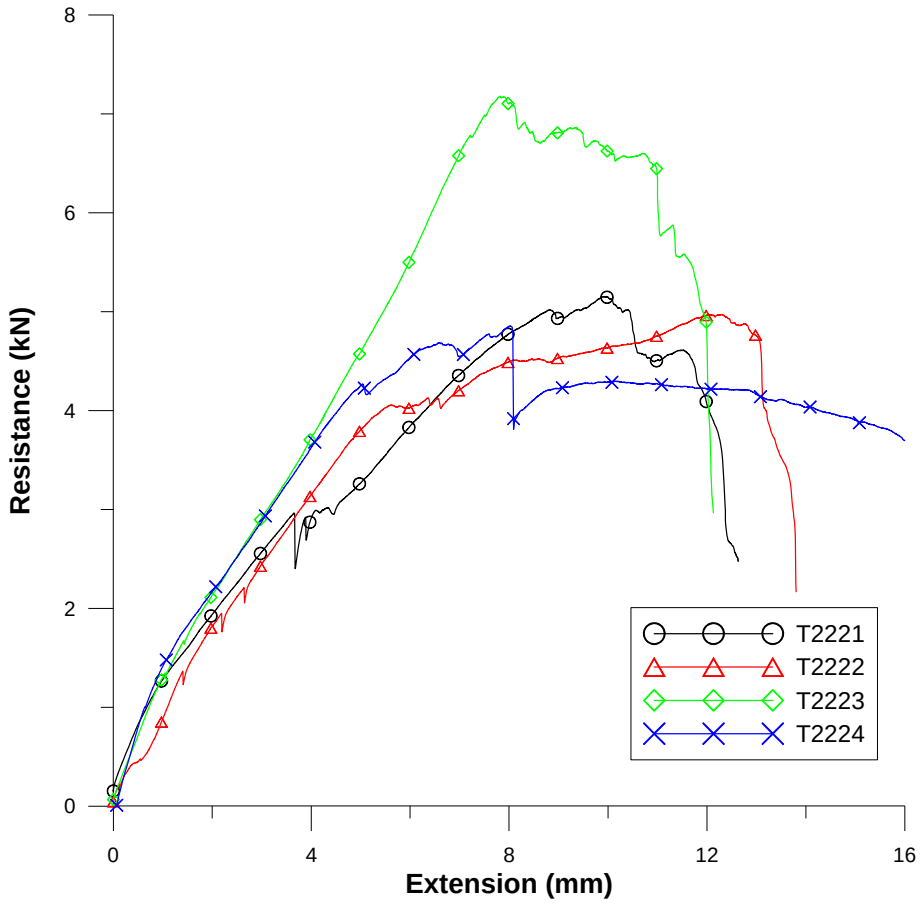

Figure G.7 2-layer tension specimens with 0.76 mm sheets and 6.4 mm angle

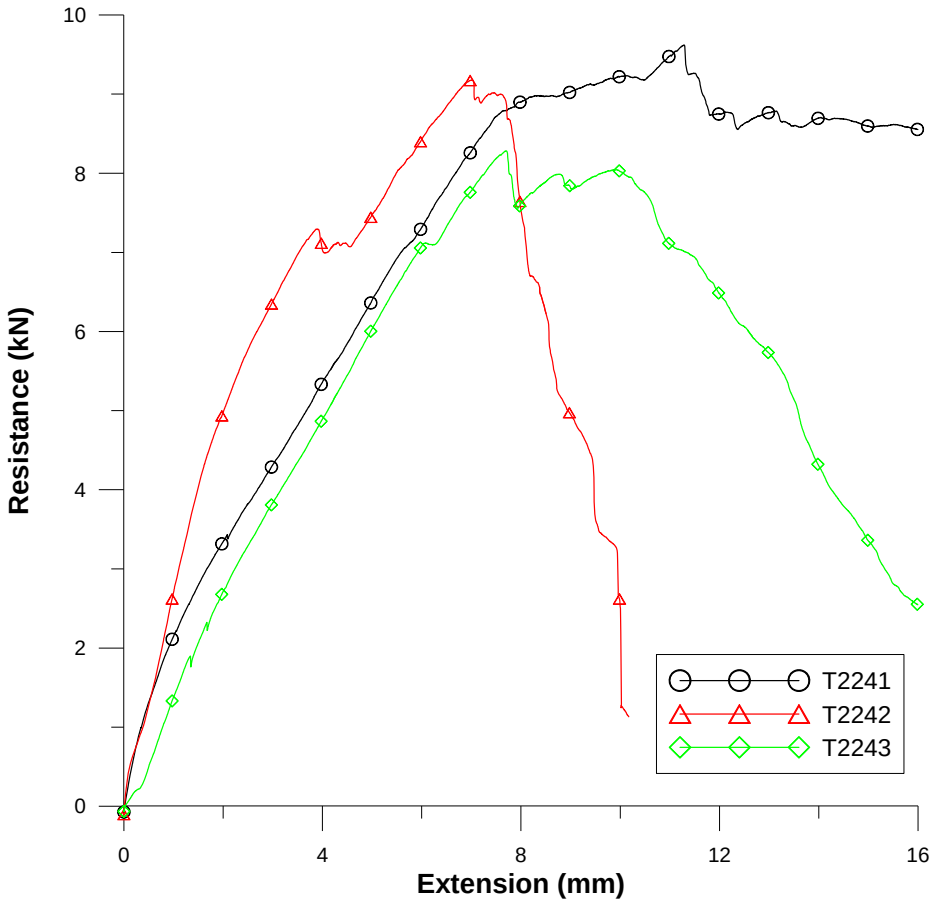

Figure G.8 4-layer tension specimens with 0.76 mm sheets and 6.4 mm angle

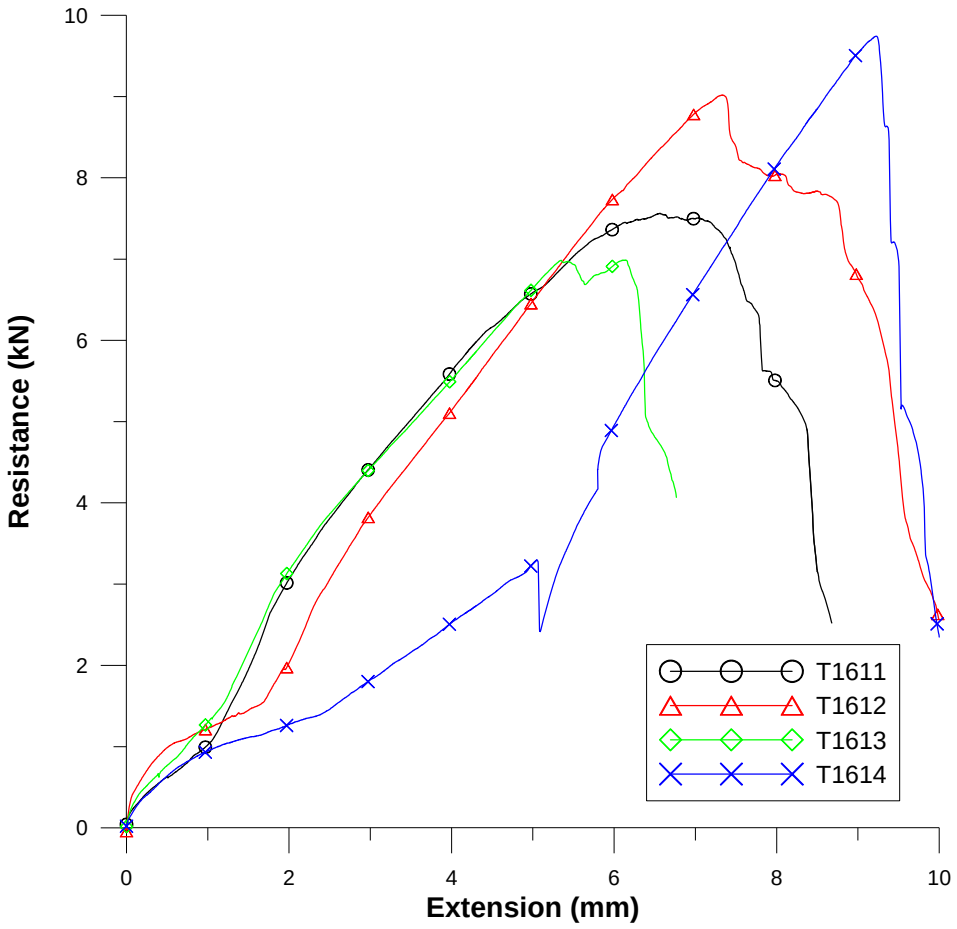

Figure G.9 1-layer tension specimens with 1.52 mm sheets and 6.4 mm angle

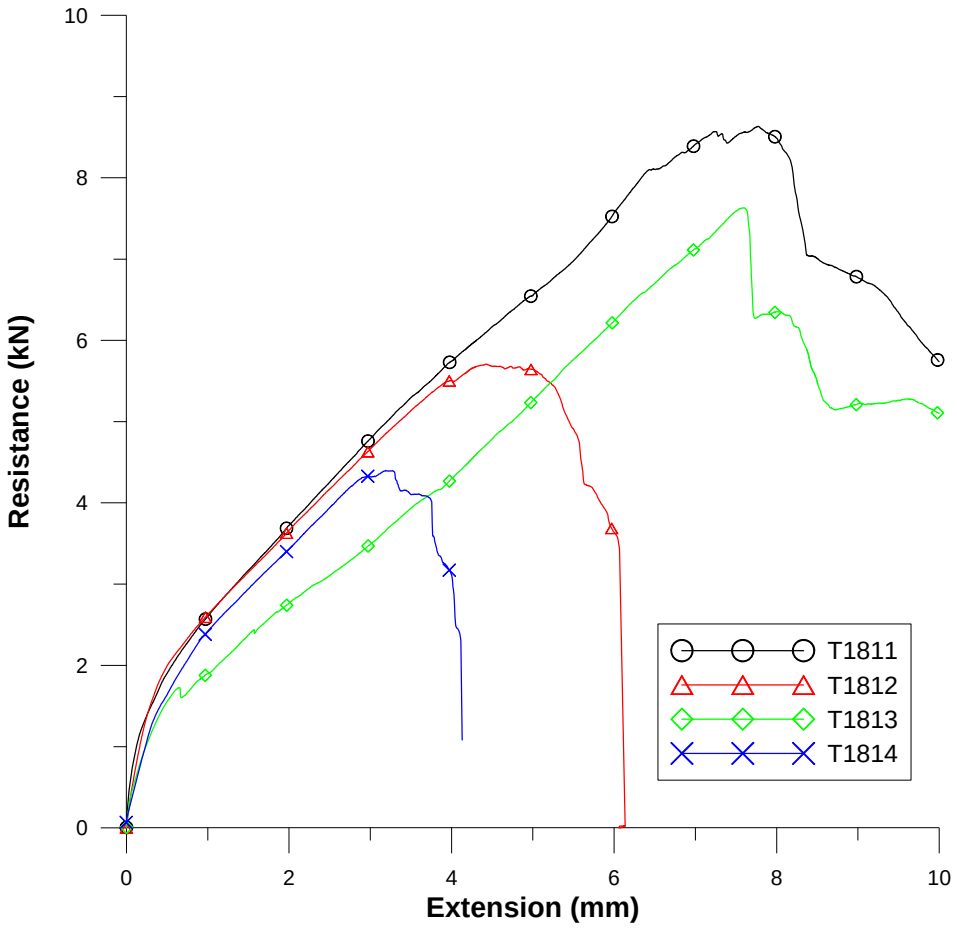

Figure G.10 1-layer tension specimens with 1.21 mm sheets and 6.4 mm angle

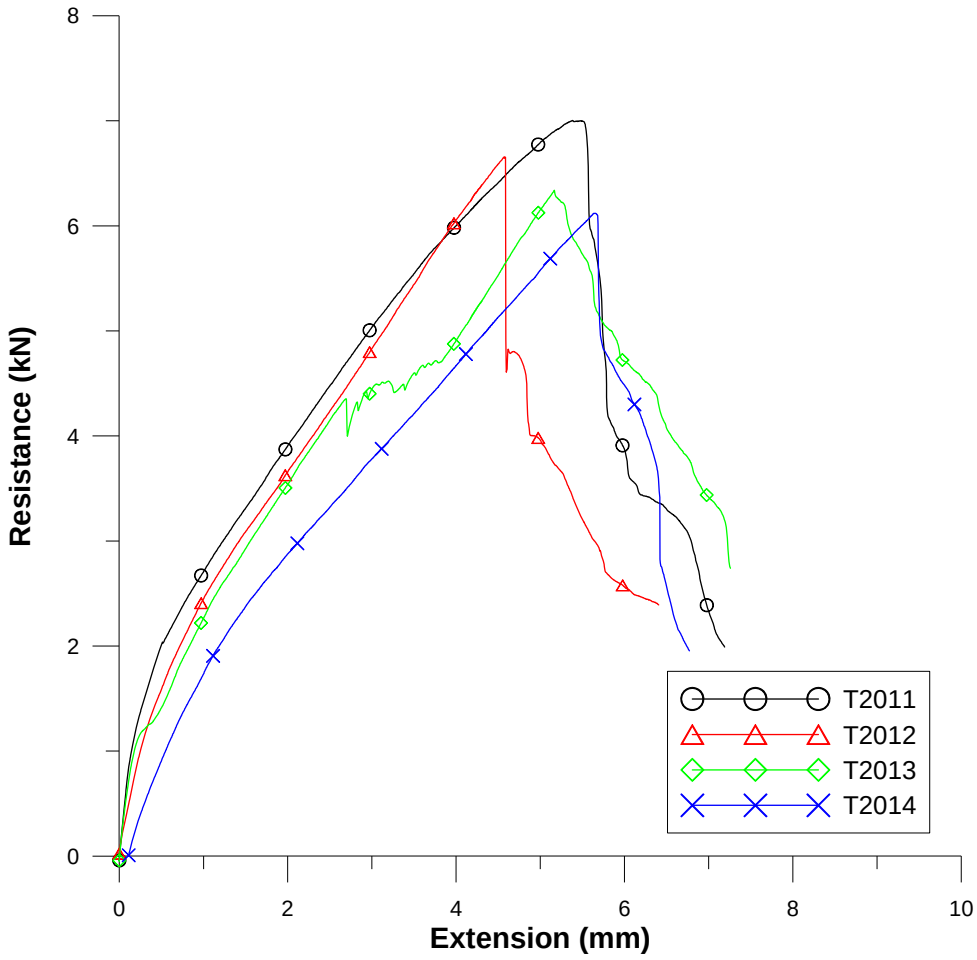

Figure G.11 1-layer tension specimens with 0.91 mm sheets and 6.4 mm angle

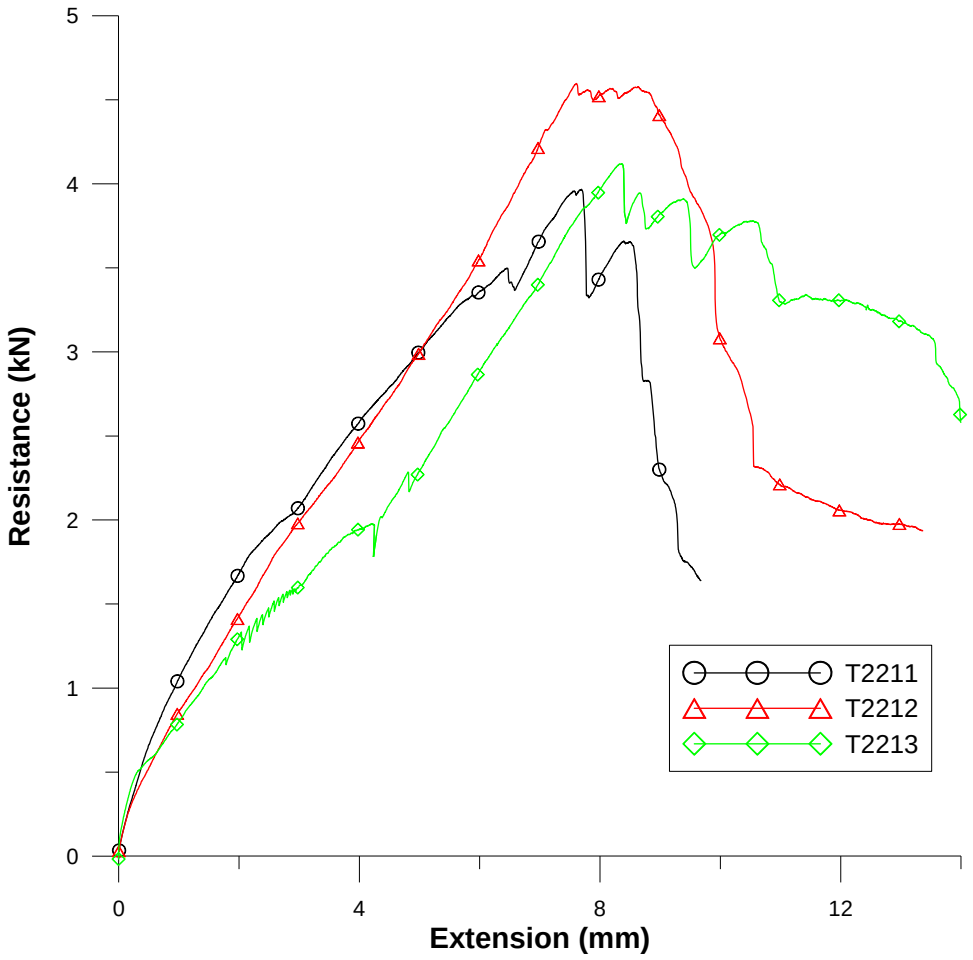

Figure G.12 1-layer tension specimens with 0.76 mm sheets and 6.4 mm angle

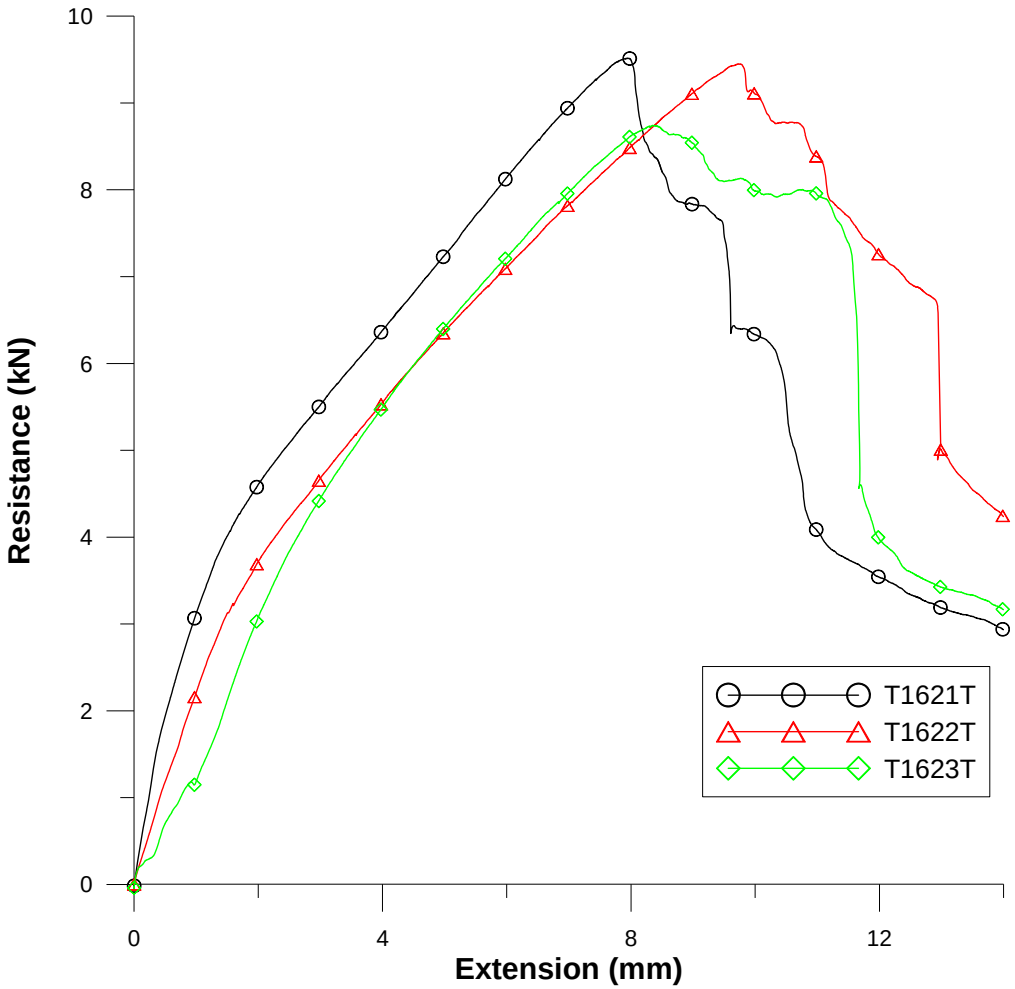

Figure G.13 2-layer tension specimens with 1.52 mm sheets and 3.2 mm angle

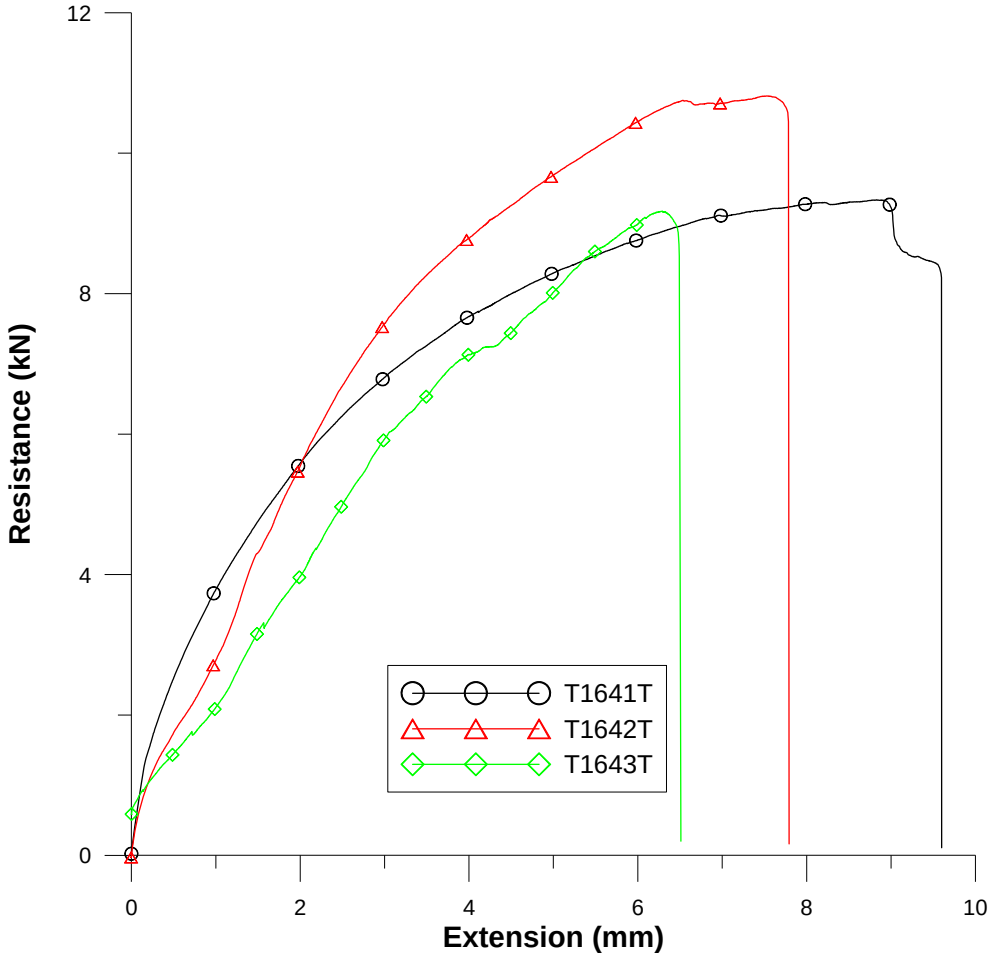

Figure G.14 4-layer tension specimens with 1.52 mm sheets and 3.2 mm angle

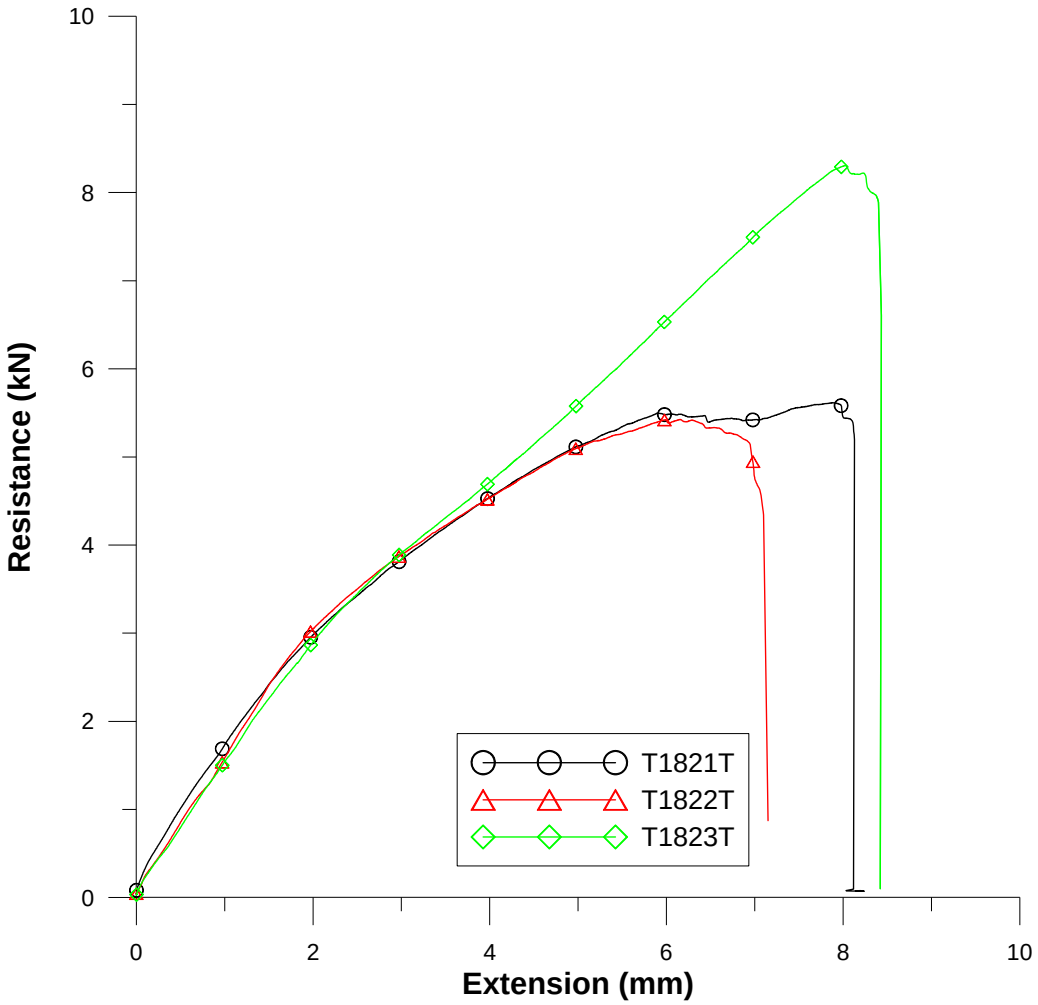

Figure G.15 2-layer tension specimens with 1.21 mm sheets and 3.2 mm angle

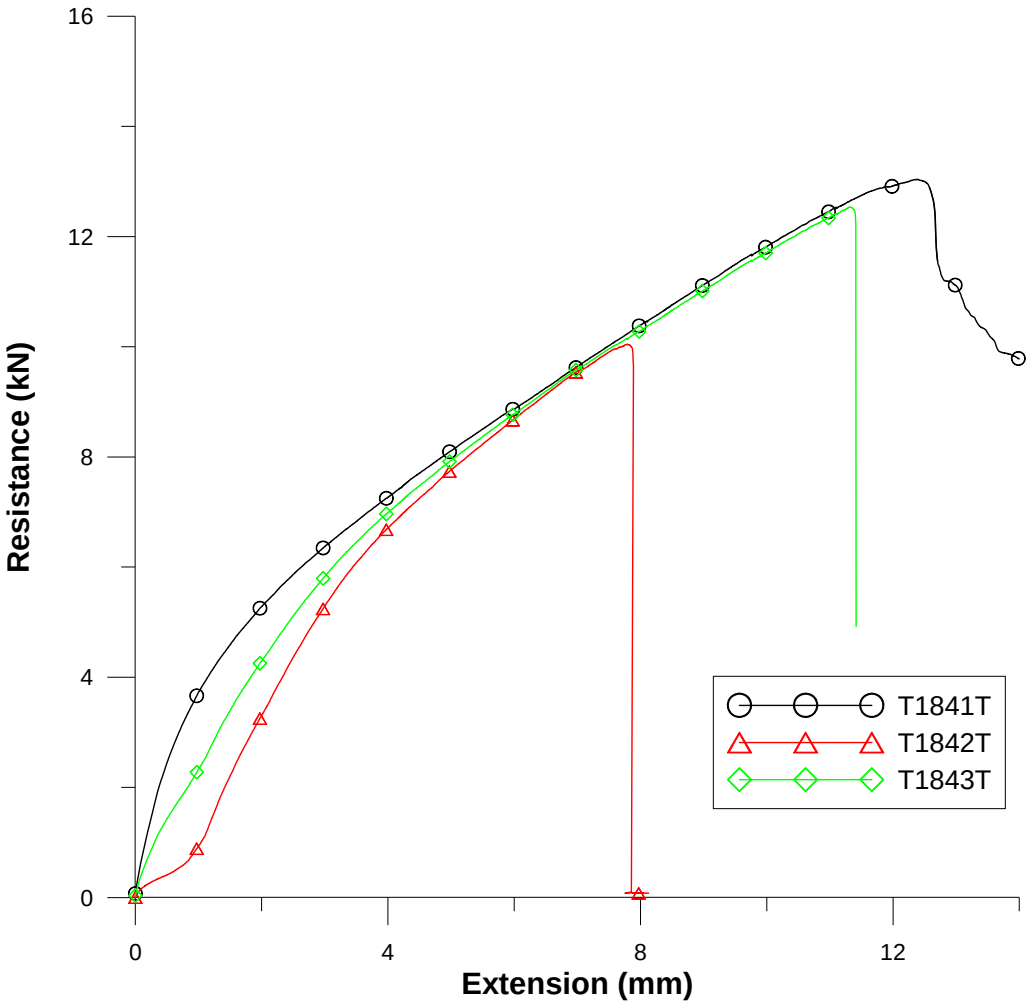

Figure G.16 4-layer tension specimens with 1.21 mm sheets and 3.2 mm angle

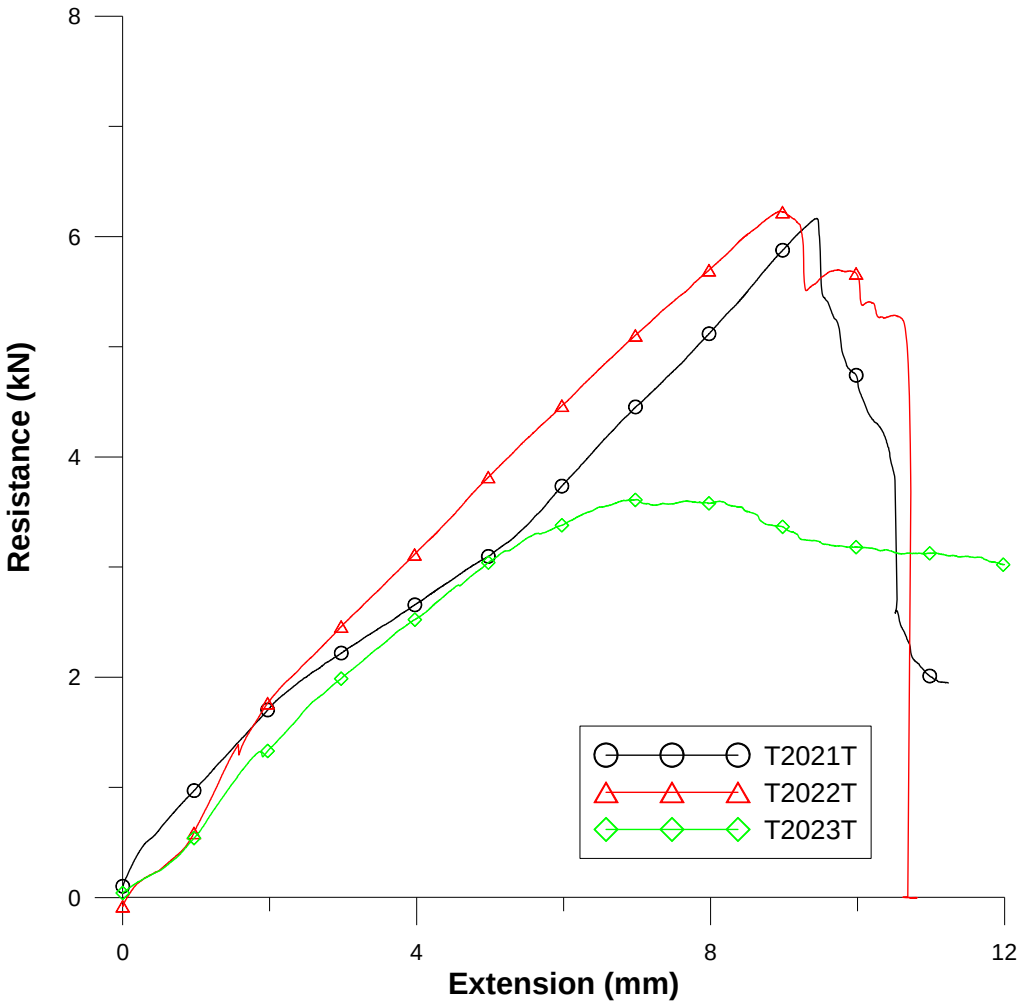

Figure G.17 2-layer tension specimens with 0.91 mm sheets and 3.2 mm angle

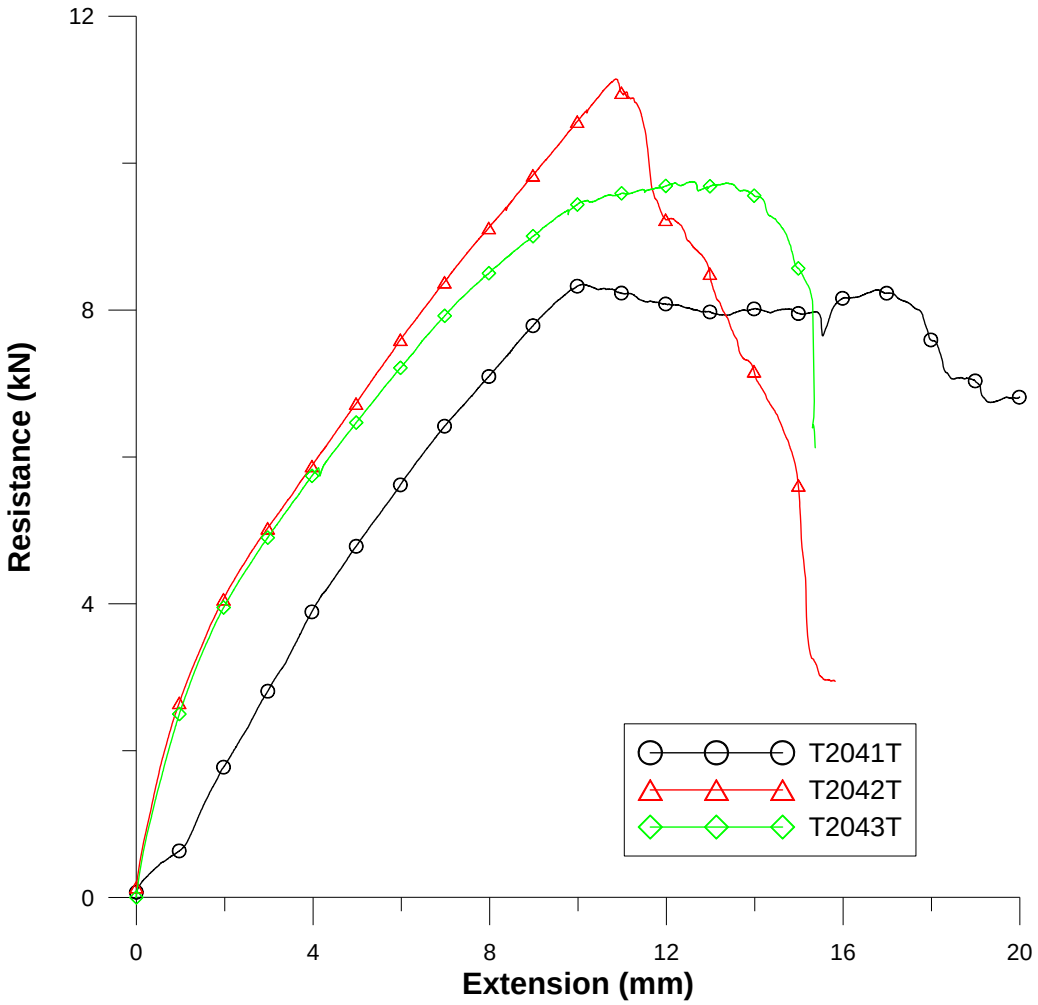

Figure G.18 4-layer tension specimens with 0.91 mm sheets and 3.2 mm angle

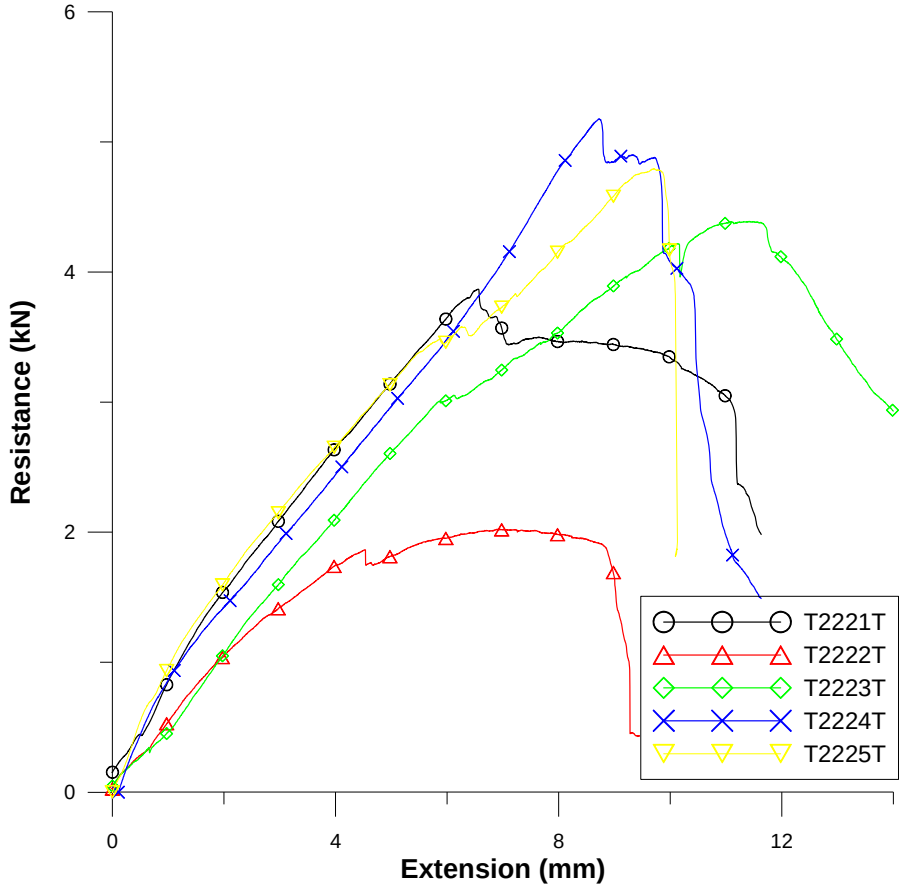

Figure G.19 2-layer tension specimens with 0.76 mm sheets and 3.2 mm angle

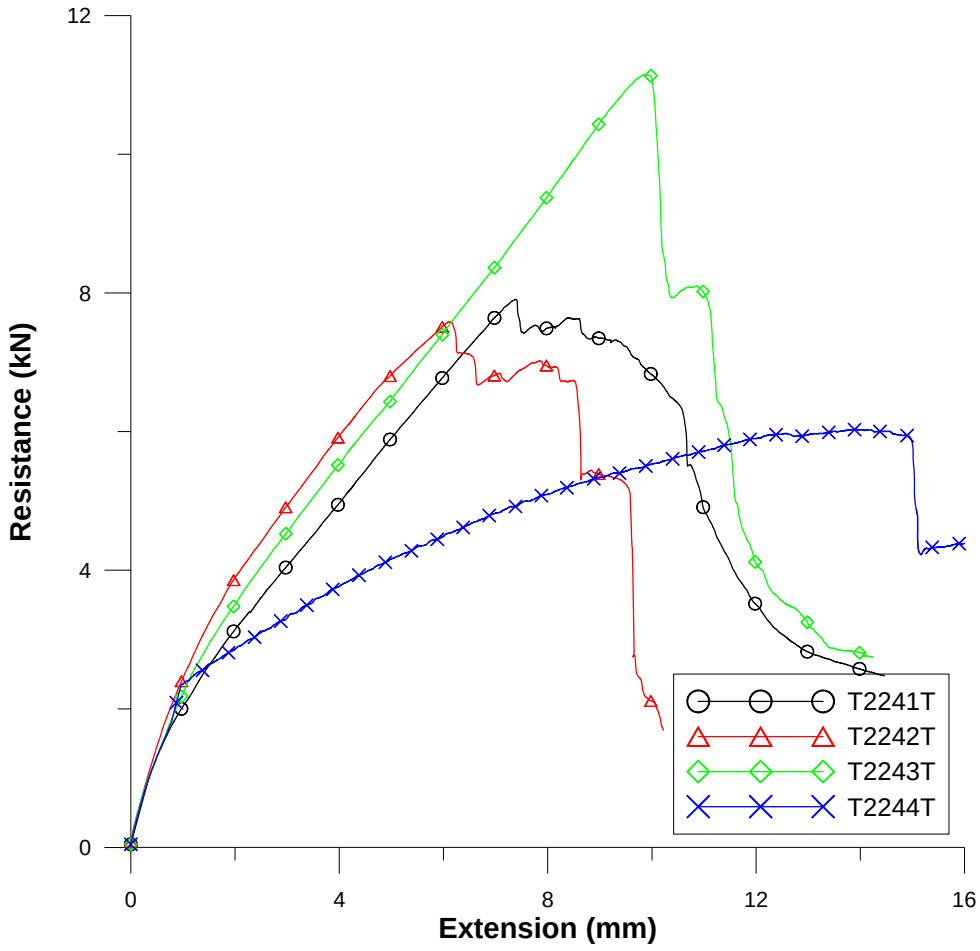

Figure G.20 4-layer tension specimens with 0.76 mm sheets and 3.2 mm angle

APPENDIX H. COUPON TEST RESULTS

Appendix H provides the results of the coupon tests described in Section 3.2.

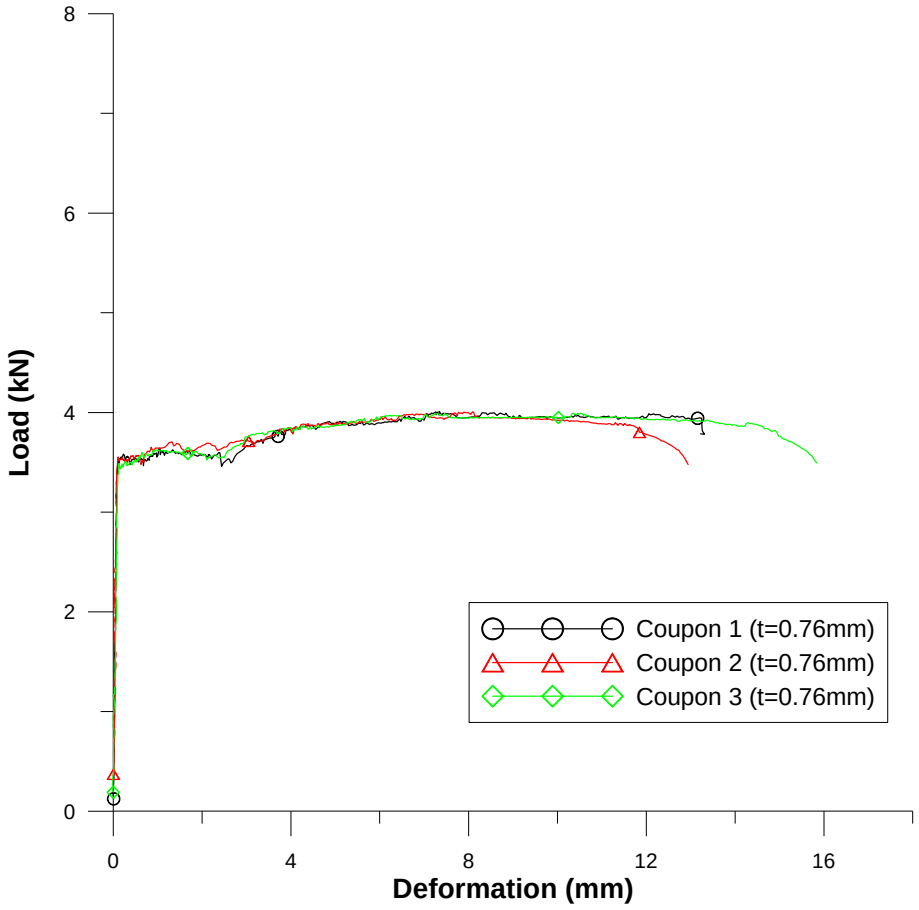

Figure H.1 Coupon test results with 22 gauge steel sheets

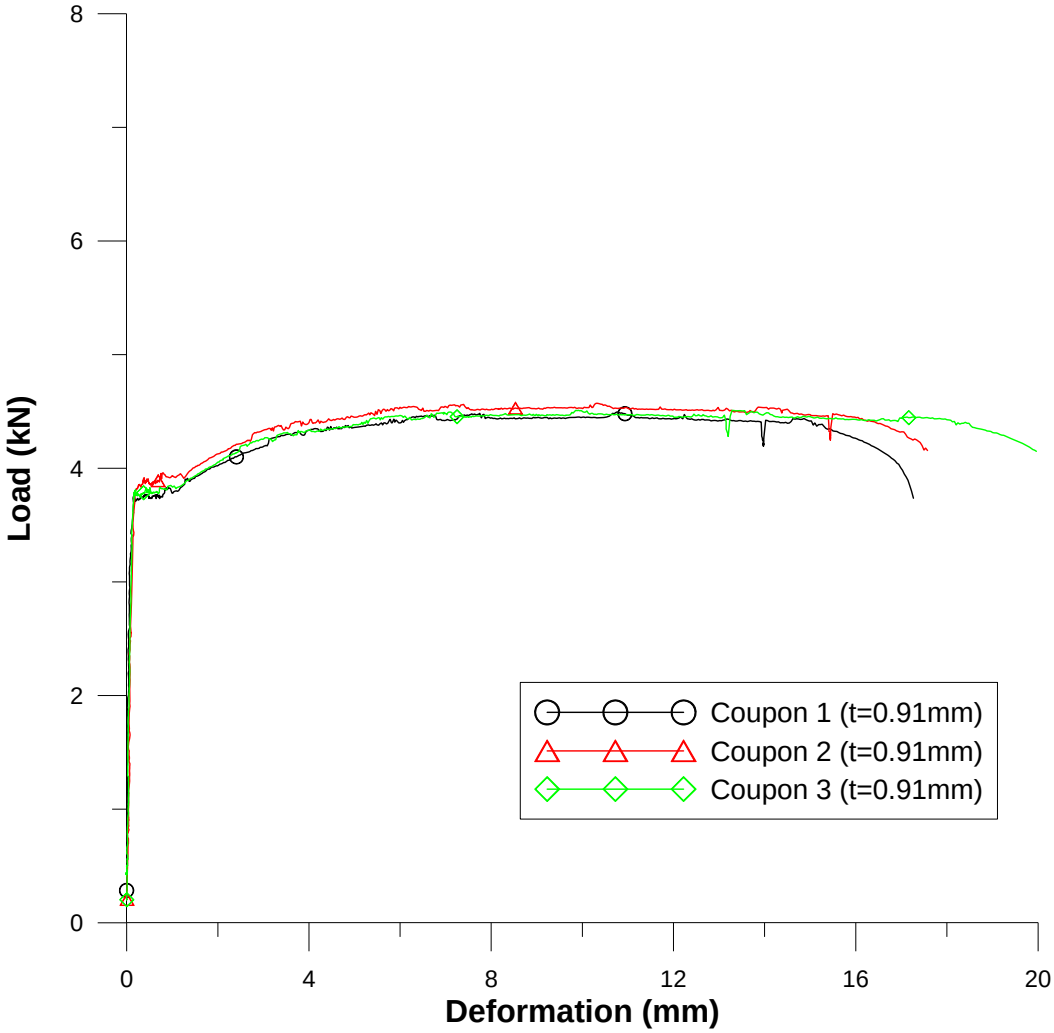

Figure H.2 Coupon test results with 20 gauge steel sheets

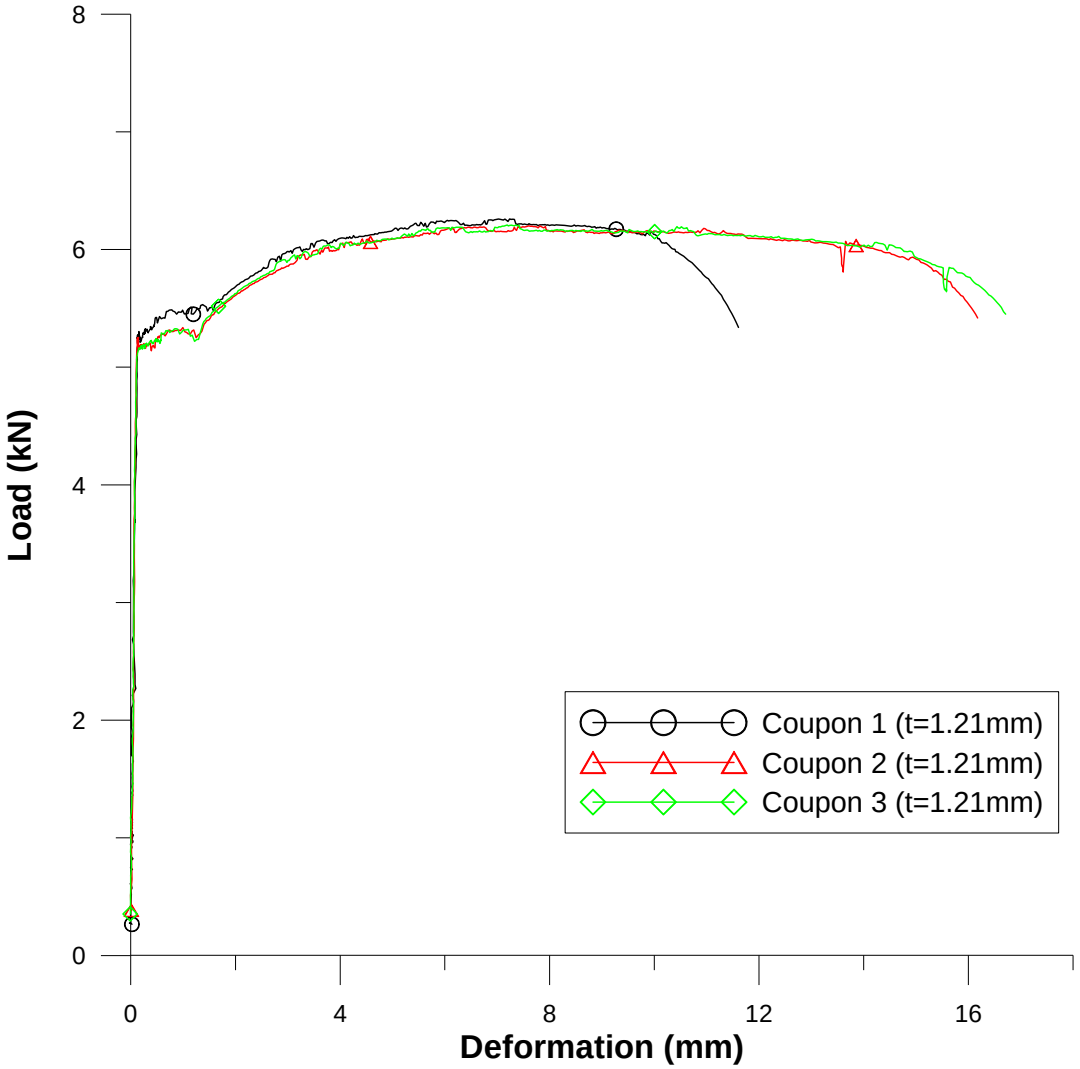

Figure H.3 Coupon test results with 18 gauge steel sheets

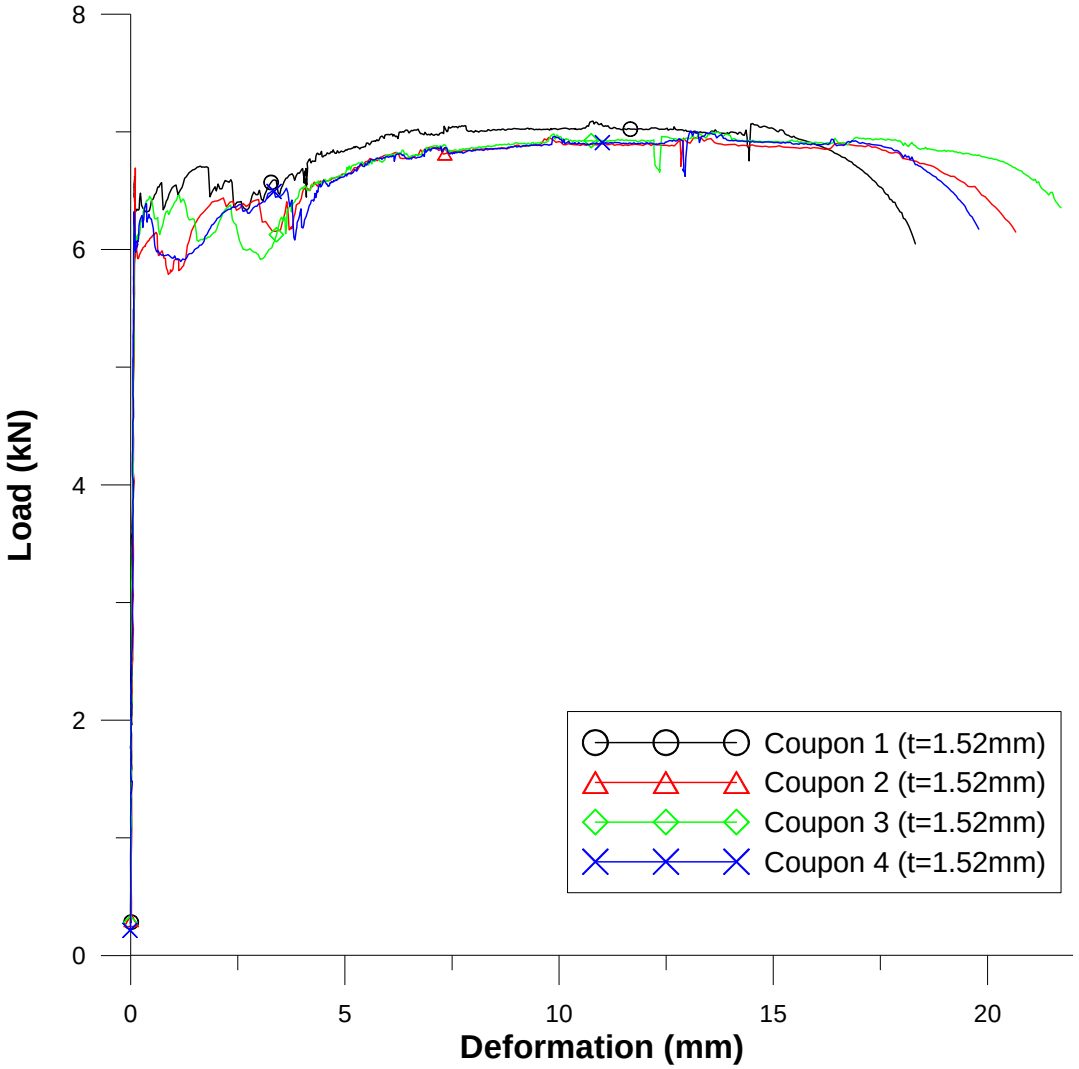

Figure H.4 Coupon test results with 16 gauge steel sheets

ARTICLE 1: SHEAR AND TENSION CAPACITY OF ARC-SPOT WELDS FOR MULTI-OVERLAP ROOF DECK PANELS

N. Guenfoud [1], R. Tremblay[1] and C.A. Rogers[2]

Abstract : Arc-spot welds fabricated in multi-overlap configurations are found in roof deck construction when steel sheets are stacked at a sidelap or endlap. A welding technique that maximizes the quality of arc-spot welds when fabricated through several layers of thick sheets is presented. Welds test specimens were fabricated through 1, 2 or 4 layers of steel sheets with thicknesses ranging from 22 gauge (0.76 mm) to 16 gauge (1.52 mm). The most important factors to control during the welding of thick steel sheets are the current (high intensity), the electrode type (E4311) and the welding technique. Various sheet steel / weld configurations found in roof deck construction were included. Adequate weld quality could be achieved in all cases except that welds were undersized when the total sheet thickness becomes twice as large as the thickness of the underlying material. A total of 76 tension tests and 107 shear tests were completed. Of these, 31 shear specimens were loaded with a reversed cyclic protocol to gain insight into the behaviour of arc-spot welds subject to seismic

[1] Dept. of Civ., Geo. and Mng. Eng., École Polytechnique, Montreal QC, Canada.

[2] Dept. of Civ. Eng. and Appl. Mech. McGill University, Montreal QC, Canada

loading. All other specimens were loaded under monotonically increasing displacement. The results were compared with the current provisions of the CSA S136 North American Specification for the Design of Cold-Formed Steel Structural Members. The CSA S136 equations for shear and tension resistance of arc-spot welds are generally conservative, even for welds fabricated through multi-overlap configurations with total sheet steel thicknesses exceeding the current limits. Nonetheless, modifications to equations E2.2.1-2 and E2.2.2-1 are recommended.

Keywords: arc-spot weld, sheet steel, deck, shear, tension, resistance

INTRODUCTION

In North America roof deck diaphragms are commonly used as part of the lateral load resisting system. These diaphragms are composed of corrugated steel panels that may be connected to the underlying structure by arc-spot welds in order to develop shear strength and stiffness. The overall shear resistance of a roof deck diaphragm is largely dependent on the strength of its connections. Due to uplift actions caused by wind loads the welded connections must also resist tension forces. The majority of the connectors are used to attach a single sheet of deck to the underlying steel frame. However, at the perimeter of each deck panel, the sidelap and endlap fasteners are used to connect the panels to one another and to the steel frame. This can result in connections comprising two and four layers of deck. Figure 1 illustrates the different fastener configurations typically found in roof deck diaphragm construction.

Provisions to determine the shear and tensile resistance of arc-spot welds can be found in the CSA S136 North American Specification for the Design of Cold-Formed Steel Structural Members (CSA, 2007). The current provisions for shear strength of arc spot welds can be traced to the research of Pekoz and McGuire (1979), while the equations given to determine the tensile resistance were recommended by LaBoube and Yu (2001). These provisions are mainly based on tests that were carried out using thin deck panels because at the time, the vast majority of roofs were composed of deck with thicknesses of 22 and 20 gauge (0.76 mm and 0.91 mm). The CSA S136 Specification currently limits

the total thickness (deck thickness times the number of deck layers) of sheet steel for an arc spot weld connection to 3.81 mm (0.15 in). Appendix B of the specification contains provisions that are applicable only to Canada. Section E2.2a of Appendix B states that the maximum single sheet thickness shall be 2.0 mm and that the maximum aggregate sheet thickness of double sheets shall be 2.5 mm. Furthermore the specification also requires that the thickness of the underlying supporting member be at least 2.5 times the steel sheet thickness.When changes were made to the seismic design provisions in the 2005 National Building Code (NRCC, 2005) and the CSA S16 Standard (CSA, 2001), a capacity based seismic design approach was adopted. This approach requires the roof deck diaphragm to have a shear resistance greater than the probable resistance of the vertical bracing system (Tremblay & Rogers, 2005; Rogers & Tremblay, 2010). Consequently, the use of 18 (1.21 mm) and 16 gauge (1.52 mm) deck has become more common as stronger and stiffer diaphragms are required.

To fasten the deck panels together they are overlapped at their perimeter. Therefore, the welds at these locations must be installed through multiple steel layers; two-layer deck situations occur when the ends or sides of two deck panels overlap, and four-layer overlap situations occur at the corners of the sheets (Fig. 1). These overlap situations are commonly found in all roof deck configurations. In the SDI Design Manual (Luttrell 2004), it is indicated *that end laps may be staggered or on a continuous line without particular effect on the diaphragm strength. However, greater care must be exercised in*

making connections through multiple layers of deck at the panel corners on the end lap. Easterling and Snow (2009) performed shear tests on single, double and four-layer arc-spot weld connections for deck ranging from 0.76 mm to 1.52 mm in thickness. These deck-to-frame connections were fabricated using a shielded metal arc welding procedure (SMAW) that involved an E4310 (E6010) electrode. It was concluded that arc-spot welds can be adequately fabricated in single and double layers of sheet steel if the total thickness does not exceed 3.81 mm (0.15 in). It was also reported that welds with sufficient penetration could not be fabricated in four layers of sheet steel regardless of the deck thickness. The current limits of the CSA S136 are exceeded when 16 and 18 gauge deck panels in the four layer sidelap/endlap configuration are required.

This research was initiated due to the inability of engineers to design arc-spot weld connections for the thicker deck sections that are now commonly specified to satisfy seismic design requirements. Given that the current design provisions are based mainly on tests where a single layer of sheet steel was welded to a steel plate the scope of research was set to address the performance of multi-layer connections of the four standard deck thicknesses found in North America. The objective was to first identify a procedure that could be used to weld the connections, and to then verify if the current design provisions in CSA S136 for arc-spot welds are applicable to these thick deck sheet assemblies. The scope of research involved the testing of arc-spot weld connections

fabricated through 1, 2 or 4 layers of steel sheets with thicknesses ranging from 22 gauge (0.76 mm) to 16 gauge (1.52 mm). A total of 76 tension resistance tests and 107 shear resistance tests were completed. Monotonic and reversed cyclic loading protocols were used. Details on the test program can be found in Guenfoud (2009)

EXPERIMENTAL PROGRAM

Test Specimens and Set-up

The test program involved the two loading conditions encountered in roof deck construction, i.e. in-plane shear due to lateral loads and tension due to uplift wind pressure, on one-layer, two-layer and four-layer welded deck-to-frame connections. Shear and tension test specimens were each fabricated using four nominal sheet steel thicknesses: 0.76, 0.91, 1.21 and 1.52 mm. All specimens were made from galvanized ASTM A653 SS230 sheet steel (nominal F_y = 230 MPa and F_u = 310 MPa) with zinc thickness corresponding to Z275 (275 g/m^2, total of two faces), representing the most commonly used material for steel deck. The actual material properties of the steel sheet were determined according to the ASTM A370 Specification using 50 mm gauge length coupons. The average measured values from three coupon tests for each sheet thickness are given in Table 1.

Separate set-ups were used for shear and tension tests. In both cases, the test rig was installed on and rigidly connected to the base cross beam of a stiff reaction frame. The prescribed specific monotonic or reversed cyclic load or displacement protocol was imposed by means of an MTS 250 kN actuator mounted vertically in the test frame. The load imposed on the test specimen was measured with the actuator load cell. Displacement protocols were imposed using the measurements from an LVDT mounted in the test set-up as feedback signal.

The shear test rig is illustrated in Figure 2 and the shear specimens are depicted in Figure 3. The test setup was similar to that described in the AISI Manual of Cold-Formed Steel Design (2002) for the "Alternate-2 Lap-Joint Shear Test". The specimens were made of two 102 mm x 280 mm overlapped steel sheets connected by a single weld. To represent the underlying joist top chord or beam top flange material, a 51 mm x 76 mm underlying plate with thicknesses of 6.4 mm (1/4") and 3.2 mm (1/8") was used. These plates were made of CSA-G40.21-350 steel with nominal F_y = 350 MPa and F_u = 450 MPa. The plates were coated with a one-coat primer according to CISC/CPMA 1-73a specification (CISC 1975) to represent typical field conditions. The four-layer specimen depicted in Figure 3 represents the case when shear is transferred between four sheets connected at their corners to a supporting beam or joist. In this case, the most critical loading condition for the weld occurs when shear induced by the upper two plies apply a horizontal load in one

direction that is resisted by the lower two sheets. The two-ply specimen represents the case of a sidelap welded connection at a joist or beam location. Again, shear in the weld is due to the force transfer from one sheet to the other sheet. The third type of specimen reproduces the situation where an end lap welded connection is used along the perimeter of the roof diaphragm. In this case, the two sheets apply a load in the same direction and maximum shear develops at the interface between the two sheets and the supporting framing member. For these specimens, the two sheets on one side are connected to a 102 mm x 280 mm x 6.4 mm steel plate fabricated to the same specifications as the underlying plates.

In the test set-up, the specimens were mounted vertically by sandwiching the pre-drilled steel sheets between two plates using pre-tensioned high strength bolts located on each side of the welded connection (Fig. 2). One side was attached to a fixed part whereas the other side was connected to an L-shaped plate that was connected to the actuator load cell. The moveable plate was carefully machined and inserted in a steel guide to ensure that longitudinal shear alone was applied to the test specimens. Brass shim plates were used in the guiding system to minimize friction. An LVDT was mounted vertically to monitor the relative longitudinal movement between the fixed and moveable parts during the tests.

The set-up used to test the tension strength of the arc-spot welds (Fig. 4) was similar to the "Modified Standard Tension-Test Fixture" described in the AISI Manual of Cold-Formed Steel Design (2002) and the set-up developed by LaBoube and Yu (1991). The tension specimens are shown in Figure 5. Steel sheets were cut and cold bent to model one flute from the common 38 mm deep x 914 mm wide trapezoidal deck profile with flutes spaced 152 mm o/c (see Fig. 1). At the bottom flange of the simulated flute, the sheets were welded to hot rolled L63x63 angles with thicknesses of 6.4 mm (1/4") and 3.2 mm (1/8") representing typical steel joist top chord conditions. The angles were made of CSA-G40.21-350 steel with nominal F_y = 350 MPa and F_u = 450 MPa and coated with a one-coat primer according to CISC/CPMA 1-73a specification. The tension strength tests comprised three configurations. The first was a two-layer connection simulating sidelap connections away from end laps or end lap connections away from sidelaps. The second was a four ply configuration simulating simultaneous sidelap and endlap connections at the corners of deck sheets. The third configuration represented a typical interior connection. In the multi-ply connections, the overlap width was 22 mm, thus greater than the visible weld diameter. In the test set-up, the angles were fixed to the load frame and the uplift load was applied by contact underneath the top flange of the simulated deck flute by means of two loading arms machined to fit the shape of the deck profile. This simulated the effect of internal and external wind pressures being transferred to the

connections through the roof steel deck. A vertical LVDT was used to monitor the vertical deformation experienced by test specimens upon loading.

Welding Protocol and Procedure

The quality of an arc spot weld is largely dependent on the skill and experience of the welder as well as the specified protocol. To maximize the quality and uniformity of the welds throughout the study, care was taken to elaborate a suitable shielded metal arc welding protocol specific to the welding of multi-overlap configurations. In collaboration with a welding engineer and experienced certified welders, the key parameters affecting weld quality in multi-overlap configurations were identified as being the electrode type, the current setting, and the welding technique. E4311 (E6011) electrodes were selected because they provided better penetration capacity than other commonly used electrodes. Peuler et al. (2002) performed static and cyclic shear tests on arc-spot welds for 22, 20 and 18 gauge thick sheet steels. Welds were made with different electrodes with and without washers. It was found that E4311 (E6011) electrodes were required to achieve better weld penetration in the underlying material. Current settings were first based on the study in which Easterling and Snow (2009) reported that the current must be set high (200± A) in order to obtain sufficient penetration when attempting to weld multi overlap configurations. Preliminary welding sessions were organized to verify the quality of welds fabricated and refine

the welding procedure. The final parameters used for the fabrication of the test specimens were as follows:

- The weld shall be circular and have a visible diameter from 16 mm to 19 mm.
- The electrode shall be 3.2 mm (1/8 in.) in diameter and meet E4311 (E6011) specifications.
- Current shall be AC and set at 195 A when welding 16 and 18 gauge steel sheets, and 160 A when welding 20 and 22 gauge steel sheets.

The following welding procedure, similar to the one elaborated by Peuler (2002), was selected because it facilitated piercing through thicker sheets while minimizing porosity. The weld was performed in the flat position. Once the arc was sparked, the electrode was pushed down vertically through the material to drill through the sheets until proper fusion of the underlying hot rolled steel was obtained. The electrode was then gradually withdrawn with a circular motion to allow the hole to be filled with molten metal. The arc was then broken vertically.

The time spent fabricating each weld was recorded for all test specimens. The average values for each configuration are given in Table 2. The amount of time necessary to fabricate the weld increases as the total thickness of sheet steel increases.

Moreover, the average welding time measured for welds fabricated with 6.4 mm thick underlying steel plates was 24% longer than the average time measured for welds fabricated with 3.2 mm thick underlying steel plates. These results indicate that the thicker underlying steel plate acts a greater heat sink which increases time required to fabricate the arc-spot weld. The SDI Design Manual suggests that 19 mm (¾ in.) welds should be fabricated in 3 to 6 seconds using 4 mm (5/32 in.) electrodes. Easterling and Snow noted that these limits may not be applicable when using 3.2 mm (1/8 in.) E4310 (E6010) electrodes. The average welding times observed for welds made through a single layer and two-layer connections by Easterling and Snow are respectively 33% and 18% longer than the average welding time measured in this study. This difference is attributed to the type of electrode used (E4311 *vs.* E4310).

Loading and Displacement Protocols

A monotonic loading protocol was used for all tension tests and 76 shear tests. The remaining 31 shear tests were carried out using a reversed cyclic loading protocol. The rate of loading for all monotonic tests was 0.5 mm/min. This rate of loading is in accordance with what has been used by Peuler (2002) and Rogers and Tremblay (2000, 2003a,b). Prior to running the cyclic tests, the data from the monotonic shear tests were compiled to provide an estimate of the average ultimate shear strength ($P_{u,avg.}$) for each connection configuration. A loading protocol specific to each

configuration was then determined. Each cyclic loading protocol was composed of three different phases. The first phase, illustrated in Figure 6, was composed of a series of load controlled cycles used to simulate the expected demand on an arc-spot weld diaphragm connection during an earthquake: 6 cycles at 1/3 and 6 cycles at 2/3 and 12 cycles at the connection factored measured resistance, i.e. $\phi P_{u,avg}$, where ϕ was determined according to the predicted failure mode. A frequency of 1.0 Hz was used, representing the fundamental period of a typical low-rise steel building with flexible steel roof deck diaphragm (Tremblay and Rogers 2005). The second phase included one displacement controlled cycle where the specimen was loaded at a rate of 0.5 mm/min., past its ultimate load (P_u) until it reached its failure point (0.8 x P_u). The load was then reversed until the failure point in the opposite direction was reached. The third phase of the reversed cyclic tests consisted of six displacement controlled cycles at a frequency of 1.0 Hz. Two cycles were completed with amplitudes of 2, 4 and 6 mm. This phase was used to observe the ductility of the specimens after failure.

Test Matrix

A listing of the test configuration, steel sheet thickness and number of test specimens is provided in Table 3. The first letter of the specimen number relates to the loading (M = monotonic, C = Cyclic, and T = tension), “xx” is the gauge number, the

following number is the number of plies, and "z" is the specimen number in a series. The letter "P" or "T" is added to identify the shear specimens at the perimeter of the diaphragm and when the thinner (3.2 mm) underlying material is used, respectively. For each connection configuration and steel sheet thickness, the number of test specimens is associated with a letter that gives the failure mode observed in the tests. These failure modes are described in the next section.

TEST RESULTS

Failure Modes

Three different failure modes were encountered during the shear strength tests: weld shear failure (W), sheet tearing failure (T) and sheet bearing failure (B). These failure modes are reported in Table 3 for each connection configuration and sheet thickness. The weld shear failure is characterized by shear fracture of the specimen through the weld nugget. Small displacements, a sudden loss in resistance and overall brittle behaviour are associated with this failure mode. Weld shear occurs mainly for the configurations that have a low weld diameter to total thickness ratio. When the effective diameter is relatively small compared to the thickness of the sheet steel plate the critical load causing failure through the weld plane is reached before the sheet steel plate can exhibit significant deformations.

When sheet tearing occurs, the failure initiates along the contour weld on the tension side of the weld with the tear typically spreading on a line perpendicular to the applied load. Out of plane deformations then occur in the sheet steel on the compression side of the weld. This failure mode occurs when the d/t ratio is high. The resistance of the connection decreases in a gradual and constant manner once the ultimate capacity has been reached. Sheet bearing failure is characterized by a ductile failure that occurs through piling of the sheet steel in front of the weld nugget and by shearing of the sheet around the contour of the weld on lines parallel to the applied load. Relatively large displacements are associated with this failure mode. Once the ultimate load has been reached the load decreases gradually. After the ultimate load there are several plateaus where the load increases slightly before decreasing again. Figures 7a to 7c show typical examples and load-deformation responses for each of these three shear failure modes.

During tension strength tests, two failure modes were encountered: weld failure (W) and sheet tearing failure (T). The weld failure occurred for configurations with low diameter to thickness ratios. This brittle failure mode occurs through the effective area of the weld. Relatively small displacements are associated with this failure mode. The sheet tearing failure mode is characterized by tearing of the sheet steel along the contour of the weld. A peeling effect caused by the geometry of the overlap

connection results in stress concentrations at the contour of the weld. During sheet tearing failure, a gradual decrease in resistance occurs once the ultimate resistance has been reached. Figures 7d & 7e show typical examples and load-deformation responses for these two tension failure modes.

Effective Weld Diameter

In CSA 136, the resistance of shear and tension specimens associated with failure of the weld is related to the effective weld diameter. This parameter must then be accurately determined for the validation of design equations. The cross-section of the weld nugget typically has a conical shape and, therefore, the diameter of the weld decreases over the depth of the weld. As illustrated in Figure 8, the visual weld diameter (d_{vis}) is measured at the surface of the weld whereas the effective weld diameter (d_{eff}) is located at the failure plane of the weld. In Figures 8a and 8b, d_{eff} is measured along the mid-thickness of the steel sheets for the four- and two-ply shear specimens. Conversely, d_{eff} is at the interface between the cold-formed steel sheets and the hot rolled steel for the two-ply shear specimens representing an end lap connection to the perimeter beams (Fig. 8b) and for the four-, two- and single-ply tension specimens.

As the total thickness of sheet steel increases above the plane of interest, the difference between the visual diameter and the effective diameter also increases. Because it is impossible for a designer to see or specify the effective weld diameter, CSA S136 provides an equation (E2.2.1-5) to determine d_{eff} :

$$d_{eff} = 0.7d_{vis} - 1.5t \leq 0.55d_{vis} \quad (1)$$

where t is the total thickness of the cold-formed steel sheets above the expected failure plane of the weld.

This equation was developed by Peköz and McGuire (1979) who indicated that the weld area obtained with d_{eff} from Equation 1 provides an accurate estimate of the net effective area of welds which contain substantial pitting and porosity. In this test program, the effective weld diameter was determined for all shear and tension specimens where weld failure occurred. On the weld failure plane, the average of two diameter measurements taken in perpendicular directions was used to calculate a gross effective weld area. These measurements were taken along the failure plane of the weld. A measure of pitting and porosity was recorded with a vernier calliper and deducted from the effective gross weld area to calculate the effective net weld area, A_{ne}. The effective net weld area was used to calculate the effective weld diameter:

$$d_{eff} = \sqrt{4A_{ne}/\pi} \quad (2)$$

This equation has previously been found to be conservative because the effective weld diameter measured by Peuler (2002) were on average 50% higher than the effective weld diameters predicted by Equation 3-1 for welds fabricated without washers. More recently, Easterling and Snow measured effective weld diameters that were on average 30% higher than those calculated using Equation 1. It must be noted that the values published by Peuler as well as Easterling and Snow do not include any reduction to account for the porosity of the welds. A plot of the data recorded from the shear and tension specimens of this test program and the data reported from previous studies by Peköz and McGuire, Peuler, Easterling and Snow is provided in Figure 9a. Only specimens fabricated without welding washers were plotted from the data from Peuler, and the data was categorized according to the type of electrode used. Only the specimens with full-time welds were plotted for the study by Easterling and Snow. The measured values of d_{vis} were used to plot the data from this study. That parameter was not found to vary with the number of sheets or the steel sheet thickness.

The results from this study support that Equation E2.2.1-5 of CSA S136 accurately predicts the effective weld diameter for the t/d_{vis} range where tests had previously been carried out. This study also provided data in a t/d_{vis} range where few tests had

previously been done. Figure 9a shows that equation E2.2.1-5 becomes overly conservative as t/d increases and that a lower limit should be added to Equation E2.2.1-5 to read:

$$d_{eff} = 0.7d_{vis} - 1.5t \quad , with\ 0.4d_{vis} \leq d_{eff} \leq 0.55d_{vis} \tag{3}$$

This lower limit should be applied only if welds are fabricated with a welding procedure using an E4311 (E6011) penetrating electrode as all the supporting data was generated using this type of electrode.

Influence of the thickness of the underlying framing material

The failure modes and ultimate resistance of the 28 shear specimens and 27 tension specimens fabricated with 3.2 mm underlying framing material were compared to those of the corresponding specimens with 6.4 mm thick framing plates or angles. For the shear specimens, the failure mode was not influenced by the plate thickness. For two-layer specimens, the strength was not found to be affected by the thickness of the supporting material, regardless of the sheet thickness, as can be observed in Figure 9b. The same holds true for the four-layer connections made with 22 to 18 gauge steel sheets. However, for the particular case of the 4-layer specimens fabricated with 16 gauge (1.52 mm) material and 3.2 mm thick underlying plates, the average measured shear resistance was 32 percent lower than the average measured shear resistance of

the 4-layer specimens with 6.4 mm thick underlying plates. In that particular case, the measured visible and effective weld diameters were respectively 13% and 28% lower for specimens fabricated with 3.2 mm thick underlying plates. As the average recorded welding time was 41% shorter for these specimens, the smaller weld dimensions were to be expected. These results show that when the underlying material to total sheet steel thickness ratio is lower than 0.5 ($3.2/(4 \times 1.52) \approx 0.5$), the welder may experience more difficulty producing welds with consistent effective weld diameters, which can result in reduced connection strength as was seen in this study. These results indicate that the limit from Appendix B of CSA S136 that requires a minimum ratio of 2.5 for the underlying material to total sheet thickness could be lowered.

Tension tests on specimens with the thinner angles were only performed with two- and four-ply specimens. In these tests, the thickness of the angle had no influence on the behaviour and strength of the specimens fabricated with 22 and 20 gauge steel sheets. For specimens with 16 and 18 gauge steel sheets, a decrease in resistance was observed when 3.2 mm thick underlying angles were used. In these tests, it was observed that the angles deformed upon loading, causing stress concentrations along the perimeter of the weld thereby reducing the tension resistance of the arc spot weld. Such deformations did not occur with the 6.4 mm thick underlying angles. Moreover, the average measured visible weld diameter of these specimens was 17% smaller,

leading to a smaller effective weld size and reduced capacities, in accordance with what was found in the shear resistance testing. For the 4-layer specimens with 3.2 mm thick underlying steel angles, the average measured effective weld area of 16 gauge specimens was 20% less than that of the specimens composed of 18 gauge steel sheets. This provides additional evidence that welders may experience difficulty producing quality welds through 4 layers of 16 gauge (1.52 mm) steel sheets if the underlying angle does not provide an adequate heat sink because it is too thin.

Analysis of shear resistance equations of CSA S136

The results of the 76 shear specimens were used to validate the CSA S136 equations. The resistance of multi-overlap specimens is governed by different factors according to their failure mode. For specimens with a failure mode related to weld fracture, the resistance of the specimen is governed by the effective diameter of the weld. When the failure mode is related to sheet failure, the thickness of the steel sheets above the plane of maximum shear, and the visible weld diameter influence the resistance of the specimen. As discussed previously, the thickness of the underlying plate does not influence the resistance of the weld although it may influence the fabrication parameters for the connection during welding.

When considering the 33 shear specimens where weld failure occurred, the comparison of the measured effective weld diameter with the values predicted by Equation E2.2.1-5 from CSA S136 provided an average measured-to-predicted ratio

of 1.13 with a coefficient of variation of 0.15. Equation E2.2.1-5 then accurately predicts the effective weld diameter for the range of t/d_{vis} ratio corresponding to the shear specimens ($0.06 < t/d_{vis} < 0.2$). Equation E2.2.1-1 of CSA S136 is used to evaluate the resistance of the connection specimens with regard to the weld shear failure mode:

$$P_u = \frac{\pi d_{eff}^2}{4} 0.75 F_{xx} \quad (4)$$

In this equation, F_{xx} is the tensile strength of the electrode. Using, the nominal tensile strength of the weld metal (F_{xx} = 430 MPa) and the effective weld diameter measured during the tests, the average measured-to-predicted resistance ratio for the shear specimens that failed due to weld fracture is 1.42 with a coefficient of variation of 0.15. This trend is similar to that obtained by Peköz and McGuire who reported an average test-to-predicted ratio of 1.22 with a coefficient of variation of 0.30 for similar tests. The relationship between P_u and d_{eff}^2 of Equation E2.2.1-1 is plotted in Figure 10 along with the data recorded during the experimental program and the data reported by Peköz and McGuire.

The comparison shows that Equation 4 consistently under-predicts the shear resistance of welded connections for the range of d_{eff} examined. This is likely caused by the difference between the actual and nominal values of the tensile strength of the

weld metal. It is difficult to measure the actual tensile strength of the weld metal in test specimens as it can vary significantly over the weld failure plane. This property was not measured in this test program. The authors have been informed, however, that the actual tensile strength of virgin electrodes can be as much as 30% higher than the nominal value. The results show that Equation E2.2.1-1 can safely be used to determine the shear resistance for arc spot weld failures in multi-overlap configurations.

Equations E2.2.1-2 to E2.2.1-4 in CSA 136 are used to predict the shear strength when shear failure occurs in the sheet material:

$$P_u = 2.20 t d_a F_u \quad , for\ (d_a/t) \leq 0.815\sqrt{E/F_u}: \tag{5}$$

$$P_u = 0.280\left[1 + 5.59\frac{\sqrt{E/F_u}}{d_a/t}\right] t d_a F_u \quad , for\ 0.815\sqrt{E/F_u} < (d_a/t) < 1.397\sqrt{E/F_u}: \tag{6}$$

$$P_u = 1.40 t d_a F_u \quad , for\ (d_a/t) \geq 1.397\sqrt{E/F_u}: \tag{7}$$

In these equations, $d_a = d_{vis} - t$, where t is the thickness of steel above the plane of maximum shear in the weld, i.e., the plane where d_{eff} was measured for the specimen with weld failure, and F_u is the tensile strength of the steel sheets. The test data was

compared to the predicted values using the measured values of d_{vis} and F_u. Of all monotonic shear specimens, 35 were governed by Equation 5 (E2.2.1-2) because $(d_a/t) \leq 0.815\sqrt{E/F_u}$. This equation is associated with a bearing failure mode. In Figure 11, Equations 5 to 7 (E2.2.1-2 to E2.2.1-4) are plotted together with the results for these 35 specimens. The data reported by Peköz and McGuire are also presented in Figure 11.

A trend can be observed where the measured resistance values are generally higher than the predicted resistance values. The average measured-to-predicted resistance ratio was 1.44 with a coefficient of variation of 0.14 for the group of specimens tested in this experimental program. Likewise, Peköz and McGuire reported an average measured-to-predicted resistance ratio of 1.15 with a coefficient of variation of 0.17 while Easterling and Snow reported a ratio of 1.28 with a coefficient of variation of 0.09 for specimens where $(d_a/t) \leq 0.815\sqrt{E/F_u}$. The difference between the three ratios may be attributed to differences in weld quality. Although this data was not recorded, some specimens may not have efficient connectivity along the entire perimeter of the weld, which would inevitably lower the resistance of the specimen. When analysing the data collected during this experimental program the best fit formula to replace equation E2.2.1-2 was found to be:

$$P_u = 2.40td_aF_u \quad , for\ (d_a/t) \leq 0.815\sqrt{E/F_u}:$$

(8)

This proposed equation was analyzed in accordance with Section F.1 of CSA S136 which specifies the statistical treatment to determine the structural performance for limit states design. When comparing the data obtained during this testing program with Equation 8, the average measured-to-predicted ratio was 1.32 with a coefficient of variation of 0.14. When using these values, the minimum required reliability index of 4.0 can be attained with a resistance factor $\phi = 0.6$.

A total of 8 specimens were governed by Equation 6 (E2.2.1-3) because $0.815\sqrt{E/F_u} < (d_a/t) < 1.397\sqrt{E/F_u}$. The average measured-to-predicted resistance ratio for specimens governed by this equation is 1.58 with a coefficient of variation of 0.04. The data measured in this study and the data by Peköz and McGuire are compared to the predicted values in Fig. 11b . Equation 6 (E2.2.1-3) generally underestimates the resistance values of the specimens tested during this experimental program. However, too few specimens were governed by this equation during this test program to warrant the modification of the current CSA S136 equation. Based on the available test data, it seems that Equation 6 (E2.2.1-3) can safely be used to predict the shear resistance of specimens with multi-overlap configurations when

$0.815\sqrt{E/F_u} < (d_a/t) < 1.397\sqrt{E/F_u}$. Further research targeting this specific range of specimens should however be carried out to validate the accuracy of Equation E2.2.1-3. Of all the specimens tested during this experimental program, none presented a d_a/t ratio indicating that Equation E2.2.1-4 would govern. As no new data was gathered during this study no suggestions can be made towards Equation E2.2.1-4.

Reversed cyclic shear resistance results

The results from the 31 reversed cyclic shear specimens provided insight into the behaviour of welds under cyclic dynamic loading. In the first phase of the tests, all specimens exhibited a stable nearly elastic response up to and including the cycles at the factored shear resistance level. This is illustrated in Figure 12 where the response of two samples: one two-ply specimen made of thin (0.91 mm) steel sheets and one four-ply specimen made of thicker (1.21 mm) steel sheets is shown. In the first half cycle of phase II, all specimens showed similar ultimate capacity compared to their monotonic equivalent. On average, the resistance was equal to 94% of the monotonic case. Differences between specimens were observed in the post-peak region and for the remaining of the tests: when sheet bearing mode was engaged the specimens could exhibit significant ductility, i.e., maintaining most of their capacity upon load reversal in phase II and developing stable, although pinched, hysteretic response under the phase III cyclic displacement protocol, whereas specimens that were

governed by other failure modes showed little ductility. This difference can be seen in Figure 12, with the specimens with the thinner total sheet thickness being more ductile than the one with greater total thickness. The difference in failure mode can be seen in Table 3. During the load reversal of phase II, the ductile specimens (bearing failure mode) could develop, on average, 74% of the peak capacity reached in the previous half-cycle. For the other specimens, that percentage reduces to 66%.

Analysis of tension resistance equations from CSA S136

Similar to what was found for the shear resistance of arc-spot welds, the results from the 72 tension specimens demonstrated that different factors influence the tensile resistance of multi-overlap specimens according to their failure mode. The results showed that when the specimens were governed by weld fracture, the effective weld diameter influenced the tension resistance. When the tension specimens were governed by sheet failure, the total thickness of sheet steel above the underlying material and the average weld diameter influenced the tension resistance. As discussed, the thickness of the underlying plate also influenced the resistance of the specimens as thinner supporting material can distort upon loading and create stress concentrations that can adversely affect the resistance of the specimen. The deformation of the support can be avoided by using hot rolled angle supports with a minimum thickness of 6.4 mm.

Section E2.2.2 of CSA S136 is used by designers to determine the tensile resistance of arc-spot welds:

$$P_u = \frac{\pi d_e^2}{4} F_{xx} \quad (9)$$

$$P_u = 0.8\left(F_u/F_y\right)^2 t d_a F_u \quad (10)$$

Equation (9) is related to weld failure in tension (Fig. 7d) whereas the Equation (10) addresses the sheet tearing failure mode. CSA S136 specifies a 30% reduction for welds fabricated in sidelap joints. As discussed later, this reduction is intended to apply to sheet tearing when only part of the weld connects to the overlapped sheet, which was not the case here. During the testing program, a total of 16 tension specimens failed due to weld fracture. The resistance of such specimens is related to the effective weld diameter of each specimen. Figure 13 contains a plot of Equation E2.2.2-1 without the 30% reduction in resistance. The results obtained in this test program and the data reported by LaBoube and Yu (1991) are also shown. The resistance values obtained from the tested specimens are plotted twice: once with the effective weld diameter measured during the tests and once with the effective weld diameter calculated using Equation 3. The thickness used to determine the effective

weld diameter is equal to the total thickness of sheet steel from the specimen as the failure plane is located between the steel sheets and the underlying steel angle.

Figure 13a shows that the best fit is obtained when using Equation 3 to predict the effective weld diameter. The average measured-to-predicted ratio was equal to 0.75 when using the measured effective weld diameter. When applying a 30% reduction, that ratio increases to 1.08 with a coefficient of variation of 0.27 when the effective weld diameters are determined using Equation 3. This suggests that the 30% reduction in resistance should be maintained when determining the tensile resistance related to weld failure. This 30% reduction in resistance should also be applied to welds that are not fabricated in multi-overlap configurations because there is no evidence that the multi-overlap configuration reduces the capacity of welds when tensile weld failure is involved. For simplicity Equation 9 (E2.2.2-1) should be modified to:

$$P_u = \frac{\pi d_e^2}{4} 0.7 F_{xx} \qquad (11)$$

This proposed equation should apply to all arc-spot welds without considering the sheet steel configuration. When the statistical treatment of Equation 4 is carried out according to Section F.1 of CSA S136 using the measured-to-predicted ratio of 1.08

and the coefficient of variation of 0.27 then the resistance factor must be lowered to 0.31 to attain the required reliability index of 4.0.

CONCLUSIONS AND RECOMMENDATIONS

The results of the 179 tests permitted the evaluation of the shear and tensile capacity of arc-spot welds fabricated in multi-overlap configurations. Through several welding sessions it was first determined that there are three important factors that must be controlled to provide quality arc-spot welds in multi-overlap configurations; type of electrode (E4311), high current setting (200± A) and proper welding technique. The amount of time necessary to fabricate the weld increases as the total thickness of sheet steel increases because the weld must pierce through more material before depositing the weld metal. In the case of multi-overlap configurations, the welding times recommended by the SDI Manual (2004) of 3 to 6 seconds to fabricate 19 mm welds should be increased when using 3.2 mm (1/8 in.) electrodes. The additional time is required to fabricate welds with thicker underlying steel plates because the thicker steel plates act as a greater heat sink. Conversely, when the total sheet thickness becomes larger than the thickness of the supporting material, the latter may not provide an adequate heat sink. Special attention must be paid to the welding protocol when the ratio of the total sheet thickness becomes twice the thickness of the underlying material.

Measurements of the net effective weld diameter of specimens that experienced weld failure were compared with the net effective weld diameter values predicted by Equation E2.2.1-5 from CSA S136. The comparison showed that when the thickness as the total thickness of sheet steel increases Equation E2.2.1-5 becomes excessively conservative. A lower limit for the net effective weld diameter should be imposed in order to improve the precision of Equation E2.2.1-5.

The shear tests carried out with monotonically increasing load confirmed which factors influenced the shear resistance of arc-spot welds. For specimens that are governed by sheet failure the total thickness of the steel sheets and the average weld diameter influence the resistance of the specimen. The resistance of specimens that are governed by weld failure are influenced by the net effective diameter of the weld. Tests also showed that the minimum ratio for the underlying material to total sheet thickness could be lowered from 2.5 to 0.5.

The behaviour of welds under dynamic loading was observed during the reversed cyclic shear tests. The results demonstrated that the resistance of arc-spot welds did not decrease after resisting several loading cycles of lower amplitude. The reversed cyclic tests also demonstrated that specimens can exhibit significant ductility when the sheet bearing failure mode is engaged.

The data obtained during the shear resistance tests enabled the evaluation of Section E2.2.1 of CSA S136 which specifies the shear resistance of arc-spot welds. The results showed that Equation E2.2.1-2 was generally conservative. When analysing the data collected during this experimental program it was determined that a modification of Equation E2.2.1-2 improves its precision.

The results of tension tests established which factors influenced the tensile resistance of multi-overlap specimens. The resistance of tension specimens governed by sheet failure is influenced by the total thickness of sheet steel and the average weld diameter. Specimens governed by weld fracture are influenced by the net effective weld diameter of the weld. The thickness of the underlying plate can influence the resistance of the specimens if the loading causes deformations in the support. These deformations can be avoided by using hot rolled angle supports with a minimum thickness of 6.4 mm.

The data obtained during the tension resistance tests were used to evaluate Section E2.2.2 of CSA S136 which specifies the tension resistance of arc-spot welds. When tension weld failure governs, the results indicate that the 30% reduction in capacity specified by Section E2.2.2 for arc-spot welds for sidelap connections should also be applied to all connections, including connections made of single sheets, because there

is no evidence to suggest that the multi-overlap configuration influences the resistance of specimens governed by this failure mode. A resistance factor $\phi = 0.31$ is proposed when applying this 30% reduction.

ACKNOWLEDGEMENTS

The authors would like to thank the Natural Sciences and Engineering Research Council of Canada (NSERC), the Canadian Sheet Steel Building Institute (CSSBI), the Steel Structures Education Foundation (SSEF) of the Canadian Institute of Steel Construction (CISC) for their support in sponsoring this project. The collaboration of the Canam Group for supplying the material for the test specimens is most appreciated. The authors also acknowledge the assistance of the laboratory technicians at École Polytechnique: P. Bélanger and D. Fortier. Additionally, appreciation is extended to G. Trigo from Consultarc for his most valuable contribution and advice on welding procedures.

REFERENCES

AISI (2002). *Cold-formed Steel Design Manual*, American Iron and Steel Institute, Washington DC

CSA (2001), *CAN/CSA-S16-01, "Limit States Design of Steel Structures*, Canadian Standards Association, Toronto, ON, Canada.

CSA, (2007), *CSA-S136-07, North American Specification for the Design of Cold-Formed Steel Structural Members*, Canadian Standards Association, Toronto, ON, Canada.

CISC. (1975), *CISC/CPMA Standard 1-73a*, *A Quick-drying One-coat Paint for Use on Structural Steel,* Canadian Institute of Steel Construction (CISC), Toronto, ON.

Easterling, W.S., and Snow, G.L. (2009), *Strength of Arc-spot Welds Made in Single and Multiple Steel Sheets*, Research Report No. CE/VPI-ST-08/02, Virginia Polytechnic Institute and State University, Blacksburg, Va, US.

Guenfoud, N. (2009), *Shear and Tension Capacity of Arc Spot Weld Connections for Multi-Overlap Roof Deck Panels*, M.Sc. Thesis, Dept. of Civil, Geological, and Mining Eng., Ecole Polytechnique of Montreal, Montreal, QC.

LaBoube, R.A., and Yu, W.W. (1991), *Tensile Strength of Welded Connections*, Final Report, Civil Engineering Studies 91-3, University of Missouri-Rolla, Rolla, MO, US.

Luttrell, L.D. (2004), *Diaphragm Design Manual*, Third Edition, Steel Deck Institute (SDI). Fox River Grove, IL.

NRCC (2005), *National Building Code of Canada 2005*,12th ed., National Research Council of Canada, Ottawa, ON, Canada.

Peköz, T., and McGuire, W. (1979), *Welding of Sheet Steel*, Report SG-79-2, American Iron and Steel Institute, Washington, DC.

Peuler, M., (2002), *Inelastic response of arc-spot welded deck-to-frame connections for steel roof deck diaphragms*, Master's Degree Project Report, Department of Civil Engineering and Applied Mechanics, McGill University, Montreal, QC, Canada.

Peuler, M., Rogers, C.A., and Tremblay, R., (2002), "Inelastic Response of Arc-Spot Welded Deck-to-Frame Connections for Steel Roof Deck Diaphragms," *Proc. 16th International Specialty Conference on Cold-Formed Steel Structures*, Orlando, USA, 763-778.

Rogers, C.A., and Tremblay, R. (2000), *Inelastic Seismic Response of Frame and Side-lap Fasteners for Steel Roof Decks*, Research Report No. EPM/CGS-2000-09, Dept. of Civil, Geological and Mining Eng., École Polytechnique, Montreal, QC, Canada.

Rogers, C.A., and Tremblay, R., (2003a) , "Inelastic Seismic Response of Side Lap Fasteners for Steel Roof Deck Diaphragms," *J. Struct. Eng.*, ASCE, 129(12) 1637-1646.

Rogers, C.A., and Tremblay, R., (2003b), "Inelastic Seismic Response of Frame Fasteners for Steel Roof Deck Diaphragms," *J. Struct. Eng.*, ASCE, Vol. 129(12) 1647-1657.

Rogers, C. and Tremblay, R. (2010), "Impact of diaphragm behaviour on the seismic design of low-rise steel buildings," *Eng. J., AISC*. (in press)

SANZ (1996). *AS/NZS 4600 – Cold Formed Steel Structures*, Standards Australia / Standards New Zealand, Sydney, NWS, Australia.

Snow, G.L., and Easterling, W. S. (2008), "Strength of Arc Spot Welds made in Single and Multiple Steel Sheets," *Proc. 19th International Specialty Conference on Cold-Formed Steel Structures*, St-Louis, MO, US.

Struble, J.W., Peköz, T., and McGuire, W. (1978), *Tests on Puddle Weld Connections*, Department of Structural Engineering, Cornell University, Ithaca, New York, US.

Tremblay, R., and Rogers, C. (2005), "Impact of Capacity Design Provisions and Period Limitations on the Seismic Design of Low-Rise Steel Buildings," *Int. J. of Steel Structures*, 5(1) 1-22.

Yarnell, R.S., and Peköz, T. (1973), *Tests on Field Weld Puddle and Fillet Welded Connections*, Department of Structural Engineering, Cornell University, Ithaca, NY.

Table 1. Average measured sheet steel material properties.

Nominal sheet thickness (mm)	Overall sheet thickness (mm)	Base metal thickness (mm)	F_y (MPa)	F_u (MPa)	F_u/F_y	% Elongation
0.76	0.786	0.728	392	446	1.14	30.1
0.91	0.912	0.880	346	415	1.20	35.5
1.21	1.209	1.169	358	429	1.20	28.0
1.52	1.513	1.458	356	388	1.09	37.3

Table 2 Average recorded welding times

Sheet Thickness (gauge)	Configuration (layers)	Total Thickness (mm)	Average Welding Time (s)
22	1	0.76	5.3
20	1	0.91	6.8
18	1	1.21	5.3
22	2	1.52	5.8
16	1	1.52	5.0
20	2	1.82	6.8
18	2	2.42	6.7
22	4	3.04	7.2
16	2	3.04	7.6
20	4	3.64	7.7
18	4	4.84	8.7
16	4	6.08	9.3

Table 3 Test matrix and observed failure modes.

Specimen No.	Sheet thickness (mm) / Gauge			
	0.76 / 22	0.91 / 20	1.21 / 18	1.52 / 16
Mxx2z	4T	4T	4T	4B
Mxx4z	2W+1T+1B	2W+1T+1B	4W	4W
Mxx2zP	2W+2T	1W+3T	4W	4W
Mxx2zT	4T	3T	4T	3W
Mxx4zT	2W+1T+1B	1W+1T+2B	3W	3W
Cxx2z	4T	4T	4T	4B
Cxx4z	1W+1T+2B	1W+1T+2B	3W	4W
Txx1z	3T	4T	4T	4T
Txx2z	4T	4T	4T	3W+1T
Txx4z	3T	1W+3T	1W+3T	3W
Txx2zT	5T	3T	3W	3T
Txx4zT	4T	1W+2T	3W	3W

Note : W = Weld failure, T = Sheet tearing failure, B = Bearing failure.

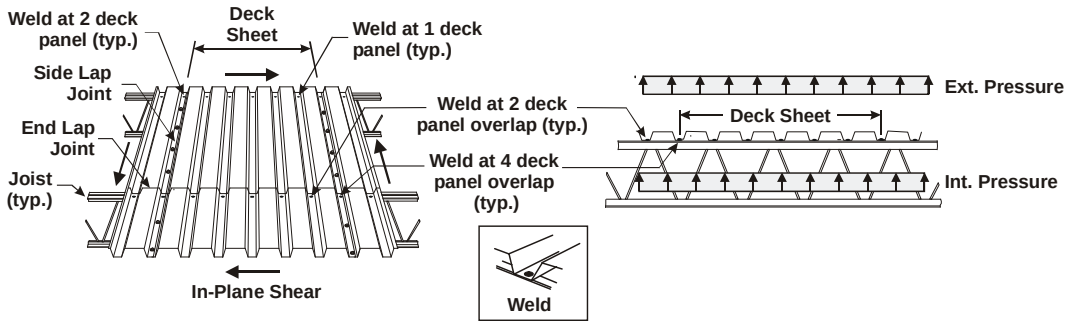

Figure 1: Steel deck sheet connections and loading

a)

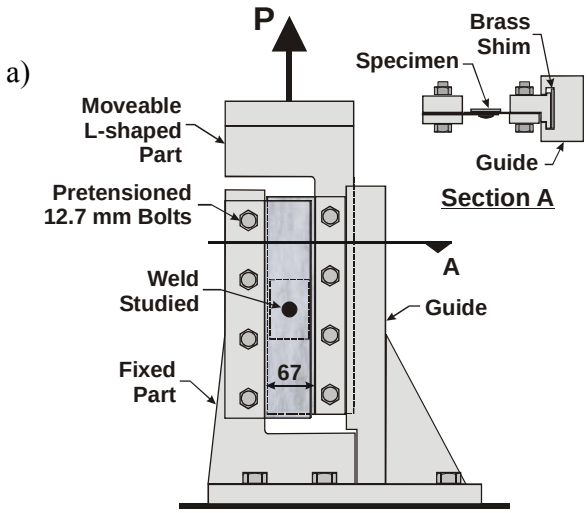

b)

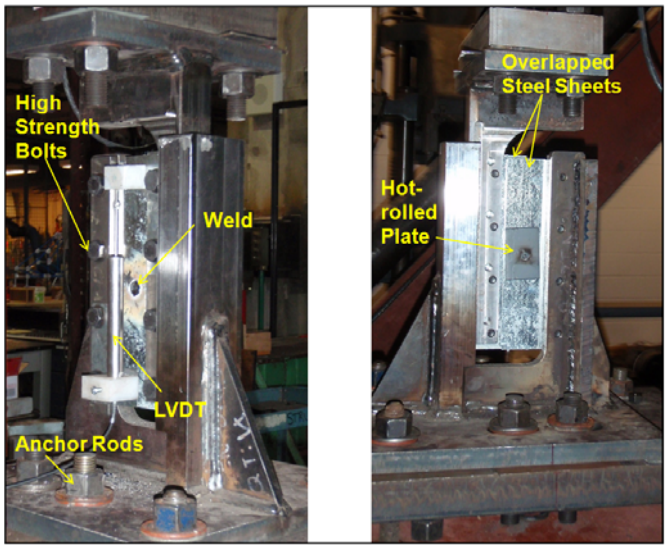

Figure 2: Shear test set-up: a) Schematic elevation view; b) Photos

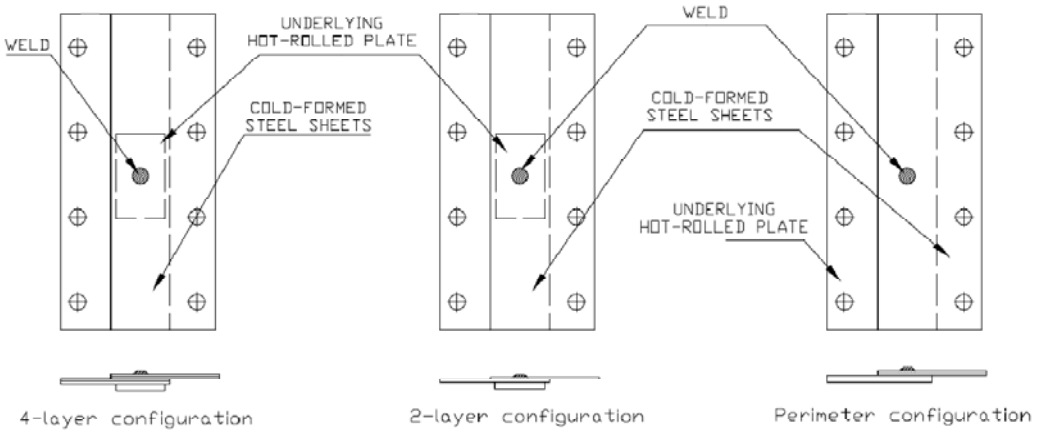

Figure 3: Shear specimen configurations

a)

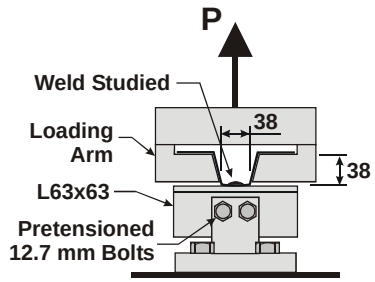

b)

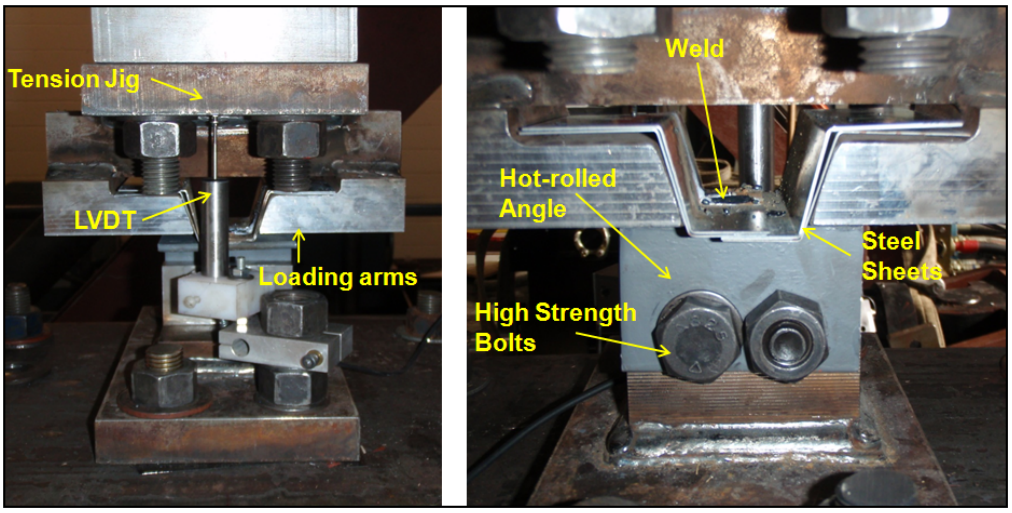

Figure 4: Tension test set-up: a) Schematic elevation view; b) Photos

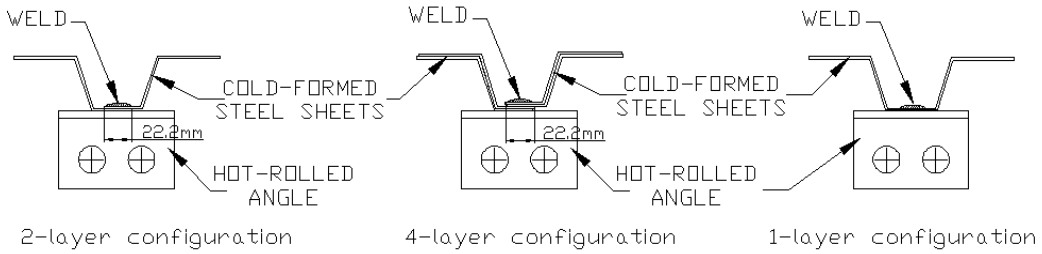

Figure 5: Tension specimen configurations

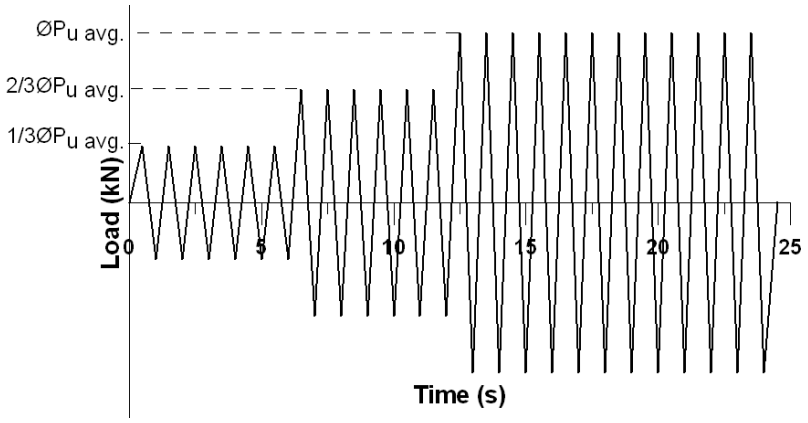

Figure 6: Displacement protocol for the first phase of reversed cyclic test

a)


P2021

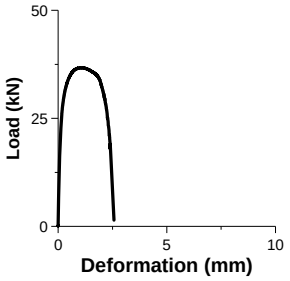
50
25
0
Load (kN)
0
5
10
Deformation (mm)

b)

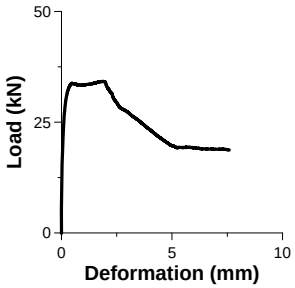
50
25
0
Load (kN)
0
5
10
Deformation (mm)

c)


A2241

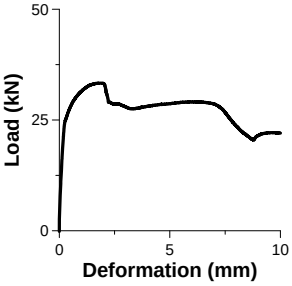
50
25
0
Load (kN)
0
5
10
Deformation (mm)

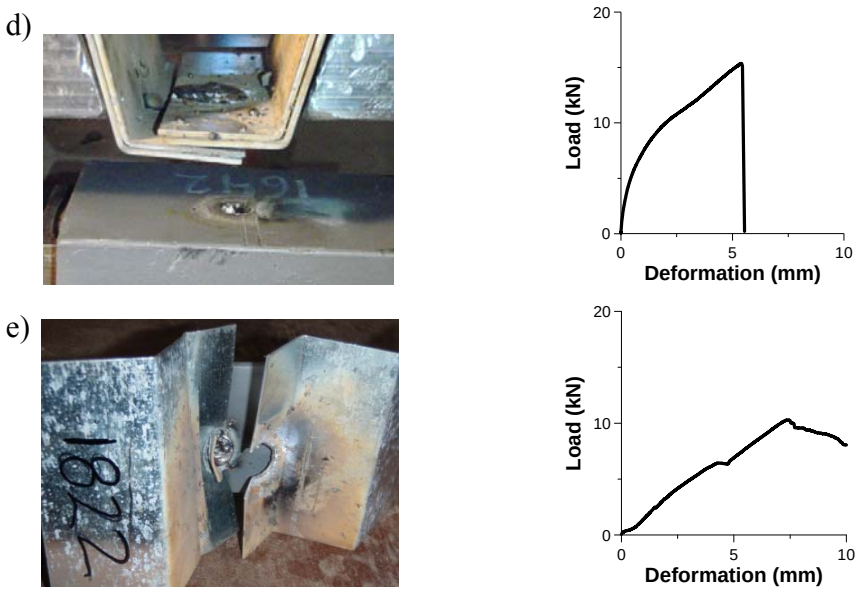

Figure 7 Typical failure modes and load-deformation responses: a) Weld failure in shear (Specimen No. P2021); b) Sheet tearing failure in shear (Specimen No. P2222); C) bearing failure in shear (Specimen No. M2241); d) Weld failure in tension (Specimen No. T1642); and e) Sheet tearing failure (Specimen No. 1822).

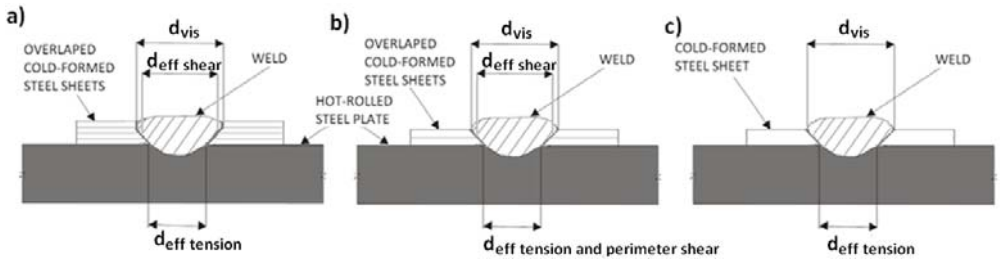

Figure 8 Schematic of cross-section showing visible and effective weld diameters for : a) Four-ply connection in shear and tension; b) Two-ply connections in shear and tension; and c) Single-ply connection in tension.

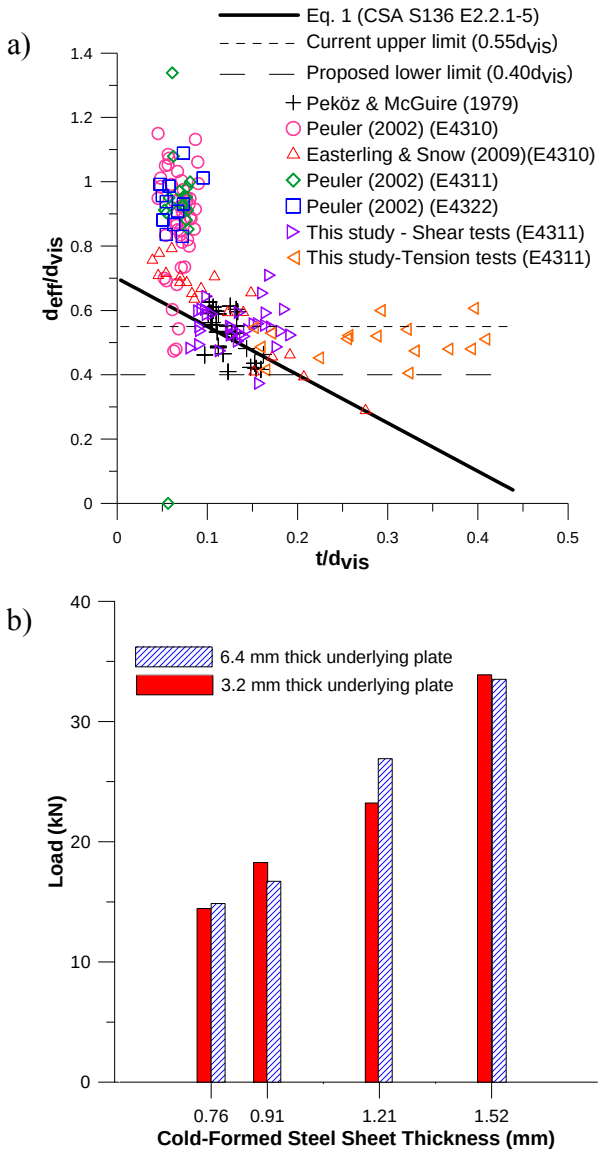

Figure 9 a) Effective weld diameter results; b) Influence of the thickness of the underlying plate on the shear strength of two-ply specimens.

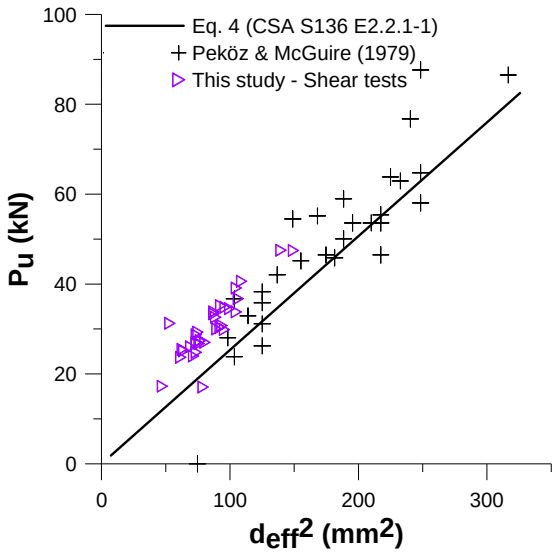

Figure 10 Relationship between measured arc spot weld shear strength P_u and $\boldsymbol{d_{eff}^2}$ of CSA S136 Equation E2.2.1-1

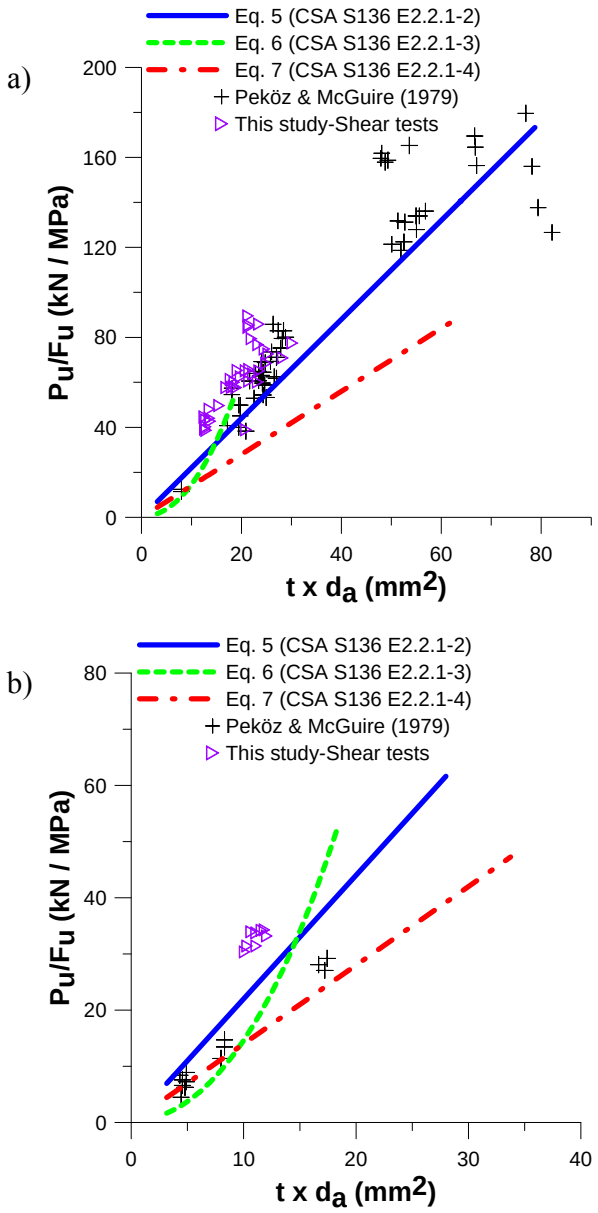

Figure 11 Relationship between measured arc spot weld shear strength and $t \times d_a$ for: a) Bearing failure; b) Tearing failure.

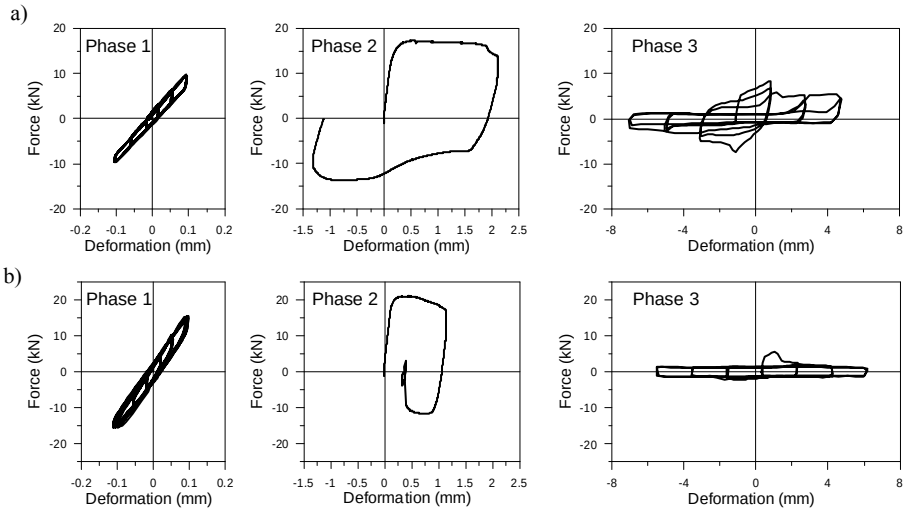

Figure 12 Cyclic load-deformation response of two-layer shear specimens made of: a) 0.91 mm steel sheets (Specimen No. SC2021); b) 1.21 mm steel sheets (Specimen No. SC1841).

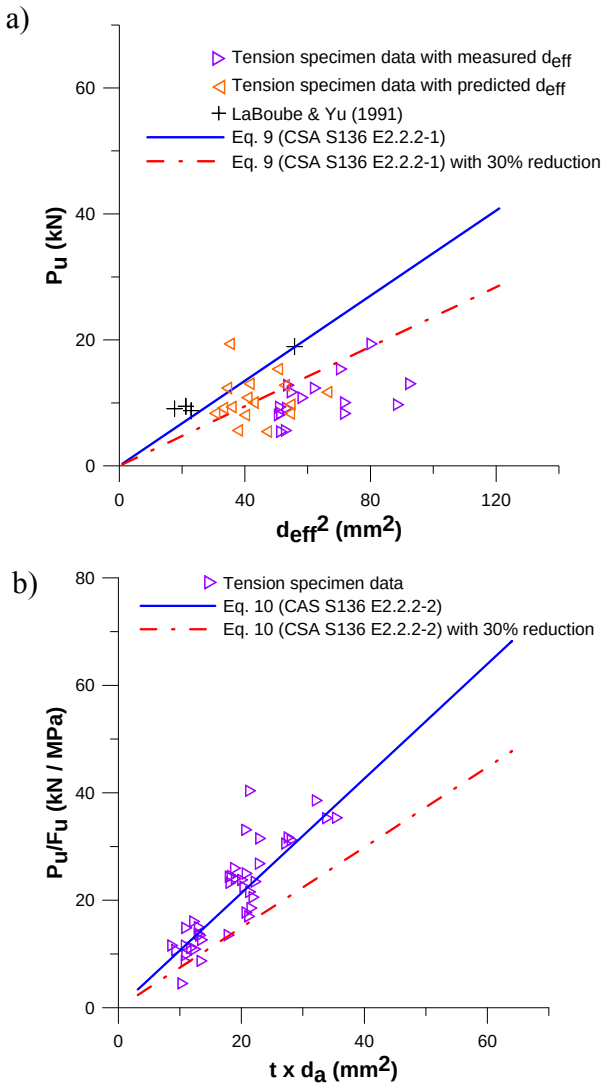

Figure 13 Relationship between measured arc spot weld tension strength and: a) $\boldsymbol{d_{eff}^2}$ for weld failure; b) t×d_a for sheet tearing failure.